

UNCLASSIFIED

AD NUMBER	
ADC007023	
CLASSIFICATION CHANGES	
TO:	unclassified
FROM:	secret
LIMITATION CHANGES	
TO:	Approved for public release, distribution unlimited
FROM:	Controlling DoD Organization. Office of Naval Research, Washington, DC 20390.
AUTHORITY	
CNO/N772 ltr N772A/6U875630 20 Jan 2006 and ONR ltr 31 Jan 2006; CNO/N772 ltr N772A/6U875630 20 Jan 2006 and ONR ltr 31	

THIS PAGE IS UNCLASSIFIED

AD-C007023

SECURITY REMARKING REQUIREMENTS

DOD 5200.1-R, DEC 78

REVIEW ON 28 MAY 96

SECRET

NUC TP 419

COPY

45 of 71

00S-2379-76



1
b.s.

ADCO07023

HORIZONTAL DIRECTIONALITY OF AMBIENT SEA NOISE IN THE NORTH PACIFIC OCEAN (U)

by

R. A. Wagstaff

J. D. Pugh

J. W. Aitkenhead

Undersea Surveillance Department

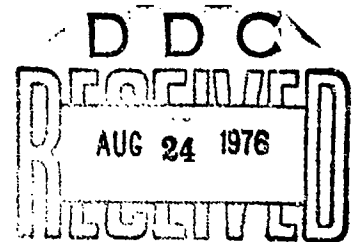
May 1976



AD No. _____
DDC FILE COPY

"NATIONAL SECURITY INFORMATION"

"Unauthorized Disclosure Subject to Criminal
Sanctions"



SECRET

UNCLASSIFIED



NAVAL UNDERSEA CENTER, SAN DIEGO, CA. 92132

AN ACTIVITY OF THE NAVAL MATERIAL COMMAND

R. B. GILCHRIST, CAPT, USN

Commander

HOWARD L. BLOOD, PhD

Technical Director

ADMINISTRATIVE STATEMENT (U)

The work reported herein was performed under ONR LRAPP Project No. R-2408 by members of the Surveillance Modeling Division. The paper covers work from September 1973 to June 1974.

The assistance of the following is gratefully acknowledged:

D. Hardman, D. Keir - data collection
G. Warner - computer program modification, runs and figure preparation
Dr. R. R. Gardner (NUC Code 502) - technical guidance
L. R. B. Duykers, W. L. Frisch - report preparation assistance
The Gould Corp. - loan of Hansen-Woodyard beamformer

Released by
M. R. AKERS, Head
Surveillance Modeling Division

Under authority of
H. A. SCHENCK, Head
Undersea Surveillance and
Ocean Sciences Department

NATIONAL SECURITY INFORMATION
Unauthorized Disclosure Subject to Criminal Sanctions

UNCLASSIFIED

SECRET

UNCLASSIFIED

SECURITY CLASSIFICATION OF THIS PAGE (When Data Entered)

REPORT DOCUMENTATION PAGE		READ INSTRUCTIONS BEFORE COMPLETING FORM
1. REPORT NUMBER NUG-TP-419	2. GOVT ACCESSION NO.	3. RECIPIENT'S CATALOG NUMBER
4. TITLE (and Subtitle) HORIZONTAL DIRECTIONALITY OF AMBIENT SEA NOISE IN THE NORTH PACIFIC OCEAN (U)		5. TYPE OF REPORT & PERIOD COVERED Research and Development Sept 1973 - June 1974
6. AUTHOR(s) R. A. Wagstaff, J. D. Pugh, J. W. Aitkenhead		7. CONTRACT OR GRANT NUMBER(s)
8. PERFORMING ORGANIZATION NAME AND ADDRESS Naval Undersea Center San Diego, California 92132		9. PROGRAM ELEMENT, PROJECT, TASK AREA & WORK UNIT NUMBERS LRAPP Project No. R-2408
10. CONTROLLING OFFICE NAME AND ADDRESS Office of Naval Research Washington, D. C. 20390		11. REPORT DATE May 1976
12. MONITORING AGENCY NAME & ADDRESS (if different from Controlling Office)		13. NUMBER OF PAGES 152 (12) 155 p.
14. DISTRIBUTION STATEMENT (of this Report)		15. SECURITY CLASS. (of this report) SECRET
15. DISTRIBUTION STATEMENT (of the abstract entered in Block 20, if different from Report)		16. DECLASSIFICATION/DOWNGRADING SCHEDULE Classified by: OPNAVINST 5510.72C Exempt from GDS of E.O. 11652 Exempt Category: 3 Declassify on 31 December 2006
17. SUPPLEMENTARY NOTES		
18. KEY WORDS (Continue on reverse side if necessary and identify by block number) Underwater acoustics Passive sonar Towed arrays Noise horizontal directionality SOFAR channel noise		
19. ABSTRACT (Continue on reverse side if necessary and identify by block number) (U) In September of 1973 the Long Range Acoustic Propagation Project (LRAPP) Office sponsored a joint exercise among various Navy Laboratories, contracting organizations and universities. This exercise, called CHURCH ANCHOR, was an acoustic and environmental measurement effort conducted in the Northeast Pacific Ocean. Results of the ambient noise horizontal directionality measurements from the CHURCH ANCHOR exercise are discussed in this report. The measurements were taken along a north-south		

DD FORM 1 JAN 73 1473 EDITION OF 1 NOV 65 IS OBSOLETE

UNCLASSIFIED
SECURITY CLASSIFICATION OF THIS PAGE (When Data Entered)

(This page is unclassified)

SECRET

DDC
RECEIVED
AUG 24 1976

The exercise discussed
the
1473

390 458

(48-173A)

deg

UNCLASSIFIED

SECURITY CLASSIFICATION OF THIS PAGE (When Data Entered)

→ base line at approximately 143° W and extending north from about 31° N to 57° N. Data from two towed arrays and a circular array are presented. The results indicate that a persistent background noise directionality pattern might exist in the Northeast Pacific Ocean basin, one upon which the fluctuations due to nearby ships and other transients can be considered superimposed. It is suggested that such a persistent noise background directionality pattern is the result of propagation mechanisms which will introduce into the SOFAR channel noise from ships along the basin boundaries and at high latitudes. Once trapped in the channel, the noise travels throughout the basin, aided by the favorable sound transmission.

14	W. 1 Section	<input type="checkbox"/>
12	W. 2 Section	<input checked="" type="checkbox"/>
11	W. 3 Section	<input type="checkbox"/>
10	W. 4 Section	<input type="checkbox"/>
9	W. 5 Section	<input type="checkbox"/>
8	W. 6 Section	<input type="checkbox"/>
7	W. 7 Section	<input type="checkbox"/>
6	W. 8 Section	<input type="checkbox"/>
5	W. 9 Section	<input type="checkbox"/>
4	W. 10 Section	<input type="checkbox"/>
3	W. 11 Section	<input type="checkbox"/>
2	W. 12 Section	<input type="checkbox"/>
1	W. 13 Section	<input type="checkbox"/>

UNCLASSIFIED

SECURITY CLASSIFICATION OF THIS PAGE (When Data Entered)

SECRET

SUMMARY

MEASUREMENT OBJECTIVES

(C) The objectives of the CHURCH ANCHOR ambient noise measurement experiments were to:

1. Obtain the azimuthal directionality of ambient noise at various locations.
2. Obtain estimates of the temporal variability of the ambient noise field.

CONCLUSIONS

(U) The analysis methods available for resolving the ambiguities in towed horizontal line array data are inherently fallible. They do not permit the accurate representation of the noise field which was measured. Several different methods have been used in an attempt to minimize the untrustworthiness of the analysis. Furthermore, because of the lack of techniques to judge the degree of similarity between the noise roses presented in this report and the noise fields which really existed at the time of the measurements, the following conclusions are stated with considerable reservation.

(C) The horizontal noise field was either stationary or the TASS experiment was incapable of assessing stationarity. If the TASS can assess stationarity, then the horizontal noise field as measured by a line-array changes significantly over a period of 15 min, a conclusion which casts doubt on the validity of the results of the deconvolution procedures used in this report. It is important to note that for the 160-Hz data the null hypothesis was rejected for all 48 legs. At 160 Hz the beams are much narrower than at the other three frequencies. For this reason, a small change in array orientation would introduce a larger degree of nonstationarity in the 160-Hz data in an otherwise stationary noise field than it would for the lower frequencies (which give wider beams).

(C) The majority of the consistently high-level, low-frequency (11-Hz to 160-Hz) noise received by a sensor located well within the Sound Fixing and Ranging (SOFAR) channel arrived via SOFAR channel propagation. The probable source of this noise was distant shipping which was crossing the waters above the continental shelf and slope along the west coast of the United States and near the Aleutian Islands. The resulting levels were from approximately 6 to 16 dB higher than the noise levels along other azimuths.

(C) Neither the beam response nor the resolved horizontal directionalities for the TASS 40-, 50-, 100-, and 160-Hz data were significantly changed when the analysis bandwidth was changed from 1/3 octave to 1/10 Hz.

SECRET

SECRET

(U) The shape of the noise field horizontal directionality and the degree of anisotropy (variability with azimuth) was found to be generally independent of frequency between 11 Hz and 160 Hz. With the exception of the absolute levels, it was possible to reproduce the low-frequency beam response results merely by smoothing or resampling the higher-frequency results to introduce the effects of the wider, and perhaps fewer, low-frequency beams.

(S) The narrowbeam data show more evidence of nearby shipping, which appeared as transients to confound the ambiguity resolution techniques. As a result, in most cases the ambiguity algorithms failed to resolve the ambiguities in the 160-Hz TASS and the 38-, 36-, and 29-Hz LAMBDA data.

(C) Only one period during TASS noise measurements passed tests for stationarity and for only the lowest frequency (40 Hz). This indicates that the assessment of noise field stationarity is not independent of the array beamwidth. As beamwidth increased, the measured data appeared more stationary, i.e., the stationarity assessment is measurement-tool dependent.

(C) All of the LAMBDA results, except for those corresponding to polygons 1 and 2, were degraded by array heading errors, which in one case was known to be approximately 30 deg.

RECOMMENDATIONS

(U) Based upon the experience gained in data collection and analysis for the experiment, the following recommendations are presented:

1. Use a source (shot or tone) prior to each measurement period to accurately establish the absolute array heading.
2. Obtain the positions, classes, courses, lengths, and speeds of nearby ships if the noise data are to be used for model validation and, if feasible, the acoustic signatures for use in spectral analysis.
3. Record both beam and hydrophone outputs whenever possible. If this is not possible, the output of at least one hydrophone should be recorded.
4. Dedicated experiments should be performed for the purpose of measuring noise data for noise model validation. In such experiments, a few (1-3) ships whose physical and acoustical characteristics are well known could be vectored along given courses to test the modules for propagation loss and surface ship source levels.
5. Investigate other techniques for comparing polygon leg beam response data to representative horizontal directionalities.
6. Initiate studies to define criteria whereby the data can be tested for stationarity. If data do not pass the tests for stationarity, ambiguity-resolution techniques requiring stationarity should be utilized.

SECRET

UNCLASSIFIED

7. Obtain ambient noise horizontal directionality measurements in the CHURCH ANCHOR project area at other times of the year to determine seasonal variability, if any exists.

8. If data from more than one measurement system are to be combined or compared, analysis compatibility with respect to beamwidth, frequency, and analysis bandwidth should be required.

UNCLASSIFIED

SECRET

CONTENTS

SUMMARY	1
Measurement Objectives	1
Conclusions	1
Recommendations	2
INTRODUCTION	9
Important Notice	10
DESCRIPTION OF THE CHURCH ANCHOR AMBIENT NOISE MEASUREMENT EXPERIMENT	11
Rationale	11
Horizontal Directionality Measurements	11
Conduct of the Experiment	14
AMBIGUITY-RESOLUTION TECHNIQUES	19
Methods	19
Effect of Noise Field Nonstationarity – A Simplified Approach	20
RESULTS	23
Baseline Results	23
SOFAR Channel Noise	39
Temporal Variability	48
Noise Field Properties	56
REFERENCES	71
APPENDICES	
A. Noise Measurement Systems Characteristics	73
B. Pre-CHURCH ANCHOR Measurements	79
C. Ambient Noise Horizontal Directionality	81
D. Ambiguity-Resolution Techniques	99
E. Environmental Data for CHURCH ANCHOR Exercise Area	113
F. Data Quality and Analysis Errors	117
G. Statistical Assessment of Randomness	129
H. Results Utilizing Adaptive Processing	141

SECRET

SECRET

LIST OF ILLUSTRATIONS

Figure

1. Locations for ambient noise horizontal directionality measurements during the CHURCH ANCHOR experiment. (U) 13
2. "Hand waving" explanation of six ambiguity resolution techniques. (U) 22
3. Horizontal directionality noise roses for a 1/8-Hz bandwidth at 38 Hz obtained from LAMBDA polygon 2 data at η -3 with Vibroseis source evident at approximately 159 deg. (S) 24
4. Horizontal directionality noise roses for a 1/8-Hz bandwidth at 29 Hz obtained from LAMBDA polygon 2 data at η -3. (S) 25
5. Horizontal directionality noise roses for a 1/8-Hz bandwidth at 23 Hz obtained from LAMBDA polygon 2 data at η -3. (S) 26
6. Horizontal directionality noise roses for a 1/8-Hz bandwidth at 11 Hz obtained from LAMBDA polygon 2 data at η -3. (S) 27
7. Horizontal directionality noise roses for a 1/3-octave bandwidth at 160 Hz obtained from TASS polygon 4 data at η -3. (C) 28
8. Horizontal directionality noise roses for a 1/3-octave bandwidth at 100 Hz obtained from TASS polygon 4 data at η -3. (C) 29
9. Horizontal directionality noise roses for a 1/3-octave bandwidth at 50 Hz obtained from TASS polygon 4 data at η -3. (C) 30
10. Horizontal directionality noise roses for a 1/3-octave bandwidth at 40 Hz obtained from TASS polygon 4 data at η -3. (C) 31
11. Typical MESA beam response data for a 1/3-octave bandwidth at 150 Hz, for 30 contiguous 1-min estimates beginning 1536Z 21 September 1973 at 45°5'54"N, 143°28'00"W. (U) 36
12. Typical MESA beam response data for a 1/3-octave bandwidth at 100 Hz, for 30 contiguous 1-min estimates beginning 1536Z 21 September 1973 at 45°5'54"N, 143°28'00"W. (U) 37
13. Typical MESA beam response data for a 1/3-octave bandwidth at 36 Hz, for 30 contiguous 1-min estimates beginning 1536Z 21 September 1973 at 45°5'54"N, 143°28'00"W. (U) 38
14. Representative relative horizontal directionality of 100-Hz ambient noise along approximately 143°W measured by MESA (above 45°N) and resolved by TASS (below 40°N). (C) 40
15. Comparison between 100-Hz average SOFAR channel noise and the resolved horizontal directionality using the MAB method and TASS all-beam data for one polygon at η -3. (C) 43

SECRET

SECRET

ILLUSTRATIONS (Continued)

Figure

- | | | |
|-----|--|----|
| 16. | Comparison between 100-Hz average SOFAR channel noise and the resolved horizontal directionality using the MAB method and TASS all-beam data for one polygon at η -2. (C) | 45 |
| 17. | Comparison between 100-Hz average SOFAR channel noise and the resolved horizontal directionality using the MAB method and TASS all-beam data for one polygon at η -1. (C) | 46 |
| 18. | Surface contacts on 3 September 1973 (reprinted from reference 9, bathymetry data added—depths in fathoms). (U) | 47 |
| 19. | High, mean, and low beam response plots for 40 Hz and leg 5 of the TASS polygons at η -3. (C) | 50 |
| 20. | High, mean, and low beam response plots for 40 Hz and leg 5 of the TASS polygons at η -1. (C) | 51 |
| 21. | MAB horizontal directionalities for the high, mean, and low beam responses for all 40-Hz TASS polygon legs at η -3. (C) | 53 |
| 22. | MAB horizontal directionalities for the high, mean, and low beam responses for all 40-Hz TASS polygon legs at η -1. (C) | 54 |
| 23. | Comparison of 29-Hz LAMBDA beam response data for leg 3 of polygons 3, 5, and 6 at η -1. (S) | 55 |
| 24. | Comparison of TASS beam response data at 160-Hz for 1/3-octave and 1/10-Hz bandwidth analysis, leg 1 of polygon 1 at station η -1. (C) | 57 |
| 25. | Comparison of TASS beam response data at 100-Hz for 1/3-octave and 1/10-Hz bandwidth analysis, leg 5 of polygon 1 at station η -1. (C) | 58 |
| 26. | Comparison of TASS beam response data at 50-Hz for 1/3-octave and 1/10-Hz bandwidth analysis, leg 3 of polygon 1 at station η -1. (C) | 59 |
| 27. | Comparison of TASS horizontal directionality noise roses at 160-Hz; 1/3-octave and 1/10-Hz bandwidth analyses for polygon 1 at station η -1. (C) | 60 |
| 28. | Comparison of TASS horizontal directionality noise roses at 100-Hz; 1/3-octave and 1/10-Hz bandwidth analyses for polygon 1 at station η -1. (C) | 61 |
| 29. | Comparison of TASS horizontal directionality noise roses at 50-Hz; 1/3-octave and 1/10-Hz bandwidth analyses for polygon 1 at station η -1. (C) | 62 |
| 30. | Comparison of TASS horizontal directionality noise roses at 40 Hz; 1/3-octave and 1/10-Hz bandwidth analyses for polygon 1 at station η -1. (C) | 63 |

SECRET

SECRET

ILLUSTRATIONS (Continued)

Figure

- | | | |
|-----|---|----|
| 31. | Comparison of LAMBDA polygon 3, leg 2, 11-Hz beam response data with 36-Hz and 36-Hz smoothed-beam response data for the same leg. (S) | 65 |
| 32. | Comparison of 29-Hz noise rose with modified (sampled and smoothed) 36-Hz noise rose for LAMBDA data, station $\eta-1$. (S) | 66 |
| 33. | Comparison of 23-Hz noise rose with modified (sampled and smoothed) 36-Hz noise rose for LAMBDA data, station $\eta-1$. (S) | 67 |
| 34. | Comparison of 11-Hz noise rose with modified (sampled and smoothed) 36-Hz noise rose for LAMBDA data, station $\eta-1$. (S) | 68 |
| 35. | Superposition of 160-Hz TASS beam response data with 29-Hz LAMBDA beam response data; both data for polygon 1, leg 1, at $\eta-3$. (S) | 70 |

SECRET

CONFIDENTIAL

INTRODUCTION

(U) The CHURCH ANCHOR experiment was a joint U.S.-Canadian long-range acoustic propagation project in the Northeast Pacific Ocean and was conducted by participants from the naval laboratories, private industry, and the universities. Acoustic propagation, ambient noise, environmental, and bathymetric measurements were taken.

(C) This document reports only the results of horizontal directionality measurements of the ambient noise. The majority of the results discussed herein were produced from the data obtained by the two towed line-arrays, the Large Aperture Marine Basic Data Array (LAMBDA) and the Towed Array Surveillance System (TASS), with some inputs of data from the Multi-Element Superdirective Array (MESA) of the Defense Research Establishment-Pacific (DREP).

(C) The Summary section of this report presents the noise measurement objectives of the CHURCH ANCHOR experiments and the conclusions and recommendations subsequently developed. The rationale of the experiments, a description of the experimental procedures, and a brief sequence-of-events narrative are presented in the section entitled Description of the CHURCH ANCHOR Ambient Noise Measurement Experiment. The ambiguity algorithms used in the data analysis phase are discussed individually in the section entitled Ambiguity Resolution Techniques. Test results and related discussion are presented in the Results section. The physical and acoustical characteristics of each system are given in Appendix A. Appendix B discusses the calibration of LAMBDA and TASS hydrophones. Appendix C contains some of the noise roses obtained from the LAMBDA and TASS data. Appendix D presents the rationale and physical interpretation of the ambiguity-resolution techniques. An example illustrating the effects of transients, such as ship noise that is dominant on only one side, or "leg", of a polygon-shaped array course, is also included. Appendix E gives pertinent environmental data for the test area. Appendix F discusses the quality of the beam response data and the sources, nature, and magnitude of the errors in the noise roses which resulted from the inaccuracies and imperfections in the ambiguity-resolution techniques. Appendix G discusses the statistical procedures utilized to assess the randomness of the TASS noise data. Finally, Appendix H discusses the horizontal directionality results which were obtained when adaptive processing was utilized to generate the effective beam response data required by the ambiguity resolution algorithms. The results are of rather limited scope since only relative, not absolute, levels were obtained.

CONFIDENTIAL

CONFIDENTIAL

IMPORTANT NOTICE

(U) The horizontal directionality noise roses (resolved noise directionality plots) presented in this report must be approached with extreme caution. This warning cannot be too strongly emphasized. Various methods have been used to obtain different bits of information about the noise field horizontal directionality. To the knowledge of the authors, there does not currently exist one method for resolving the ambiguities in the data measured by a horizontal line-array that is capable of answering all of the questions which could be asked regarding the directional character of the noise. The methods used herein are no exception. Each method is incomplete but supplies at least one bit of information about the noise field which the other methods do not, and each method contains its own peculiar deficiencies and errors. Thus, by utilizing each method to supply those unique pieces of information about the noise field, while fully realizing and understanding the faults and pitfalls as well, a better reconstruction of the noise field can be achieved. Unfortunately, at the time these analyses were conducted, there did not exist a method of estimating the degree of similarity between the reconstructed noise fields and the noise fields which really existed at the time of the measurements. Hence, conclusions based on these analyses are stated with a moderately low confidence.

CONFIDENTIAL

CONFIDENTIAL

DESCRIPTION OF THE CHURCH ANCHOR AMBIENT NOISE MEASUREMENT EXPERIMENT

RATIONALE

(C) In general, the CHURCH ANCHOR experiment was designed to provide a data base for select regions of the Northeast Pacific which would permit the:

1. Formulation of decisions related to design, development and deployment of new-generation ASW systems.
2. Performance prediction of various ASW system options.
3. Diagnosis of specific system detection performance characteristics.
4. Evaluation and refinement of prediction techniques.

(C) Knowledge of the characteristics of the ambient noise field is pertinent to all of the above. Expected levels of omnidirectional noise measured near the ocean surface are well established. The information on directional characteristics for noise measured at significantly greater depths and lower frequencies is not as well known. It is the purpose of this report to (1) provide a documented noise-measurement data base and (2) discuss directional ambient noise as measured by TASS, LAMBDA, and MESA at frequencies below 200 Hz.

HORIZONTAL DIRECTIONALITY MEASUREMENTS

(C) The horizontal directionality characteristics of the noise field were sampled independently by three different arrays; i.e., LAMBDA, TASS, and MESA. Table 1 contains the deployment data for these three arrays and Fig. 1 pinpoints the geographical locations where the noise measurements were taken.

(C) Both the TASS array (USNS S. P. LEE) and the LAMBDA array (PACIFIC APOLLO) were towed along five different headings during the noise measurement periods to enable unambiguous reconstructions of the noise field. The tow-depths of both arrays were well within the SOFAR channel. For the present discussion the SOFAR channel will refer to the region in the vertical water column over which continuously refracted rays travel. The MESA array (ENDEAVOUR) was deployed either on, or near, the SOFAR channel axis.

(C) The TASS and LAMBDA arrays were towed at approximately 3.5 kt. Both ships utilized onboard computers to reconstruct the noise field horizontal directionality from ambiguous beam outputs obtained during the polygon maneuvers.

CONFIDENTIAL

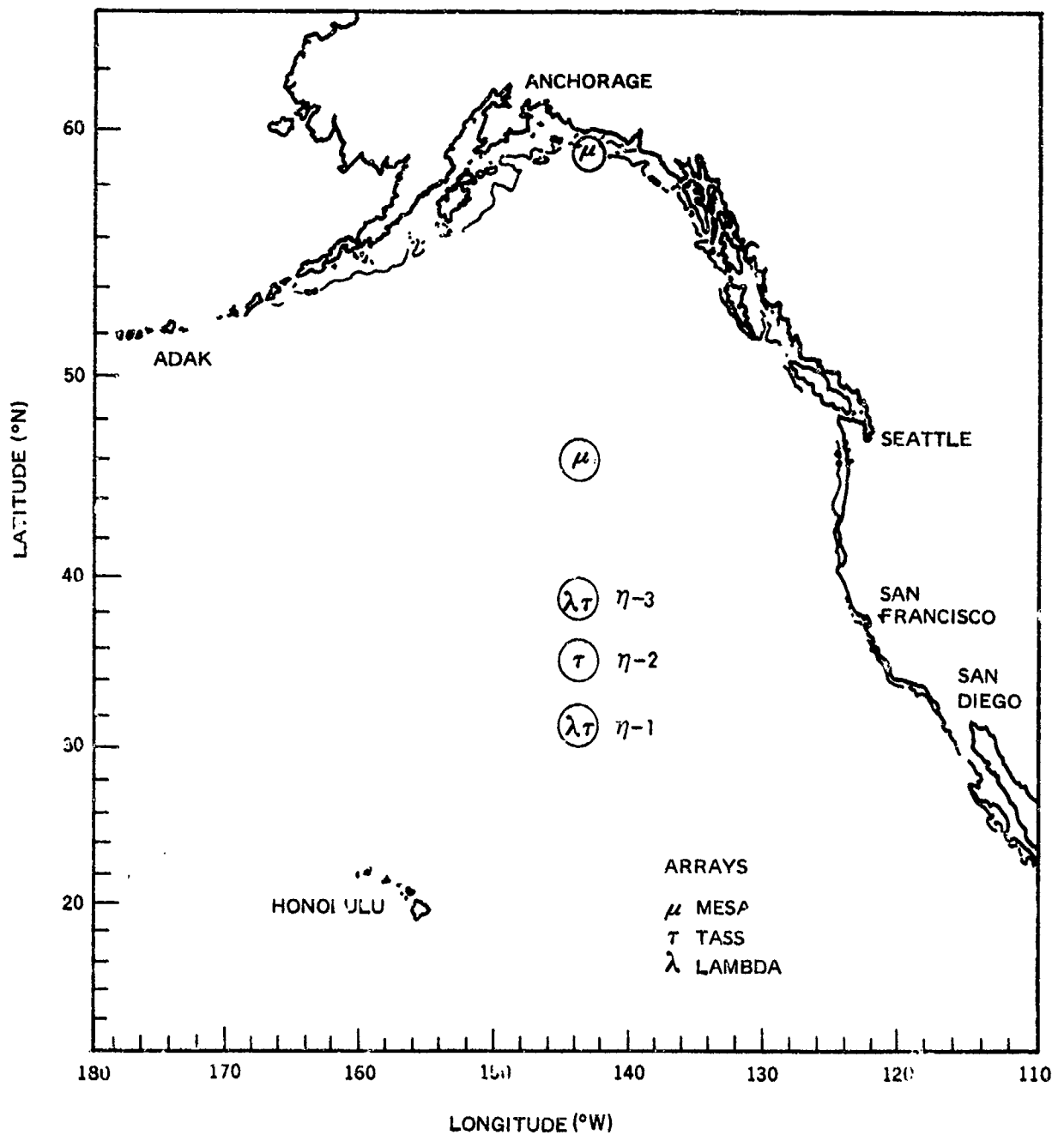
CONFIDENTIAL

(C) Table 1. Deployment of the horizontal arrays. (U)

Array	September 1973 Date/Time (ZULU)		Latitude (N) (deg)	Longitude (W) (deg)	Designation	Depth	Mode
	Start	Finish					
LAMBDA	021400	031000	38	143	η -3	457	Tow
	082200	091800	31	143	η -1	457	Tow
	192100	201930	31	143	η -1	457	Tow
TASS	021430	030945	38	143	η -3	457	Tow
	052042	061547	34	143	η -2	457	Tow
	082230	091245	32	143	η -1	457	Tow
MESA	100400	100414	57	143	---	100	Moored
	102313	102327	57	143	---	100	Moored
	110206	110236	57	143	---	100	Moored
	110443	110457	57	143	---	100	Moored
	110759	110813	57	143	---	100	Moored
	111144	111213	57	143	---	100	Moored
	111950	112004	57	143	---	100	Moored
	190809	190838	45	143	---	460	Moored
	200228	200258	45	143	---	460	Moored
	210512	210541	45	143	---	400	Moored
	210913	210942	45	143	---	400	Moored
	211536	211605	45	143	---	400	Moored
	220405	220420	45	143	---	400	Moored
	222310	222324	46	143	---	400	Moored

CONFIDENTIAL

CONFIDENTIAL



(C) Figure 1. Locations for ambient noise horizontal directionality measurements during the CHURCH ANCHOR experiment. (U)

CONFIDENTIAL

CONFIDENTIAL

(U) During each noise day, as many as four polygons were executed by the USNS S. P. LEE. Each polygon consisted of five sides separated in azimuth by approximately 72 deg. Each leg was of 1 hr duration; 30 min for array equilibration and 30 min for data acquisition.

(C) The Hansen-Woodyard beamformer was also utilized to form relatively narrow endfire beams, enabling TASS to better assess the horizontal directionality of the noise field. The Hansen-Woodyard endfire beam data were taken throughout all polygons at the four primary analysis frequencies of 160, 100, 50, and 40 Hz.

CONDUCT OF THE EXPERIMENT

USNS S. P. LEE - TASS Array

(C) Aboard the LEE, a NOVA 800 computer sampled and stored for onboard analysis all TASS low-frequency beams while the analog outputs were being simultaneously recorded on magnetic tape. The analog tapes included channels for time-code and voice. Calibration signals were periodically introduced to enable post-exercise analysis. Each 30-min measurement period was divided into two 15-min periods. The first 15-min period was originally intended to be devoted to measurements at 0-dB system gain, while the second was set apart for measurements with 20-dB system gain.

(U) During the 30 min required to stabilize the array following a course change, the data for the previous leg was to be analyzed by the statistical algorithms and beam-response plots generated. A result of this onboard analysis capability was the early discovery that the beam responses corresponding to low system gain remained relatively constant from leg to leg. A noise of high level and low variability remained on the broadside beam even though the array heading changed radically from leg to leg. The most likely source of this noise was judged to be the beamformer, i.e., the "floor" of the beamformer was being measured, not ambient noise. As a result, the Technical Director granted permission to take all subsequent measurements in the high-gain mode.

(U) At the completion of each noise measurement day, the beam response data from each polygon were processed by the ambiguity-resolution algorithms. The results were beam response plots and tables of statistical analysis results for all legs, frequencies, and measurement time periods. Hydrophone profiles were also taken periodically to insure data quality.

(C) A log of all ships within radar range (about 20 nmi) was maintained during all noise measurement periods, and the TASS lofargrams* were annotated and data recorded to facilitate the post-exercise interpretation of the measured noise data.

*Low-frequency analysis and recording.

CONFIDENTIAL

CONFIDENTIAL

Shipping surveillance data, however, had very little influence on the interpretation of the noise data because (1) the aerial surveillances were conducted during the day following the noise measurements, (2) surveillances near the arrays were sparse, and (3) the recorded ship positions were not dead-reckoned for times during the noise measurement periods. Therefore, when a high-level noise was evident in the beam response data, there was no way to establish the nature and range of the source, unless that ship (the noise source) passed the tow ship within the vicinity of the affected azimuth.

(C) During the first polygon of the first noise measurement day, the ship LONGVIEW VICTORY came within 500 yd of the LEE to evacuate the ship's master and an oiler for unavoidable medical and personal reasons, respectively; however, only one leg of TASS data appeared to have been adversely affected. Two other deviations from the exercise plan occurred:

1. Electrical power to the array was accidentally turned off; however, only one of the two 15-min measurement periods was affected. This was not considered to be serious, since only one would be used in the final analysis.
2. Computer failure was experienced and the stored data for several previous legs were lost. To restore the data, the analog tapes were played back through the system at the end of the noise measurements taken that day and the beam data re-sampled and stored. Data recovery was complete, with no adverse effects caused by the reconstruction process. This incident demonstrated the utility of the onboard data analysis capability.

(C) During the noise measurements at $\eta-1$, noises from explosive sources were received by the TASS array. The explosions were spaced some 8 min apart in an apparent coded sequence. The effects were observed both in real time and later in the statistical data (see Appendix G). The real-time effects appeared as overload signals from the onboard computer, level changes in the Hansen-Woodyard endfire beam strip-chart recorder, and were visible on the Sanders "waterfall-type" spectrum analyzer. The regularity of the explosions was such that the time of each event could usually be predicted with reasonable accuracy. A more complete discussion of the explosions, their sound levels, and their probably sources and locations is given in Ref. 1. Because of the short duration and long time interval between each event, the explosions were not visible in the averaged beam response data of either LAMBDA or TASS; in fact, they were barely detectable on the TASS lofargrams even though the gram readers had been alerted to their occurrence.

(C) Post-exercise analysis included quality assurance checks of the onboard results and narrowband (1/10-Hz) analysis of selected TASS analog data. A result of the narrowband analysis was the discovery that all 50-Hz, 1/3-octave data analyzed onboard were low by approximately 3 dB. The discrepancy was first

CONFIDENTIAL

CONFIDENTIAL

discovered when trying to compare the 1/10-Hz results with the 1/3-octave results. Select portions of the back-up tapes were then analyzed for the same times and for the same 1/3-octave bands used when the onboard data were obtained. Agreement at 40, 100, and 160 Hz was generally within a fraction of a dB, while the onboard 50-Hz data were approximately 3 dB low. This error was attributed to a defective filter in the onboard 1/3-octave analyzer and was corrected by adding 3.2 dB to the affected data.

PACIFIC APOLLO - LAMBDA Array

(C) Unlike the TASS system, the LAMBDA system utilizes hydrophone outputs in digital format as "back-up" rather than analog beam responses. Beams, however, are formed in real time, and the onboard Data Acquisition System (DAS) accepts the LAMBDA beam responses and processes them with the All-Bearings ambiguity-resolution algorithm to yield noise roses. During onshore post-analysis, these beam responses were utilized in the same ambiguity-resolution algorithms as were the TASS beam response data. The ambiguous noise-level-versus-azimuth data resulting from the post-exercise adaptive beamforming analysis of the hydrophone data were also utilized in the ambiguity resolution techniques. The results of the analysis are discussed in Appendix H.

(C) During the second LAMBDA polygon at η -3, the Vibroseis source was operating on one of the analysis frequencies of LAMBDA. The azimuth from LAMBDA to the source was approximately 159 deg and the source was clearly evident in the LAMBDA beam response data for all legs of the polygon. Although this event was not originally scheduled, it was of major importance in that it accurately established the array headings for this polygon. The heading errors ranged from 6 to 30 deg, all in the same direction.

(C) During the first leg of polygon 3, the ship GOOD MARINER passed over the array cable 1,000 ft aft of the PACIFIC APOLLO, contaminating the LAMBDA beam response data for that leg. As a result, only four legs were used in the assessment of the horizontal directionality from the data of polygon 3. During the execution of polygon 4, a system failure occurred, resulting in the loss of all data for polygon 4. Data recovery was not possible. Just prior to the execution of polygon 5, the array struck an unidentified underwater object (probably a sub-surface buoy) damaging the exterior covering of the array. The first and second legs of polygon 5 were successfully completed before flooding of the components in the damaged section adversely affected the acoustical performance of the array. Prior to the start of the third leg, the damaged section was replaced and the measurement experiment resumed some 2 hr behind schedule. The delay is not believed to have had a detrimental effect on the results.

CONFIDENTIAL

UNCLASSIFIED

ENDEAVOR – MESA Array

(U) The MESA data presented later in this document are results obtained from the processing of only four of the seven elements of the array. A loose connector discovered after 21 September made a three-element group inoperable. Also, in order to be consistent, all of the MESA data reported herein are from the same four elements. A discussion of the MESA experiment and data from the entire array will be published at a later date by DREP.

UNCLASSIFIED

CONFIDENTIAL

AMBIGUITY-RESOLUTION TECHNIQUES

METHODS

(U) The analysis of the noise directionality as sampled by a line-array was accomplished by the use of various (six) algorithms and techniques. Each one provides a different aspect of the noise field, but none yields the entire picture. The following gives a short description of the six techniques. Supplementary information is given in Appendices D and F.

All-Bearings

(U) The All-Bearings method attempts to calculate representative values for the noise along each azimuth. The utilization of normalized beam outputs (beam-response levels reduced by 10 times the log of the beamwidth) from an array having nonuniform beamwidths, the addition and subtraction of noises from different azimuths and the nonstationary noise field over the duration of a polygon combine to degrade the effectiveness of this method. The net results are that a large percentage (sometimes in excess of 40 percent) of azimuths are assigned negative noise power levels and the ambiguities of transients are not resolved, giving rise to "ghosts" in the noise roses. The All-Bearings result in Fig. F-7 has been shaded appropriately to distinguish the regions of positive and negative power.

Bearing Ambiguity Resolution (BAR)

(C) The BAR method utilizes the lowest level of measured noise in a given direction for the noise along that azimuth. If the level along a given azimuth is 4 dB below the average level, the assumption is made that the noise was received equally from that azimuth and the ambiguous azimuth. For such azimuths the levels are reduced by 3 dB.

Modified All-Bearings (MAB)

(U) The MAB estimate for the noise in a given direction is simply the maximum of the All-Bearings and the BAR methods. This union overcomes the negative power problem of the All-Bearings method by substituting a measured value for the negative intensity and replacing low BAR levels along some azimuths with higher levels which may be more indicative of the average during the measurement time period. Figure F-7 illustrates the negative power problem for the All-Bearings method and the result obtained when the BAR values are substituted for the affected azimuths.

CONFIDENTIAL

CONFIDENTIAL

HIBAR

(U) This method selects the highest of the normalized levels along a given azimuth. The result along a given azimuth is an upper bound for the normalized data for the duration of the polygon. All other normalized levels along a given azimuth must be less than, or equal to, the HIBAR value. The results are necessarily ambiguous in a nonstationary field since the ambiguity of a transient, which appears as a high level on the ambiguous beam during only one leg, cannot be resolved.

LOBAR

(U) The LOBAR method is essentially the BAR method modified by the assumption that for all azimuths the noise came equally from both ambiguous directions (beams). Hence, the LOBAR results will be identical to the BAR results in low-noise directions and 3 dB lower than the BAR results in high-noise directions. The LOBAR results for a given azimuth represent the lowest level the array could have measured during the measurement time and for the given array orientations. The LOBAR value along a given azimuth therefore represents a lower bound for the normalized data.

Hansen-Woodyard Endfire Beam

(C) Throughout each polygon executed by TASS, the Hansen-Woodyard endfire beamformer (Ref. 2) was utilized to form relatively narrow endfire beams to obtain unambiguous estimates of the noise field horizontal directionality. At 100 Hz, for example, beamwidth was approximately 23 deg. The SOFAR channel limiting angles at the CHURCH ANCHOR locations and depths for the TASS were such that this beam was, for all practical purposes, entirely enclosed within the SOFAR channel. Hence, the Hansen-Woodyard beam at this frequency was measuring only noise which arrived by way of the SOFAR channel. By this means the noise which arrives via SOFAR channel propagation can be measured without interference from nearby noise sources on the surface.

EFFECT OF NOISE FIELD NONSTATIONARITY— A SIMPLIFIED APPROACH

(U) The following discussion presents a simplified view of a complex problem. Readers interested in more complete or more rigorous treatments are referred to appendix D and Refs. 3 and 4.

(U) None of the present methods (see Fig. 2) for resolving the ambiguities in the beam response data acquired by a horizontally towed line-array adequately accounts for the nonstationarity of the noise field. Implicit in each method is the assumption that the noise field does not change significantly over the time required to execute the

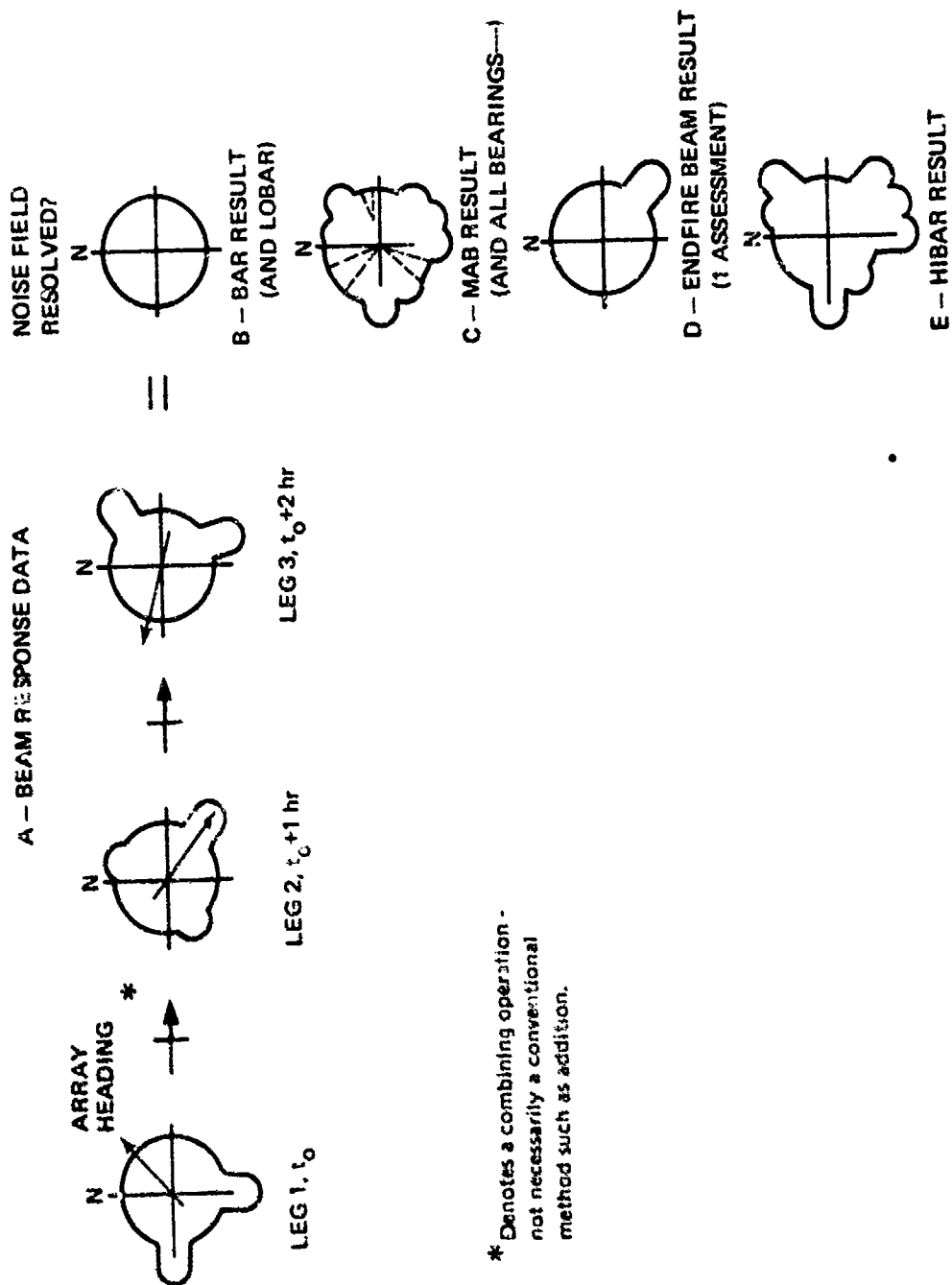
CONFIDENTIAL

UNCLASSIFIED

necessary towing maneuvers required for deconvolution. Unfortunately, very little of the CHURCH ANCHOR noise data satisfied this assumption. However, before new methods can be derived which account for the nonstationarity of the noise field, it is the opinion of the authors that the type of end result which will be meaningful or representative must first be determined. Then and only then should the necessary mathematics or algorithms be derived which accomplish the desired objective. This in itself may be an impossible task. For example, consider the three consecutive hypothetical beam response patterns in part A of Fig. 2. Each might be analogous to what would be obtained during a three-sided polygon maneuver in a simplified nonstationary noise field. This is clearly a case of combining "apples" and "oranges" to get something else. In the case of the BAR and LOBAR solutions, the resolved horizontal directionality pattern in part B does not resemble any of the three input beam response patterns (apples + oranges + pears = bananas). The MAB and All-Bearings (part C) result has some features of all the patterns (apples + oranges + pears = fruit salad). The endfire analysis (part D) is different (apples + oranges + pears = fruit cocktail) and the HIBAR result (part E) is different yet (apples + oranges + pears = fruit bowl). Whether any of these six can be considered representative of the noise at the times during which the measurements were taken is doubtful. It is easy to find fault with each method and difficult to arrive at a tractable solution. What the answer should be, or if there even exists one answer which is suitable for all purposes, the authors do not know. However, it is evident that a thorough understanding of each method is required before the resolved noise field directionalities can be properly interpreted. Also, because of the imperfections in the present ambiguity-resolution techniques, the original beam response data have been preserved in Ref. 5; hence, if and when an improved method is devised, the data can be reprocessed.

UNCLASSIFIED

UNCLASSIFIED



(U) Figure 2. "Hand waving" explanation of six ambiguity resolution techniques. (U)

UNCLASSIFIED

SECRET

RESULTS

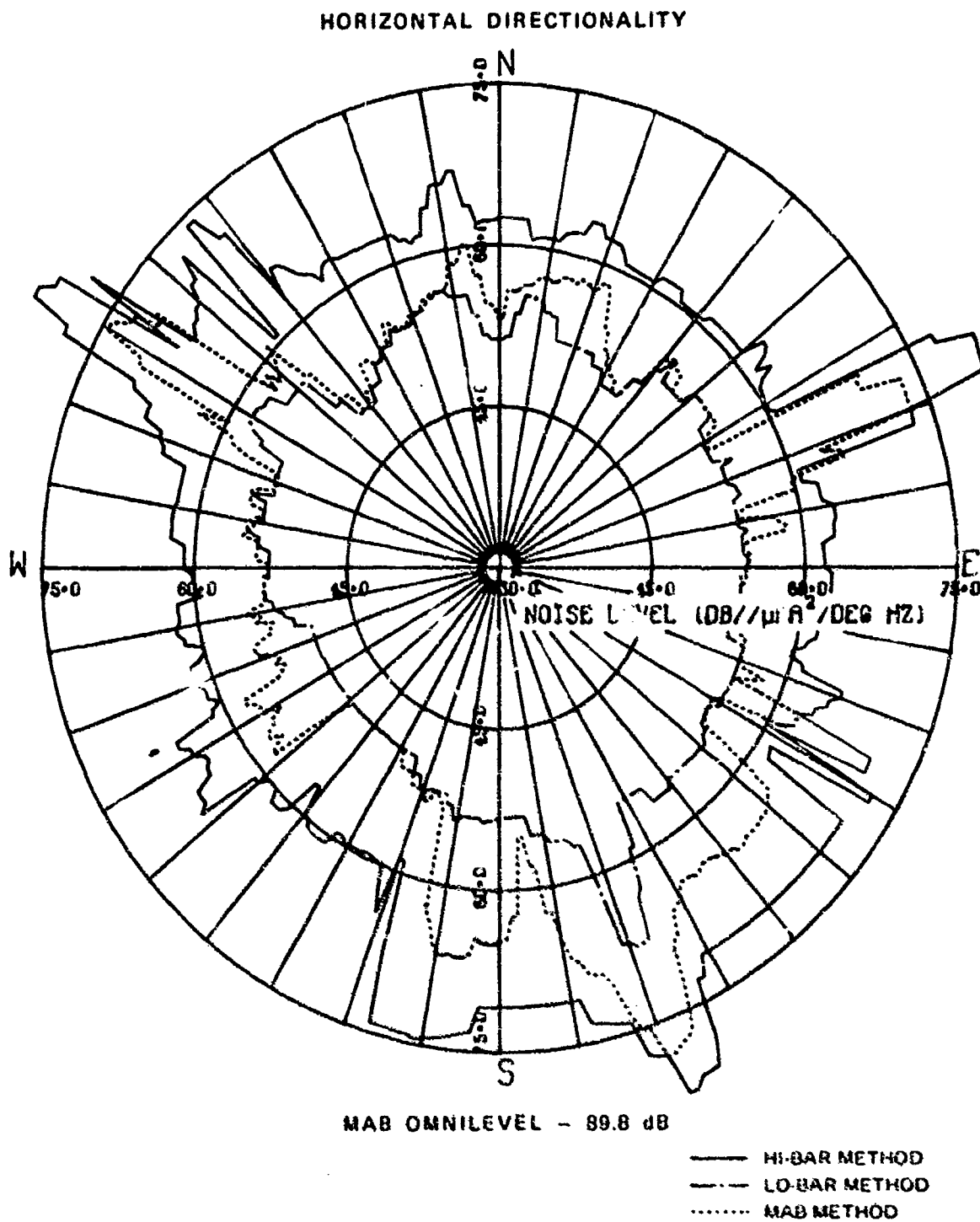
BASELINE RESULTS

(C) The results in the following examples are presented in terms of normalized levels and have been plotted on a per-degree basis. The necessity for this convention arises when the data are taken by arrays having nonuniform beams as a function of relative bearing. For analysis purposes, the assumption is made that the noise received on a beam comes from a continuous distribution of sources, where it may in fact, effectively come from only one source. Hence, the proper interpretation of the results requires the reader to keep in mind that the noise along a given azimuthal sector of width equal to the beamwidth of the array from which the data were measured is approximately equal to the average level in that sector plus 10 times the log of the beamwidth. In the cases of the TASS results this would mean an additional 6 to 16 dB, and for the LAMBDA results the increase would be from 6 to 14 dB. Furthermore, the noise could well be due to a single discrete source, such as a nearby ship.

(S) Figures 3 through 6 and 7 through 10 give the noise field horizontal directionalities obtained from the LAMBDA and the TASS beam-response data, respectively, for one polygon each during the noise measurement period starting 2 September. The LAMBDA results are for 1/8-Hz bands centered at 38, 29, 23, and 11 Hz. The TASS results are for 1/3-octave bands centered at 160, 100, 50, and 40 Hz respectively. Each figure contains the results obtained from the HIBAR (solid), LOBAR (chain dot), and MAB (dotted line) methods. Similar plots of results for the other two noise measurement days for the two systems are included in appendix C as figures C-1 through C-16. The original beam response data from which these results were generated are given in Ref. 5 and pertinent environmental data are included in Appendix E. More complete documentation on the environmental data and shipping surveillance will be published by the participating organizations as outlined in the data analysis plan (Ref. 6).

(S) The second polygon of the measurement period was selected to illustrate the noise measured by the LAMBDA system, since the Vibroseis source was operating at 38 Hz during this polygon and the array heading can be accurately established. The selection of the TASS polygon data believed to be the most representative of the ambient noise conditions for that day was based on careful consideration of the statistical data obtained during the onboard data analyses. These analyses are discussed in Appendix G and the pertinent statistical data are included in Ref. 5.

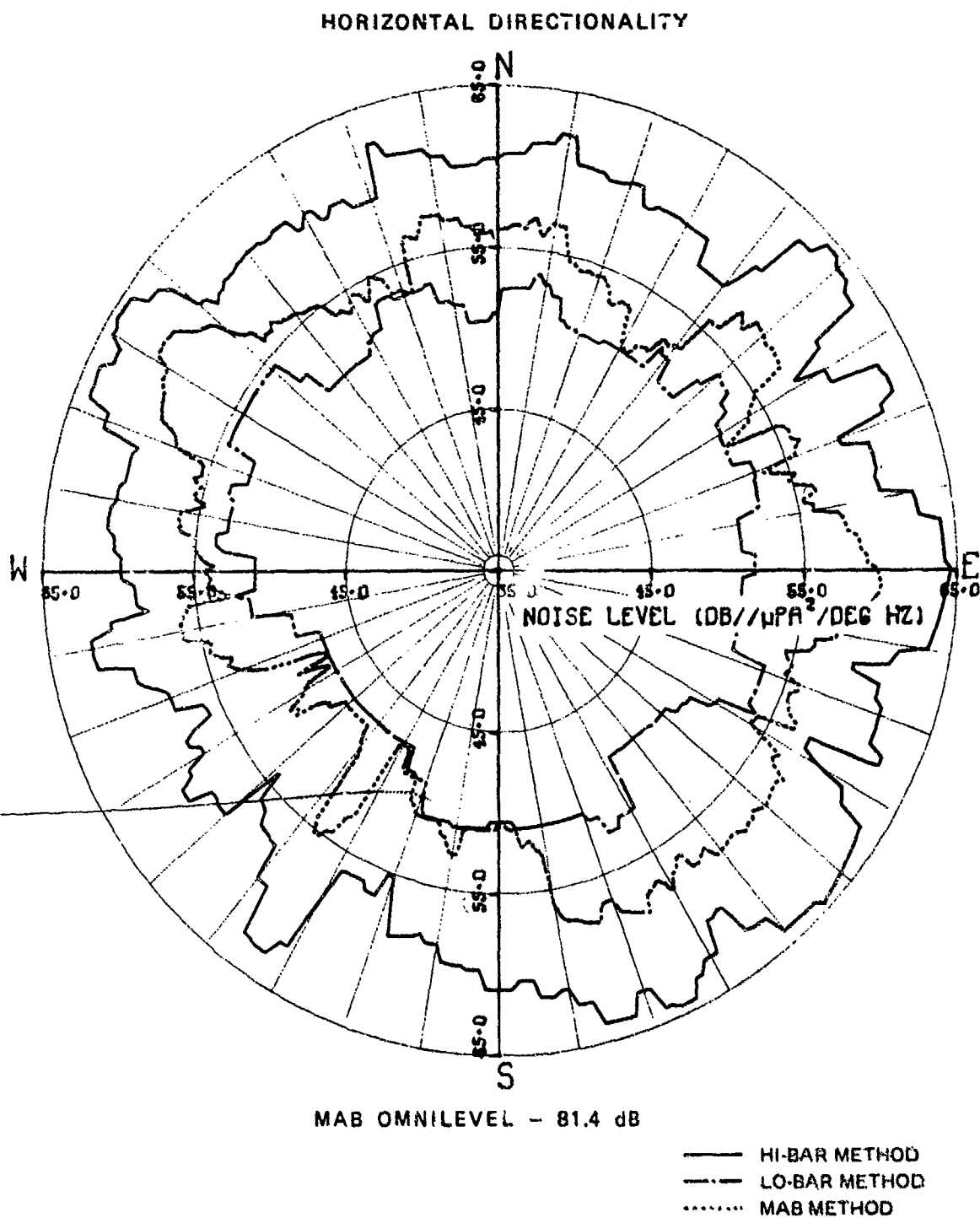
SECRET



(U) Figure 3. Horizontal directionality noise roses for a 1/8-Hz bandwidth at 38 Hz obtained from LAMBDA polygon 2 data at η -3 with Vibroseis source evident at approximately 159 deg. (S)

SECRET

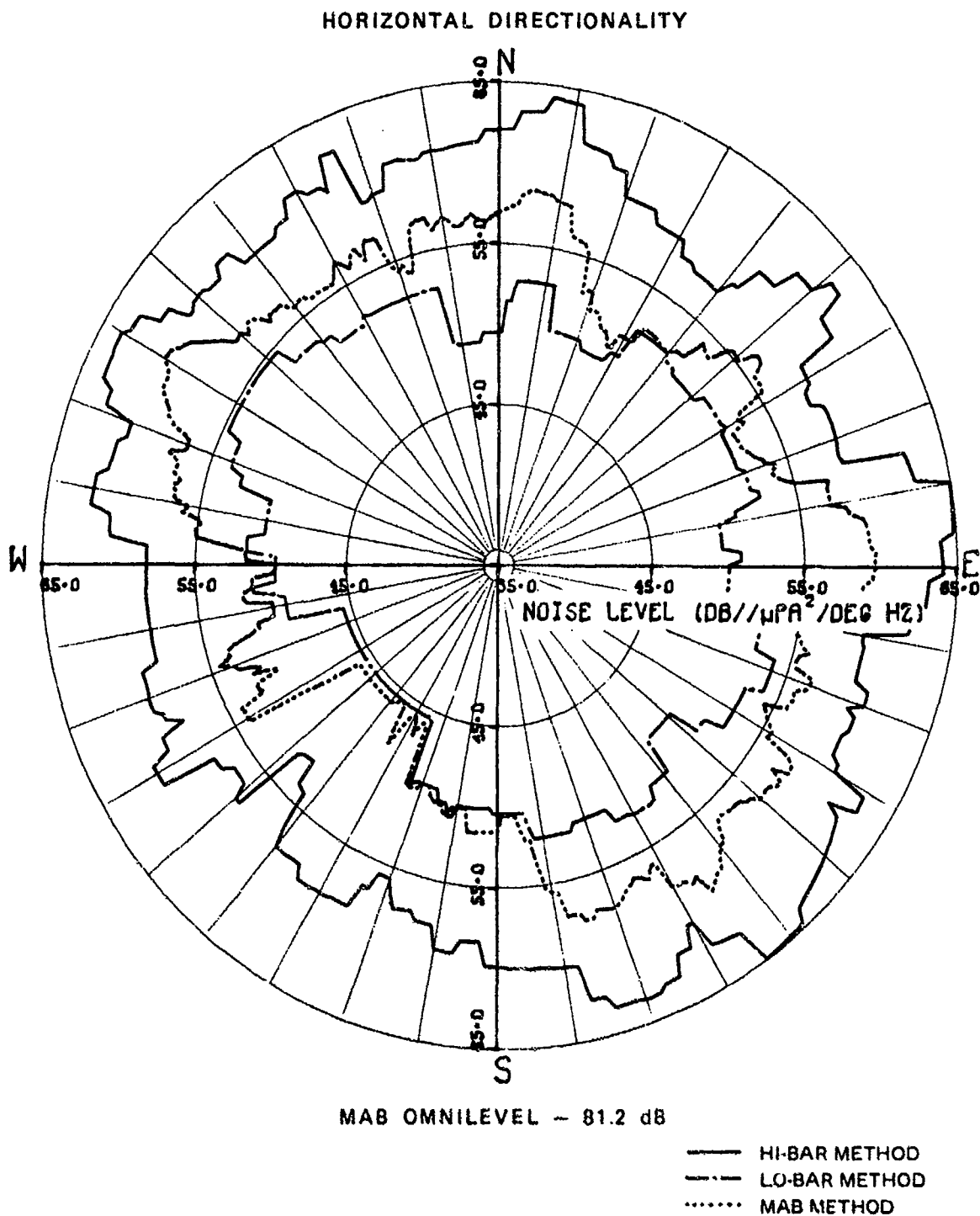
SECRET



(U) Figure 4. Horizontal directionality noise roses for a 1/8-Hz bandwidth at 29 Hz obtained from LAMBDA polygon 2 data at $\eta=3$. (S)

SECRET

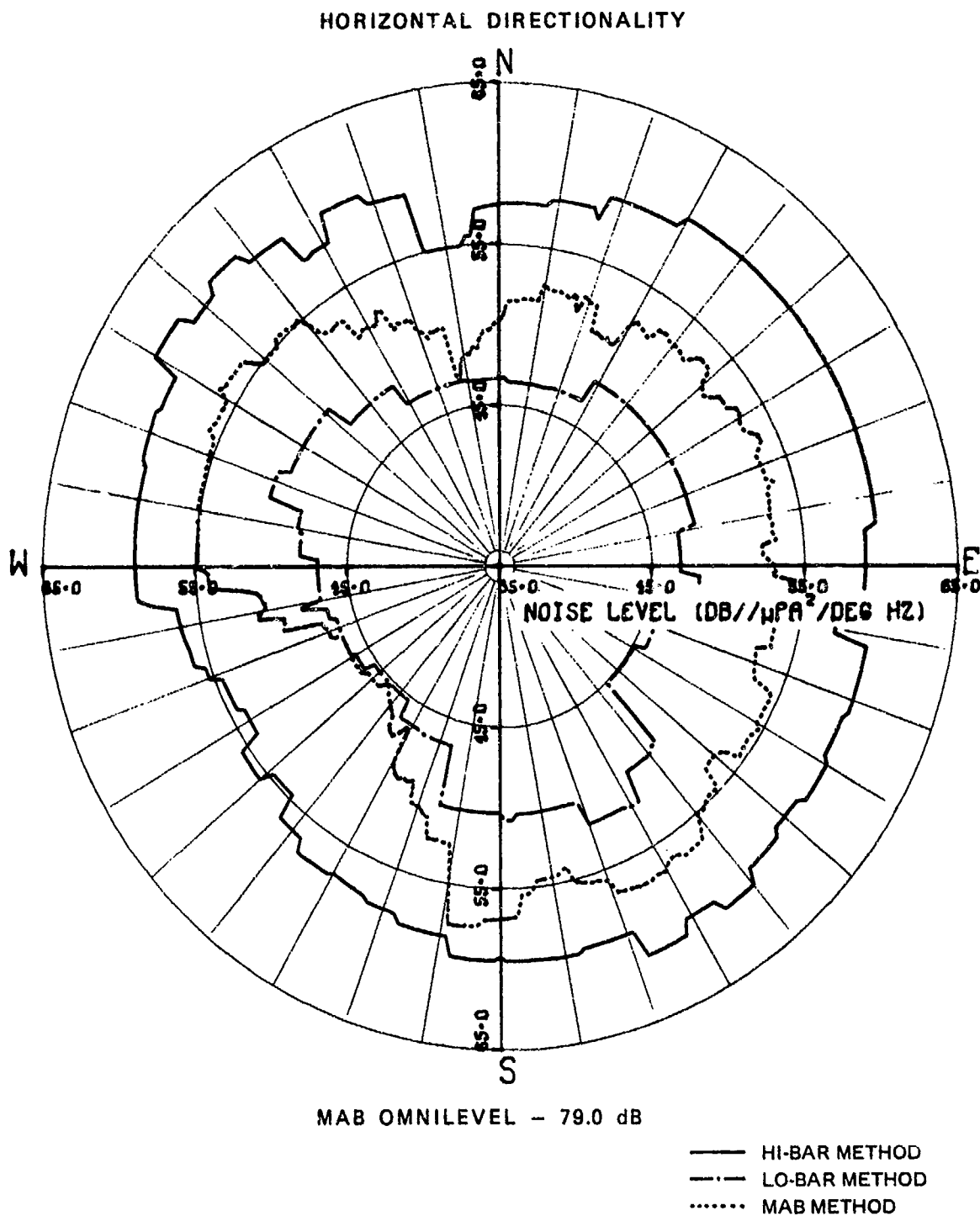
SECRET



(U) Figure 5. Horizontal directionality noise roses for a 1/8-Hz bandwidth at 23 Hz obtained from LAMBDA polygon 2 data at η -3. (S)

SECRET

SECRET

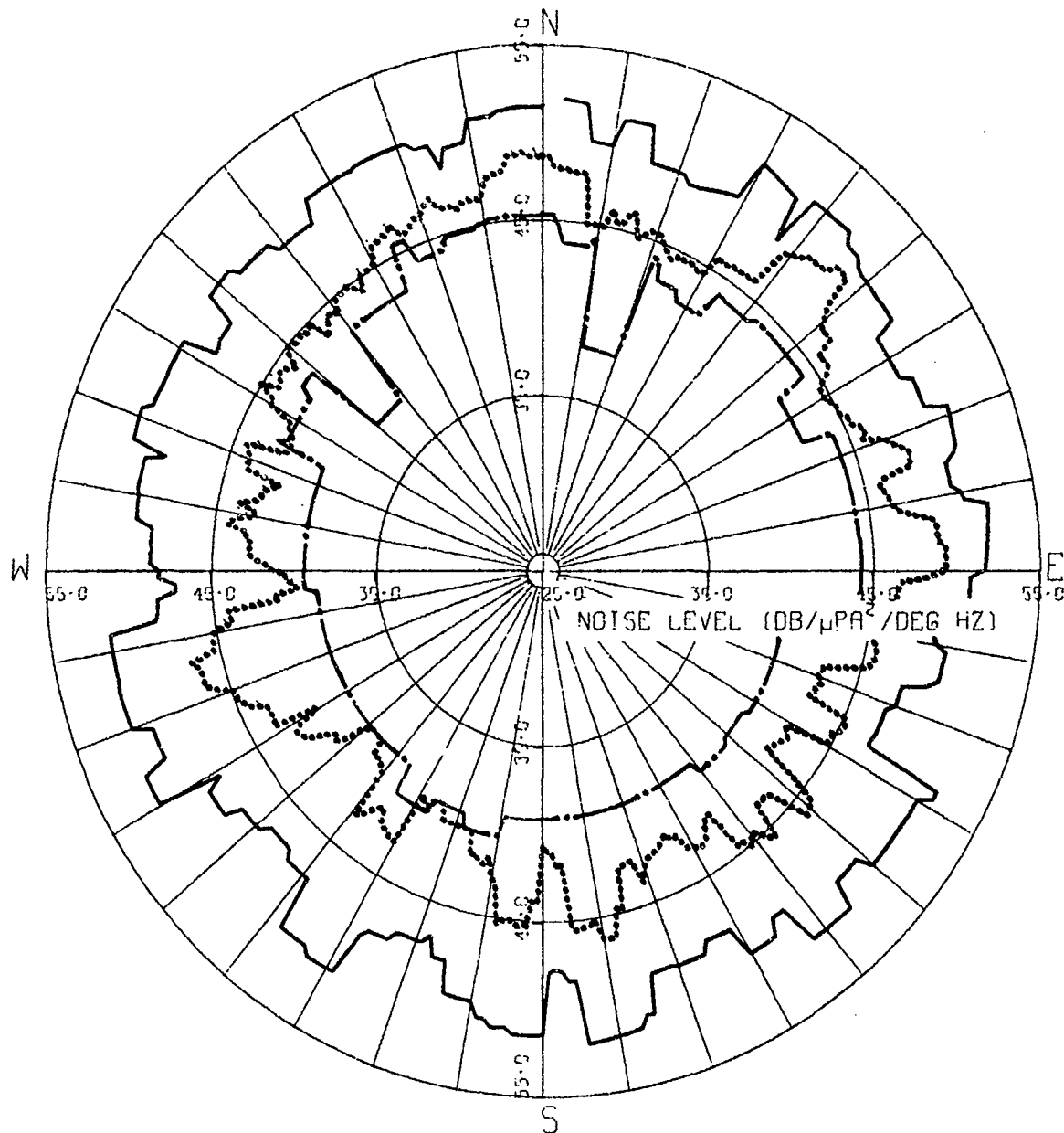


(U) Figure 6. Horizontal directionality noise roses for a 1/8-Hz bandwidth at 11 Hz obtained from LAMBDA polygon 2 data at η -3. (S)

SECRET

SECRET

HORIZONTAL DIRECTIONALITY



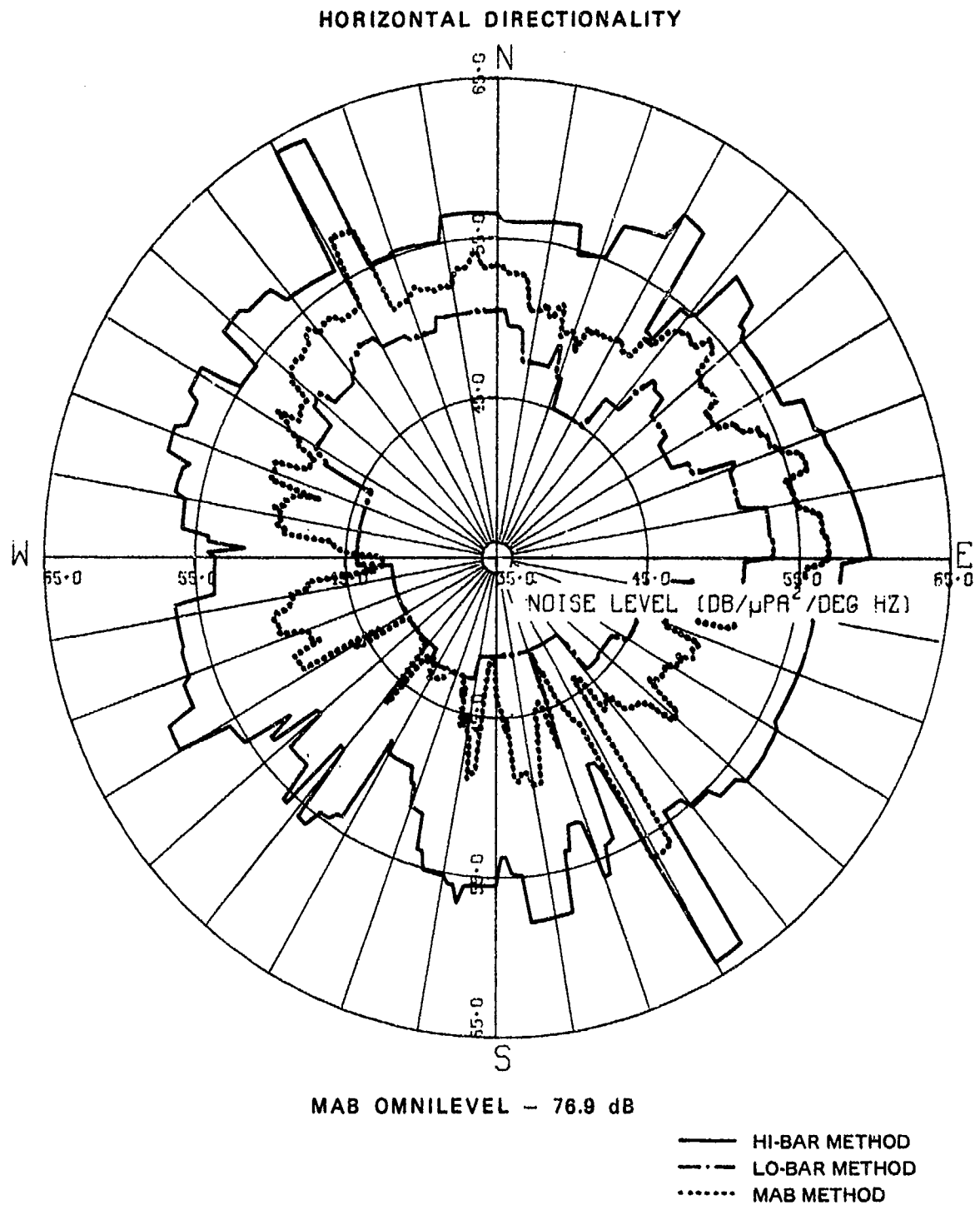
MAB OMNILEVEL - 70.6 dB

— HI-BAR METHOD
- - - LO-BAR METHOD
..... MAB METHOD

(U) Figure 7. Horizontal directionality noise roses for a 1/3-octave bandwidth at 160 Hz obtained from TASS polygon 4 data at $\eta=3$. (C)

SECRET

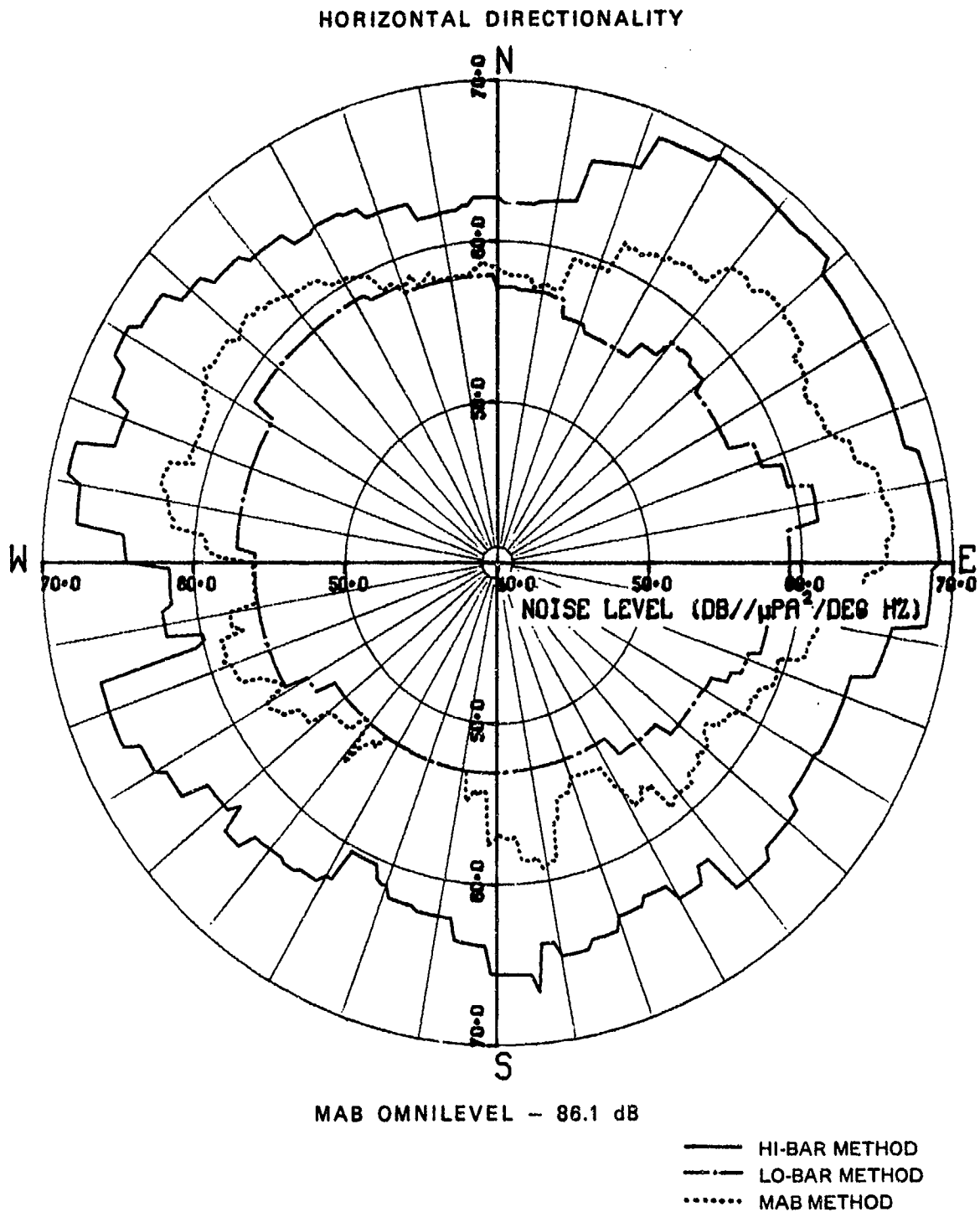
CONFIDENTIAL



(U) Figure 8. Horizontal directionality noise roses for a 1/3-octave bandwidth at 100 Hz obtained from TASS polygon 4 data at η -3. (C)

CONFIDENTIAL

CONFIDENTIAL

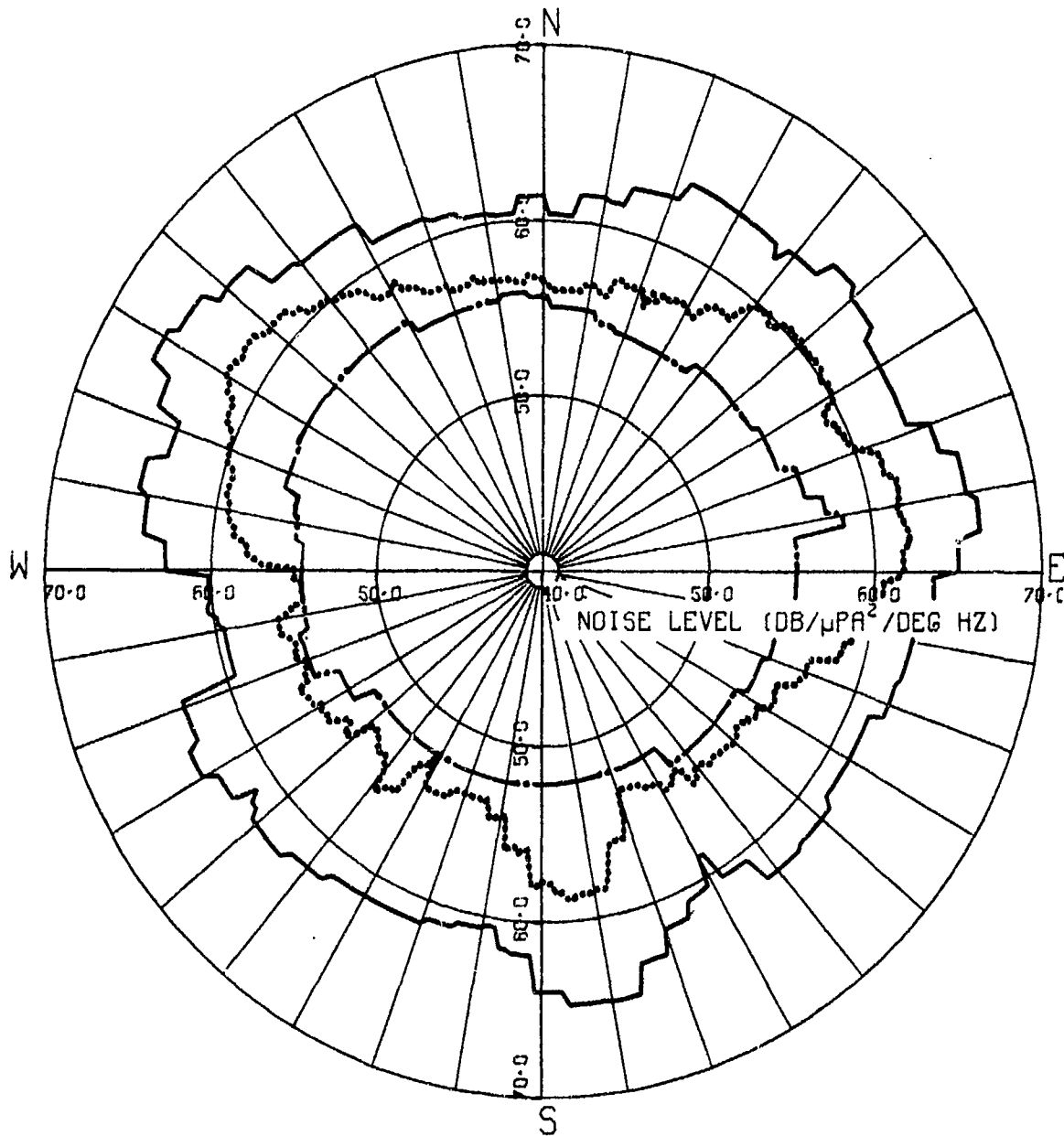


(U) Figure 9. Horizontal directionality noise roses for a 1/3-octave bandwidth at 50 Hz obtained from TASS polygon 4 data at $\eta=3$. (C)

CONFIDENTIAL

CONFIDENTIAL

HORIZONTAL DIRECTIONALITY



MAB OMNILEVEL - 83.6 dB

— HI-BAR METHOD
- - - LO-BAR METHOD
..... MAB METHOD

(U) Figure 10. Horizontal directionality noise roses for a 1/3-octave bandwidth at 40 Hz obtained from TASS polygon 4 data at $\eta=3$. (C)

CONFIDENTIAL

CONFIDENTIAL

(U) By displaying the results of three different analysis methods (MAB, HIBAR, and LOBAR) on the same plot, a qualitative assessment of the various results can be obtained. The HIBAR method selects the highest normalized beam response value from the set of all normalized beam responses which are along that azimuth, irrespective of the leg of the polygon on which it occurs. This method was not designed to resolve the ambiguity. The LOBAR method is similar to the HIBAR method except that the lowest normalized beam response is selected and then reduced by 3 dB. This method, unlike the HIBAR, does give an unambiguous assessment of the noise, since the low noise level does come from both ambiguous directions, i.e., neither of the ambiguous directions could have had noise greater than that measured, or the low level could not have been measured. How low the level of noise from each ambiguous direction actually was remains indeterminate. For this reason, the noise is assumed to come equally from both directions, requiring 3-dB reduction in the ambiguous normalized beam responses. This clearly establishes a lower bound for the normalized beam noise data. The MAB method was designed to resolve the ambiguity and its result must always be less than the HIBAR value and greater than, or equal to, the LOBAR value. Now, by comparing the relationships between the different results, the assessment of the most representative noise level for a given azimuth can be made.

(C) For purpose of illustration, consider the 38-Hz results in Fig. 3 (because of the large variability in levels, the grid for this figure is 15 dB per inch) for LAMBDA polygon 2 at $\eta=3$. During this polygon the Vibroseis source was along an azimuth of approximately 159 deg at a range of 115 nmi and radiating sound energy at 38 Hz. Hence, the extremely high noise levels in Fig. 3 near 159 deg are due to the Vibroseis and the high levels near 65 deg and 300 deg are artifacts ("ghosts") resulting from the inability of the MAB method to adequately resolve the ambiguity in the source direction. The beam response plots for each leg of polygon 2 are included in Appendix F together with a discussion of bearing errors. The results in Fig. 3 are for corrected bearings.

(U) The potential capability of the MAB method to discriminate against transients or resolve the ambiguity of a high-level noise is approximately equal to $10 \log n$ in dB, where n is the number of legs of the polygon. In the case of a pentagon, approximately 7 dB discrimination is possible. The high levels in Fig. 3 near 65 deg and 300 deg are excellent examples. Along these azimuths relatively low levels were measured on four legs, and levels approximately 15 to 20 dB higher were measured on only one leg each. These were the ambiguous images of the real source at 159 deg. The MAB value is approximately 7 dB below the HIBAR value, indicating that levels of the order of the HIBAR occurred only on one leg. Hence, the MAB result along these azimuths cannot be considered representative of the noise along these two directions. Either the LOBAR level or something between the MAB and LOBAR would be more indicative of a representative value. Along

CONFIDENTIAL

SECRET

159 deg, the HIBAR and MAB are in close agreement, indicating that the high levels along this azimuth occurred on more than one leg; thus, the MAB is indeed representative of the noise levels in that direction. When the HIBAR and the LOBAR differ by only a few dB, nearly any level between the two including the MAB value could be considered to be representative.

(U) Similar reasoning can be applied to the results in Figs. 4 through 10. In the TASS results of Fig. 7 for example, the MAB levels are within 3 dB of the HIBAR level between the 40- and 50-deg azimuths and again near the 90- 110-deg azimuths. Thus, normalized levels on the order of the MAB results could be accepted as representative levels with a high degree of confidence for these azimuths. Reasonable confidence could also be placed on the normalized noise levels to the north, since the MAB-HIBAR differences there are close to 3 dB. For many of the other azimuths, however, the differences in the HIBAR and MAB results are close to, or exceeding 7 dB. Hence, the MAB results are representative of the noise field for those azimuths only when they are close to the LOBAR values. As the MAB and LOBAR results approach the same value, between 270-deg and 360-deg for example, both become more representative of the normalized noise field. This, however, is not true when the two results are equal, because this only happens when the All-Bearings algorithm calculates a negative intensity which is replaced by the BAR result in the MAB method. Finally, when the MAB result is not close to either the LOBAR or the HIBAR results, a valid assessment cannot be made beyond the realization that if a level exists which is indeed representative of the noise in that direction, it must lie between the LOBAR and HIBAR value. This is the case in Fig. 3 in the southwest directions, and from about 245 to 260 deg. With these results in mind, it can be concluded that the azimuths toward the north, northeast, and east were approximately 5 to 8 dB noisier than the other azimuths during the measurement time period.

(C) Utilizing the same analysis philosophy discussed above makes the 100-Hz TASS results in Fig. 8 more amenable to interpretation. The high levels of noise at approximately 150 and 330 deg occurred only on one leg, since the differences between the MAB and HIBAR results exceed 7 dB. Therefore, the MAB results cannot be considered representative. In fact, since the HIBAR values are equal, and both occurred on only one leg, they must necessarily be ambiguous pairs. Again, the levels to the north and east are higher than the levels along other azimuths and the agreement between the HIBAR and MAB results is good. Similarly, the variability along the other azimuths precludes the estimation of a representative level. And again the conclusion that azimuths to the north and east had consistently higher level noise is made with a reasonable degree of confidence.

(C) The 50- and 40-Hz TASS results in Figs. 9 and 10, respectively, are more readily interpreted than the previous two. The MAB result approaches either the HIBAR or LOBAR results over large azimuthal sectors, with relatively smooth transition from one to the other. In these cases, the MAB result is considered a

SECRET

SECRET

good estimate of a representative value and the conclusion that the noise was 6 to 8 dB higher along azimuths to the northwest, the east, and the northeast than along any other azimuths can be made with a high degree of confidence. Great-circle paths from the array locations along these azimuths of high-level noise intersect the west coast of the United States to the east and the Aleutian Islands to the north and northeast. As the latitude of the noise measurement location decreases (going from η -3 to η -2 to η -1) the azimuths of high-level noise migrate toward the north, as would be expected if shipping near the west coast and the Aleutians was the responsible source.

(S) The analysis of the LAMBDA results for 38, 29, 23, and 11 Hz presented in Figs. 3 through 6, and Figs. C-9 through C-16 are nearly identical in nature to the TASS results previously discussed. The results for the higher LAMBDA frequencies (38, 36, and 29 Hz) show a high degree of variability with azimuth; the poor agreement between the MAB method and the other two methods indicates that determining representative levels with a reasonable degree of confidence would be extremely difficult, if not impossible. The results for the lower two frequencies (23 and 11 Hz), however, are another matter. These results are quite similar to the 40- and 50-Hz TASS results.

(C) When the shape of the HIBAR and MAB results are compared for the 38-, 36-, and 29-Hz data (with an approximate 7-dB displacement in the MAB values), the two curves on each plot are nearly identical. This is interesting in view of the fact that the HIBAR method was not designed to resolve ambiguities. Hence, the agreement between the two is evidence that the MAB method failed to resolve the ambiguities in these cases. The same was found to be true of much of the 160-Hz TASS data.

(U) The reason for the failure of the ambiguity-resolution methods to give reasonable estimates of the noise field horizontal directionalities at the high frequencies of each system is not a frequency-dependent property of the noise field. Instead, it is a result of making noise measurements in a nonstationary field with an array having relatively narrow beamwidths at the high frequencies. The degradation with increasing frequency is caused by the beamwidth of the array decreasing and the noise field appearing more nonstationary because the capability of spatial averaging decreases with the beamwidth.

(S) The time required to complete the polygon maneuver also has a detrimental effect on the ambiguity-resolution results. As the time from the start of the first leg to the end of the last leg increases, the sources of noise, such as nearby and distant ships, are more likely to exhibit significant changes in range and azimuth, with corresponding changes in the horizontal directionality of the noise. Hence, as the nonstationarity of the noise field increases, the allowable time for the polygon maneuver decreases. Additionally, the problem is compounded by the frequency-dependent characteristics of the beam patterns. A noise field which appears relatively

SECRET

SECRET

stationary in the low-frequency results may appear quite nonstationary at higher frequencies, where the beamwidths are significantly reduced. This is the case in much of the TASS 40- and 160-Hz data, respectively. The 40-Hz beam response data and horizontal directionality results show considerably less variability than the data for 160 Hz. This is especially true at the first noise station, η -3. Evidence that this is not a noise-field-frequency dependence is obtained by comparing the beam response data and resolved directionality results for 36 and 11 Hz. This comparison yields results similar to the previous comparison. The 36-Hz results for the narrow beamwidths show the effects of the noise field nonstationarity more than do either the 11-Hz results or the TASS results at nearly the same frequency (40 Hz). In the latter case, both the longer time required to execute a polygon with LAMBDA and the beamwidths being approximately 80 percent narrower than those of TASS combined to increase the effective noise field nonstationarity seen by LAMBDA at 36 Hz. As a result, the horizontal directionalities obtained from the LAMBDA 36-Hz data are of questionable validity. This is fairly evident in the figures when the MAB results are compared with the LOBAR and HIBAR results. Certainly, very little confidence can be associated with "representative values" obtained from these data. The same appears true for both the LAMBDA 29-Hz results and the TASS 160-Hz results.

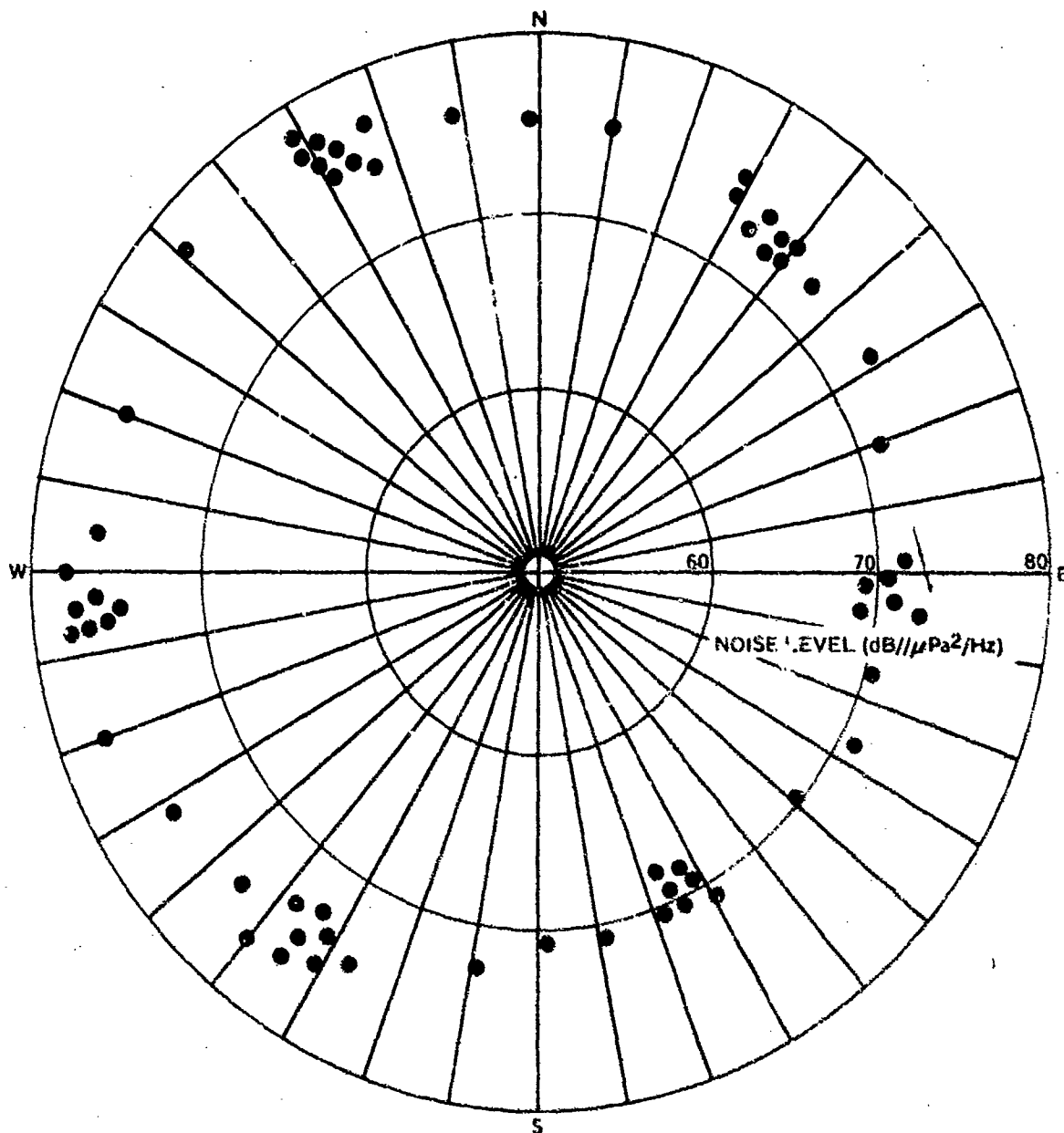
(S) The conclusion that the LAMBDA 36- and 29-Hz and TASS 160-Hz directionalities are of questionable value does not imply that either the corresponding beam response data are of little or no value, or that measurements should not be taken by a narrowbeam array. In fact, the converse is true. If a narrowbeam deconvolution assessment is required it must be accomplished over a smaller time period. If it is not required, then the narrow beam will give higher resolution in the beam response data. It must be remembered that the beam response data is the measured quantity and should be used by those making system design decisions or performing model validations. The beam response data contain none of the artificial factors introduced by the different methods in attempting to resolve the ambiguities. In the event that resolved horizontal directionalities are required, the beam responses from the narrowbeam array can be either sampled or smoothed to create new beam responses; these would be applicable to an effective array having beamwidth characteristics compatible with the nonstationarity of the noise field in order to yield meaningful results after ambiguity resolution. Such a procedure was demonstrated to be feasible on the present data. The results are discussed in a later section.

(U) Figures 11, 12, and 13 are typical examples of beam response levels from MESA for 1/3-octave bands centered at 150, 100, and 36 Hz, respectively, for 30 contiguous 1-min estimates starting on 20 September at 0228Z hours. These data, as well as the MESA data for the other measurement times and locations, show single broad maxima and minima. Generally the total excursion from the low levels to the high levels are approximately 6 to 12, 5 to 10, and 2 to 5 dB for the

SECRET

SECRET

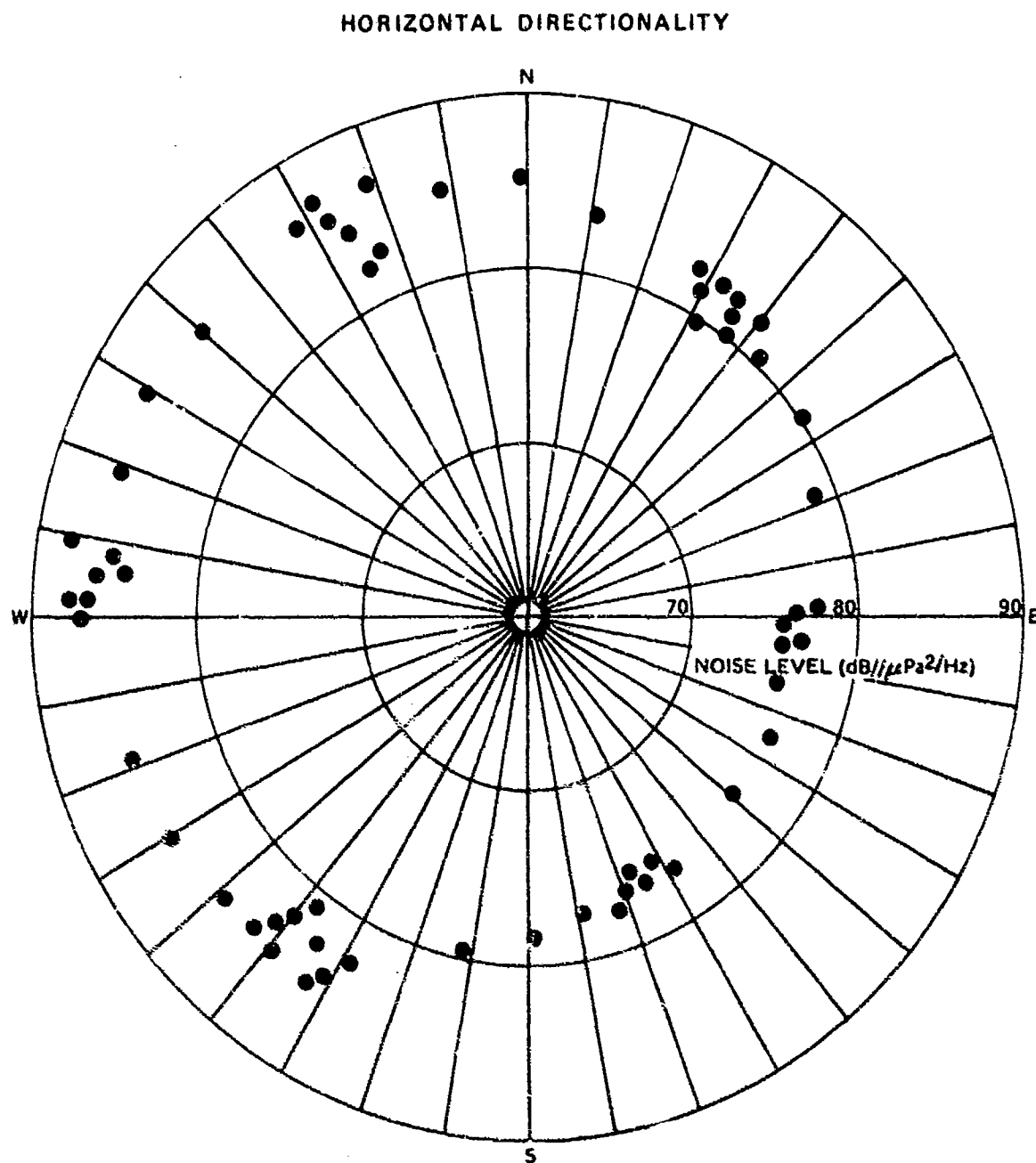
HORIZONTAL DIRECTIONALITY



(U) Figure 11. Typical MESA beam response data for a 1/3-octave bandwidth at 150 Hz, for 30 contiguous 1-min estimates beginning 1536Z 21 September 1973 at 45°5'54"N, 143°28'00"W. (U)

SECRET

UNCLASSIFIED

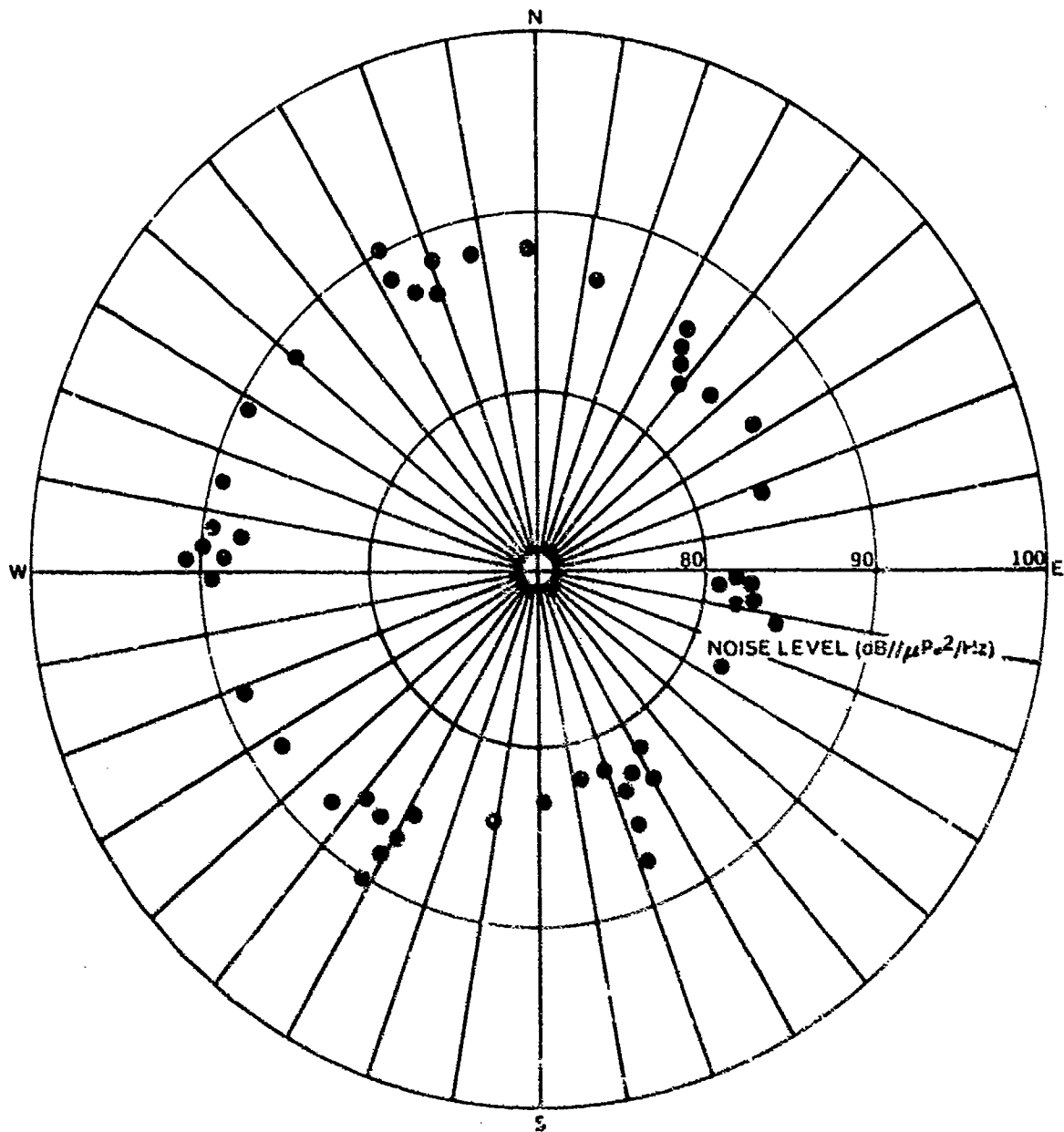


(U) Figure 12. Typical MESA beam response data for a 1/3-octave bandwidth at 100 Hz, for 30 contiguous 1-min estimates beginning 1536Z 21 September 1973 at 45°3'54"N, 143°28'00"W. (U)

UNCLASSIFIED

UNCLASSIFIED

HORIZONTAL DIRECTIONALITY



(U) Figure 13. Typical MESA beam response data for a 1/3-octave bandwidth at 36 Hz, for 30 contiguous 1-min estimates beginning 1536Z 21 September 1973 at 45° 5' 54" N, 143° 28' 00" W. (U)

UNCLASSIFIED

CONFIDENTIAL

1/3-octave bands centered at 150, 100, and 36 Hz, respectively.

(U) The MESA array broad beamwidths (75 deg) and its location (45°05'54"N, 143°28'00"W) create difficulties in interpreting the horizontal directionality of the ambient noise shown in figures 11, 12 and 13. This location was in the transpacific shipping lanes; hence, the array was potentially subject to nearby shipping noise. And the broad beamwidths will effectively smear out the dimensions of a sector of pre-dominantly high-level noise. This appears to be the case in Figs. 11, 12 and 13; noise emanating from ships over or near the slopes of the Aleutian and Kuril Islands would arrive at the MESA array in a sector from 295 deg to 320 deg, yet the figures indicate relatively high ambient noise levels from about 210 deg to 10 deg.

(C) At first glance these data do not appear entirely consistent with the TASS and LAMBDA data, since the levels toward the west coast of the United States are relatively low, and the TASS and LAMBDA data generally show high levels along corresponding azimuths. The reasons for this inconsistency will be discussed in the following section.

(C) The general trend of the ambient noise north-south spatial variability along approximately 143°W is summarized in Fig. 14. The two curves above 45°N were derived from an "eyeball" analysis of the MESA data, while those below 45°N are "eyeball" results of resolved TASS data. All results in this figure are for 100 Hz and the levels are relative since only the general shape of the pattern is of importance here and the gross features of the patterns were found to be relatively insensitive to frequency. More detailed results can be obtained from the previous figures in this section, from appendix C, or from Ref. 5.

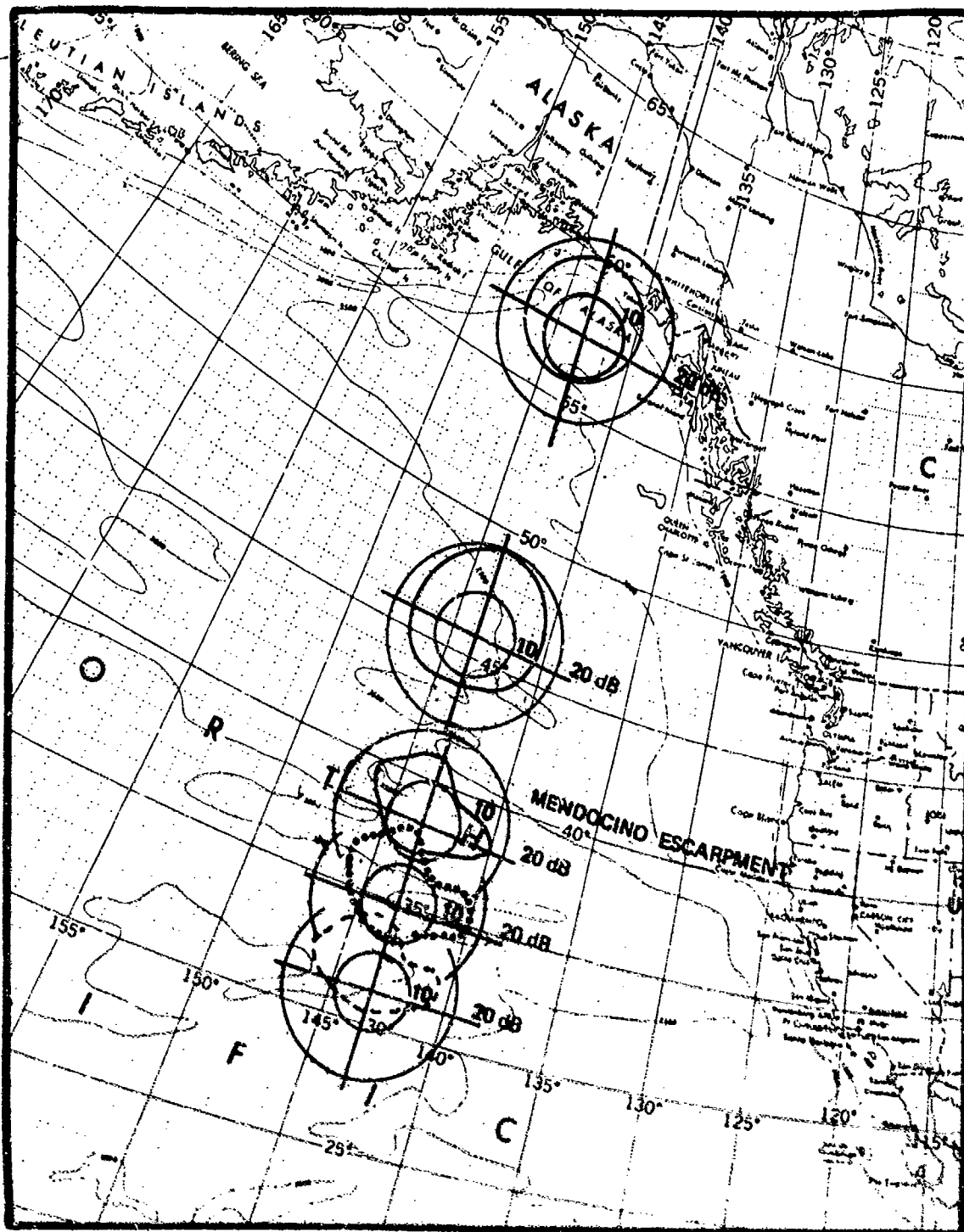
SOFAR CHANNEL NOISE

(U) The noise recorded by a sensor in the deep ocean comes from many sources. In the low-frequency range from 11 to 160 Hz the major contributions are usually wind wave interaction below 17 Hz, and shipping, biological, and seismic noise throughout the band. During the late summer the winds and seas in the CHURCH ANCHOR area were expected to be mild and the biological and seismic noise were expected to be minimal. Shipping was anticipated to be the major source of low-frequency noise.

(U) The noise due to shipping can be divided into two separate and nearly mutually exclusive categories. The first category is the noise due to the ships over the deep ocean. This noise generally reaches a deep sensor by way of paths which intersect the surface and/or bottom and generally has a vertical arrival angle greater than the SOFAR channel limiting angle (vertical angle for which all rays having a smaller vertical arrival angle are trapped in the channel). (In the present discussion the SOFAR

CONFIDENTIAL

CONFIDENTIAL



(U) Figure 14. Representative relative horizontal directionality of 100-Hz ambient noise along approximately 143°W measured by MESA (above 45°N) and resolved by TASS (below 40°N). (C)

CONFIDENTIAL

CONFIDENTIAL

channel will refer to the region in the vertical water column over which continuously refracted rays travel.) At the TASS and LAMBDA array depths, the channel-limiting angle was about 14 deg from horizontal. The noise model studies conducted by Wagstaff (Ref. 7) suggest that the contribution to this category of noise by ships more distant than a few hundred miles (with the distance increasing with decreasing nearby shipping density) is usually negligible. The second category includes the noise having vertical arrival angles less than the channel limiting angle. This noise arrives at the measurement location by way of continuously refracted paths within the channel. Since the propagation loss along these types of paths is relatively small compared to paths for noise in the first category, noise from more distant sources can make a significant contribution to the noise levels measured by the in-channel sensor. The only requirement is that a mechanism exist which will efficiently introduce the noise from the distant sources into the SOFAR channel. In the CHURCH ANCHOR case the responsible mechanism is believed to be the response of the reflection characteristics of the continental slopes and shelves to the sound radiated from ships transiting directly above them. This mechanism will be discussed in more detail below.

(U) In order to gain a better understanding of the noise field in the CHURCH ANCHOR area it would be desirable to separate the contributions due to these two different categories of noise. However, in order to do this the array must have the capability of accepting all SOFAR channel arrivals while rejecting the higher angle arrivals of sound generated by nearby shipping, and vice versa. The horizontal line-array, however, due to the conical shape of the beams, cannot completely accomplish this. By utilizing the output of the endfire beams, providing they are well matched to the angular dimensions of the channel, an assessment of the channel energy can be made which is independent of the noise from the nearby sources. Then by utilizing the endfire beam outputs for all directions during all of the polygons for one measurement day, a reasonably accurate reconstruction of the horizontal directionality of the noise which remains trapped in the SOFAR channel can be made. Once this has been accomplished the results can be compared with the directionalities obtained from the all-beam results and a relative assessment of the noise contributed by the nearby ships obtained.

(U) An assessment of both the noise due to nearby sources and that due to distant sources is vital to the thorough understanding of the noise field for at least two reasons. In order to validate noise models, the two different categories of noise must first be adequately modeled and then actual noise measurement data must exist to enable the validation of each model separately and together. The second reason is of a more scientific nature. The depth dependence of the noise field is believed to be dependent upon the relative amounts of noise received from the nearby sources at large vertical arrival angles and from distant sources at vertical arrival angles within the SOFAR channel limiting angles (Ref. 8). Only when the two types of noise are treated separately can the noise depth dependence be understood and, perhaps, predicted.

CONFIDENTIAL

CONFIDENTIAL

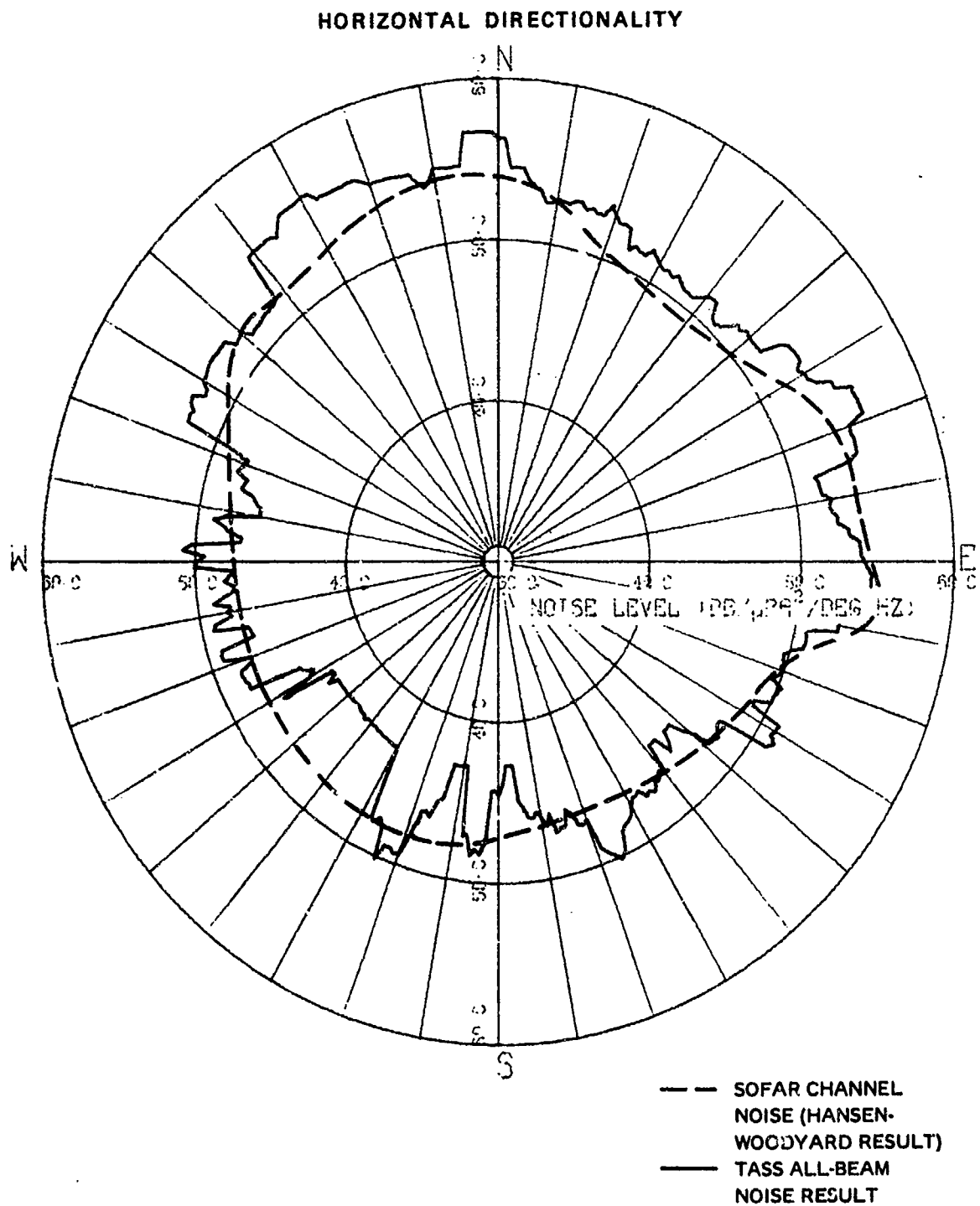
(C) To accomplish the objective of separating the SOFAR channel noise from the noise due to nearby (usually within a few hundred miles) sources, the Hansen-Woodyard beamformer (Ref. 2) was utilized aboard the LEE in conjunction with TASS to form relatively narrow endfire beams throughout the CHURCH ANCHOR noise measurement periods. At 100 Hz the Hansen-Woodyard beam is approximately 23 deg between the half-power points, with sidelobes suppressed about 20 dB. For the TASS noise measurement depths the entire beam was contained within the acoustical limits of the SOFAR channel. Therefore, a noise value obtained by the Hansen-Woodyard beam for 100 Hz was effectively a measure of the noise which reached the array from a relatively wide azimuthal sector (about 23 deg) by way of the SOFAR channel. The dashed curve in Fig. 15 was obtained by constructing a smooth curve between the average levels obtained from the Hansen-Woodyard beam during the 20-hr noise-measurement period at the η -3 location. Approximately 150 data samples were taken along various azimuths during the 20-hr period while four polygons (four revolutions of the array) were being executed. The measured levels appropriately reduced to account for beamwidth did not deviate more than about 2 dB from the dashed curve of Fig. 15. It is concluded, therefore, that the noise in the 1/3-octave band centered at 100 Hz, which arrived at this measurement location via the SOFAR channel, was relatively stationary over the 20-hr time period and that this curve is a reasonable representation of the SOFAR channel noise spatially averaged over the width of the Hansen-Woodyard endfire beam.

(U) The continuous curve in Fig. 15 is the result obtained when the ambiguities in the all-beam data for a polygon maneuver at the same location were resolved using the MAB procedure. The similarities between the two curves are significant when one realizes that the all-beam data are a sampling of the entire noise field with relatively narrow beams (6-18 deg) and the Hansen-Woodyard beam at this frequency has a wider beam (23 deg) and samples only the noise which arrives via the SOFAR channel. The irregularities in the noise field directionality curve derived from the all-beam data are attributed to the presence of nearby ships, the instabilities in the MAB ambiguity-resolution technique and the increased spatial resolution possible with the relatively narrow TASS beams.

(U) There are two sectors of high-level noise indicated by the curves shown in Fig. 15. The first extends from 70 deg to 100 deg. Great circles passing through the measurement location within this sector would intersect the coast of California. The second sector of high-level noise extends from 310 deg to 010 deg. Great circles passing through the measurement point within this sector would intersect the southern coast of Alaska and the Aleutian Islands.

CONFIDENTIAL

CONFIDENTIAL



(U) Figure 15. Comparison between 100-Hz average SOFAR channel noise and the resolved horizontal directionality using the MAB method and TASS all-beam data for one polygon at η -3. (C)

CONFIDENTIAL

CONFIDENTIAL

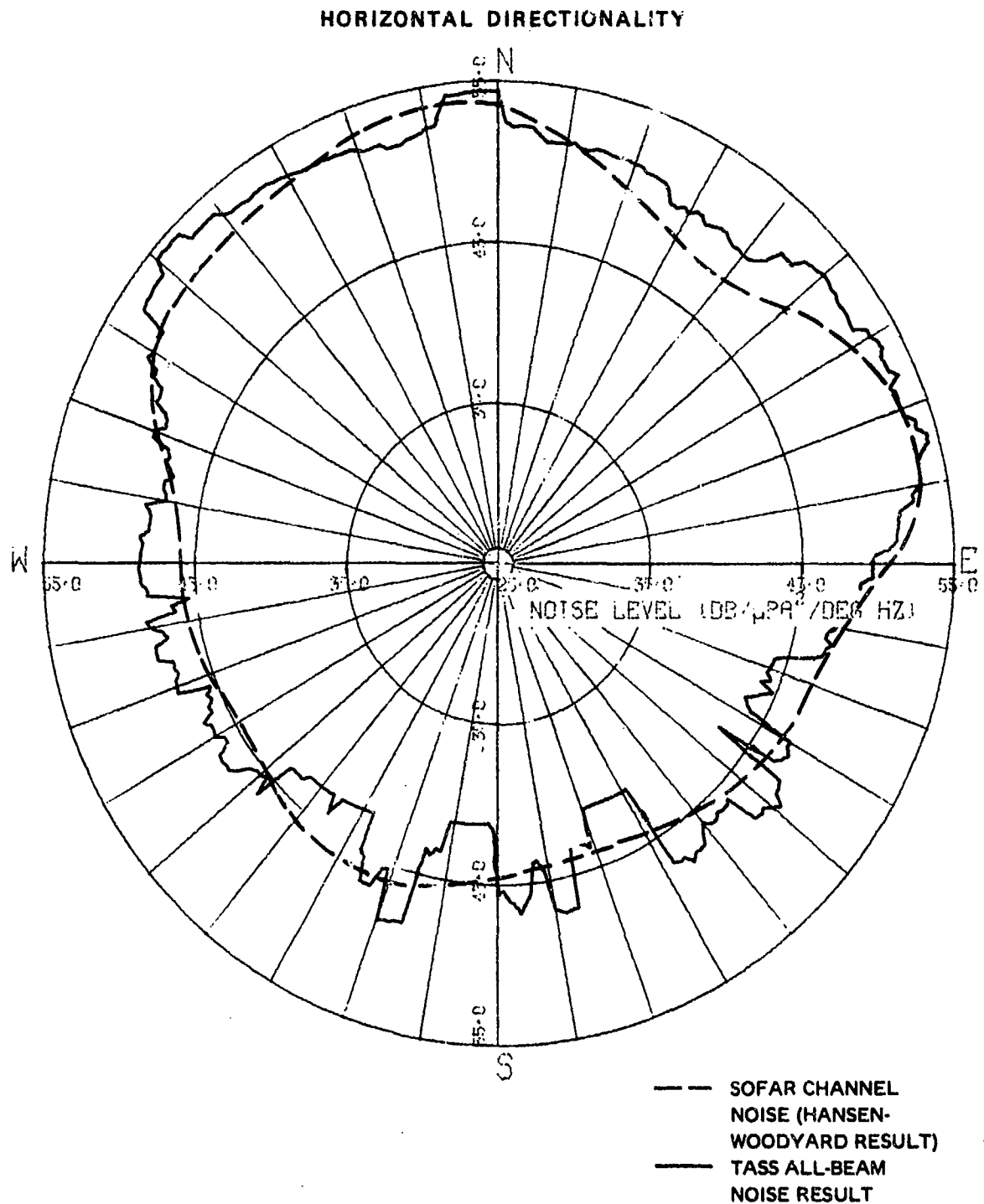
(U) The corresponding curves for locations η -2 and η -1 are shown in Figs. 16 and 17, respectively. The expected northerly migration of the eastward-looking high-level-noise sector as the measurement location shifts to the south is apparent. Also, in these figures, the high-level-noise sector which looks northwest includes a portion of the Kuril Islands and the Kamchatka Peninsula.

(U) Figure 18 (Ref. 9) illustrates the shipping count for the day following the first noise measurement period. If it is assumed that this distribution is indicative of the shipping for the days when the noise measurements were taken, the results in Figs. 15, 16, and 17 are not difficult to explain. As the range from the nearby ships to the array increases, the corresponding contribution to the directionality and total noise decreases. For intermediate and long ranges, the contributions are negligible. Ships over a rapidly sloping continental shelf and slope are another matter, however; each reflection down a sloping bottom reduces the reflected angle by twice the angle of the bottom slope. With relatively few reflections, a ray can become sufficiently horizontal to become continuously refracted and trapped within the SOFAR channel, a phenomenon hereinafter referred to as "downslope conversion." By the conversion of reflected rays into continuously refracted rays, the noise from relatively few ships many hundreds of miles away can dominate the noise field horizontal directionality and the total noise level at a location. This is believed to have been true in the case of the low-frequency noise at CHURCH ANCHOR locations. This mechanism is more thoroughly discussed in Ref. 8.

(U) Sound transmission enhancement due to downslope conversion of reflected rays into continuously refracted rays from the west coast of the United States has been substantiated by a previous experiment. Northrop, Loughridge, and Werner (Ref. 10) give an example for noise (explosive sources) originating in shallow water off Point Arena, California, being recorded by hydrophones at SOFAR channel depths near Eniwetok and Midway. The maximum levels received corresponded to shots over the edge of the continental shelf, with levels decreasing seaward and shoreward. The shoreward reduction was attributed to the increased number of bounces necessary to get the sound into the channel. The seaward reduction resulted from the bottom being below channel depth. For sound generated over the slope, they state "the first bottom reflection is from the continental slope, where the effect of the steeper bottom slope (3-1/2 deg) becomes important in channeling BR/SR (bottom reflected/surface reflected) rays into RRR (continuously refracted) rays. For example, for a surface shot in 300 m of water a ray that is initially the 0-deg ray steepens to 11 deg before it strikes the bottom at a depth of 475 m. Upon bottom reflection, the ray angle is reduced to 4 deg, and the ray becomes continuously refracted. Steeper rays become RRR after one or more bottom reflections on the lower continental slope." Officer (Ref. 11) also discusses this same mechanism for sound becoming trapped in a SOFAR channel.

CONFIDENTIAL

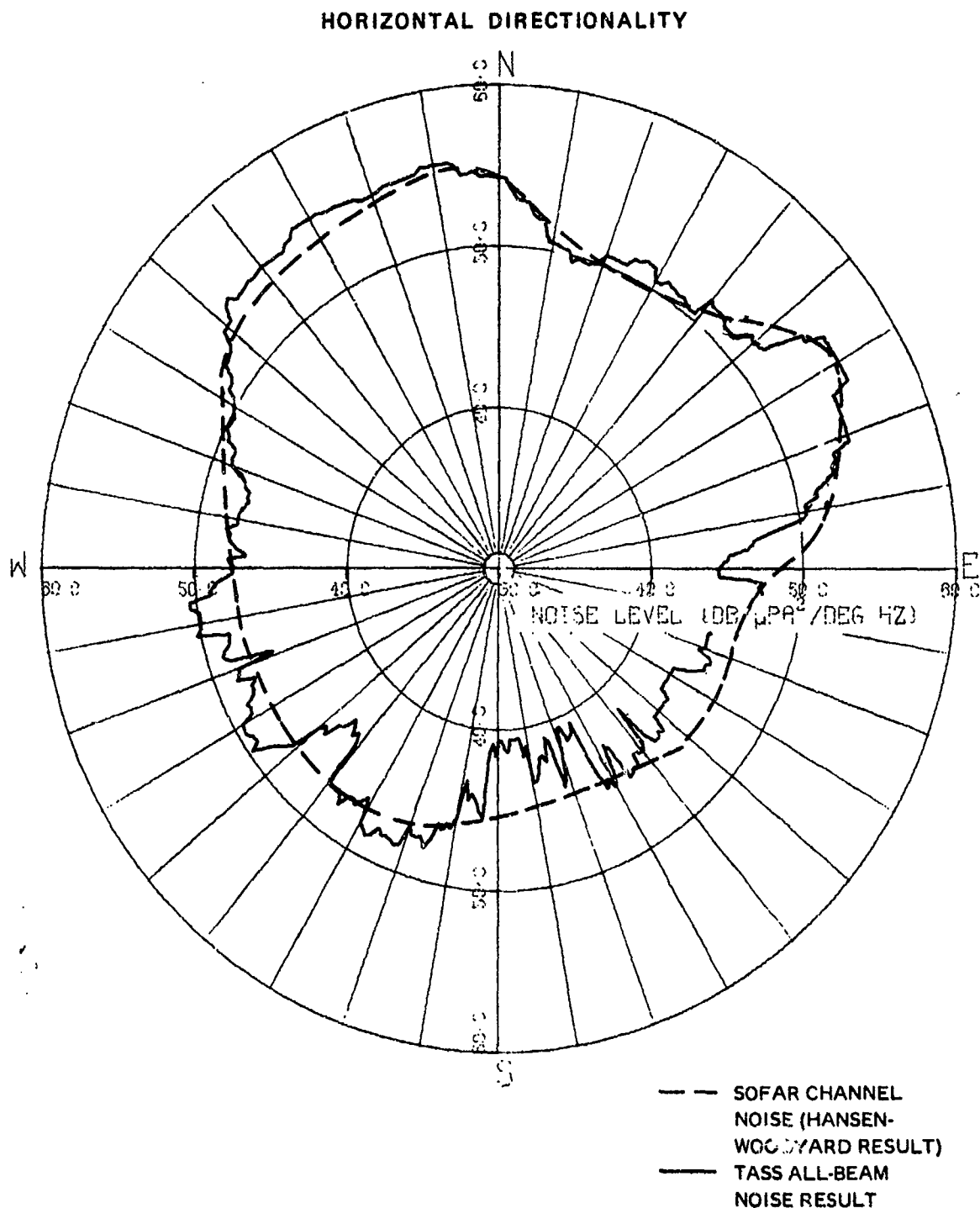
CONFIDENTIAL



(U) Figure 16. Comparison between 100-Hz average SOFAR channel noise and the resolved horizontal directionality using the MAB method and TASS all-beam data for one polygon at $\eta=2$. (C)

CONFIDENTIAL

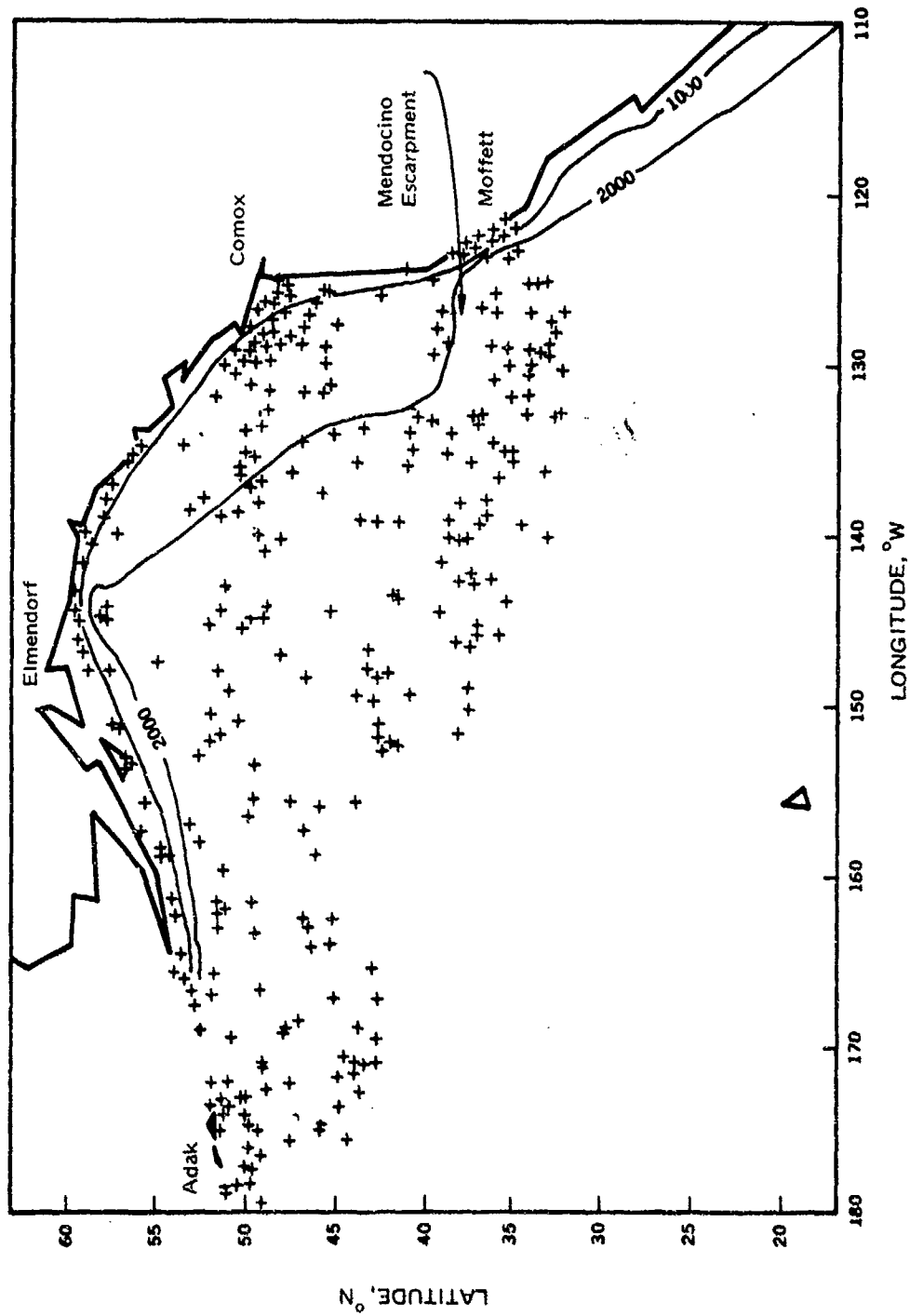
CONFIDENTIAL



(U) Figure 17. Comparison between 100-Hz average SOFAR channel noise and the resolved horizontal directionality using the MAB method and TASS all-beam data for one polygon at $\eta=1$. (C)

CONFIDENTIAL

CONFIDENTIAL



(C) Figure 18. Surface contacts on 3 September 1973 (reprinted from Ref. 9, bathymetry data added—depths in fathoms). (U)

CONFIDENTIAL

CONFIDENTIAL

(C) Another indication that downslope conversion is the responsible mechanism is the low level of noise measured along azimuths to the Juan De Fuca Strait. More than 200 ships were observed in the immediate vicinity of the straits during the aerial surveillance flights. However, the measured noise levels along these azimuths were on the order of 7 to 8 dB lower than along the azimuths to the much less dense shipping region south of the Mendocino Escarpment. By comparing the bathymetry of the two regions, it is observed that the 2000-fathom line is nearly 400 miles from the Juan De Fuca Strait, whereas it lies less than 60 miles from the coast south of the Mendocino Escarpment. This clearly indicated that noise originating near the shelf and slope south of the escarpment requires fewer reflections to enter the SOFAR channel than does noise originating near the Juan De Fuca Strait. Fewer reflections to become channelized means less power loss due to bottom contact. Therefore, a few ships along the continental slope and shelf below the Mendocino Escarpment can introduce the same amount of noise into the SOFAR channel as can a greater number of ships north of the escarpment.

(C) Similar high levels of noise along azimuths toward the west coast and the Aleutian Islands were observed in the Hansen-Woodyard endfire beam data and the unambiguous (bearing ambiguity resolved) data for other frequencies (Ref. 5). The effect, however, is less pronounced; this is believed to result from (1) the width of the Hansen-Woodyard beam not being as well matched to the limiting angle of the SOFAR channel at the other frequencies, (2) the smearing effect of the increased TASS beam-widths at lower frequencies, and (3) the increased attenuation at high frequencies for the noise from distant sources.

(C) The effect of this same mechanism is observable in the MESA data and provides an explanation for the presence of only one region of high-level noise and not two as in the TASS and LAMBDA data. The high levels of noise in the MESA data are along azimuths of great-circle paths to the Aleutian Islands, and the responsible mechanism is believed to be downslope transmission in this case as well. Toward the east and south-east along azimuths of great-circle paths to the west coast of the United States, the levels are not significantly high. This is probably due to the MESA noise measurement locations (above 45°N) being considerably higher in latitude than those of TASS and LAMBDA (below 39°N). As a result, great-circle paths from the MESA locations to the west coast of the United States are nearly parallel to the coast. The slope of the continental shelf and slope is very shallow along these paths, eliminating the downslope conversion effect from the west coast to the MESA locations. Hence, the absence of the high-level noise along easterly azimuths in the directionalities measured by MESA is to be expected if downslope conversion is actually the mechanism responsible for the sectors of high-level noise. The downslope conversion effect will deflect the paths from the west coast out into the ocean basin and prevents these paths from reaching the MESA locations.

TEMPORAL VARIABILITY

(U) Since the temporal variability in the CHURCH ANCHOR ambient noise horizontal directionality data cannot be assessed for time periods longer than 11 days, only the short-term variability will be discussed in this section.

CONFIDENTIAL

CONFIDENTIAL

(C) Forty-eight of the fifty-five polygon legs (TASS) executed by the LEE at stations η -3, η -2, and η -1 contained two contiguous 15-min measurement periods in which the beamformer gain remained unchanged. The manner in which these acoustic measurements were acquired made possible an objective comparison of the first measurement period data with data from the second measurement period for each of the 48 legs. The 23 samples of 1/4 sec each, 1 per beam, acquired within a 6-sec period were treated as a sample from a multivariate population. Hence, each measurement period produced 150 23-element vectors.

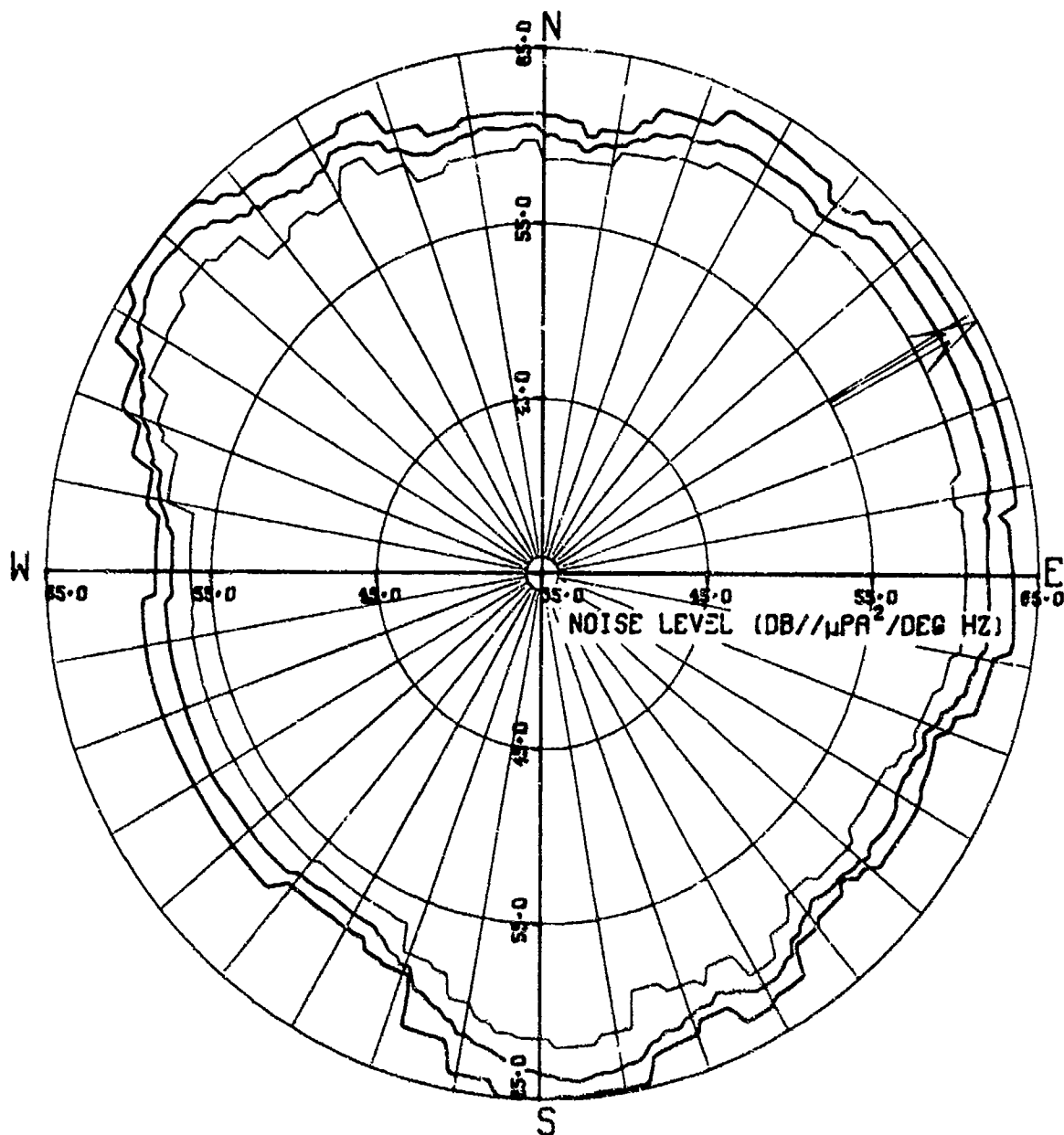
(C) If the average level for each beam remained unchanged in the 1/2 hr which contained two measurement periods, the average of the difference between corresponding samples from the two measurement periods would not be expected to differ significantly from zero. Zero, in this sense, means a 23-element vector with all 23 elements equal to zero. The Hotelling T^2 -Test for paired data, the multivariate analog of Student's t -Test for paired scalar data, was used to test the hypothesis of no change in beam response between the two measurement periods. At the 1-percent significance level there were only two of the 48 legs for which the hypothesis could not be rejected for all four frequencies under study (40, 50, 100, and 160 Hz). For one of these legs the 40-, 50-, and 100-Hz data were not significantly different from zero. For the other leg, the 40- and 50-Hz data were not significantly different from zero. Both of these legs occurred at station η -2:

(C) In general, then it is reasonable to conclude that the TASS experiment was incapable of detecting the stationarity of the horizontal noise field, assuming that the field was, in fact, stationary, or - alternatively - that if the TASS was able to assess stationarity, then the horizontal noise field as measured by a line-array changed significantly over a period of 15 min, a conclusion which casts doubt on the validity of the results of the deconvolution procedures used in this report. It is important to note that for the 160-Hz data the null hypothesis was rejected for all 48 legs. At 160 Hz the beams are much narrower than at the other three frequencies. For this reason, a small change in array orientation would introduce a larger degree of nonstationarity in the 160-Hz data in an otherwise stationary noise field than it would for the lower frequencies (which give wider beams).

(C) The temporal variability in the TASS and LAMBDA noise measurements, as determined by comparing average beam response measurements between measurement periods which are separated in time by at least 5 hr for TASS and 10 hr for LAMBDA, was greatest for the data from location η -3. The variability at all locations decreased with decreasing frequency, a manifestation of the inverse relationship between beamwidth and frequency. Figures 19 through 22 illustrate the extremes in this variability for the 40-Hz TASS results. Figures 19 and 20 are plots containing three curves each. These curves were obtained by plotting the maximum, mean, and minimum values for the 40-Hz TASS results. Figures 19 and 20 are plots containing three curves each. These

CONFIDENTIAL

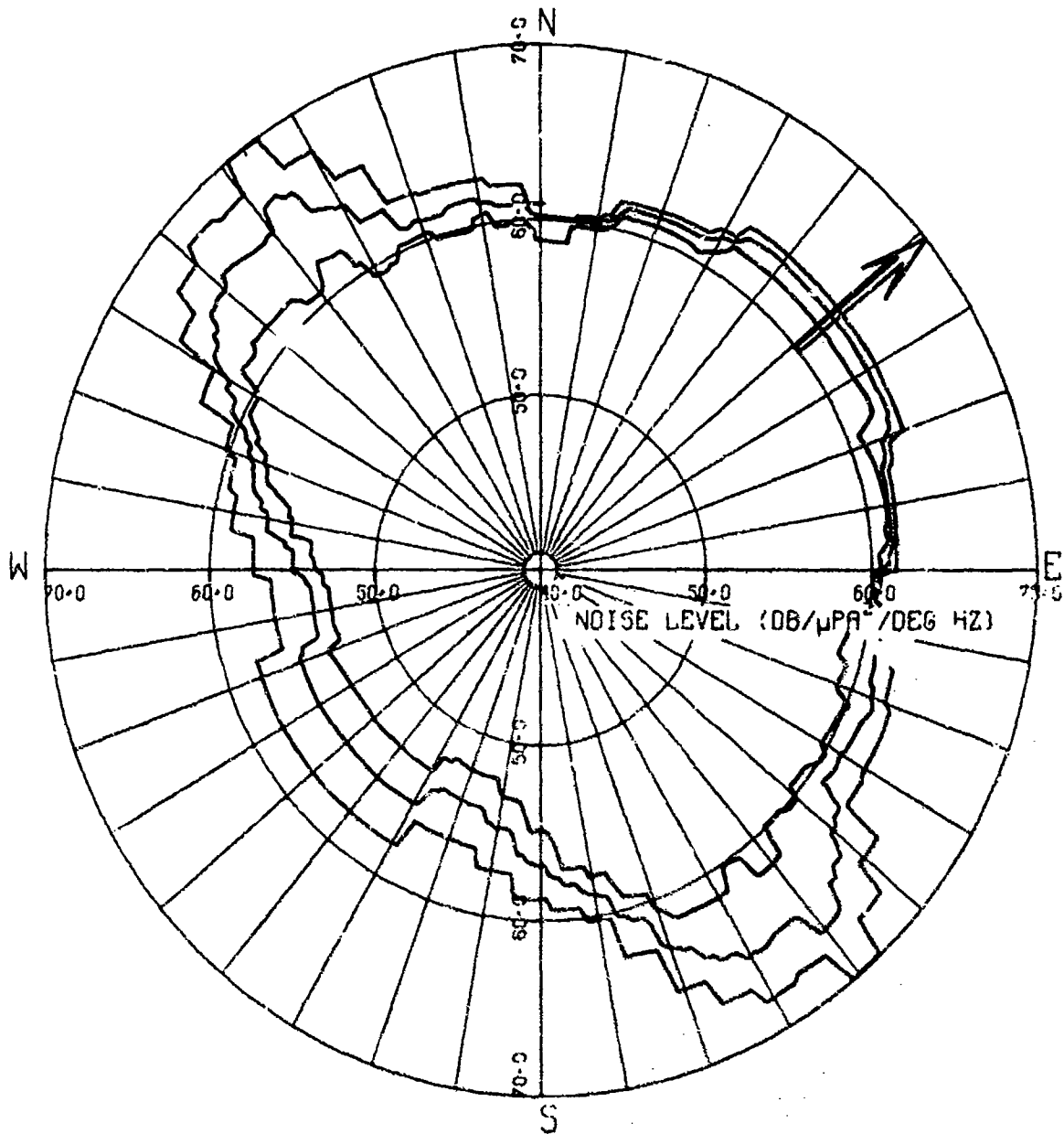
CONFIDENTIAL



(U) Figure 19. High, mean, and low beam response plots for 40 Hz and leg 5 of the TASS polygons at $\eta=3$. (C)

CONFIDENTIAL

SECRET



(U) Figure 20. High, mean, and low beam response plots for 40 Hz and leg 5 of the TASS polygons at η -I. (C)

SECRET

SECRET

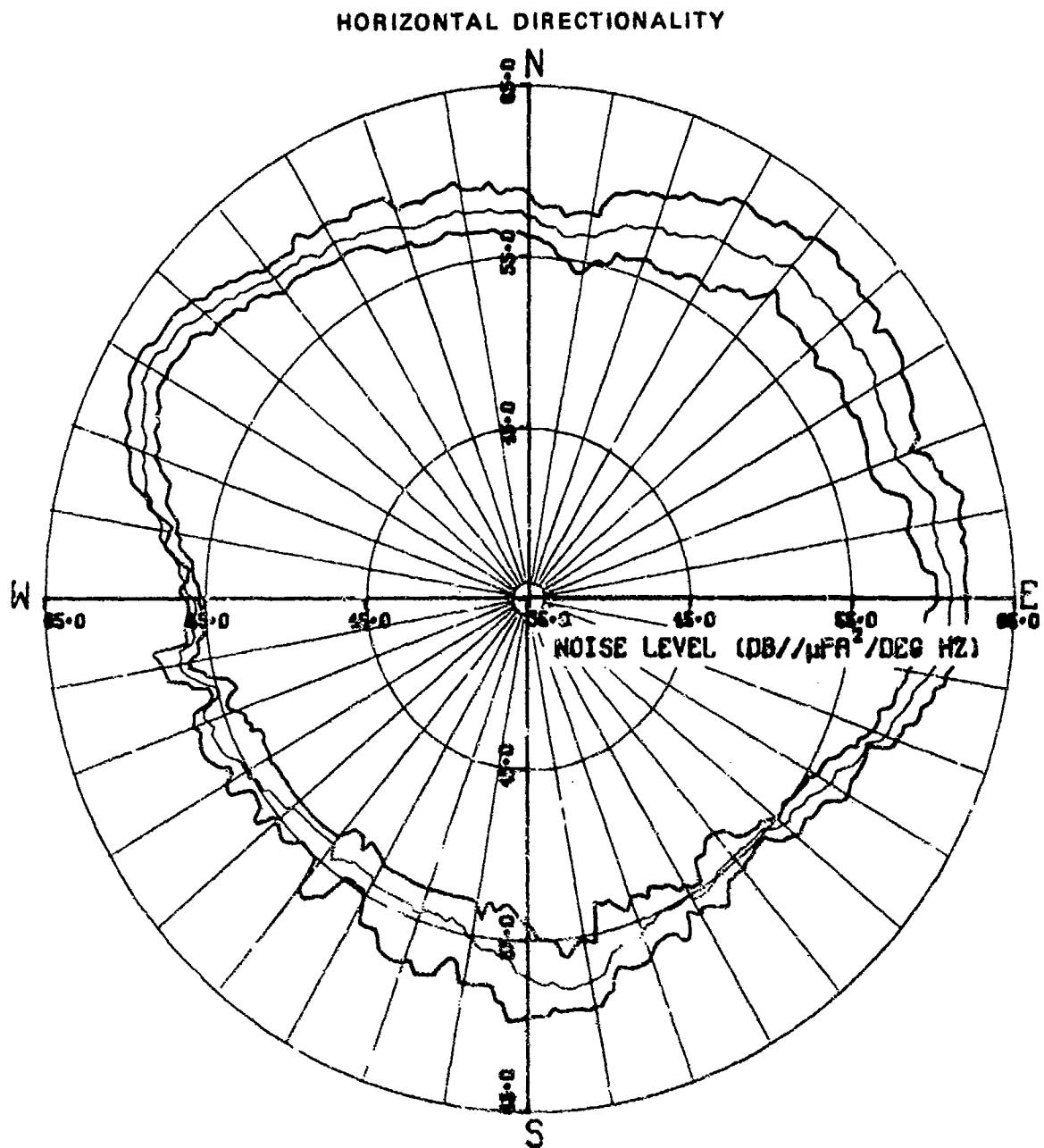
curves were obtained by plotting the maximum, mean, and minimum values for the 40-Hz all-beam outputs for the last leg of each polygon at $\eta-3$ and $\eta-1$, respectively. Hence, the values which make up the high and low curves in Fig. 19 are outputs of the highest and lowest recorded levels, respectively, for each of the 23 TASS beams for the last leg of each of the 4 polygons at $\eta-3$. The curve within these 2 extremes is composed of the 23 mean values for the 4 sets of 23 beams. Figure 20 is the same type of plot for the three polygons executed at $\eta-1$. The results shown in these figures are indicative of the magnitude of the fluctuation as a function of azimuth for the times when the data were taken. Similar results were obtained for the other four sets of legs at these two locations.

(S) The three curves in both Figs. 21 and 22 were obtained by utilizing the MAB method to resolve the ambiguity in the five sets of high, low, and mean beam responses for $\eta-3$ and $\eta-1$, respectively. The regions of high-level noise in these figures are toward the Kuril and Aleutian Islands to the northwest and toward the west coast of the United States in the easterly directions. Sectors in which the noise was relatively stationary are delineated by the proximity of the high and low noise-level curves. Even when the maximum levels in the low-level-noise direction are combined with the minimum levels in the high-level-noise direction, the general shape of the directionality pattern is the same. The two high-level-noise regions remain high-level-noise directions. This is an indication that the fluctuations in the "widebeam" data do not seriously degrade the horizontal directionality results. This conclusion cannot, however, be generalized to include other ocean areas where the acoustic propagation and shipping conditions are different, or include results at the same location for frequencies yielding significantly narrower beamwidths. The 11-Hz LAMBDA results would fit into the same category as the 40-Hz TASS results; the 36- or 38-Hz LAMBDA results, however, would not. Even though the noise field at 36 and 38 Hz is nearly the same as that at 40 Hz, the smaller beamwidths of LAMBDA at these frequencies increase the average beam response fluctuations seen on each beam. The same is true for the 160-Hz TASS results. Again it should be stressed that this effect is a beamwidth-related phenomenon and not a frequency-dependent property of the noise field.

(S) The maximum time TASS occupied one station was 20 hr, the duration of four polygons. LAMBDA, however, executed polygon 3 at $\eta-1$ on 8 and 9 September and 11 days later executed polygons 5 and 6 at the same location, thus achieving the longest time lapse at one station. When the beam response data were compared for the 10-hr separation between polygons 5 and 6 and then each of these compared to the beam response data for polygon 3 taken 11 days earlier, no trend in the data was detected. Figure 23 is a typical example of the results obtained when the three 29-Hz beam response plots for the third leg of each polygon were compared. The dashed, solid, and chain-dot curves are for polygons 3, 5, and 6, respectively. These results were indicative of the same type of comparison for other legs and for the 36-Hz data.

SECRET

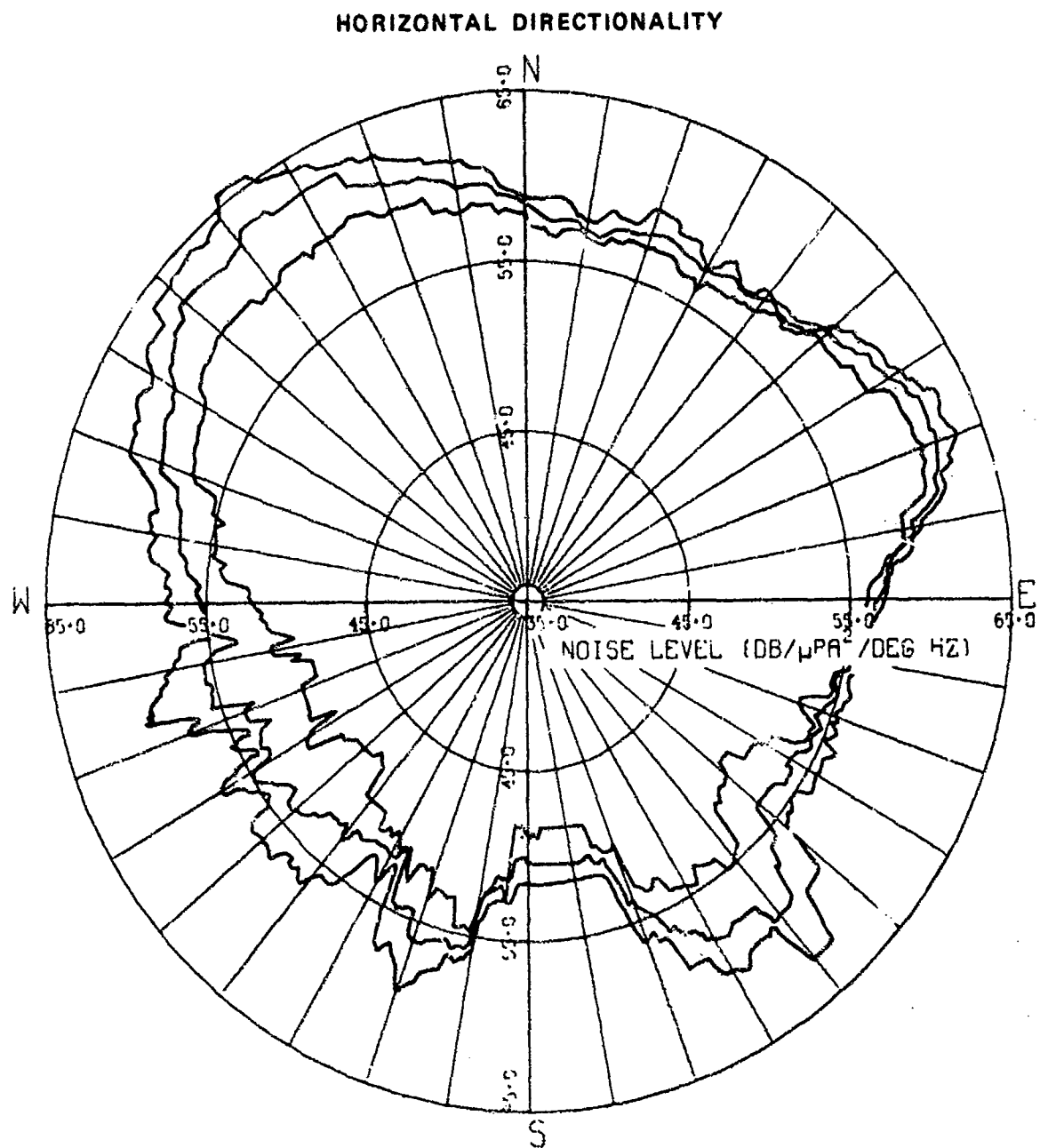
CONFIDENTIAL



(U) Figure 21. MAB horizontal directionalities for the high, mean, and low beam responses for all 40-Hz TASS polygon legs at η -3. (C)

CONFIDENTIAL

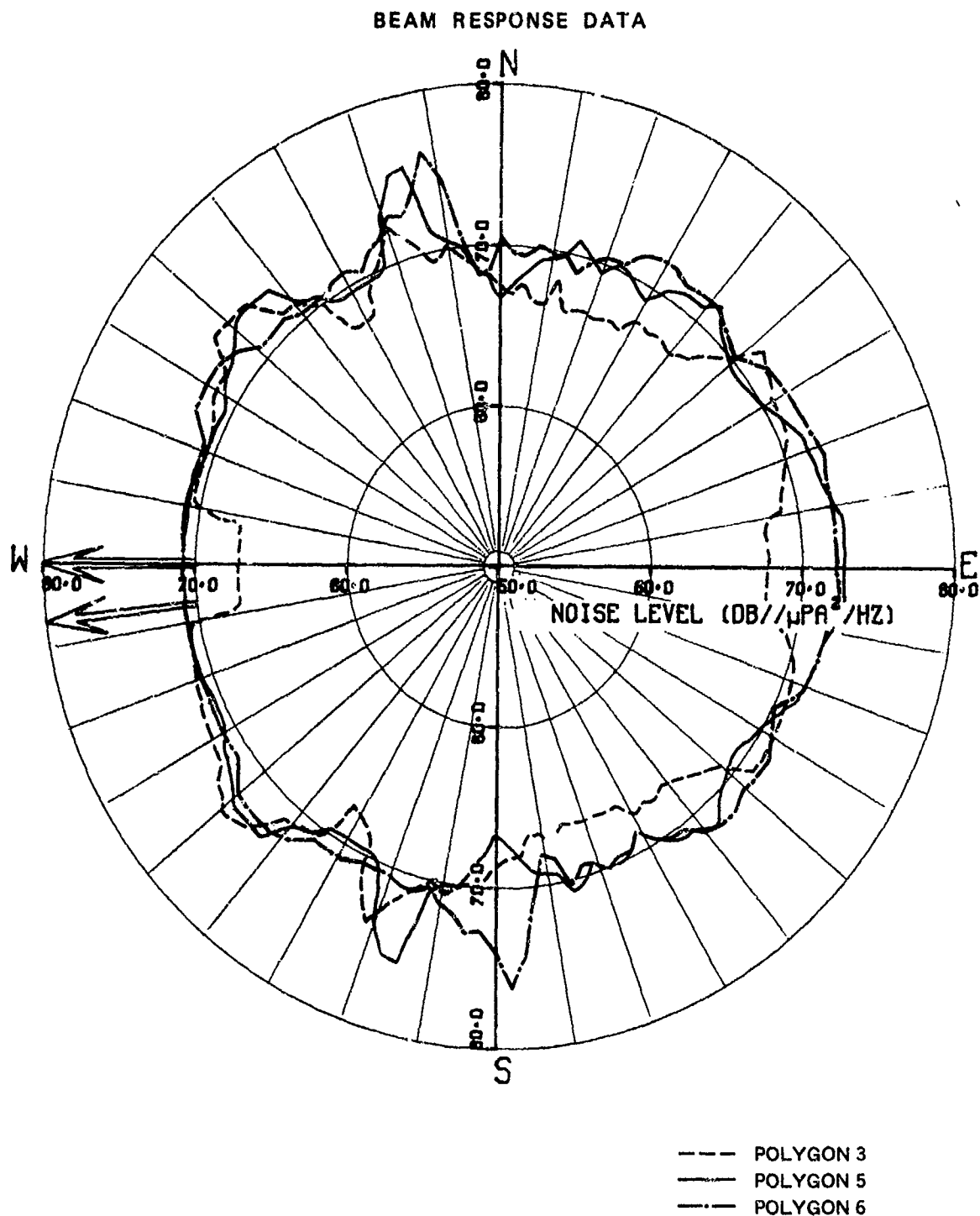
CONFIDENTIAL



(U) Figure 22. MAB horizontal directionalities for the high, mean, and low beam responses for all 40-Hz TASS polygon legs at $\eta=1$. (C)

CONFIDENTIAL

SECRET



(U) Figure 23. Comparison of 29-Hz LAMBDA beam response data for leg 3 of polygons 3, 5, and 6 at $\eta=1$. (S)

SECRET

SECRET

(U) No trend in the temporal variability for time periods up to 11 days was evident in any of the CHURCH ANCHOR horizontal directionality data. Longer term trends, however, are expected and would probably be correlated with seasonal changes in propagation conditions, shipping routes, and commercial fishing.

NOISE FIELD PROPERTIES

Narrowband Versus Wideband Results

(C) Three different bandwidths were used to assess the horizontal directionality of the noise field. One-third octave bandwidths were used on both the TASS and the MESA data. A 1/10-Hz bandwidth was also used on selected TASS data and a 1/8-Hz bandwidth on the LAMBDA data. In order to compare data taken by one system with data taken by another system, the effect of the differences in analysis bandwidth must first be understood. To facilitate this, the TASS beam response data and resulting horizontal directionalities for the two different bandwidths were compared.

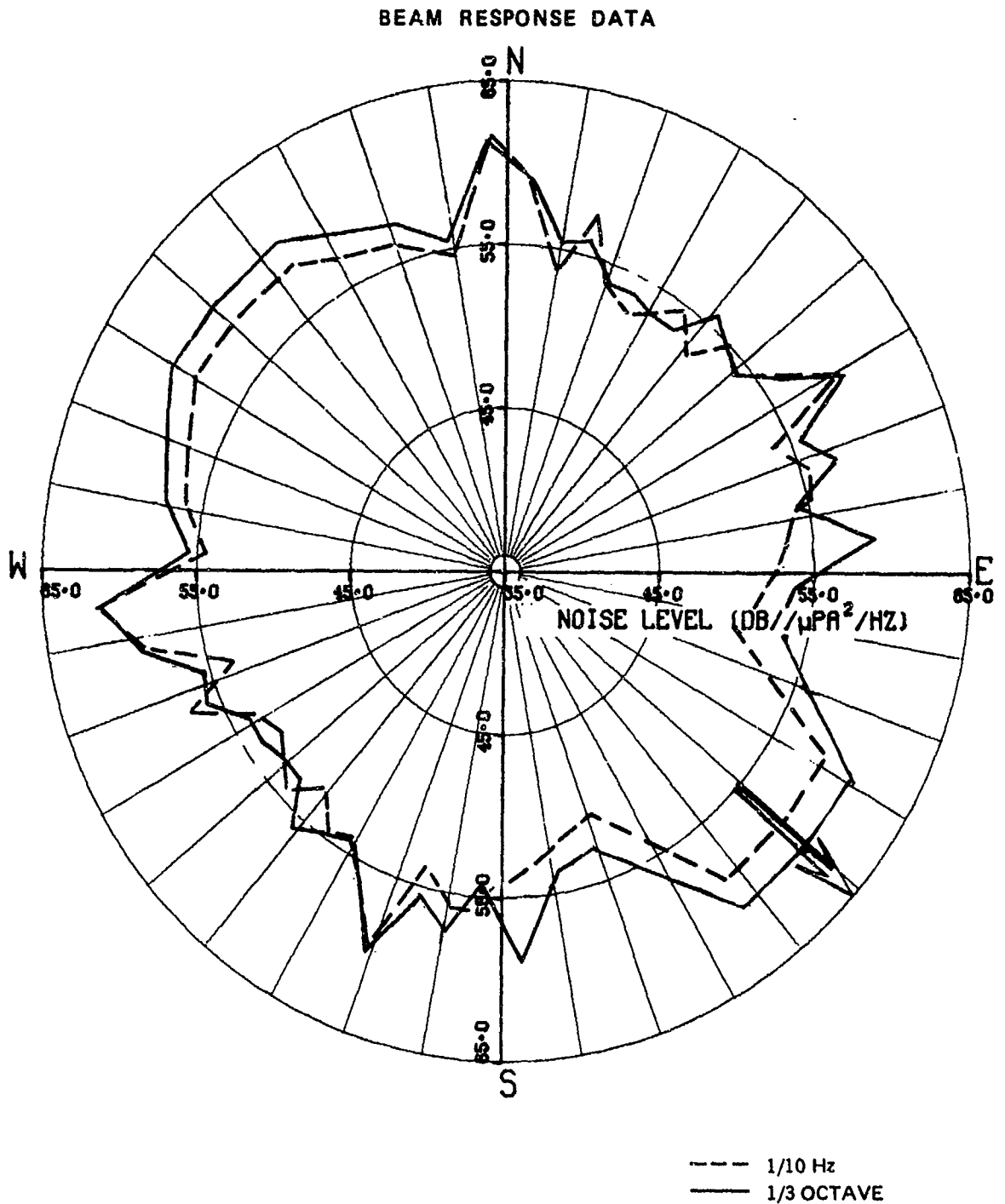
(C) Figures 24, 25, and 26 are typical examples of the comparison between the 1/3-octave and 1/10-Hz beam response data. These data were acquired during the first polygon at station η -1 for the 8 to 9 September measurement period. In some cases the levels differ by as much as 4 to 5 dB along a given azimuth but the total noise level is not significantly different. These differences may result because the 1/10-Hz analysis covered only 320 sec within a 15-min measurement period. Differences may also result when the 1/10-Hz band is a poor estimate of the spectral content in the 1/3-octave band. In general, however, the beam responses have the same shapes and the same degree of anisotropy. The reconstructed noise fields for the same time period and the two different analysis bands are compared in Figs. 27 through 30 for 160, 100, 50, and 40 Hz, respectively. The solid curves in these figures are the 1/3-octave results, and the dashed curves are the 1/10-Hz results. It is evident from these figures that the directionalities are not significantly different. The azimuths of high-level noise for one analysis bandwidth are the same for the other bandwidth. The differences between the absolute levels along any one azimuth are generally less than 2 or 3 dB. The total noise or equivalent omni-levels differ at most by approximately 2 dB for all frequencies. No significant difference in horizontal directionality is attributable to analysis bandwidth for any of the CHURCH ANCHOR data.

Noise Field Directionality Characteristics – Frequency Independence

(S) The beam response data for the LAMBDA, TASS, and MESA systems indicate that the degree of anisotropy measured by each system decreases with decreasing frequency. Whether this phenomenon is a property of the noise field, a result of the frequency characteristics of the measuring tool, or a combination of

SECRET

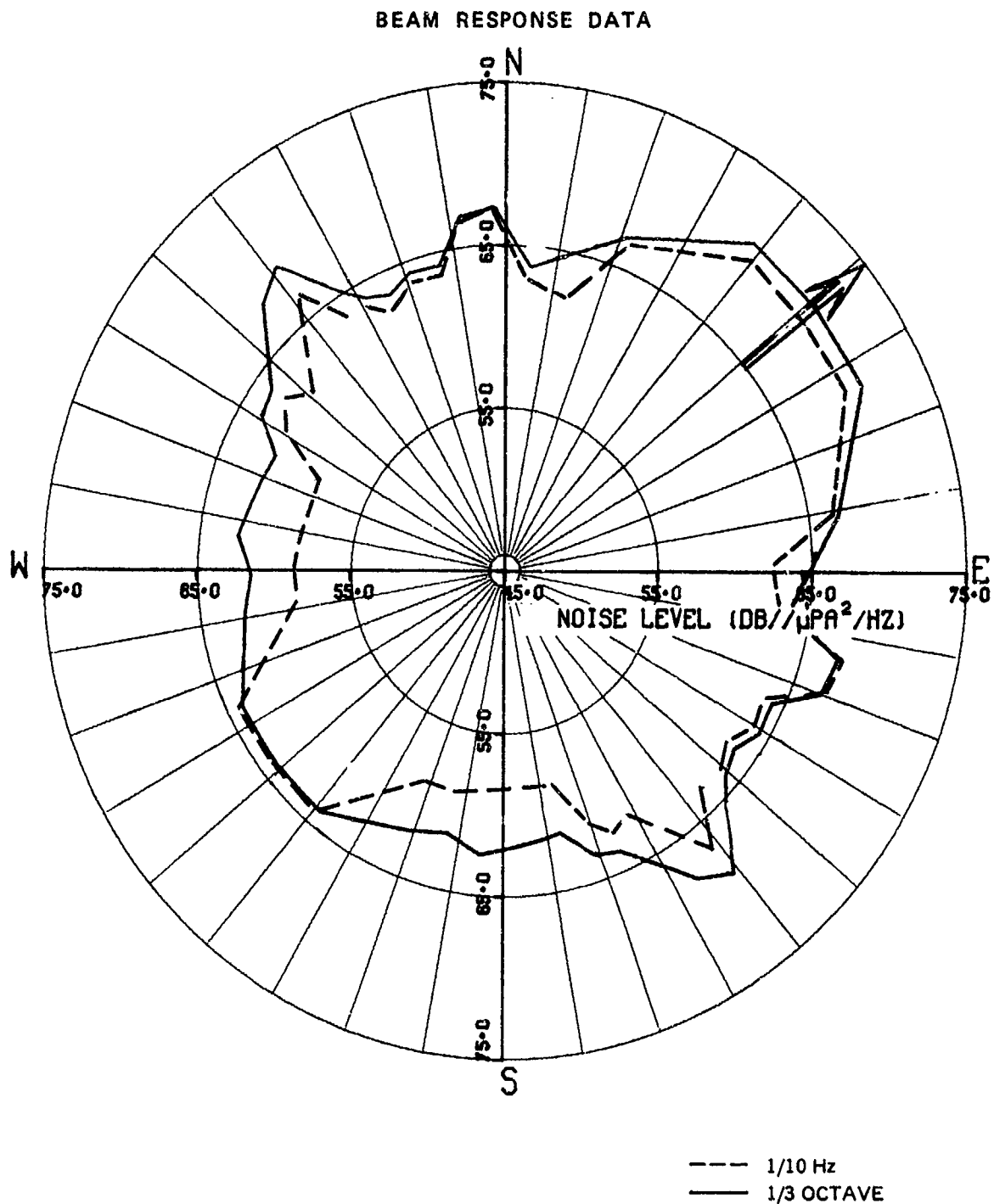
CONFIDENTIAL



(U) Figure 24. Comparison of TASS beam response data at 160-Hz for 1/3-octave and 1/10-Hz bandwidth analysis, leg 1 of polygon 1 at station η -1. (C)

CONFIDENTIAL

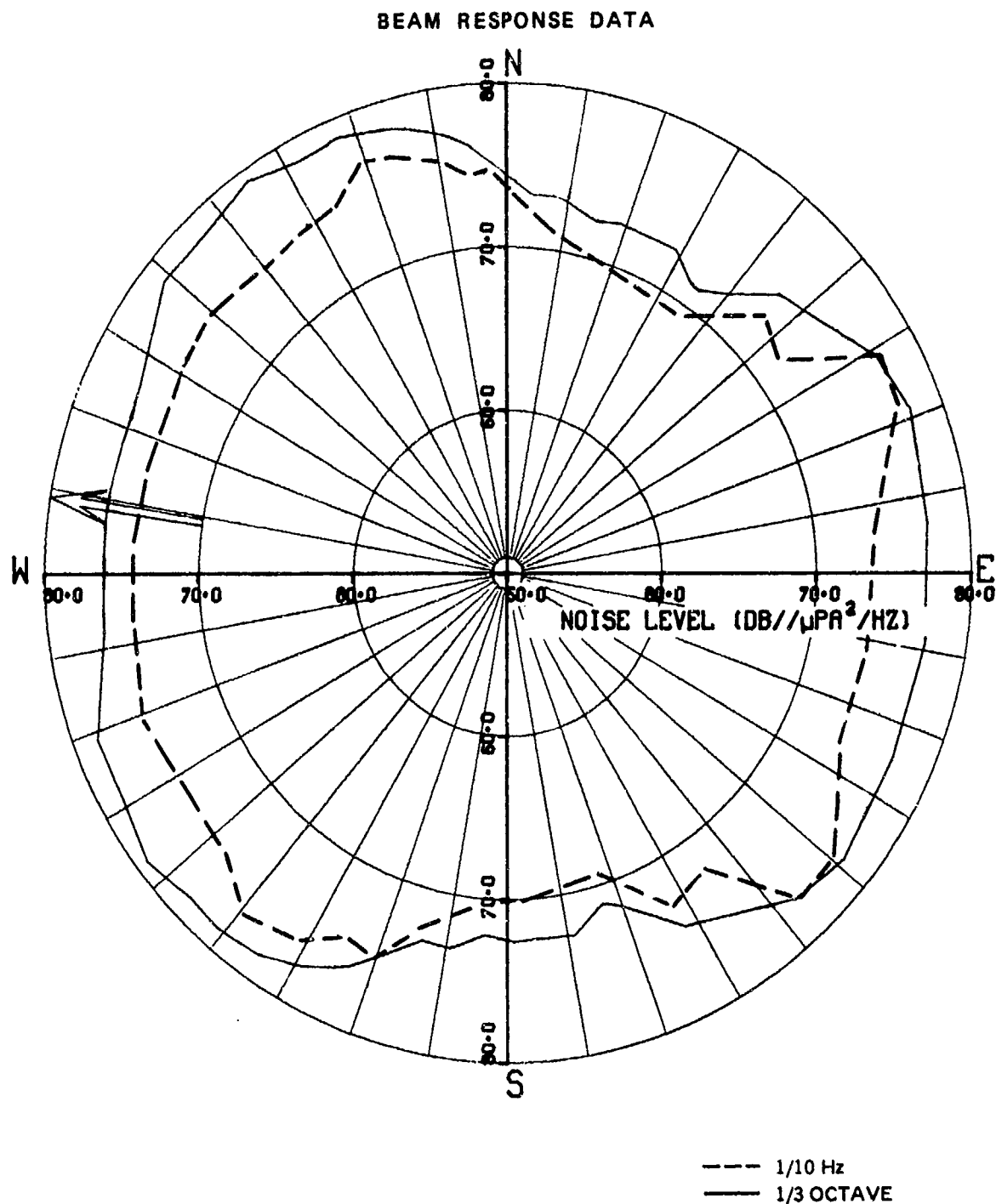
CONFIDENTIAL



(U) Figure 25. Comparison of TASS beam response data at 100-Hz for 1/3-octave and 1/10-Hz bandwidth analysis, leg 5 of polygon 1 at station η -1. (C)

CONFIDENTIAL

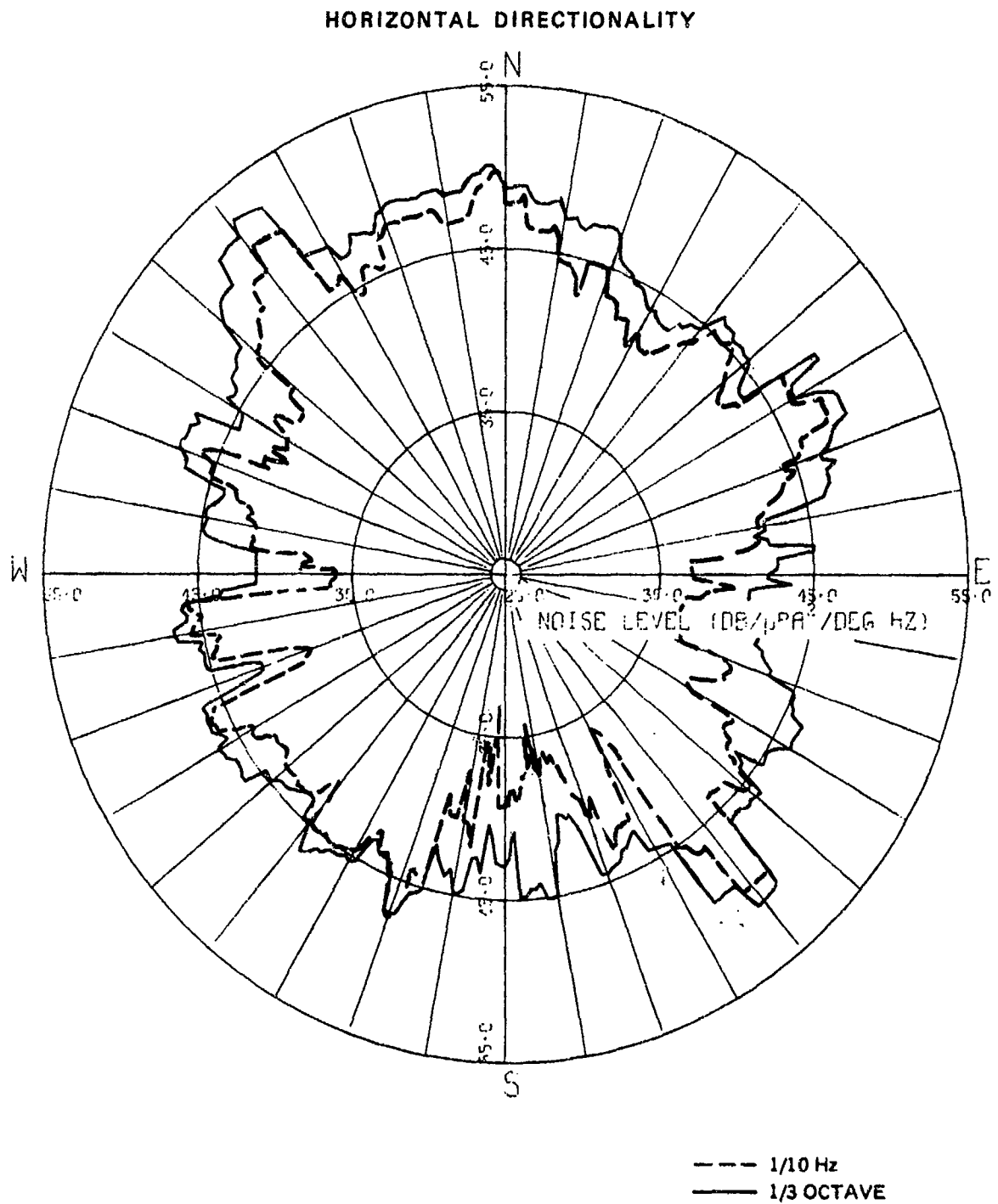
CONFIDENTIAL



(C) Figure 26. Comparison of TASS beam response data at 50-Hz for 1/3-octave and 1/10-Hz bandwidth analysis, leg 3 of polygon 1 at station η -1. (C)

CONFIDENTIAL

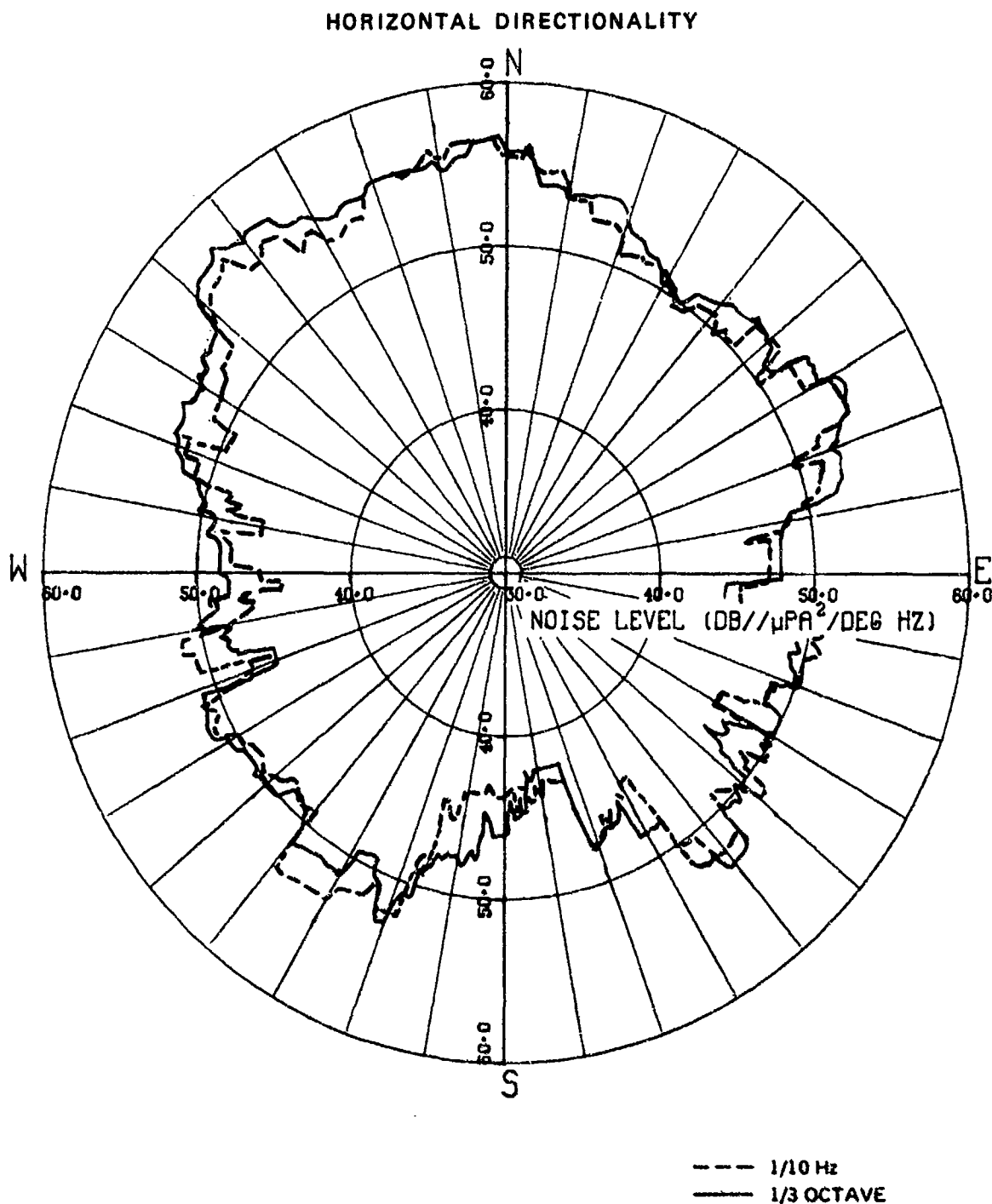
CONFIDENTIAL



(U) Figure 27. Comparison of TASS horizontal directionality noise roses at 160-Hz; 1/3-octave and 1/10-Hz bandwidth analyses for polygon 1 at station η-1. (C)

CONFIDENTIAL

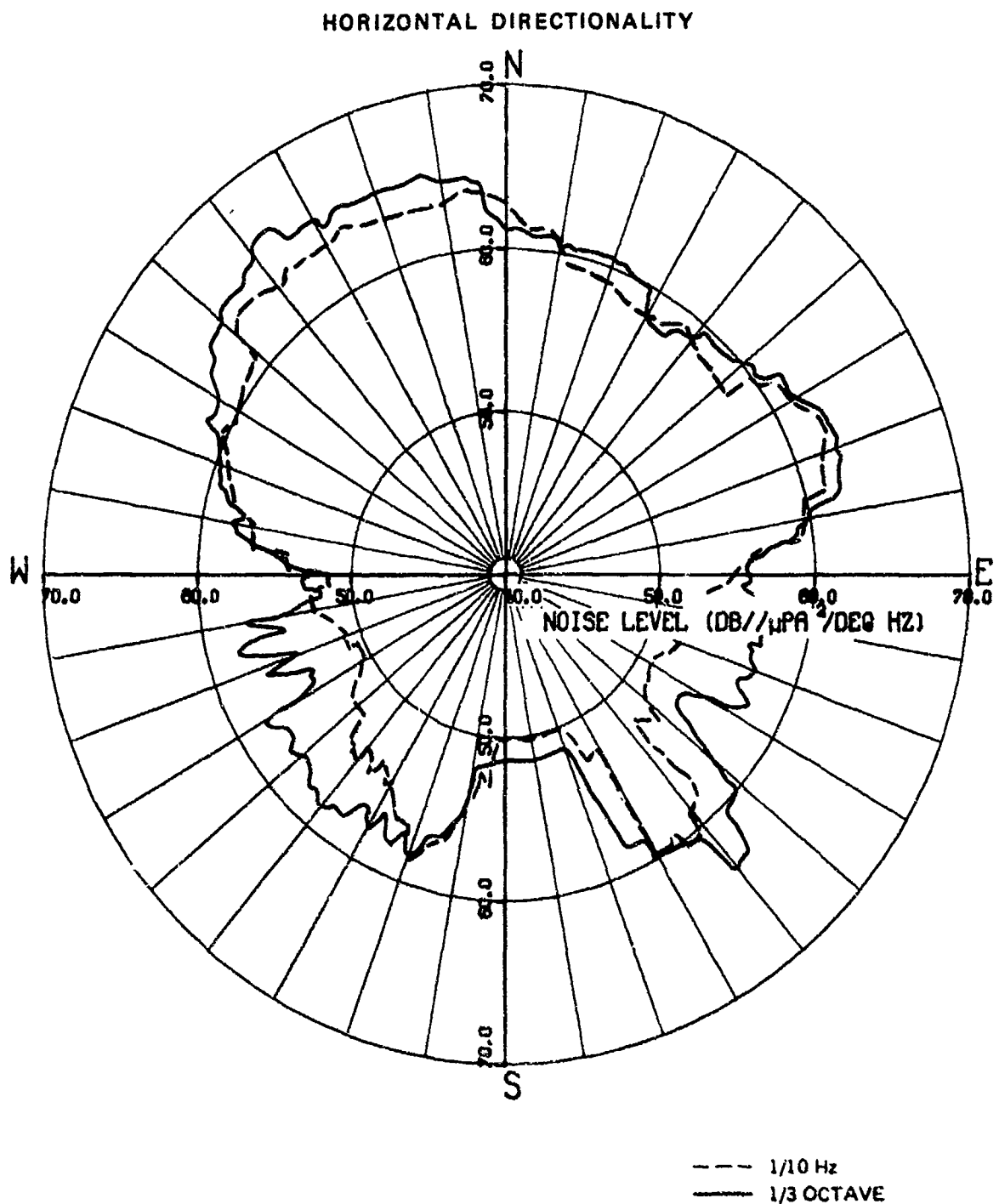
CONFIDENTIAL



(U) Figure 28. Comparison of TASS horizontal directionality noise roses at 100-Hz; 1/3-octave and 1/10-Hz bandwidth analyses for polygon 1 at station η -1. (C)

CONFIDENTIAL

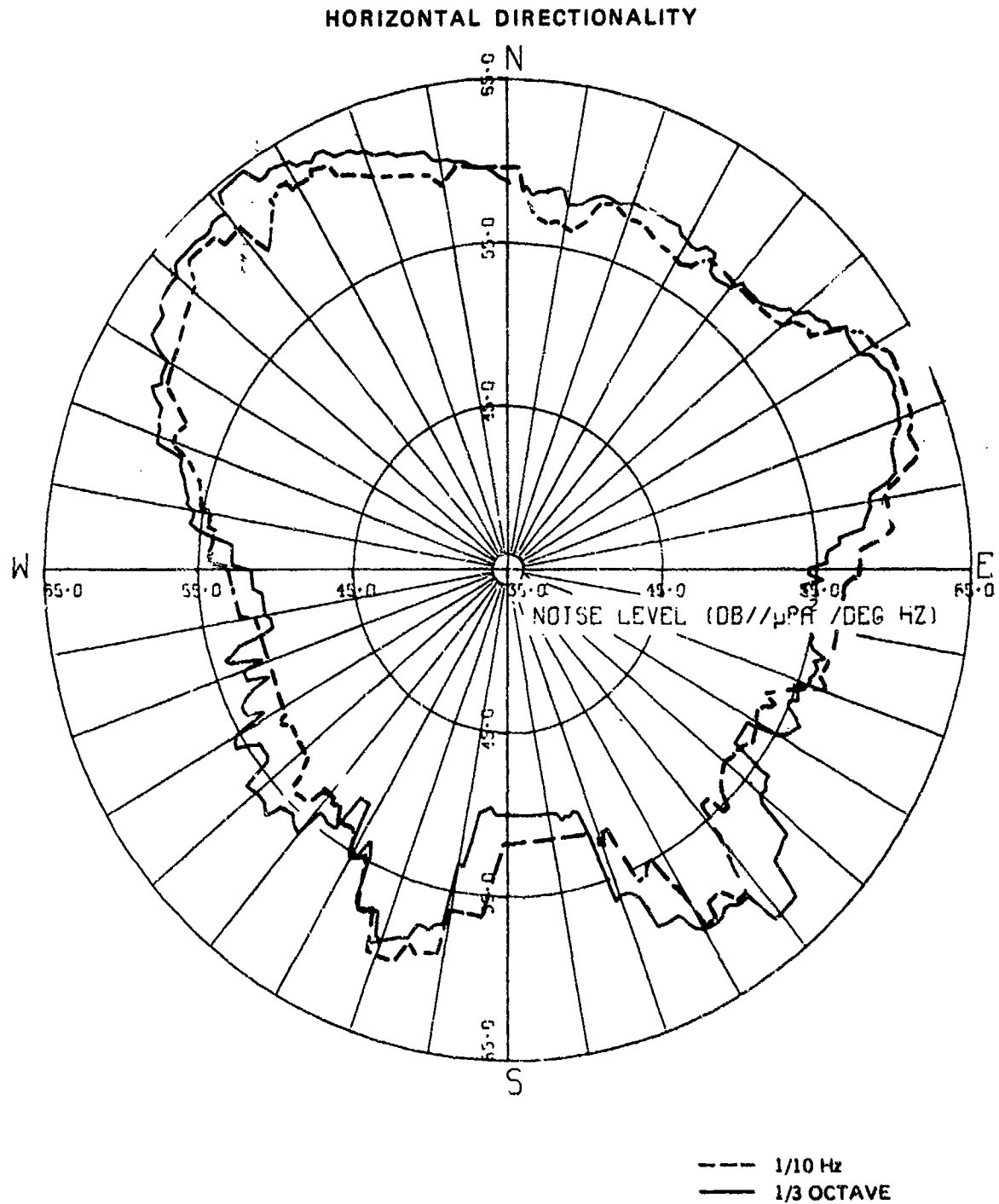
CONFIDENTIAL



(U) Figure 29. Comparison of TASS horizontal directionality noise roses at 50-Hz; 1/3-octave and 1/10-Hz bandwidth analyses for polygon 1 at station η -1. (C)

CONFIDENTIAL

SECRET



(U) Figure 30. Comparison of TASS horizontal directionality noise roses at 40-Hz; 1/3-octave and 1/10-Hz bandwidth analyses for polygon 1 at station η -1. (C)

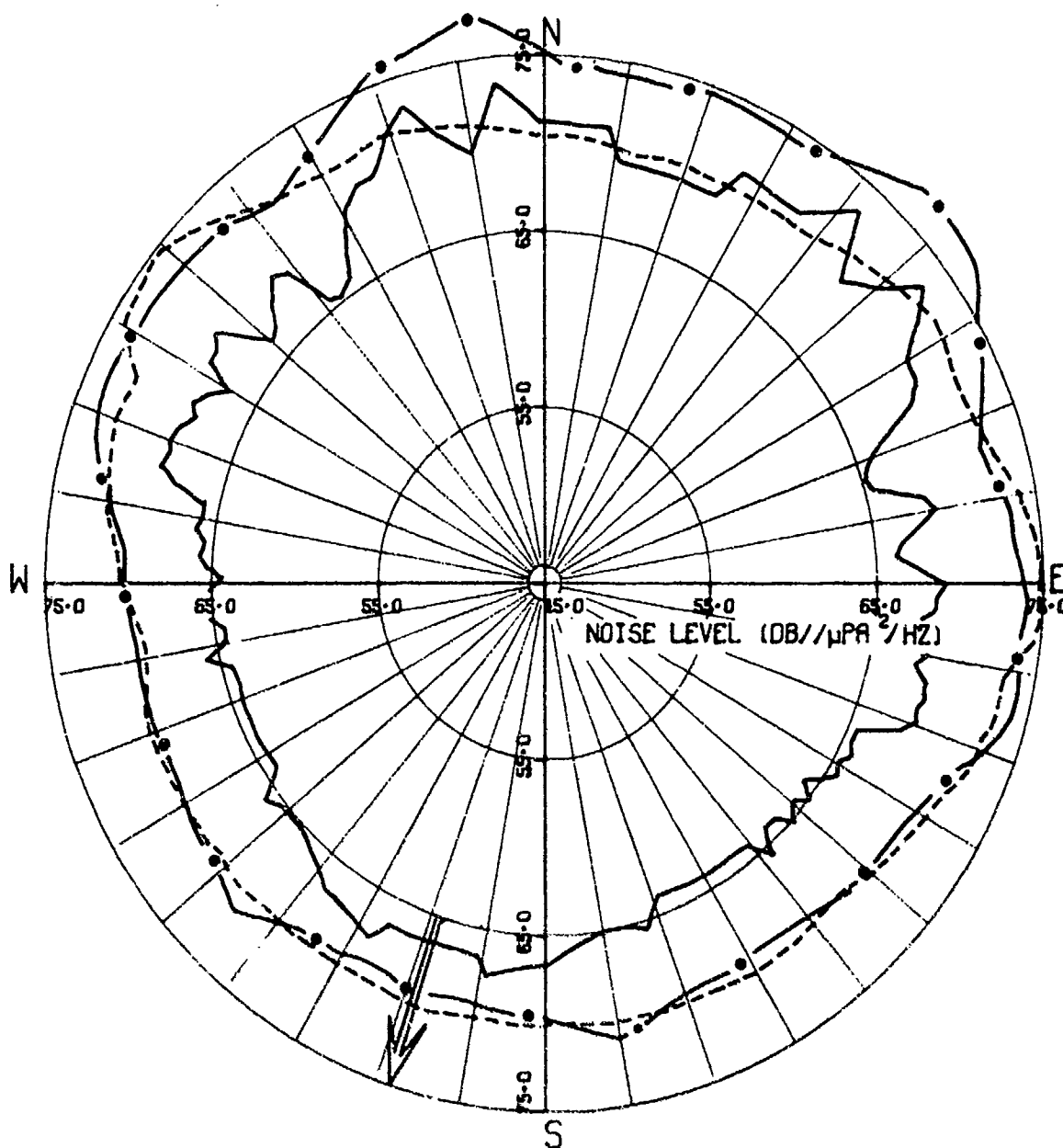
SECRET

these and possibly other effects is open to question. A partial, but not complete, resolution can be obtained by comparing the data from the different systems and by applying special analysis procedures. Consider, for example, the beam response curves in Fig. 31. The solid curve is the plot of the 61 beam response levels at 36 Hz for the second leg of the third LAMBDA polygon. Variations in level of 4 or 5 dB within 10 deg of azimuth for this curve are not uncommon. The dashed curve in this figure is the plot of the 21 beam response levels at 11 Hz for the same time period. This curve is smoother than the previous one, with variations in level less than 2 dB within 10 deg generally being the rule. The third curve is the result of sampling the 61 beam response data points of the 36-Hz data to generate 21 new beam response values, which include the effect of the increased beamwidth at 11 Hz. This last curve compares very favorably with the curve for 11 Hz. The degree of smoothness and general shape are the same. This type of comparison was made for other legs and other frequencies, with the results being essentially the same. In addition, the modified or smoothed beam responses for the 36-Hz data were utilized in the MAB method to obtain horizontal directionality estimates. The resulting comparisons between the horizontal directionality plots for the modified 36-Hz data and the 29-, 23-, and 11-Hz measured data are given in Figs. 32, 33, and 34. The overall agreement in the directionalities is reasonably good.

(S) The fact that data at one frequency can be smoothed to produce the general shape and reduction in the degree of anisotropy seen in lower frequency data taken by the same system indicates that the phenomenon is related to the measurement tool and is not a characteristic of the noise field. This is also suggested by the degree of anisotropy obtained by each of the three measurement systems for frequencies near 36 Hz. The LAMBDA, for example, which has beamwidths nearly an order of magnitude narrower than TASS, shows excursions in the beam response levels in excess of 8 dB within 10 deg of azimuth. The TASS, however, shows less than 4 dB in 10 deg of azimuth. The MESA, whose beamwidths are nearly five times those of TASS, generally measured less than 2 or 3 dB in 60 deg of azimuth. Hence, the anisotropy which is measured appears to be dependent on the acoustical characteristics of the measurement tool. There is no evidence in the CHURCH ANCHOR horizontal noise data which suggests this phenomenon is other than a result of the frequency-dependent acoustical characteristics of the measurement tools. It can be explained simply in terms of the frequency-dependent characteristics of the measurement tool.

(S) Further evidence of the frequency independence of the directional characteristics of the noise field can be obtained by comparing TASS and LAMBDA results at frequencies for which the beamwidths are approximately equal and for measurement periods which are nearly coincident in time. The beamwidths for TASS at 160 Hz and 100 Hz compare favorably with those for LAMBDA at 29 Hz and 23 Hz, respectively, although the number of LAMBDA beams at each frequency

SECRET
BEAM RESPONSE DATA



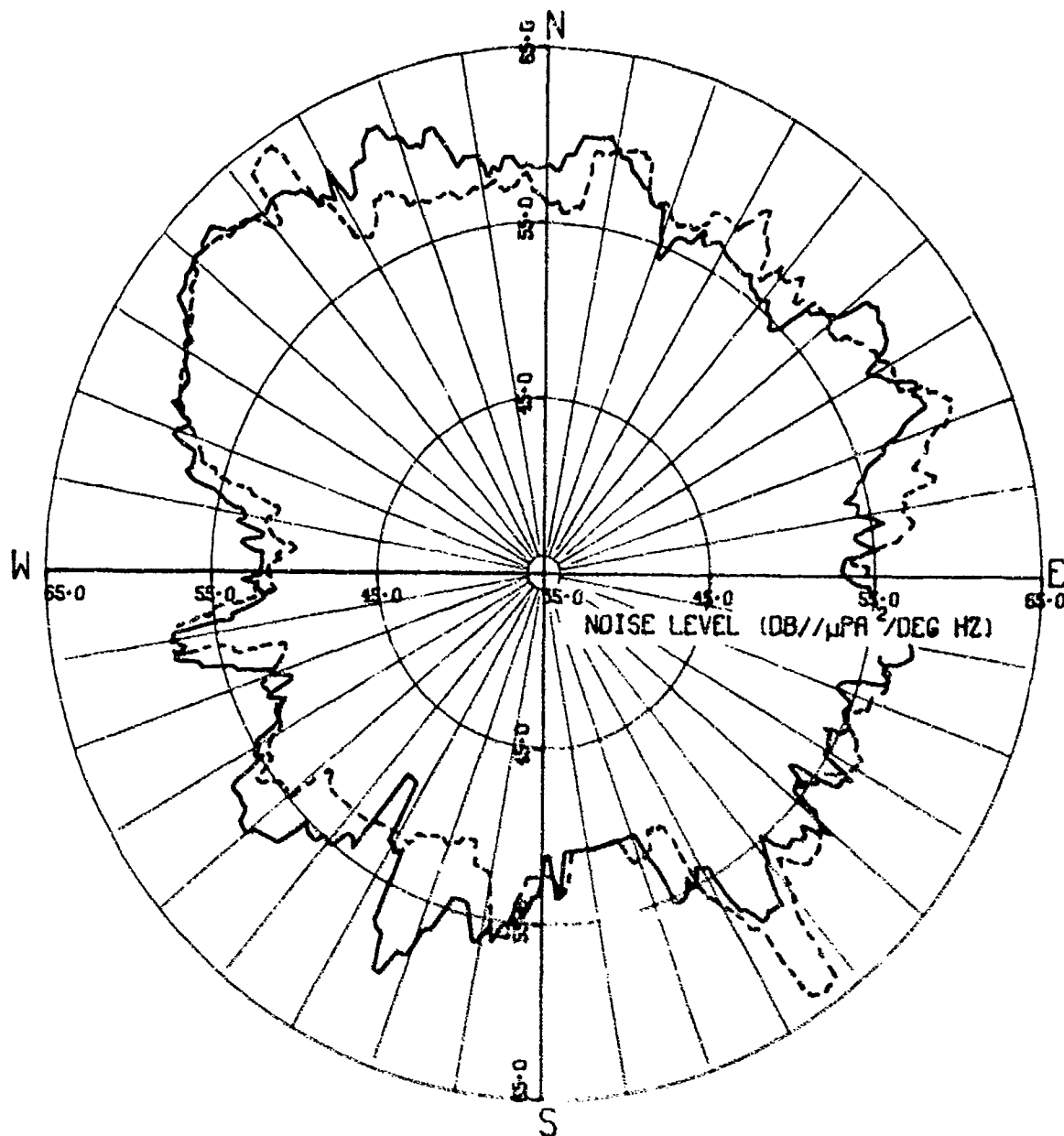
— 36 Hz (ORIG)
 - - 11 Hz (ORIG)
 - • - 36 Hz (11-Hz
 BEAMWIDTH)

(U) Figure 31. Comparison of LAMBDA polygon 3, leg 2, 11-Hz beam response data with 36-Hz and 36-Hz smoothed-beam response data for the same leg. (S)

SECRET

SECRET

HORIZONTAL DIRECTIONALITY

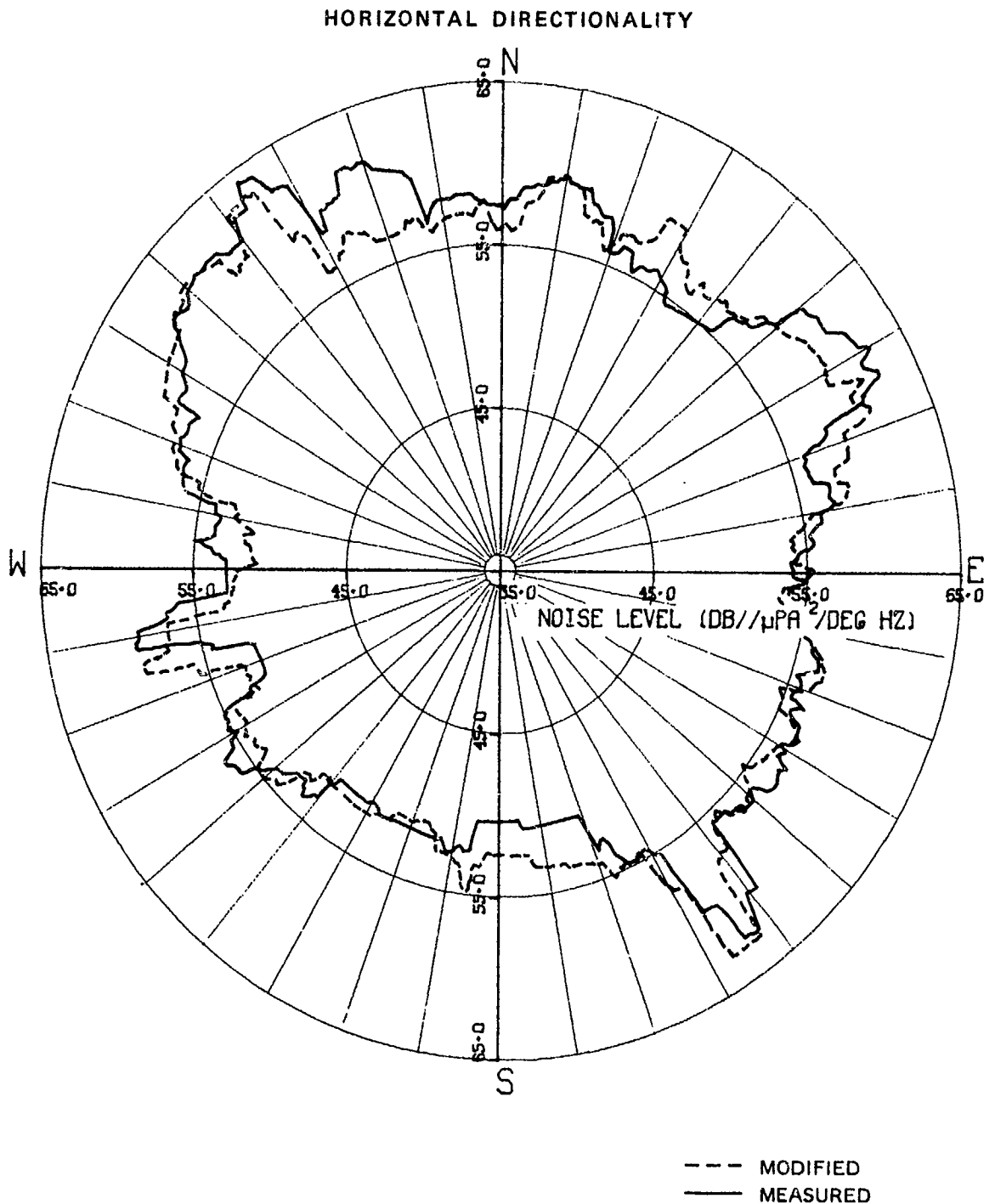


--- MODIFIED
— MEASURED

(U) Figure 32. Comparison of 29-Hz noise rose with modified (sampled and smoothed) 36-Hz noise rose for LAMBDA data, station η -1. (S)

SECRET

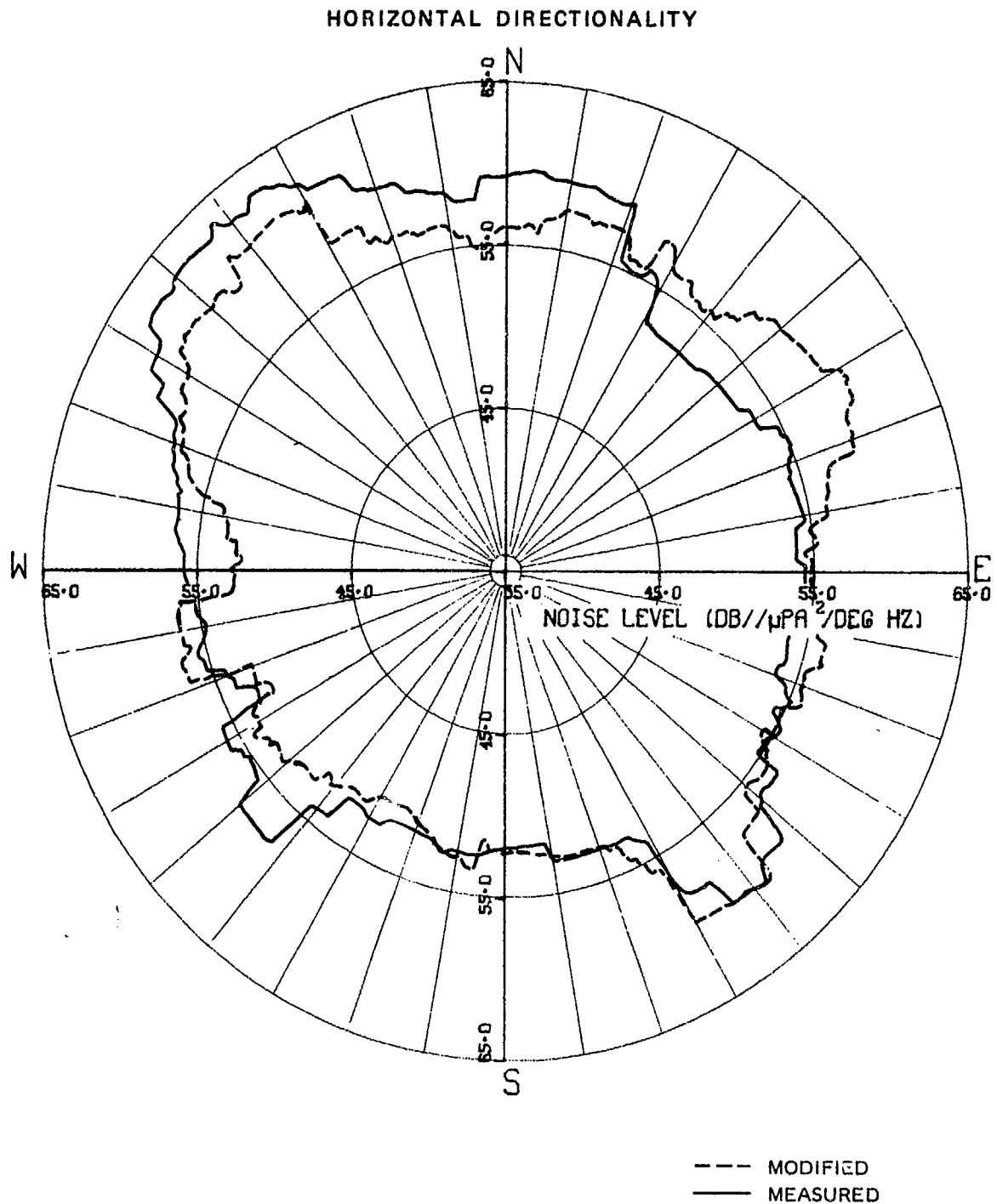
SECRET



(S) Figure 33. Comparison of 23-Hz noise rose with modified (sampled and smoothed) 36-Hz noise rose for LAMBDA data, station η -1. (S)

SECRET

SECRET



(S) Figure 34. Comparison of 11-Hz noise rose with modified (sampled and smoothed) 36-Hz noise rose for LAMBDA data, station η -1. (S)

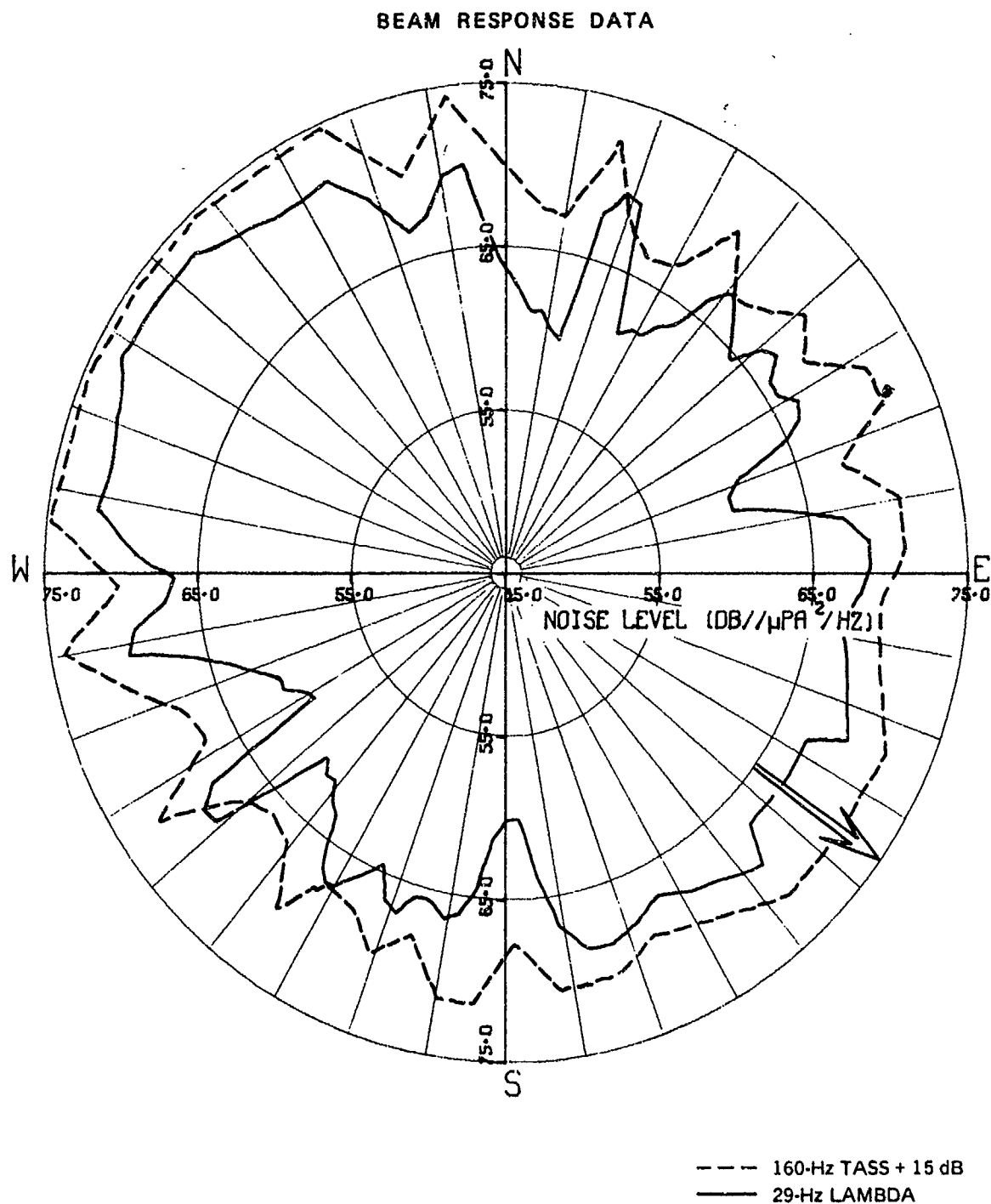
SECRET

greatly exceeds the number of TASS beams. In comparing these data, note that because of the length of time required to complete a leg (LAMBDA, 2 hr; TASS, 1 hr), only LAMBDA legs 1, 5, 6, and 10 have the same headings at approximately the same times as TASS legs 1, 10, 11, and 20, respectively, on a given noise measurement day.

(S) Figure 35 illustrates the results of one such comparison. Here the dashed curve is for the TASS 160-Hz beam response data for leg 1 of polygon 1 at $\eta=3$. The solid curve is the LAMBDA 29-Hz beam response for leg 1 of polygon 1, also at $\eta=3$. The separation distance between the two arrays at this time was about 20 nmi, with LAMBDA being approximately due east of TASS. An additional 15 dB has been added to the 160-Hz data to facilitate directionality comparison; no comparison of the absolute levels will be attempted, since the two sets of data are for radically different frequencies. The analysis bandwidths are also different, 1/3-octave for the TASS data and 1/8-Hz for the LAMBDA data, but this was shown previously to have a negligible effect.

(S) The two directionality patterns displayed in Fig. 35 are remarkably similar considering the differences in the two corresponding frequencies and considering that at 29-Hz LAMBDA has more than twice as many beams as TASS. All of the high-noise sources in one curve are present in the other and on nearly the same azimuths, despite the spatial separation of the two arrays. This indicates that the sources are fairly distant from both arrays. The 160-Hz data appears more "spikey" in nature as a result of TASS having only 23 beams; hence, a noise from a discrete source would most likely appear on only one beam. LAMBDA, however, has 49 beams at 29 Hz and a discrete source will appear on at least two beams, thus giving a less "spikey" appearance to the beam response data. Also, the LAMBDA data exhibits 3 to 4 dB more anisotropy (excursion in level with azimuth) than the TASS data. This is believed to be due to the wind noise, which established the background noise threshold at 160 Hz but not at 29 Hz, and to the lesser capability for sidelobe suppression of TASS as compared to LAMBDA. Similar results were observed at other times, frequencies, and locations.

SECRET



(U) Figure 35. Superposition of 160-Hz TASS beam response data with 29-Hz LAMBDA beam response data; both data for polygon 1, leg 1, at η -3. (S)

SECRET

UNCLASSIFIED

(U) REFERENCES

1. Naval Undersea Center, NUC TP 422, Detection, Localization, and Classification of Some Unusual Transient Signals in the Pacific (U), by J. Northrop, D. L. Keir, and J. D. Pugh, November 1974, (S).
2. Naval Undersea Center, NUC TN-834, A Short Method of Calculating the Response Pattern of a Line Array Having Dolph-Chebyshev Shading, by H. S. Aurand, August 1972.
3. Arthur D. Little, Inc., Working Memorandum, Case 74014-8, Ambiguity Resolution, Appendix A, by G. Raisbeck, 18 December 1972.
4. Naval Undersea Center, NUC TP-374, A Discussion and Comparison of Five Methods Utilizing the Towed Array to Assess the Azimuthal Directionality of Ambient Noise (U), by R. A. Wagstaff, January 1974, (C).
5. Naval Undersea Center, NUC TN-1387, CHURCH ANCHOR Ambient Noise Horizontal Directionality Data Base (U), by Undersea Surveillance Dept. (in publication) (S).
6. Maury Center for Ocean Sciences, Plan MC-001, CHURCH ANCHOR Data Analysis Plan (U), October 1973, (S).
7. Naval Undersea Center, NUC TN-1039, Ambient Noise: Comments on its Causes, Variability, and Measurement, by R. A. Wagstaff, May 1973.
8. R. A. Wagstaff, Ambient Noise Depth Dependence (U), *JUA*, Vol 23, No. 4, pp 543-549 (C).
9. Planning Systems, Inc., TR-004002, CHURCH ANCHOR: Aircraft Surveillance of Shipping (U), January 1974 (S).
10. J. Northrop, M. S. Loughridge, and E. W. Werner, "Effect of Near-Source Bottom Conditions on Long-Range Sound Propagation in the Ocean," *J. Geophys. Res.*, Vol. 73, No. 12, June 1968.
11. D. B. Officer. *Introduction to the Theory of Sound Transmission with its Application to the Ocean*, McGraw-Hill, New York, 1958, p. 159.
12. Naval Undersea Center, NUC TN-1088, Implementation of Raisbeck's Technique to Resolve Left/Right Ambiguity Inherent in Beam Patterns of a Line Array, Using Real-Time Data Processing, by N. J. Martini, August 1973.
13. Naval Undersea Center, LAMBDA Project, Quick Look Report, LAMBDA Sea Test No. 3 (U), by C. L. Meland and S. J. McCarthy, September 1973 (S).
14. Naval Undersea Center, NUC TN-989, TASS Test Bed Project, Quick Look Report, Hydrophone Sensitivities and Beam Patterns (U), by J. W. Reese and D. L. Keir, April 1973 (S).

UNCLASSIFIED

UNCLASSIFIED

15. Naval Undersea Center, NUC TN-988, TASS Test Bed Project Quick Look Report, TASS Self-Noise Operations, 12-16 March 1973 (U), by A. G. Fabula, April 1973 (S).
16. Naval Undersea Center, NUC TN-1038, Part II, NUC Participation in Eastern Pacific LRAPP Operations, June and September 1972 (U), by R. Gardner, et al., May 1973 (S).
17. Naval Undersea Center, NUC TN-877, SONODIVER/SPARBUOY/TASS Preliminary Data Analysis (U), by C. W. Johnson, November 1972 (C).
18. Naval Undersea Center, NUC TN-941, Quick Look Report, TASS Self-Noise Operations, 15-29 January 1973, Phase I (U), by A. G. Fabula, February 1973 (S).
19. Maury Center for Ocean Science, Plan MC-011, CHURCH ANCHOR Exercise Plan - Long Range Acoustic Propagation Project (U), July 1973 (16 July 1973 Revision) (C).
20. Maury Center for Ocean Science, Plan MC-0011A, Supplement A to CHURCH ANCHOR Exercise Plan - Long Range Acoustic Propagation Project (U), with Appendix B-III, PACIFIC APOLLO Array (U) and Appendix B-IV, LEE Array, 16 July 1973 (SNF).
21. J. V. Bradley. *Distribution-Free Statistical Tests*, Prentice-Hall, Inc., Englewood Cliffs, N. J., 1968.
22. S. Siegel. *Nonparametric Statistics for the Behavioral Sciences*, McGraw-Hill, Inc., New York, 1956.
23. B. I. Hart. "Significance Levels for the Ratio of the Mean-Square Successive Difference to the Variance." *The Annals of Mathematical Statistics* 12:445-447 (1942).
24. D. B. Owen. *Handbook of Statistical Tables*, Addison-Wesley, Palo Alto, 1962.
25. K. A. Brownlee. *Statistical Theory and Methodology In Science and Engineering*. John Wiley and Sons, Inc., New York, 1965.
26. D. J. Edleblute, J. M. Fisk, and G. L. Kinnison. "Criteria for Optimum-Signal-Detection Theory for Arrays." *JASA* Vol 41, No. 1, 1967, pp 199-205.

UNCLASSIFIED

APPENDIX A

NOISE MEASUREMENT SYSTEMS CHARACTERISTICS

(S) Three systems were deployed for horizontal directionality data acquisition in CHURCH ANCHOR. They were the LAMBDA system, the TASS, and the MESA. LAMBDA and TASS are towed line-arrays 1219 m and 207.3 m in length, respectively. LAMBDA has the additional capability of operating in a stationary mode by means of a drogue chute. The MESA system consists of a seven-element (only four were used in CHURCH ANCHOR due to equipment failures), 6-ft-diameter circular or hexagonal array with one of the seven hydrophones suspended 20 ft below it. It is relatively stationary, once launched. The acoustic characteristics of all three systems are summarized in Table A-1, and the data analysis summarized in Table A-2.

(S) Table A-1. Measurement systems acoustic characteristics. (U)

Array Characteristics	LAMBDA	TASS	MESA
Number of Hydrophones	44	34	7*
Hydrophone Spacing	62.5 ft	14.5 ft	Circular array of six elements around a 6-ft dia. and one suspended below
Frequency Response	4.5 – 53 Hz	10 – 160 Hz	20 – 800 Hz
Array Acoustic Aperture	2750	478.5 ft	6 ft
Number of Preformed Beams	65 at 38 Hz	23	6
Bearing Resolution	1.8° (broadside at 38 Hz)	5.0° (broadside at 160 Hz)	37.5° at 150 Hz (with seven elements)
Sidelobe Suppression	~30 dB	22 dB	17 dB
Minimum Beamwidth	3.5° at 38 Hz	5.0° at 160 Hz	75° below 200 Hz

*Due to an electrical difficulty, only four were used in the data reported herein.

SECRET

(S) Table A-2. Data analysis for LAMBDA, TASS, and MESA. (U)

Frequency (Hz)			Time (sec)		
Array	Center	Bandwidth	Sample	Integration/Averaging	
LAMBDA	11	1/8 Hz	--	2400	
	23	1/8 Hz	--	2400	
	29	1/8 Hz	--	2400	
	36	1/8 Hz	--	2400	
	38	1/8 Hz	--	2400	
TASS	40	1/3 oct	0.25	37.5	One hundred fifty 1/4-sec samples per 15-min measurement period (each frequency)
	50	1/3 oct	0.25	37.5	
	100	1/3 oct	0.25	37.5	
	160	1/3 oct	0.25	37.5	
	40	1/10 Hz	10.0	320	
	50	1/10 Hz	10.0	320	
	100	1/10 Hz	10.0	320	
	160	1/10 Hz	10.0	320	
MESA	23	1/3 oct	60	60 to 300	
	36	1/3 oct	60	60 to 300	
	100	1/3 oct	60	60 to 300	
	150	1/3 oct	60	60 to 300	

SECRET

LAMBDA

(C) Figure A-1 is a data-flow diagram for the onboard data acquisition and reduction system used to analyze the LAMBDA ambient noise beam data. The onboard data analysis technique to derive an estimate of the noise field directionality utilizes data from multiple array headings, the All-Bearings algorithm, and the DAS. The algorithm is described in Appendix D, and Ref. 12 describes the DAS, a programmable analyzer based on a mini-computer (HP 2100A). In this application it has been programmed to accept the amplitude-versus-azimuth data from the oscilloscope of the LAMBDA array system for five different course headings. An estimate of the ambient noise field directionality is derived from these data using the All-Bearings algorithm. During post-analysis, the MAR, HIBAR, and LOBAR algorithms were used to resolve the ambiguities. These methods are also discussed in Appendix D.

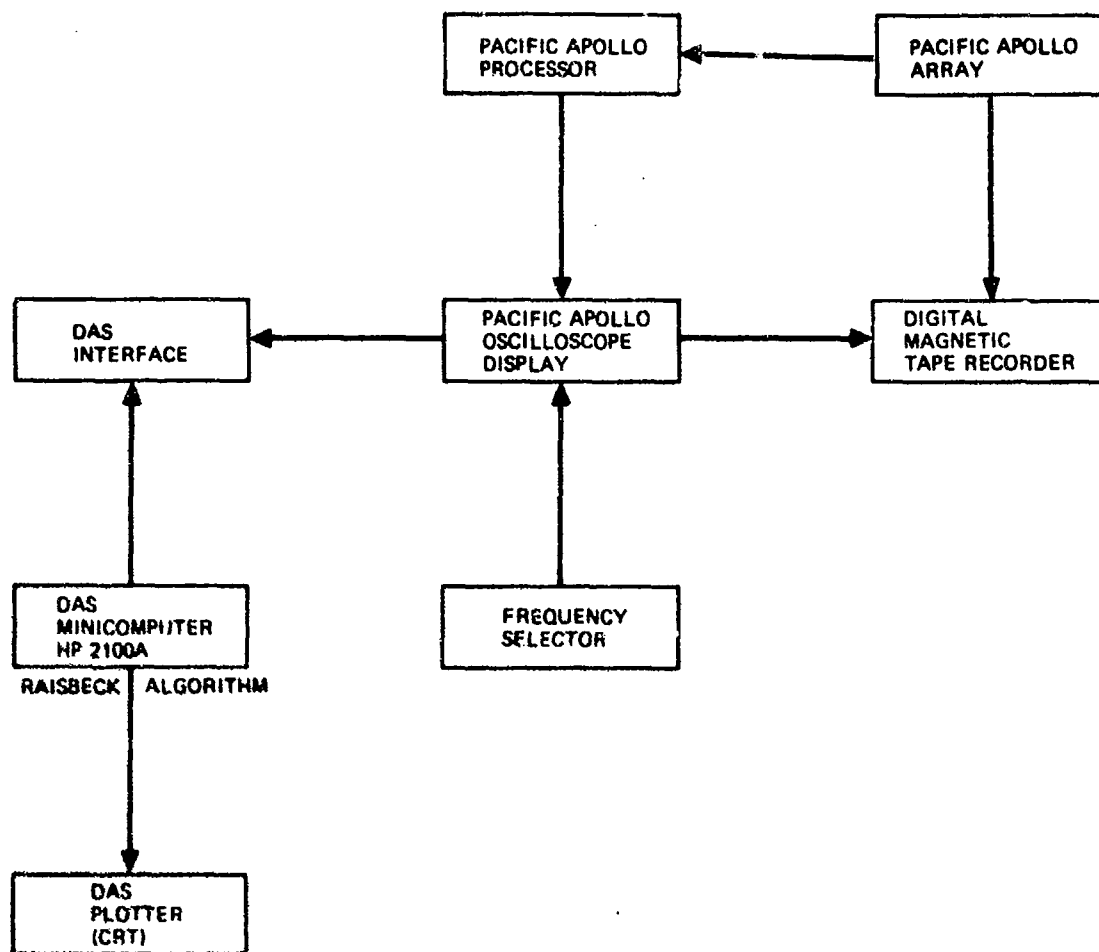
TASS

(C) Figure A-2 illustrates the data flow for the noise data acquisition and reduction system used to analyze the TASS ambient noise beam data. Noise intensity data sequences for 23 beams in four frequency bands were retrieved from storage at the completion of the final leg of each polygon. Polygons were executed with the beamformer in high gain or low gain, a 20-dB gain difference. The mean intensity of each sequence except the Hansen-Woodyard endfire beam data is utilized by the All-Bearings, BAR, HIBAR, and LOBAR algorithms. These algorithms are described in Appendix D. Use of these algorithms yields assessments of the noise field azimuthal directionality for each setting, frequency, and polygon.

MESA

(U) Figure A-3 illustrates the MESA noise data acquisition and reduction system. Outputs of six hydrophones are processed in analog electronics to form six super-directive beams at 60-deg intervals with widths ranging from 112 deg below 80 Hz to 75 deg near 200 Hz. These beams are digitally sampled and spectrum-analyzed simultaneously, using a system based on an HP 2100 digital computer and Fast Fourier Transform (FFT) hardware package. Noise measurements are averaged and recorded on digital magnetic tape, while the spectra are displayed on a CRT and hard copies are produced for monitoring purposes. In addition to these digital records, the outputs from the array are recorded on a 14-track FM tape recorder, together with voice and time code information.

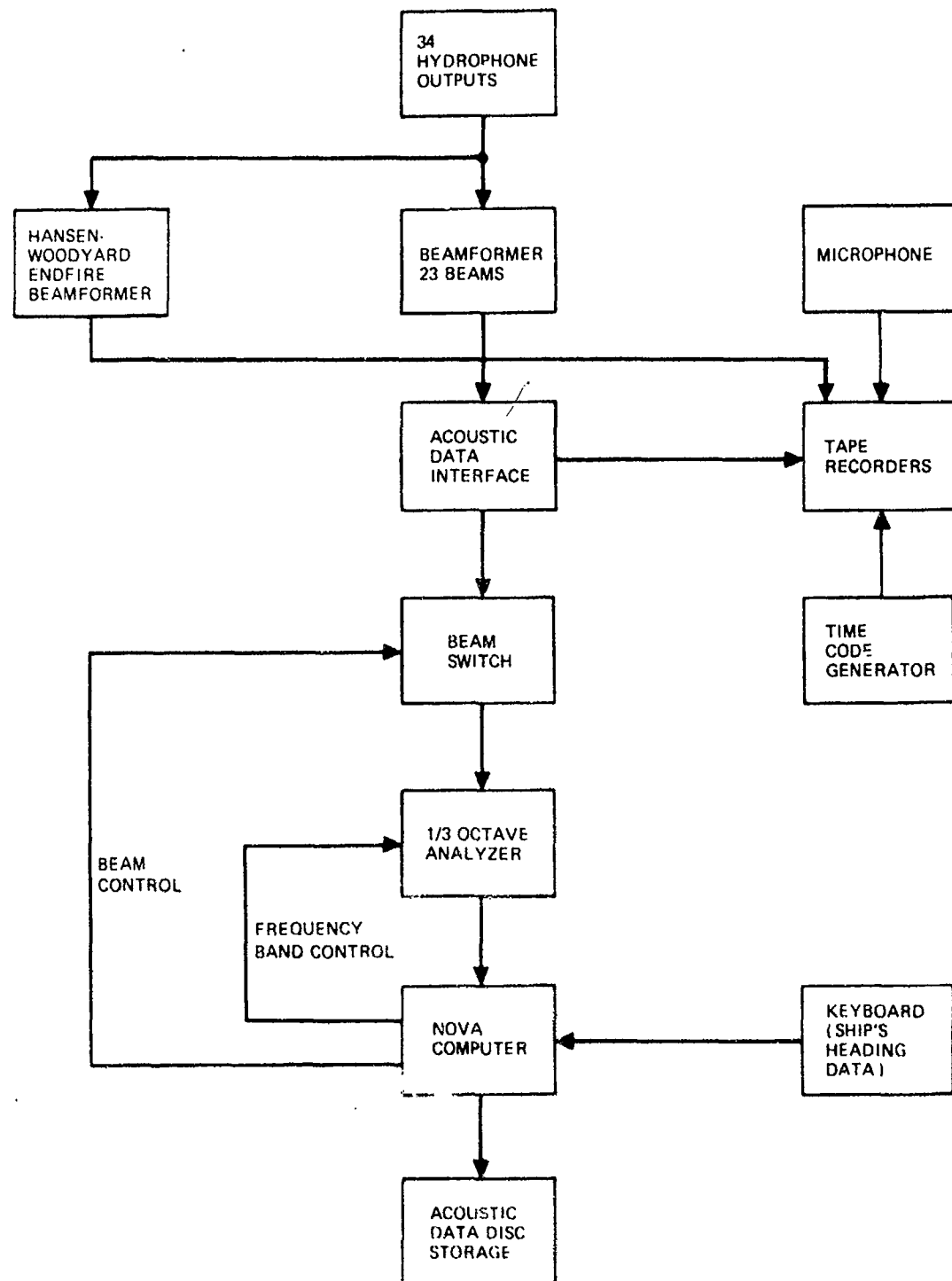
CONFIDENTIAL



(U) Figure A-1. PACIFIC APOLLO onboard data flow diagram. (U)

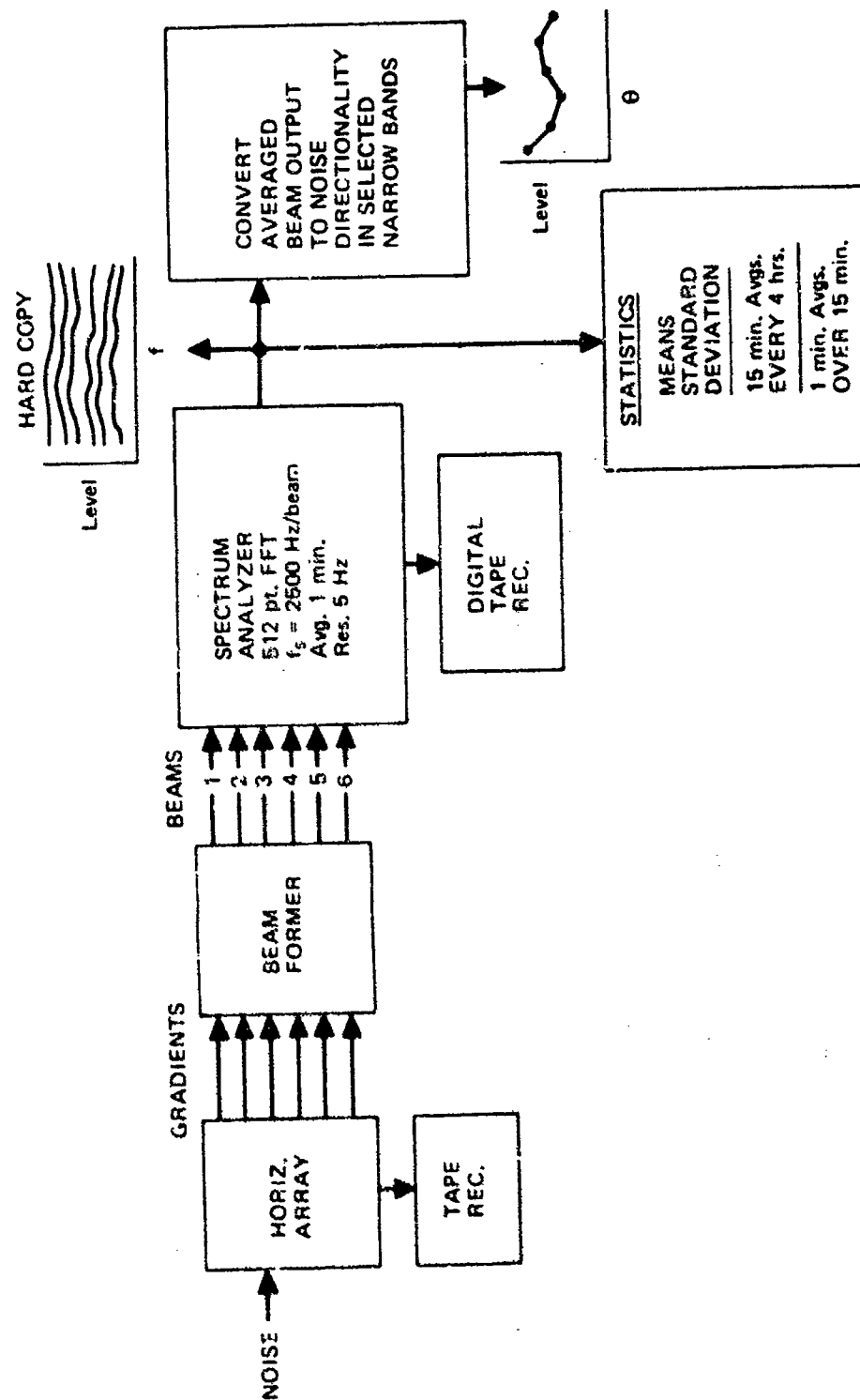
CONFIDENTIAL

UNCLASSIFIED



(U) Figure A-2. LEE data flow diagram for ambient noise assessment. (U)

UNCLASSIFIED



(U) Figure A-3. Flow diagram of ambient noise receiver on MESA array. (U)

SECRET

**APPENDIX B
PRE-CHURCH ANCHOR MEASUREMENTS**

CALIBRATION OF INDIVIDUAL HYDROPHONES

LAMBDA

(S) Hydrophone calibration was done in two parts. Five hydrophones were calibrated at the NUC TRANSDEC facility. An effort was made to calibrate the remaining hydrophones at sea, utilizing towed sources at 11, 23, and 38 Hz. This scheme produced results that suggested a range in sensitivity of 12 dB for all the LAMBDA hydrophones. These calibration data are contained in Ref. 13.

TASS

(C) The bulk of calibration data for TASS was accepted from Chesapeake Instruments Corporation. At the NUC calibration facility at Lake Pend Oreille, an independent calibration was performed on one portion of the array for both low and high frequencies (30 to 300 Hz and 150 to 1000 Hz). A detailed description of the procedure and results of the TASS hydrophone sensitivity measurements can be found in Ref. 14. In general, the fluctuation in sensitivity of all hydrophones in the array showed maximum excursions of approximately 4 dB.

INTERSYSTEM CALIBRATION COMPARISON TESTS

TASS

(C) At-sea tests prior to CHURCH ANCHOR related to a number of noise-reduction experiments. Some made use of vibration isolation modules in an effort to reduce self-noise contamination (see Ref. 15). At-sea experiments were also conducted with the NUC SPARBUOY and SONODIVER (quiet untethered vehicles for measuring ambient sea noise) to determine the minimum tow speed and frequency at which TASS becomes self-noise limited. Results of these measurements showing noise as a function of tow speed and frequency with associated components of tow-cable vibration and/or radiated noise from the tow vessel are contained in part II of Refs. 16 and 17, and Ref. 18.

(C) A discussion of errors inherent in the systems used to acquire the noise data and the methods employed in the analysis is, of necessity, complex. Measurement errors are complex functions of:

SECRET

SECRET

1. Ambiguity caused by the conical shape of the beam in determining direction of sound arrival, the vertical angle of sound arrival, and the finite beamwidths.
2. Possible beam pattern degradation caused by minor nonstationarity perturbations in the array geometry including array tilt and curvature.
3. Beam pattern degradation caused by variation in hydrophone sensitivities.
4. Beamformer errors (including data transmission system).
5. Accuracy of the array heading sensor (LAMBDA had no sensor).
6. Calibration of the beam sensitivities.

(U) One error caused by beam shape is that different beams aligned along the same azimuth will measure a different noise field. This factor would be present even if each beam were unambiguous. The resultant error decreases as the arrival angles of the significant noise contributions approach the horizontal and as the array beamwidth increases.

(U) The combined effect of items 2, 3, and 4 is measurable and shows that for the main lobes there is no significant degradation from the theoretical in shape and sensitivity (± 1 dB), and the sidelobe levels are better than 17 dB below the main lobe levels.

(C) The combined effects of items 2, 4, and 5 on bearing accuracies have been measured for TASS and found to be approximately 2 deg to 3 deg.

(C) The array heading error alone for LAMBDA was approximately 30 deg in one instance during the CHURCH ANCHOR noise measurement experiments.

SECRET

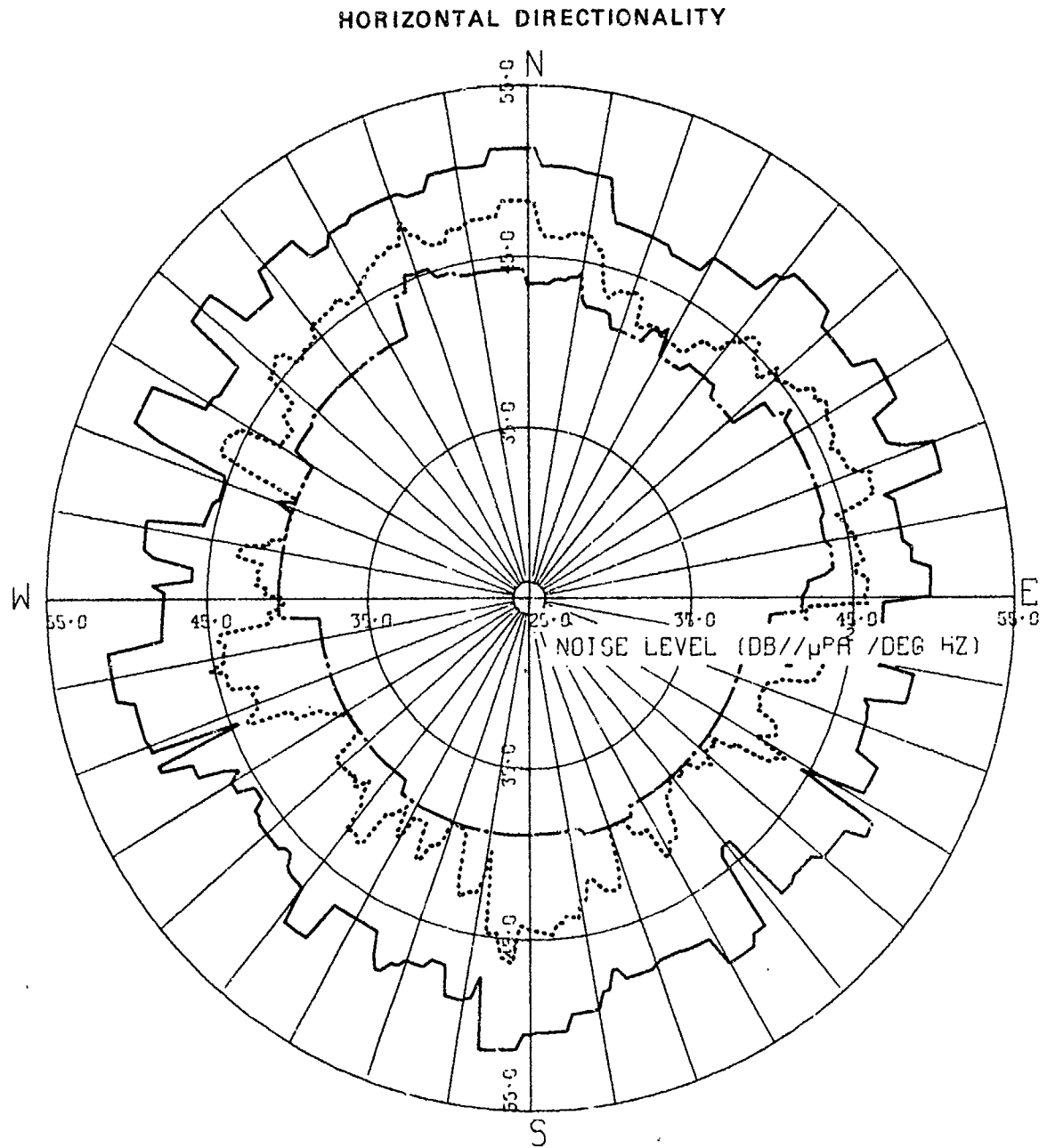
SECRET

**APPENDIX C
AMBIENT NOISE HORIZONTAL DIRECTIONALITY**

(S) The figures in this appendix show the ambient noise horizontal directionality as measured by the LAMBDA and TASS arrays, with the bearing ambiguities resolved by the HIBAR, MAB, and LOBAR methods. Figures C-1 through C-8 are TASS results for 160, 100, 50, and 40 Hz. Figures C-9 through C-16 are LAMBDA results for 36, 29, 23, and 11 Hz.

SECRET

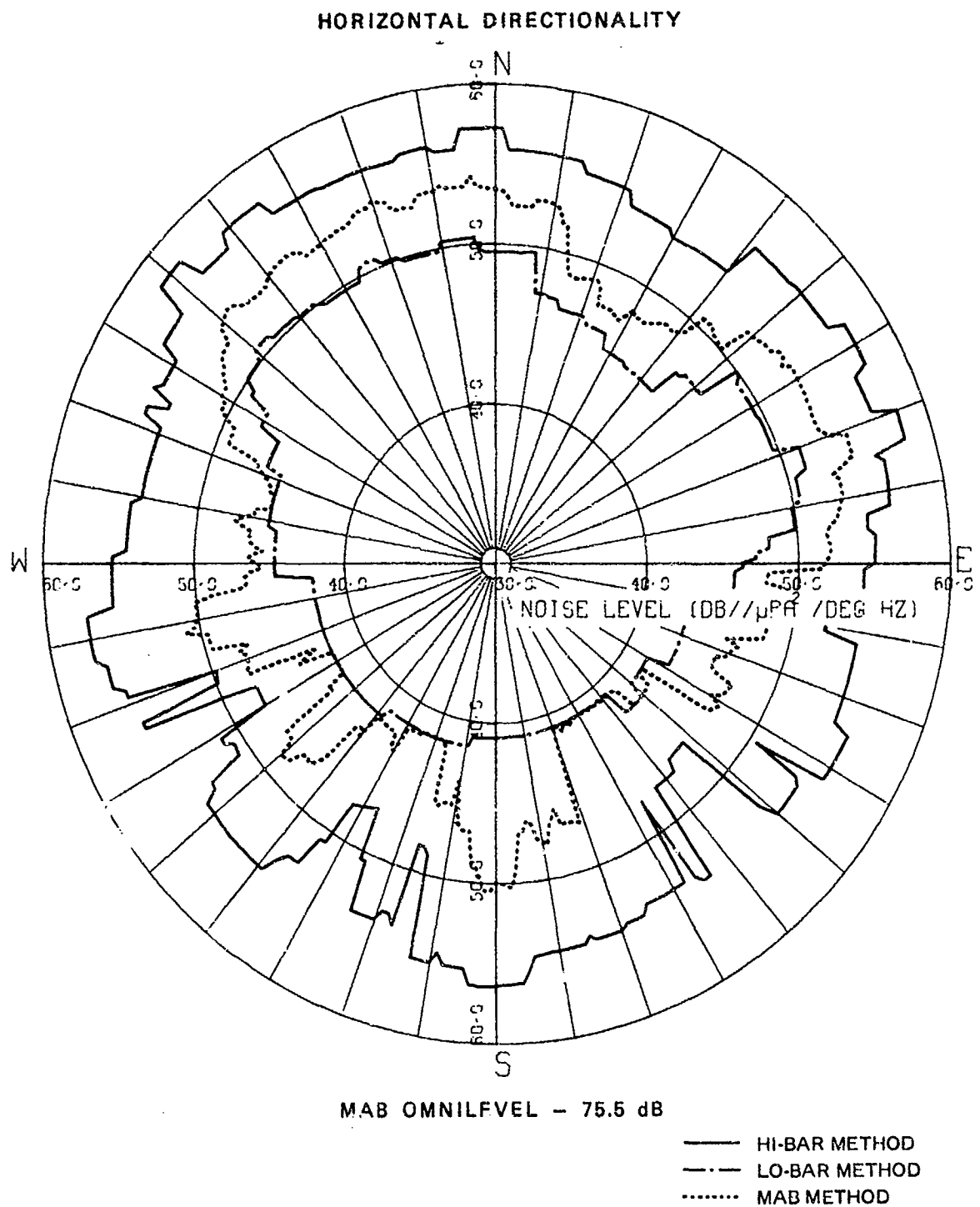
SECRET



(U) Figure C-1. Horizontal directionality noise roses for a 1/3-octave bandwidth at 160 Hz obtained from TASS polygon 3 data at η -2. (C)

SECRET

CONFIDENTIAL

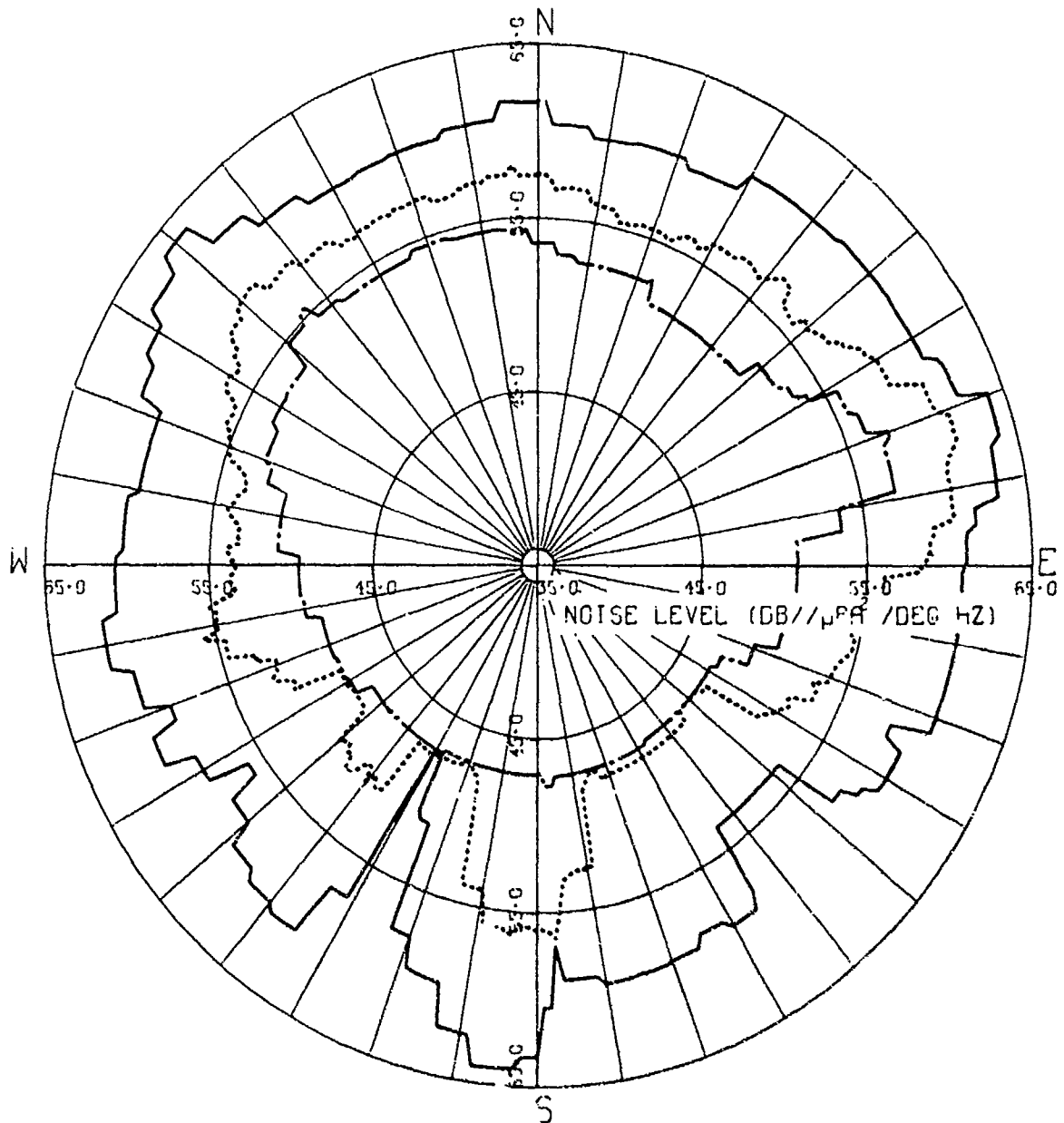


(U) Figure C-2. Horizontal directionality noise roses for a 1/3-octave bandwidth at 100 Hz obtained from TASS polygon 3 data at $\eta=2$. (C)

CONFIDENTIAL

CONFIDENTIAL

HORIZONTAL DIRECTIONALITY



MAB OMNILEVEL - 84.4 dB

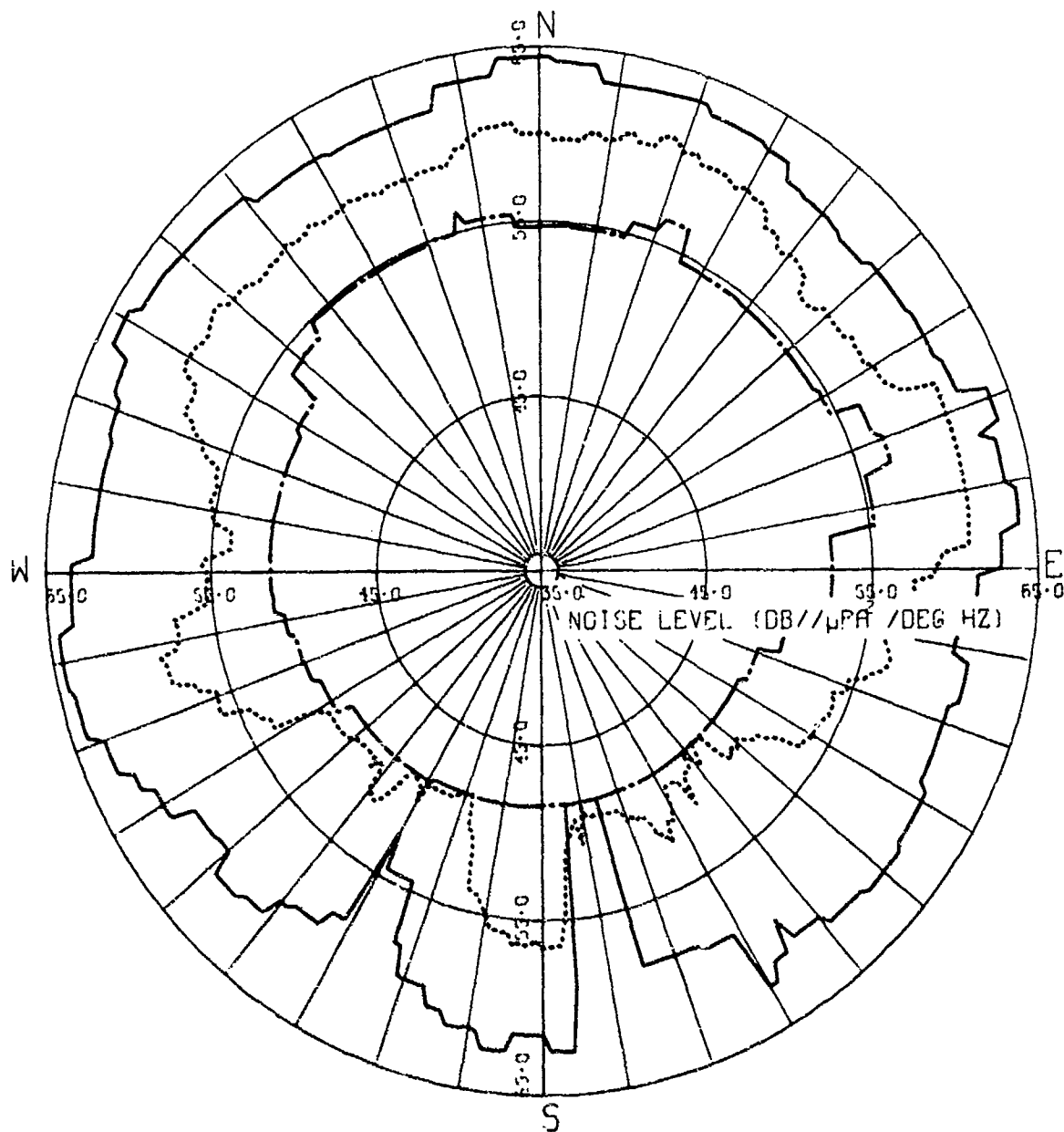
— HI-BAR METHOD
- - - LO-BAR METHOD
..... MAB METHOD

(U) Figure C-3. Horizontal directionality noise roses for a 1/3-octave bandwidth at 50 Hz obtained from TASS polygon 3 data at $\eta=2$. (C)

CONFIDENTIAL

CONFIDENTIAL

HORIZONTAL DIRECTIONALITY



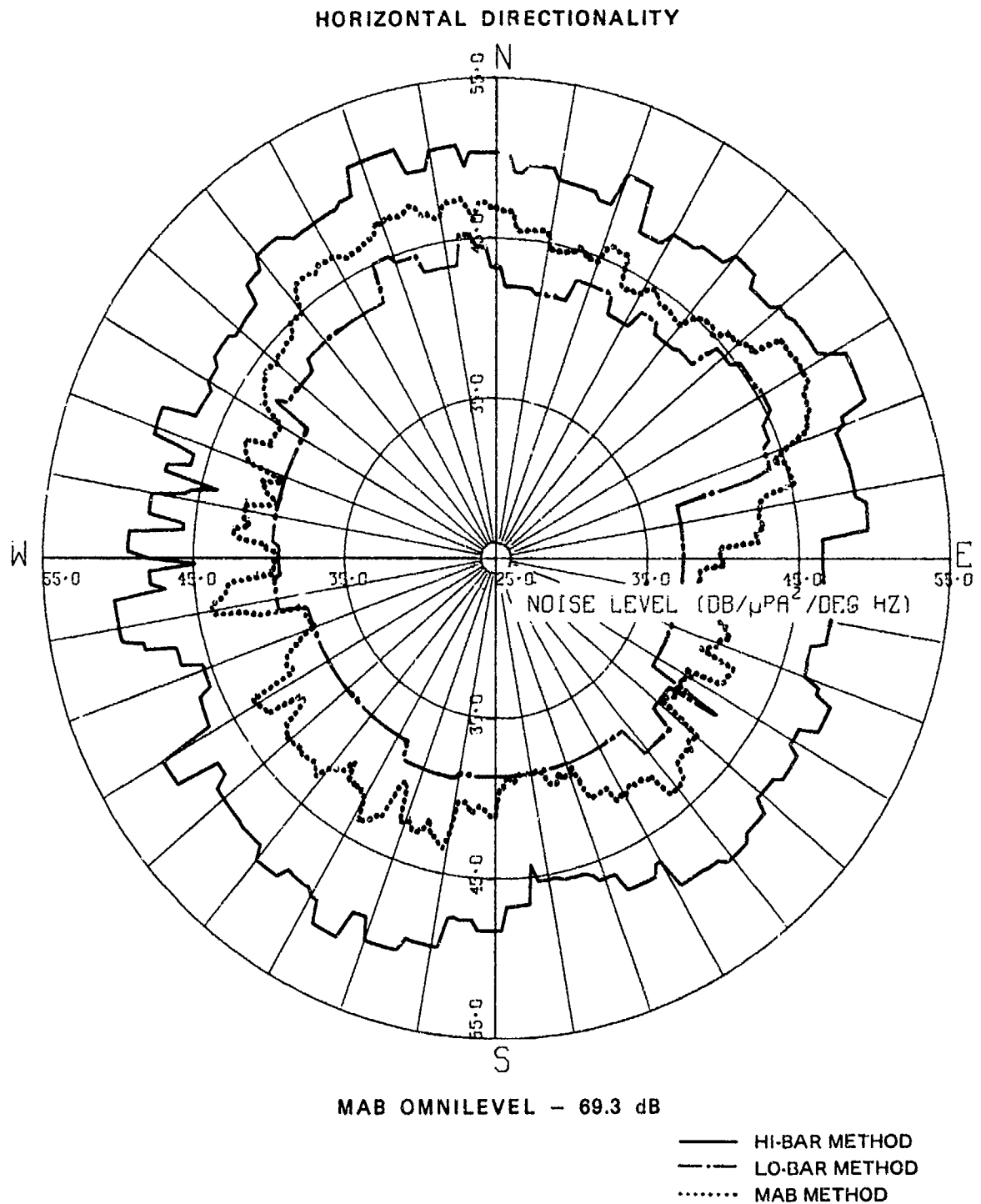
MAB OMNILEVEL - 82.9 dB

— HI-BAR METHOD
- - - LO-BAR METHOD
..... MAB METHOD

(U) Figure C-4. Horizontal directionality noise roses for a 1/3-octave bandwidth at 40 Hz obtained from TASS polygon 3 data at $\eta=2$. (C)

CONFIDENTIAL

CONFIDENTIAL

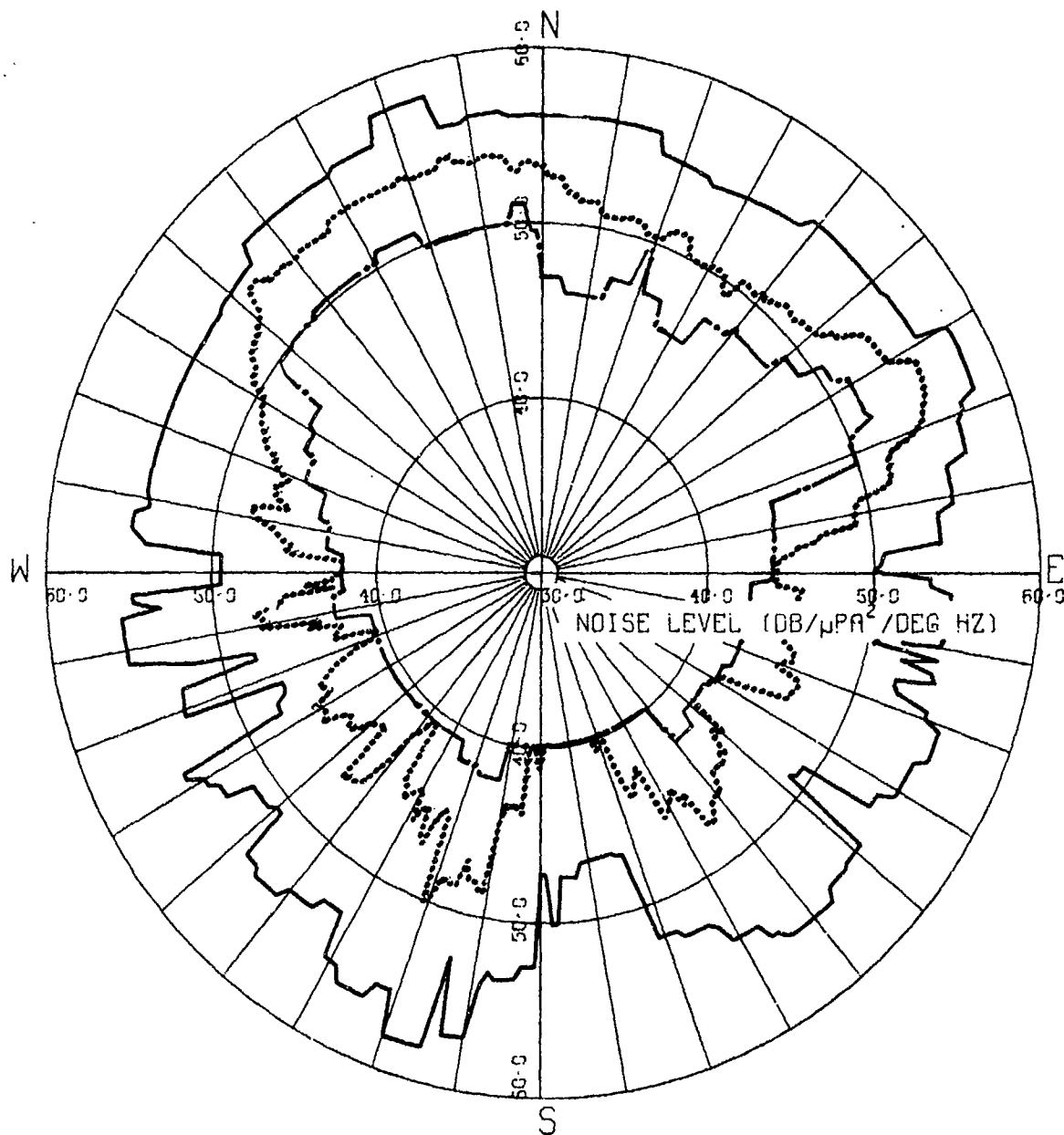


(U) Figure C-5. Horizontal directionality noise roses for a 1/3-octave bandwidth at 160 Hz obtained from TASS polygon 2 data at $\eta=1$. (C)

CONFIDENTIAL

CONFIDENTIAL

HORIZONTAL DIRECTIONALITY



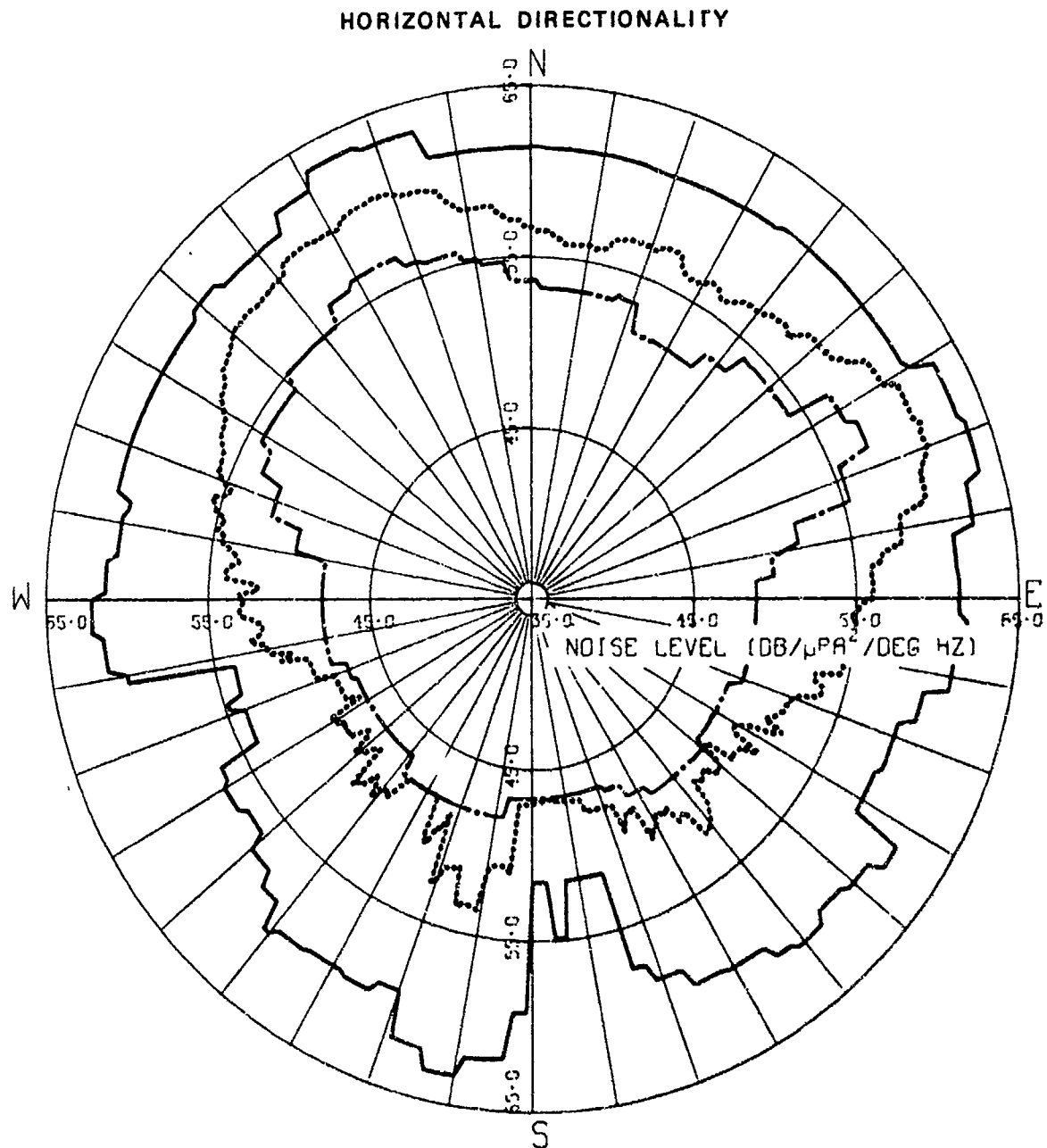
MAB OMNILEVEL - 75.2 dB

— HI-BAR METHOD
- - - LO-BAR METHOD
..... MAB METHOD

(U) Figure C-6. Horizontal directionality noise roses for a 1/3-octave bandwidth at 100 Hz obtained from TASS polygon 2 data at $\eta=1$. (C)

CONFIDENTIAL

CONFIDENTIAL

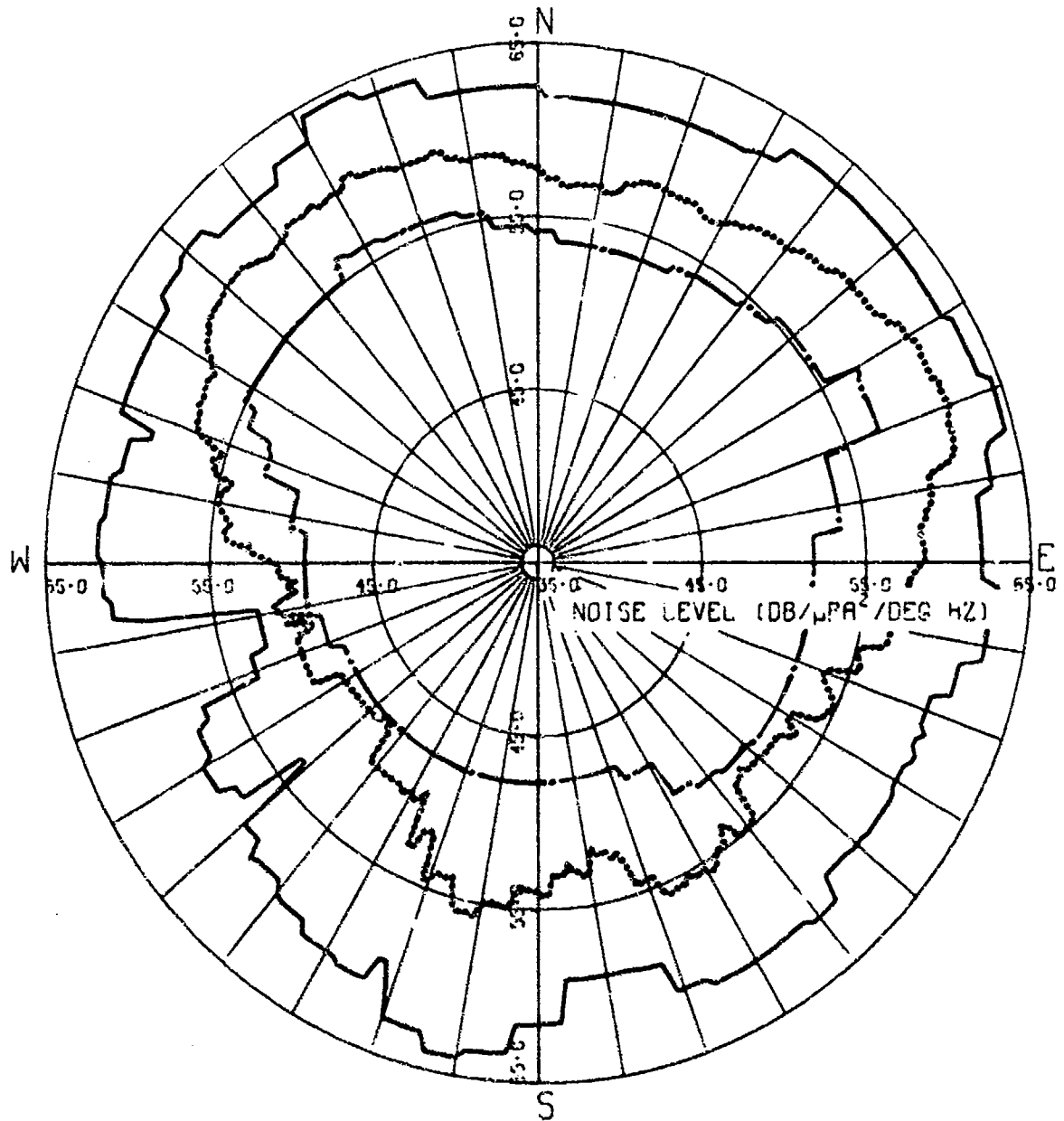


(U) Figure C-7. Horizontal directionality noise roses for a 1/3-octave bandwidth at 50 Hz obtained from TASS polygon 2 data at $\eta=1$. (C)

CONFIDENTIAL

SECRET

HORIZONTAL DIRECTIONALITY



MAB OMNILEVEL - 82.5 dB

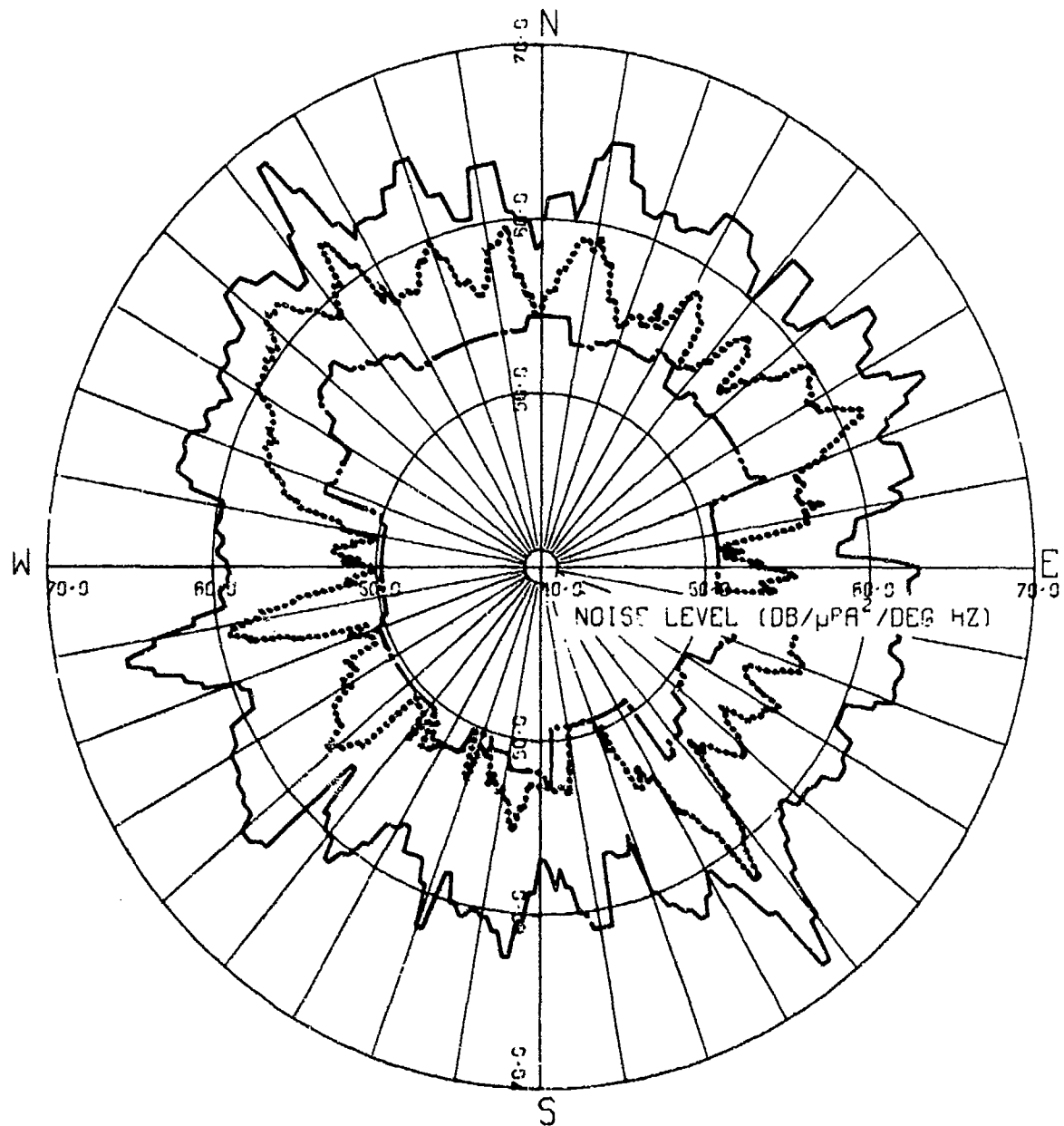
—— HI-BAR METHOD
- - - LO-BAR METHOD
..... MAB METHOD

(U) Figure C-8. Horizontal directionality noise roses for a 1/3-octave bandwidth at 40 Hz obtained from TASS polygon 2 data at $\eta=1$. (C)

SECRET

SECRET

HORIZONTAL DIRECTIONALITY



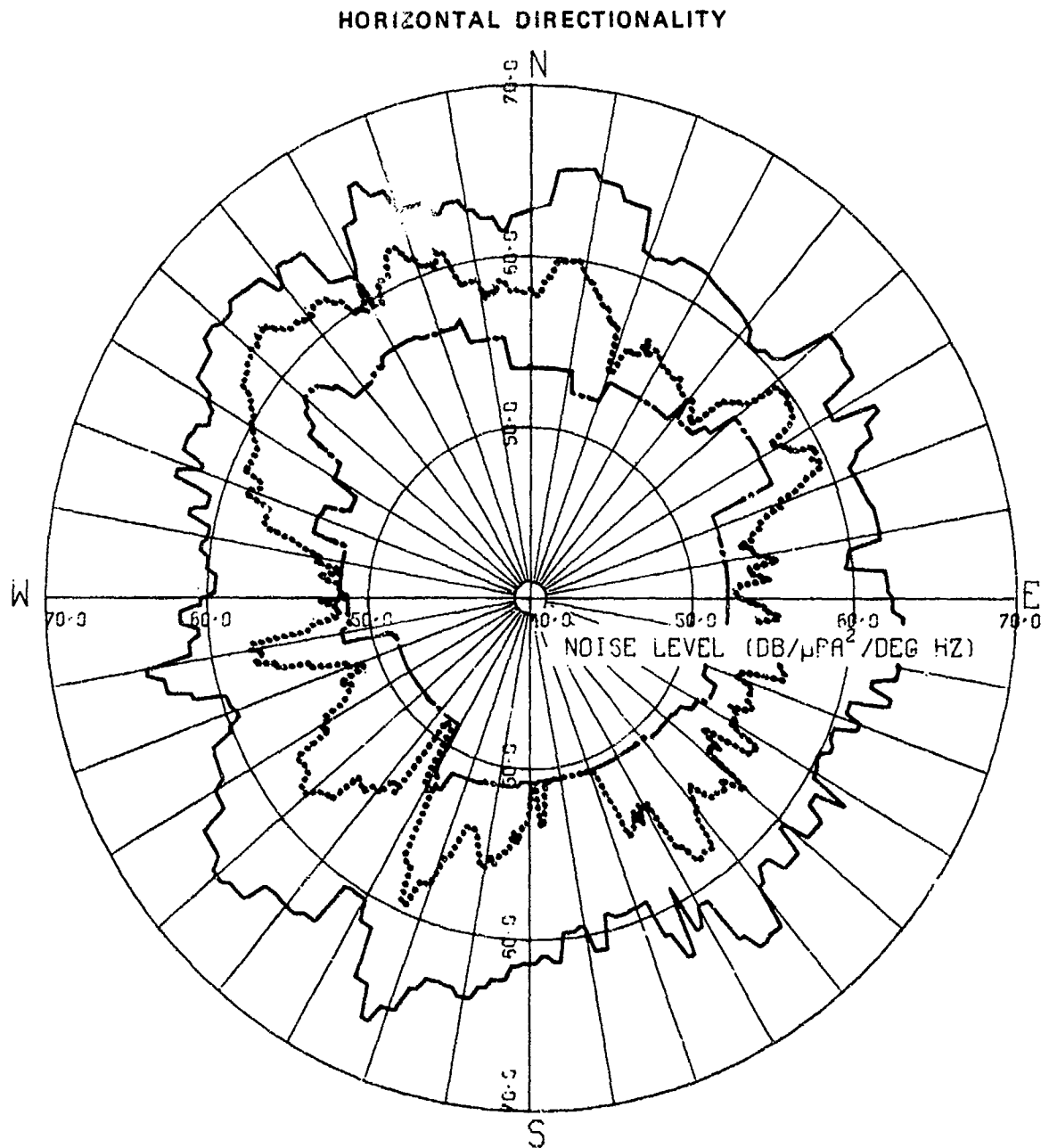
MAB OMNILEVEL - 82.1 dB

— HI-BAR METHOD
- - - LO-BAR METHOD
..... MAB METHOD

(U) Figure C-9. Horizontal directionality noise roses for a 1/8-Hz bandwidth at 36 Hz obtained from LAMBDA polygon 3 data at $\eta=1$. (S)

SECRET

SECRET



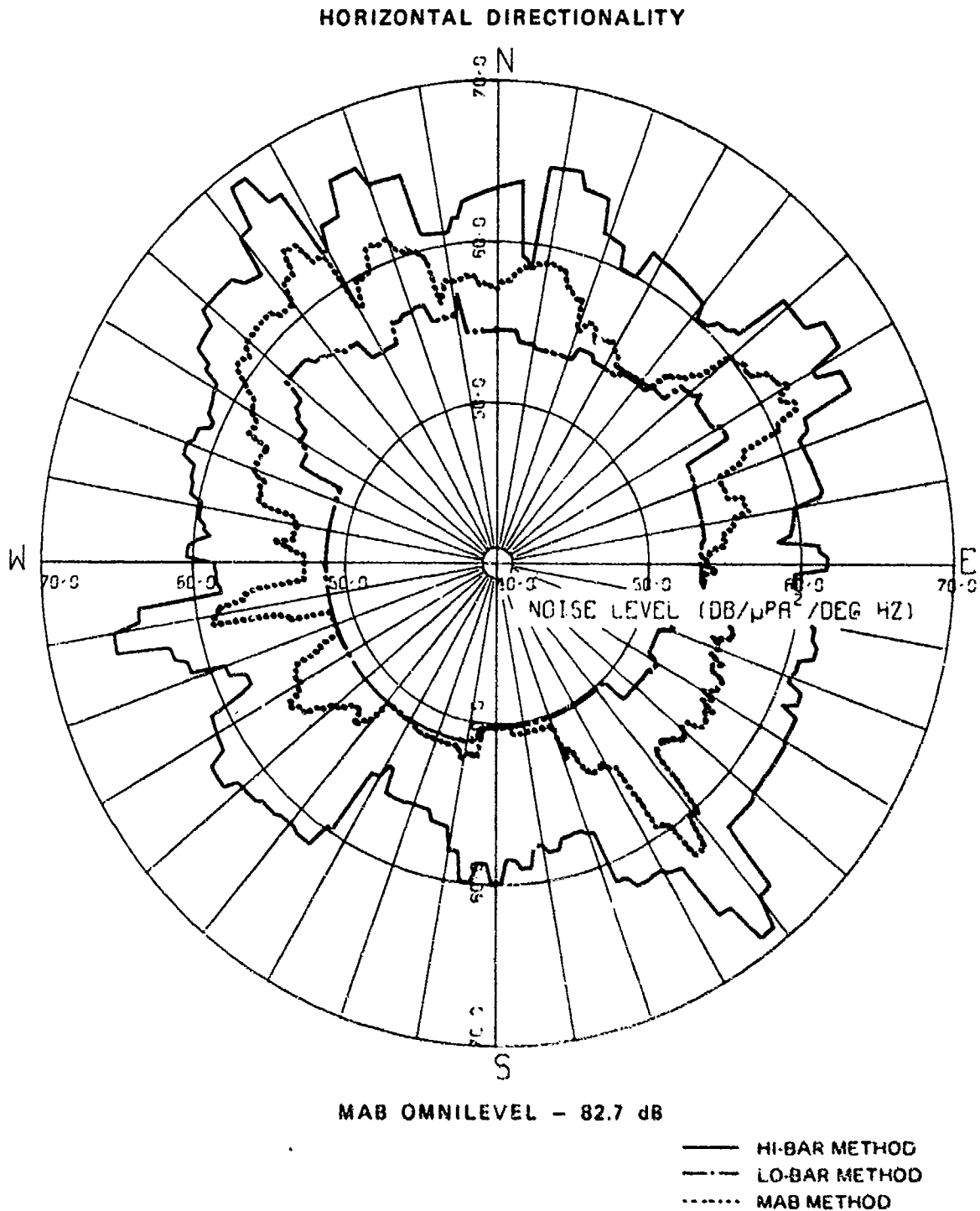
MAB OMNILEVEL - 82.8 dB

— HI-BAR METHOD
- - - LO-BAR METHOD
..... MAB METHOD

(U) Figure C-10. Horizontal directionality noise roses for a 1/8-Hz bandwidth at 29 Hz obtained from LAMBDA polygon 3 data at $\eta=1$. (S)

SECRET

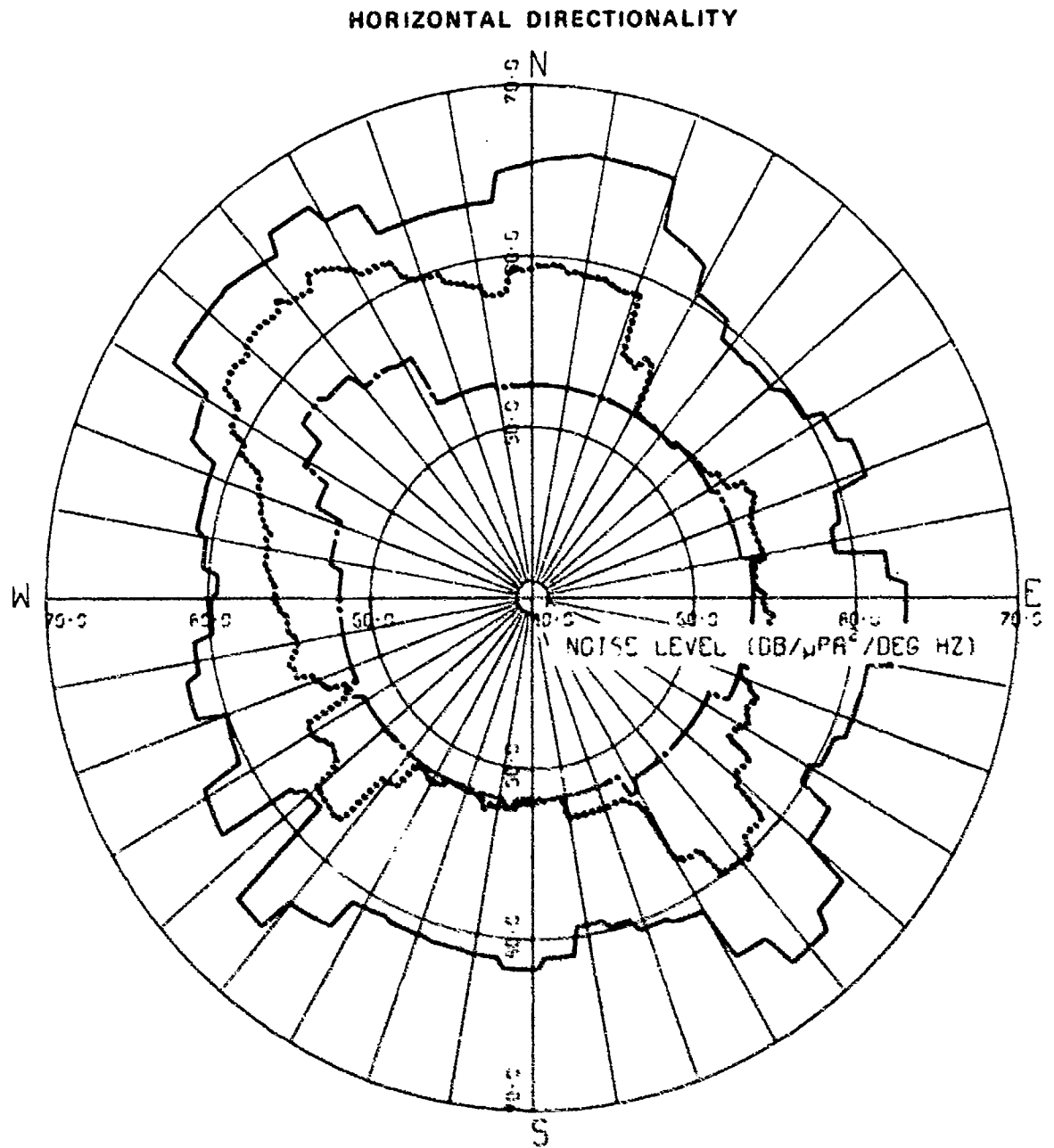
SECRET



(U) Figure C-11. Horizontal directionality noise roses for a 1/8-Hz bandwidth at 23 Hz obtained from LAMBDA polygon 3 data at $\eta=1$. (S)

SECRET

SECRET



MAB OMNILEVEL - 82.9 dB

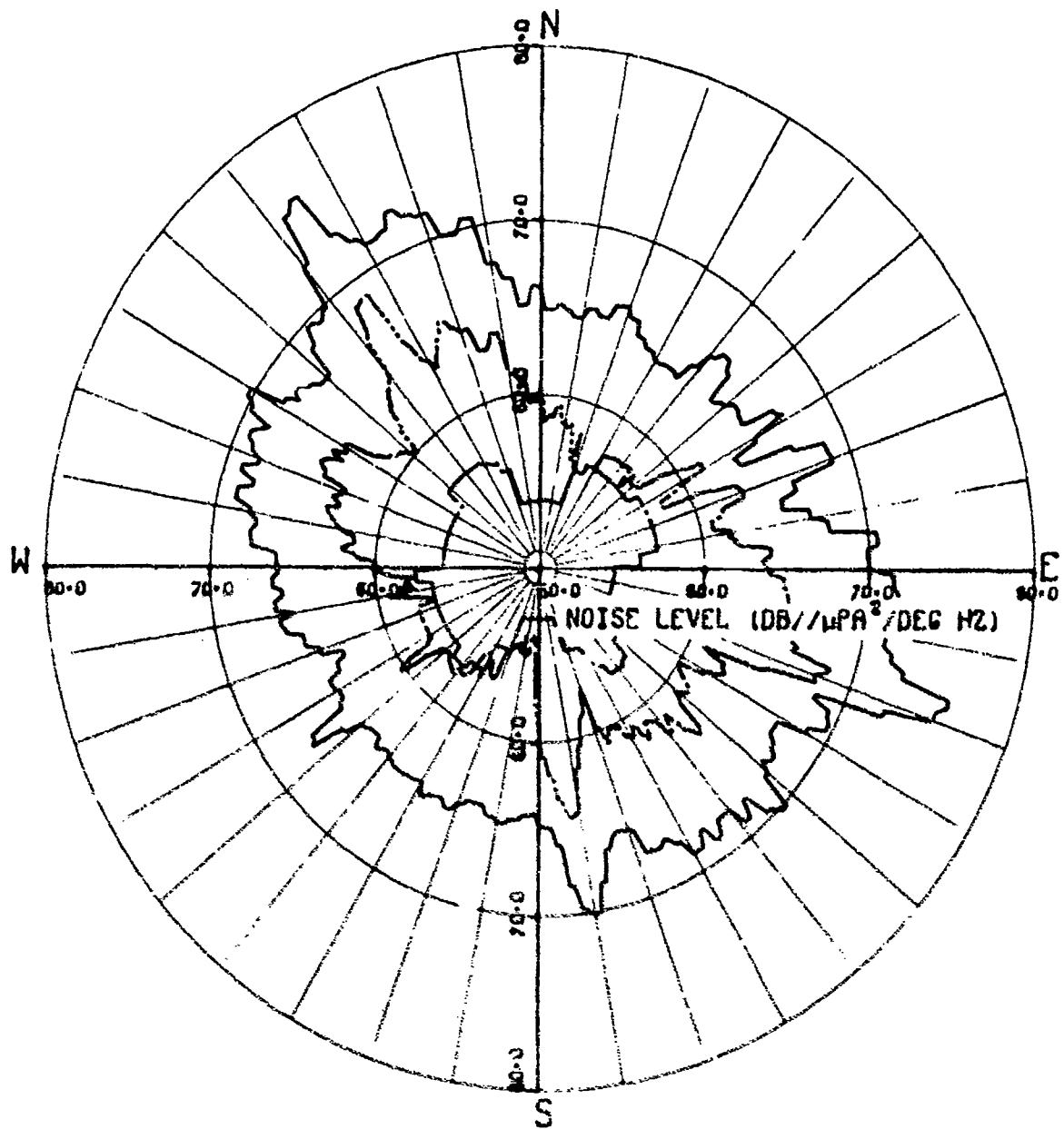
—— HI-BAR METHOD
- - - LO-BAR METHOD
..... MAB METHOD

(U) Figure C-12. Horizontal directionality noise roses for a 1/8-Hz bandwidth at 11 Hz obtained from LAMBDA polygon 3 data at $\eta=1$. (S)

SECRET

SECRET

HORIZONTAL DIRECTIONALITY



MAB OMNILEVEL - 87.2 dB

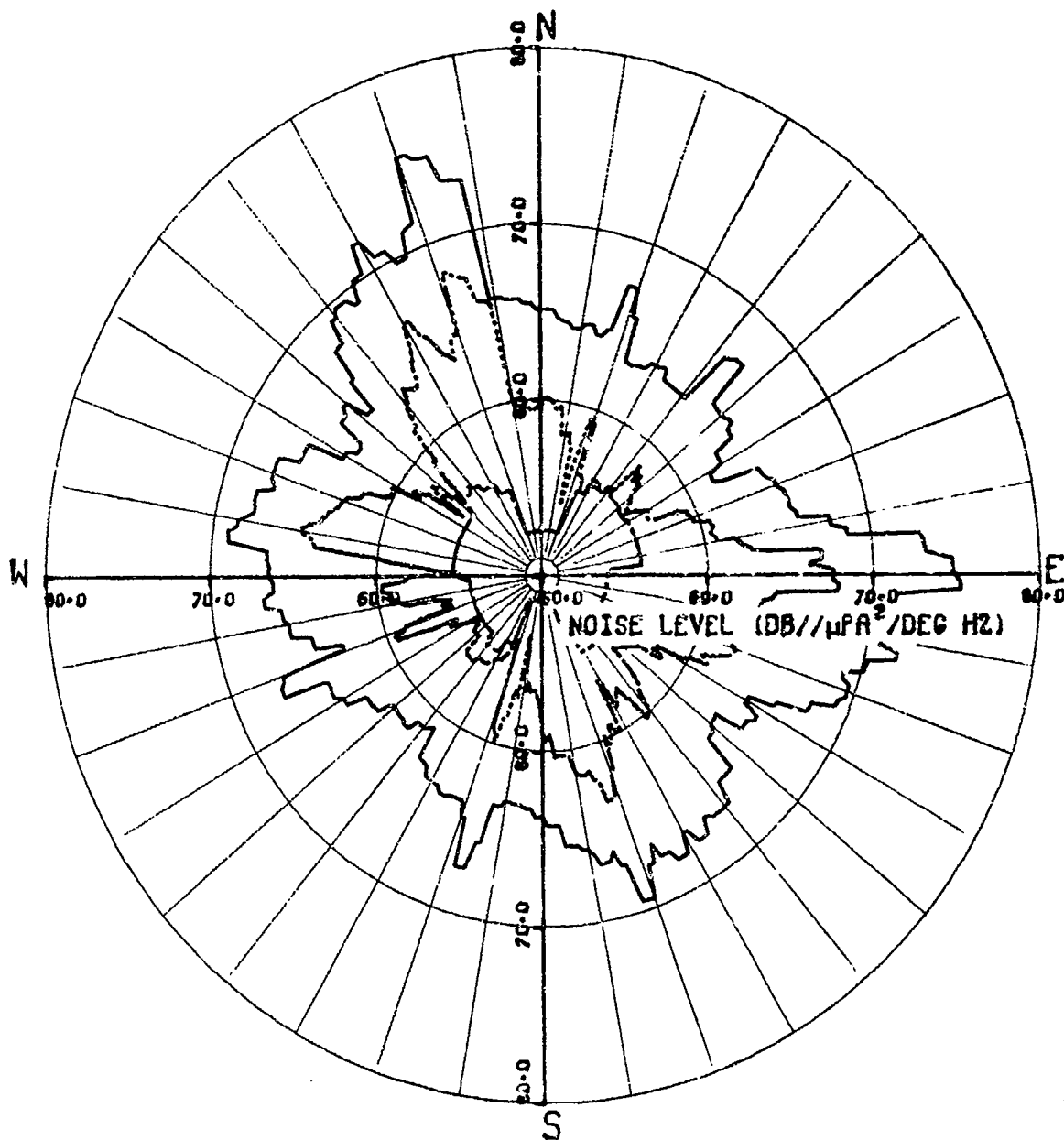
— HI-BAR METHOD
- - - LO-BAR METHOD
... MAB METHOD

(U) Figure C-13. Horizontal directionality noise roses for a 1/8-Hz bandwidth at 36 Hz obtained from LAMBDA polygon 6 data at η-1. (S)

SECRET

SECRET

HORIZONTAL DIRECTIONALITY



MAB OMNILEVEL - 86.4 dB

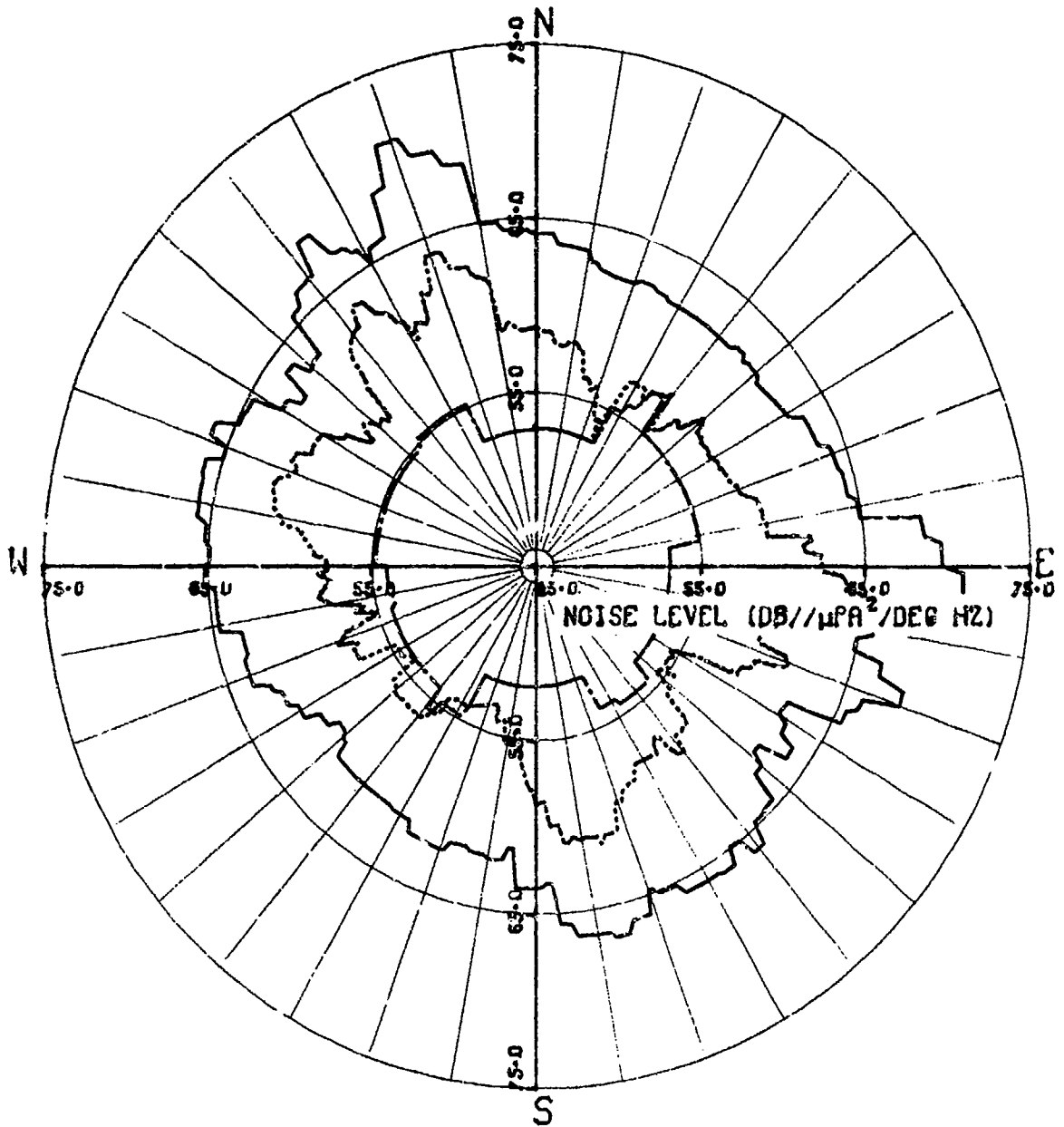
— HI-BAR METHOD
- - - LO-BAR METHOD
..... MAB METHOD

(U) Figure C-14. Horizontal directionality noise roses for a 1/8-Hz bandwidth at 29 Hz obtained from LAMBDA polygon 6 data at $\eta=1$. (S)

SECRET

SECRET

HORIZONTAL DIRECTIONALITY



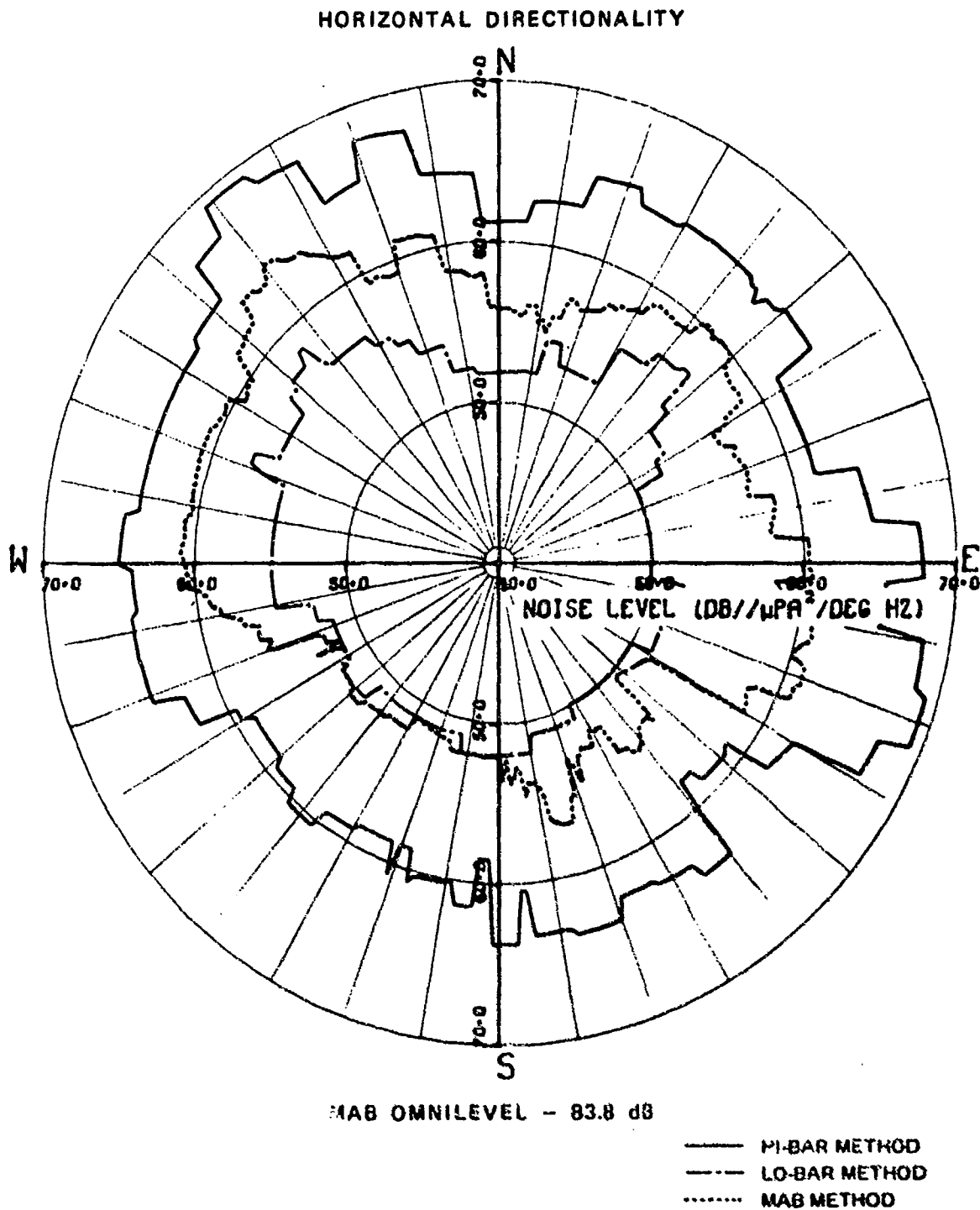
MAB OMNILEVEL - 84.5 dB

— HI-BAR METHOD
- - - LO-BAR METHOD
..... MAB METHOD

(U) Figure C-15. Horizontal directionality noise roses for a 1/8-Hz bandwidth at 23 Hz obtained from LAMBDA polygon 6 data at $\eta=1$. (S)

SECRET

SECRET



(U) Figure C-16. Horizontal directionality noise roses for a 1/8-Hz bandwidth at 11 Hz obtained from LAMBDA polygon 6 data at $\eta=1$. (S)

SECRET

UNCLASSIFIED

APPENDIX D AMBIGUITY-RESOLUTION TECHNIQUES

METHODS

All-Bearings

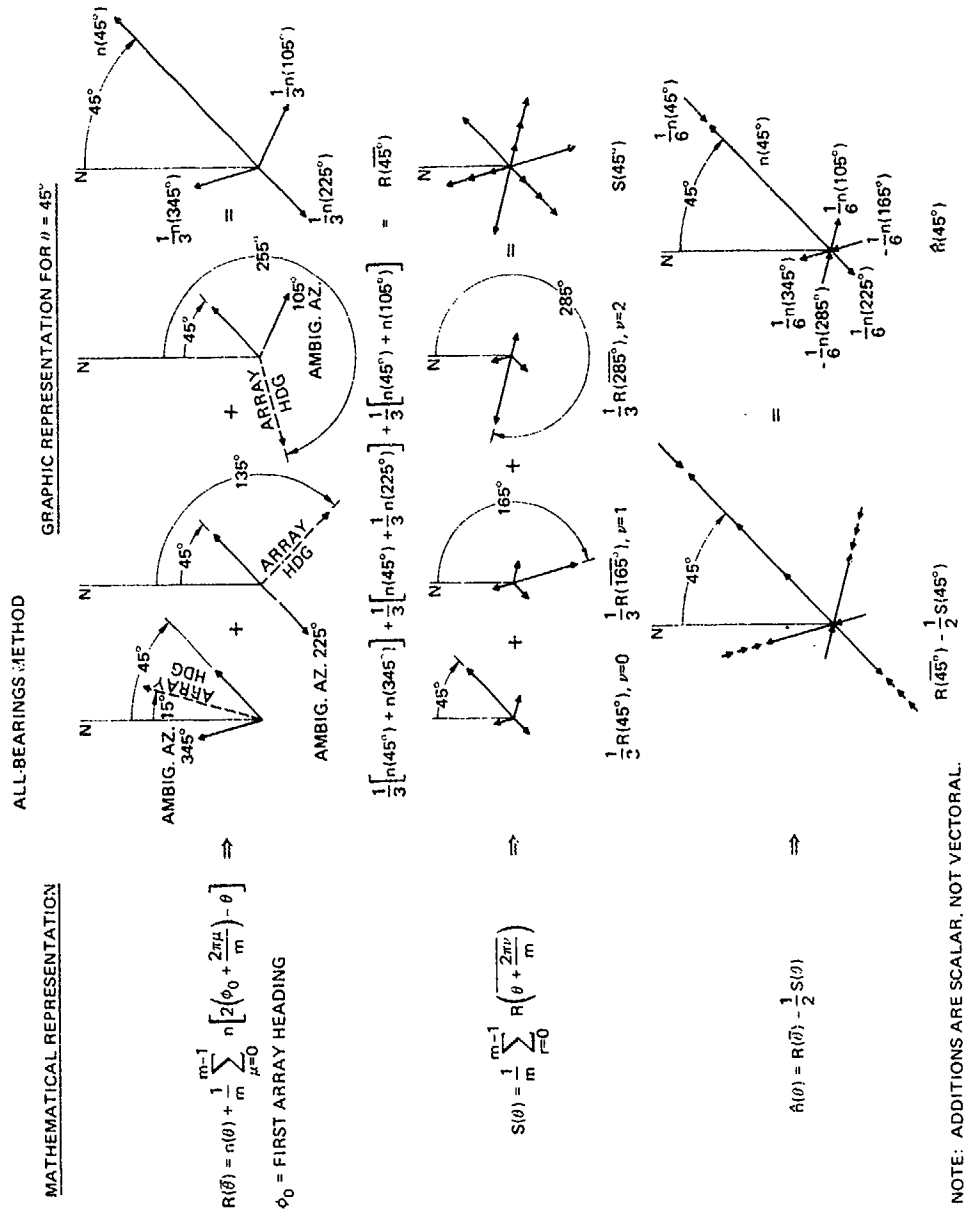
(U) The mathematical formulation and the basic rationale for the All-Bearings method is discussed by Raisbeck in Ref. 3. The extent of the mathematical detail, unfortunately, is an obstacle to the immediate understanding of the method. A more simplified approach to the mathematics presented herein enables the physical significance of the cancellation process to be more easily understood. A more rigorous approach is given by Wagstaff in Ref. 4.

(U) A pictorial representation of the method is given in Fig. D-1 for a three-sided equiangular polygon ($m=3$) with array headings of 15, 135, and 255 deg. The arrows (the length is proportionate to the magnitude and the direction of the arrow denotes the arrival direction of the scalar noise) indicate that the quantity $R(\theta)$ includes all of the noise $n(\theta)$ (normalized to be noise-per-unit beamwidth) in the estimating direction plus $1/3$ the noise, respectively, from three other directions. Three of the medium-length arrows in $R(\theta)$ denote the ambiguous beam contributions. The function $S(\theta)$ is introduced in an attempt to cancel out the noises due to the ambiguous beams. This gives rise to the smallest and additional medium-sized arrows. For example, the noise estimation functions, for the case illustrated, in the direction of $\theta=45$ deg is obtained by the appropriate substitution in the equation for $\hat{n}(\theta)$ and reduced to obtain

$$\hat{n}(45) = n(45) + \frac{1}{6} [-n(45) + n(105) - n(165) + n(225) - n(285) + n(345)] \quad (1)$$

Hence the error in the noise estimation is the term within the brackets of Eq. (1). When this error is more negative than the first term on the right-hand side of Eq. (1) is positive, a negative intensity results. Such an occurrence is not uncommon. If, for example, the noise field has approximately equal noise in the direction of 45, 105, 225, 345, and 165 deg but noise is some 10 dB higher in the direction 285 deg, a negative intensity would be estimated in the direction of 45 deg. In such a case, functions having a period equal to $360/m$ deg (m equals the number of sides of the polygon) are arbitrarily added to the calculated azimuthal directionalities. These functions are of sufficient amplitude to eliminate the negatives without causing additional negative intensities along the other azimuths. The rationale behind such an approach is that the intensity is exactly offset by subtracting an equal intensity from the ambiguous beam. The net change in the total beam output is zero, and the array is incapable of measuring the presence of the added periodic function. The net effect on the directionality, however, is not zero. With sufficiently large negative intensities, the added function can be a major source of error in the reconstructed horizontal directionality pattern.

UNCLASSIFIED



(U) Figure D-1. All-Bearings method mathematical and graphical representation. In the graphical representation the noise is being estimated for an azimuth of 45 deg. Lengths of arrows are proportional to the percentage of the noise along the array azimuth being used to estimate the noise along 45 deg. (U)

UNCLASSIFIED

Bearing Ambiguity Resolution (BAR)

(U) The BAR method, illustrated in Fig. D-2, utilizes normalized (noise-per-unit beamwidth) beam outputs while the array is towed in at least three different directions. Each output is a measure of the noise arriving from a common direction and from the directions of the three ambiguous beams. The noise arriving from the common direction is assumed to be the lowest of the three measured levels when more than 4 dB above the mean level along all azimuths. The value of 4 dB is arbitrarily chosen to represent the level above which the beam output is assumed to be dominated by the noise in the given direction, with the ambiguous direction having no significant effects. If this condition is not met, the ambiguous direction is assumed to contribute equally, and the lowest level minus 3 dB ($10 \log 2$) is assigned the noise coming from the common direction. This process is repeated for all azimuths to complete the assessment of the horizontal directionality.

(U) Consider the example in Fig. D-2. Suppose a noise of 80 dB is arriving from the common direction with negligible contribution from the ambiguous directions. Also, suppose that the three beams pointed along the common direction have beamwidths of 4, 5.6, and 10 deg. Then the normalized levels per azimuthal degree would be 74, 72.5, and 70 dB, respectively. The per-degree level for noise in the common direction obtained by the BAR method would be either 70 dB or 70 minus 3 dB. The 3 dB subtraction would occur if 70 dB was more than the arbitrary limit of 4 dB below the mean of all the beam outputs. The noise would then be assumed to originate equally from both sides of the array. Hence, the accepted noise on the beam originating from the direction of interest would be 67 dB ($70 - 3$ dB). There is no provision for the highest normalized level (74 dB) to be accepted even though it may be a more realistic estimate of the noise in the given direction. This is a major source of error in the BAR method.

Modified All-Bearings (MAB)

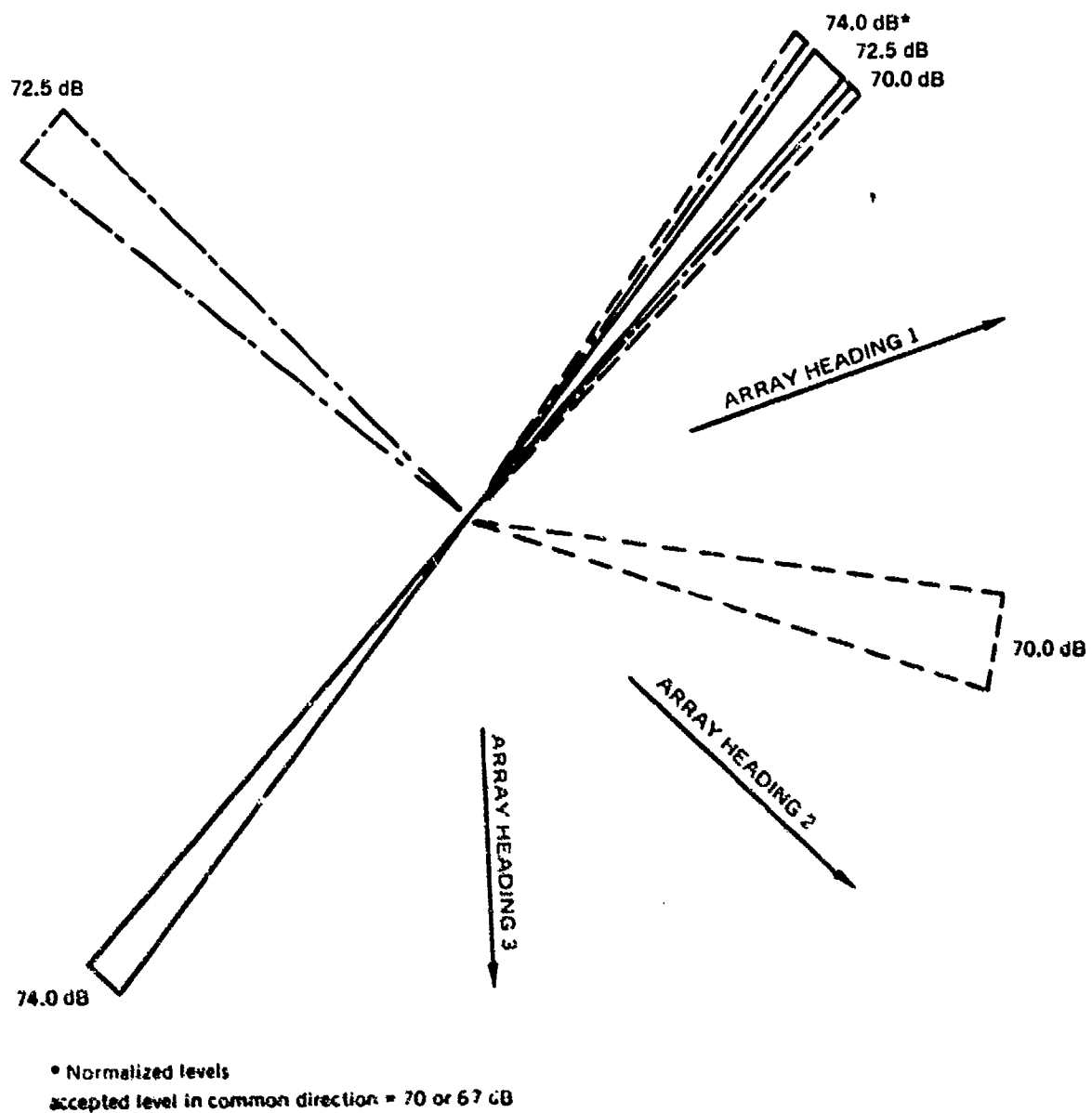
(U) This method is a combination of the previous two methods. It selects the maximum of the All-Bearings and the BAR methods for any given azimuth. This union overcomes the negative power problem of the All-Bearings method by the substitution of a measured value for the negative intensity and the replacement of low noise levels along some azimuths by higher levels which may be more indicative of the average for the measurement time period.

HIBAR

(U) The HIBAR method is nearly identical to the BAR method, but instead of the lowest value being retained for the noise assessment along a given azimuth, the highest value is retained.

UNCLASSIFIED

UNCLASSIFIED



(U) Figure D-2. BAR method (reprinted from Ref. 4).

UNCLASSIFIED

SECRET

(U) This method is designed to provide information concerning transient point sources and to provide an upper bound for the normalized data.

LOBAR

(U) In contrast with the previous method, this one selects the lowest value measured along any one azimuth during the noise measurements. In this approach, it is assumed that equal amounts of noise energy are received by the array from the direction of a given beam axis as well as its ambiguous counterpart. Hence, 3 dB is subtracted from all normalized beam data, and the lowest value obtained for any one azimuth for all legs of a polygon is selected. The 4-dB criterion utilized in the BAR method is not used in the LOBAR approach. This method provides a lower bound for the normalized data.

Hansen-Woodyard Endfire Beam

(U) The Hansen-Woodyard endfire beam (Ref. 2) analysis yields an unambiguous assessment of the noise field without the need for ambiguity algorithms, since the endfire beams are unambiguous. However, the resulting horizontal directionality is sensitive to array orientation when the noise field is nonstationary and the sample size is small.

EFFECT OF TRANSIENTS ON RESOLUTION TECHNIQUES

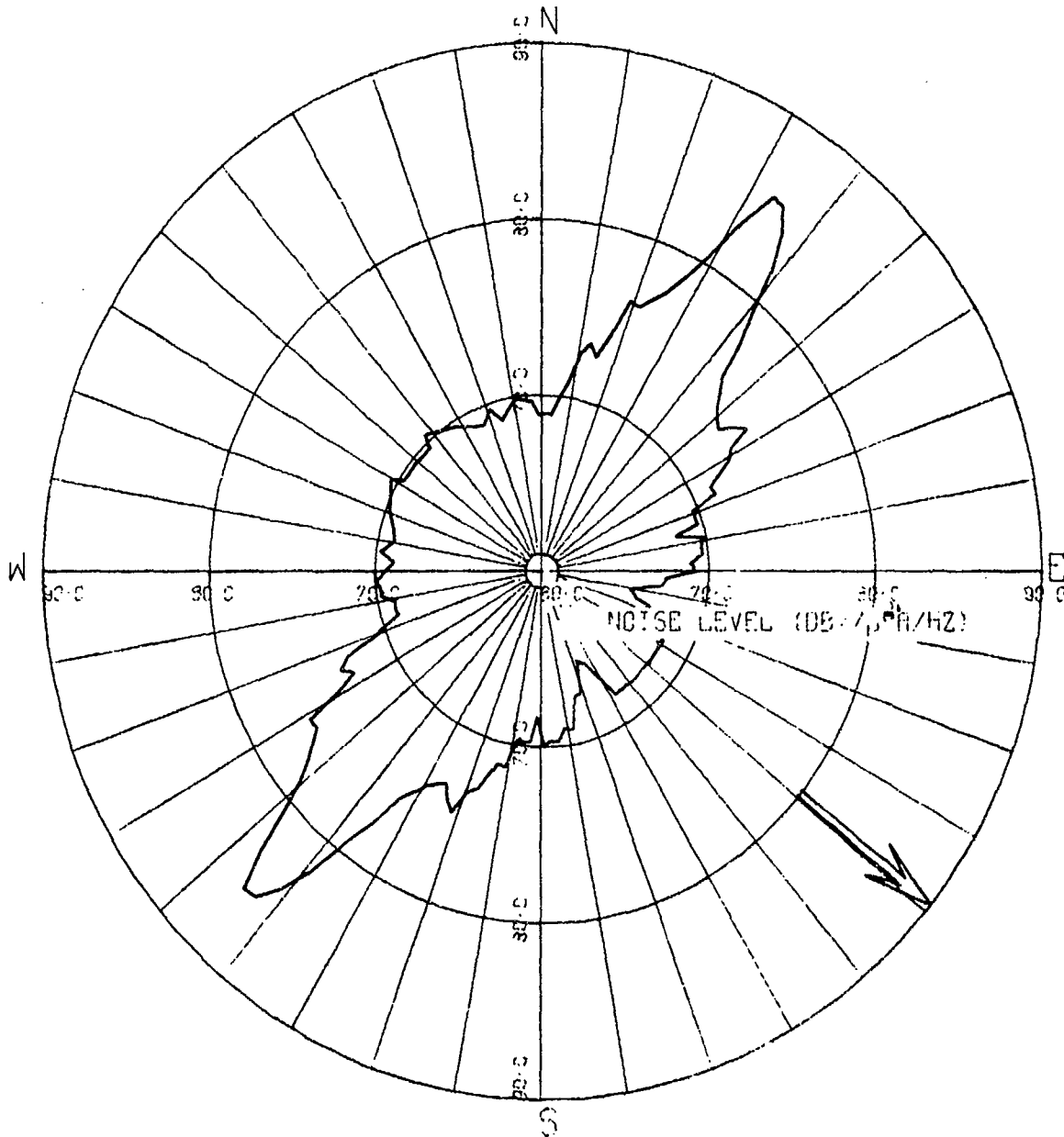
(U) Of the various methods used to obtain the horizontal directionality of the noise field, the two most affected by nonstationarity are the endfire beam and the MAB (and hence the All-Bearings to a greater degree) methods.

(C) The difficulties in the endfire method have been overcome by taking many data samples over the duration of three or four polygons in order to average out the nonstationary effects. In the MAB method, however, the solution is not as easily obtained. The nature of the method is such that high-level transients can bias the directionalities by causing angular regions of abnormally low or negative intensities, while simultaneously causing other areas to have abnormally large intensities. Consider, for example, the LAMBDA beam response plots for the first polygon at $\eta = 1$. These are included as Figs. D-3 through D-7. There is a strong source evident in the first leg which appears on the broadside beam. This source is not evident, however, on the other four legs. Hence, in some type of average assessment of the horizontal directionality of the noise as arrived at from these five legs, the first leg would, it is hoped, have only a minimal influence on the final pattern, since the other four legs are reasonably similar in shape.

SECRET

SECRET

BEAM RESPONSE DATA



OMNILEVEL - 90.89 dB

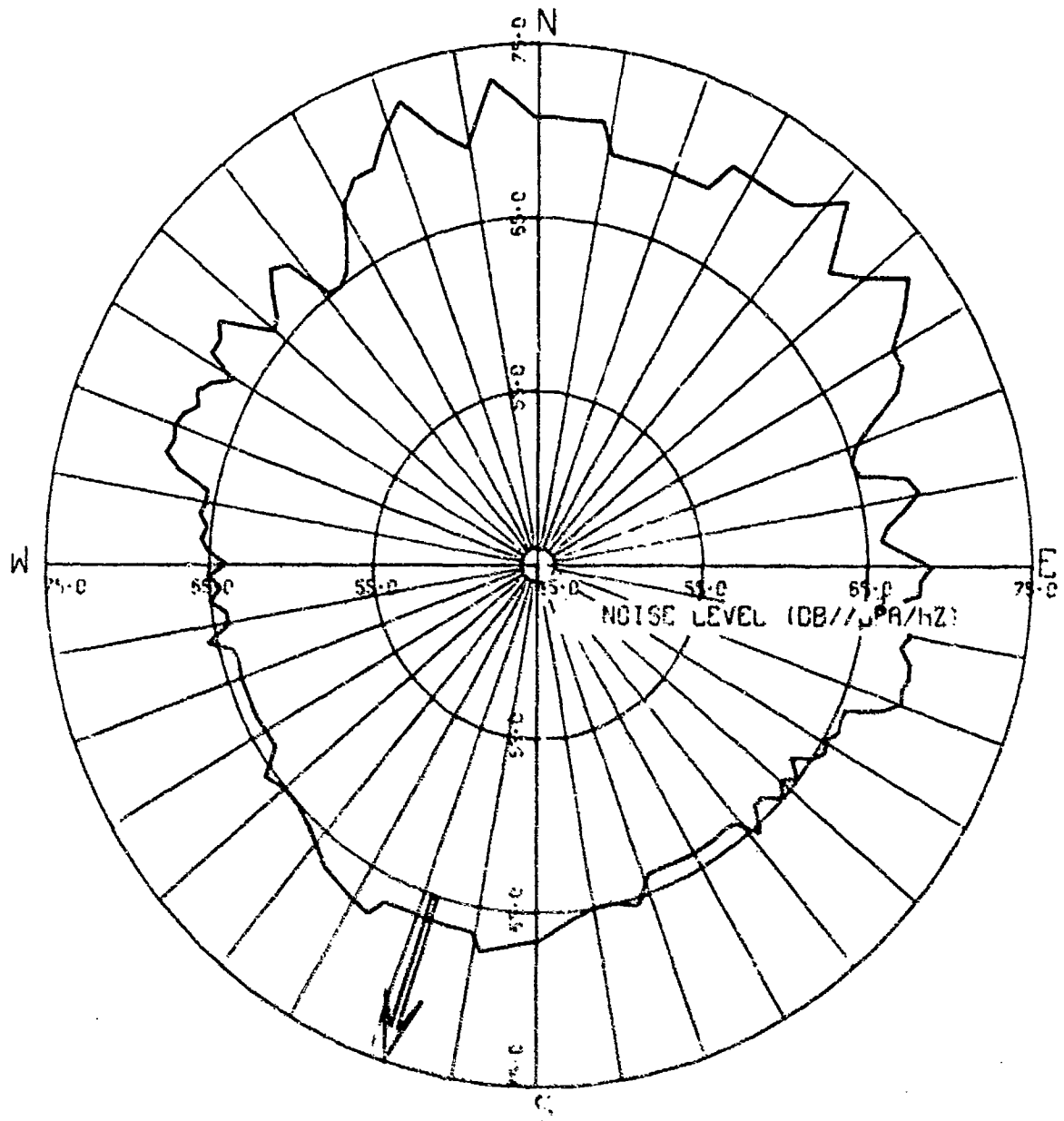
POLYGON 3, 36 Hz, LEG 1, 129 DEG BEARING

(U) Figure D-3. Beam response data for LAMBDA
polygon 3, leg 1, 36-Hz at station η -1. (S)

SECRET

SECRET

BEAM RESPONSE DATA



OMNILEVEL ~ 82.46 dB

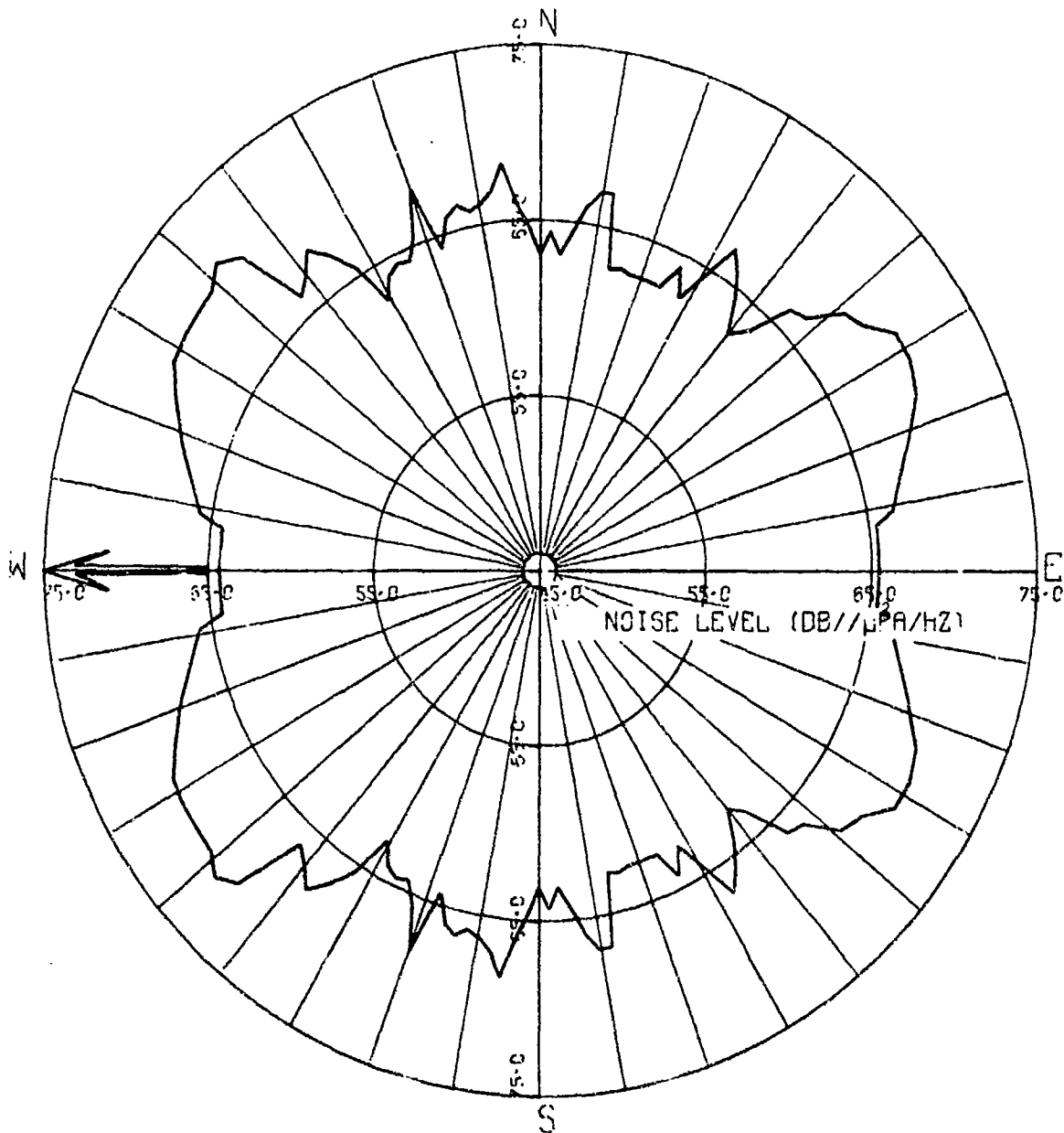
POLYGON 3, 36 Hz, LEG 2, 198 DEG BEARING

(U) Figure D-4. Beam response data for LAMBDA
polygon 3, leg 2, 36-Hz at station η-1. (S)

SECRET

SECRET

BEAM RESPONSE DATA



OMNILEVEL - 81.77 dB

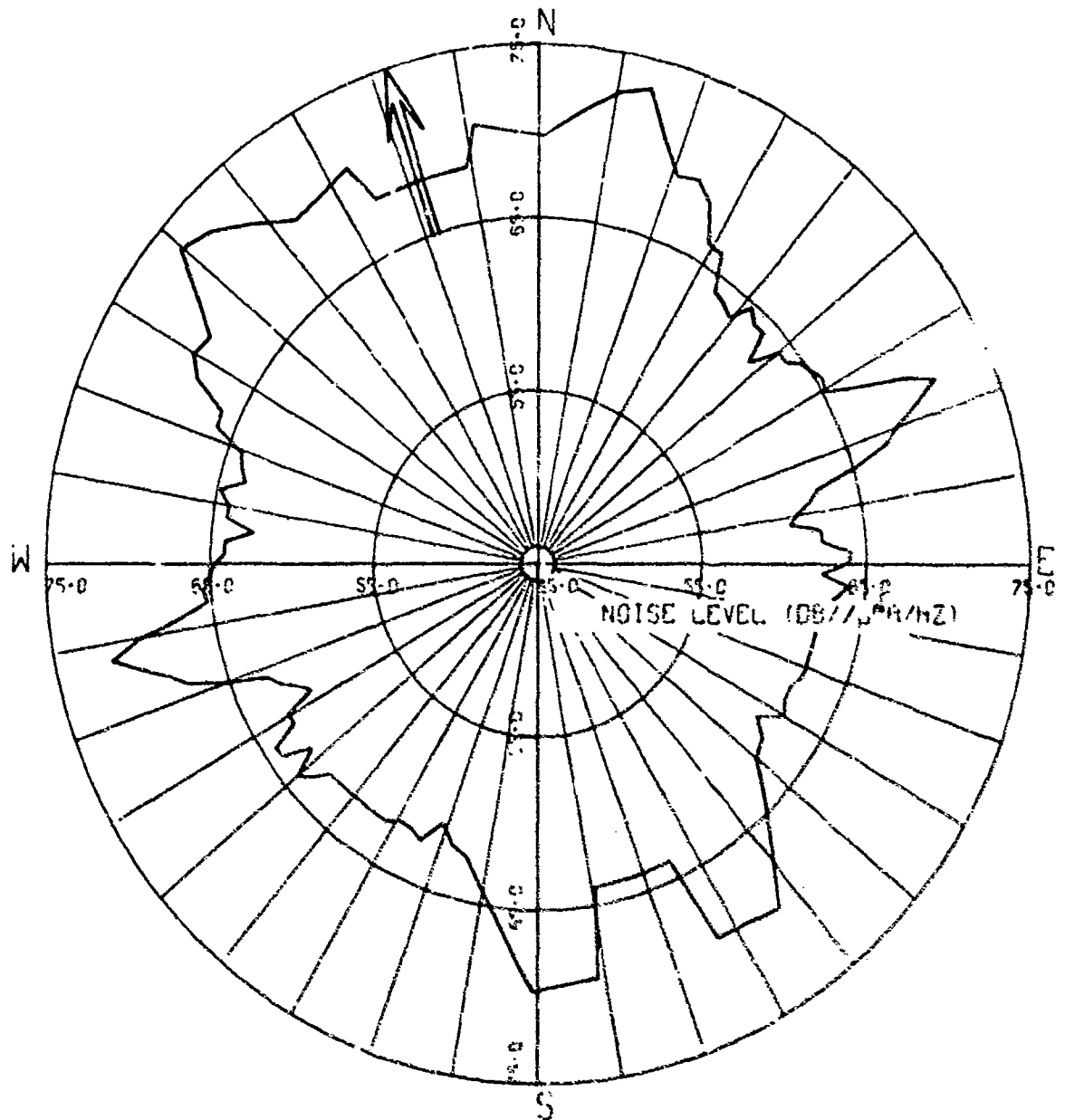
POLYGON 3, 36 Hz, LEG 3, 270 DEG BEARING

(U) Figure D-5. Beam response data for LAMBDA
polygon 3, leg 3, 36-Hz at station η-1. (S)

SECRET

SECRET

BEAM RESPONSE DATA



OMNILEVEL - 81.55 dB

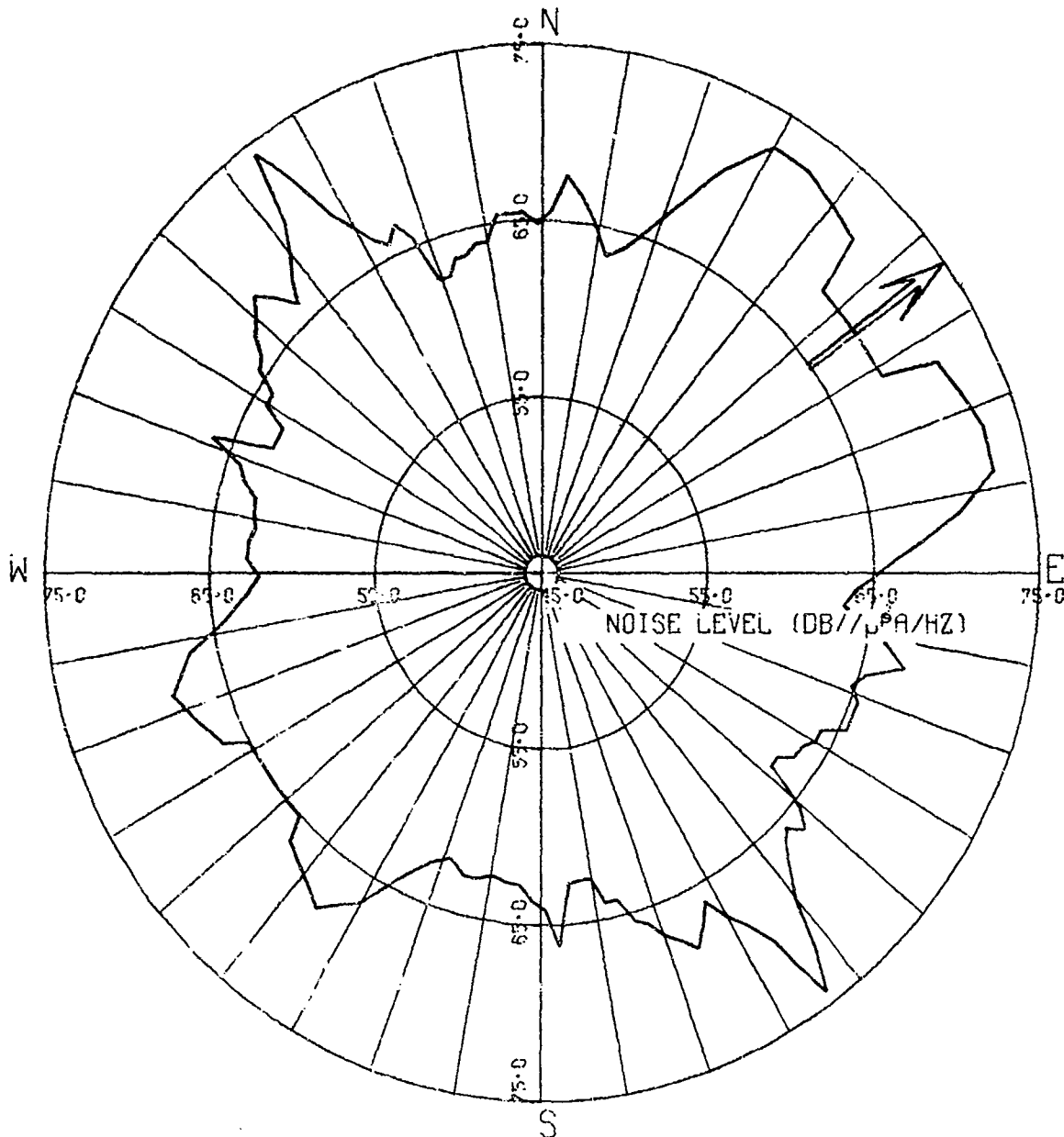
POLYGON 3, 36 Hz, LEG 4, 342 DEG BEARING

(U) Figure D-6. Beam response data for LAMBDA
polygon 3, leg 4, 36-Hz at station η-1. (S)

SECRET

SECRET

BEAM RESPONSE DATA



OMNILEVEL - 82.00 dB

POLYGON 3, 36 Hz, LEG 5, 54 DEG BEARING

(U) Figure D-7. Beam response data for LAMBDA
polygon 3, leg 5, 36-Hz at station η-1. (S)

SECRET

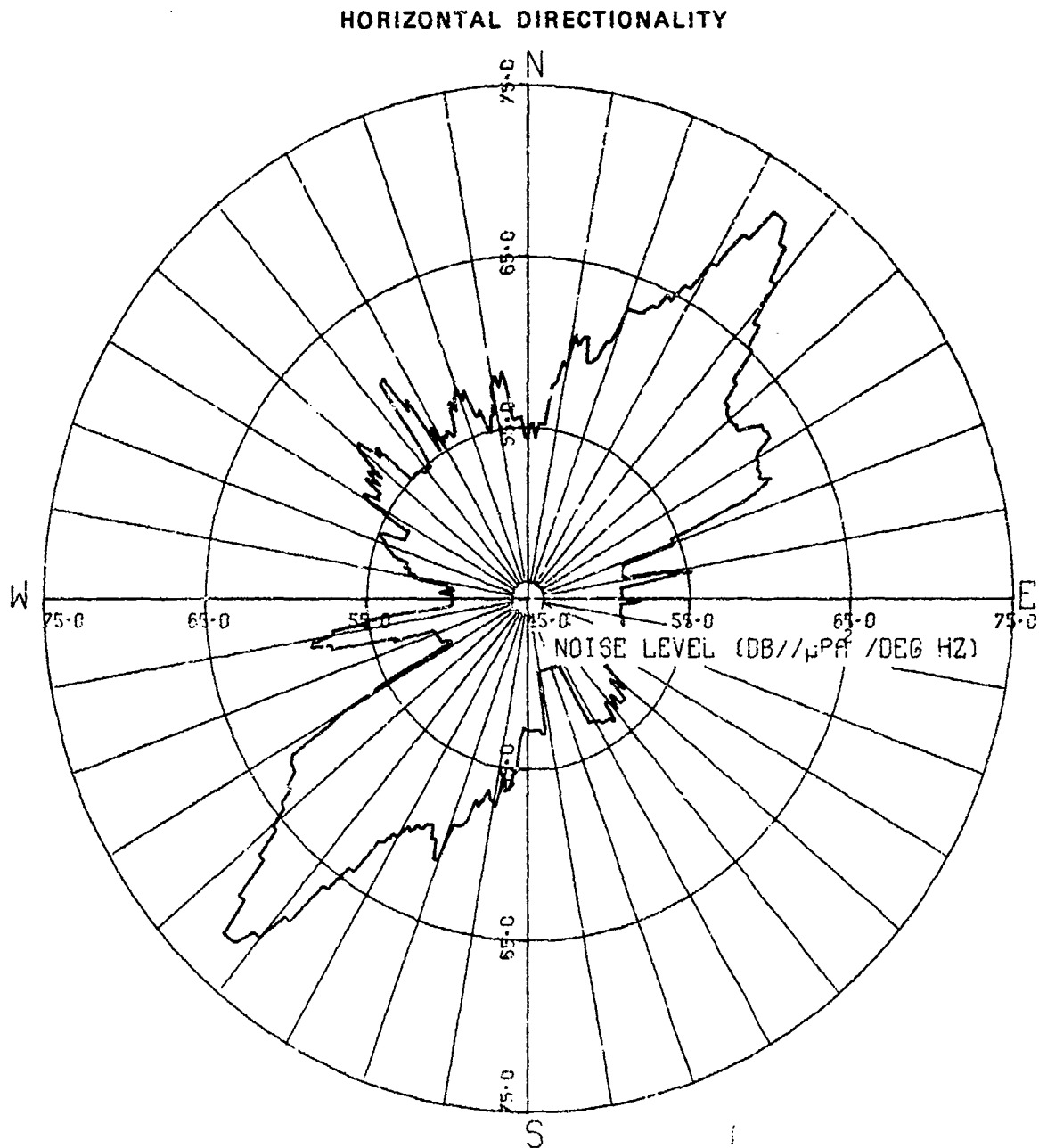
SECRET

(C) Figure D-8 gives the resulting noise field directionality. When this directionality is compared with the ambiguous beam response data of the first leg, Fig. D-3, it is obvious that the ambiguity has not been resolved. When the first leg is omitted from the ambiguity resolution process and only the remaining four are used, the result in Fig. D-9 is obtained. The differences between Figs. D-8 and D-9 are striking. Conclusions drawn from each of these two figures regarding the noise field directionality characteristics would no doubt be radically different.

(U) In the above example the first leg was easily recognized as being contaminated by a transient. However, this same situation occurs on a smaller scale in all of the data processed by the All-Bearings and MAB methods. The transients which do not dominate the data cannot be as easily recognized and removed. Therefore, they remain to become sources of abnormally low or high levels of noise in the final result.

SECRET

SECRET



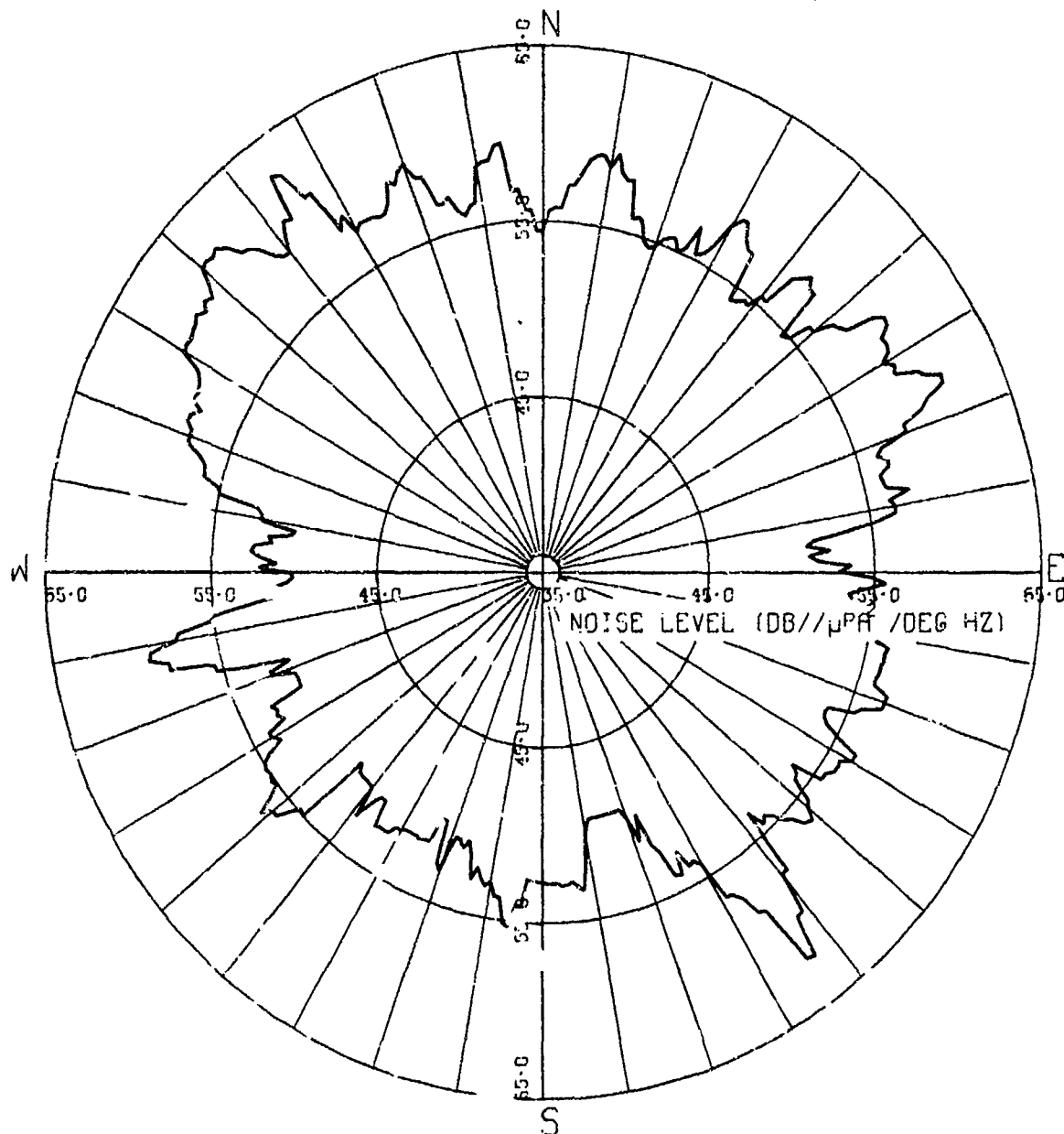
OMNILEVEL - 86.6 dB
POLYGON 3, 5 SIDES, 36 Hz

(U) Figure D-8. MAB horizontal directionality assessment of 36-Hz ambient noise obtained by using beam response data for all five legs of LAMBDA polygon 3 at η -1. (S)

SECRET

SECRET

HORIZONTAL DIRECTIONALITY



OMNILEVEL - 82.1 dB

POLYGON 3, 4 SIDES, 36 Hz

(U) Figure D-9. MAB horizontal directionality assessment of 36-Hz ambient noise obtained by using only beam response data for legs 2 through 5 of LAMBDA polygon 3 at $\eta-1$. (S)

SECRET

CONFIDENTIAL

**APPENDIX E
ENVIRONMENTAL DATA FOR CHURCH ANCHOR EXERCISE AREA**

(C) Table E-1 contains wind and wave data for times during the ambient noise horizontal directionality measurements. These data were taken at the positions of the PACIFIC APOLLO (LAMBDA array) and are assumed to be representative of the conditions at the USNS S. P. LEE (TASS array) location. Figure E-1 presents sound-speed-versus-depth information for locations along a north-south track through the CHURCH ANCHOR area. More complete environmental, bathymetric, acoustic, and shipping data can be obtained from the publications of the participants as prescribed by Refs. 6, 19, and 20.

CONFIDENTIAL

CONFIDENTIAL

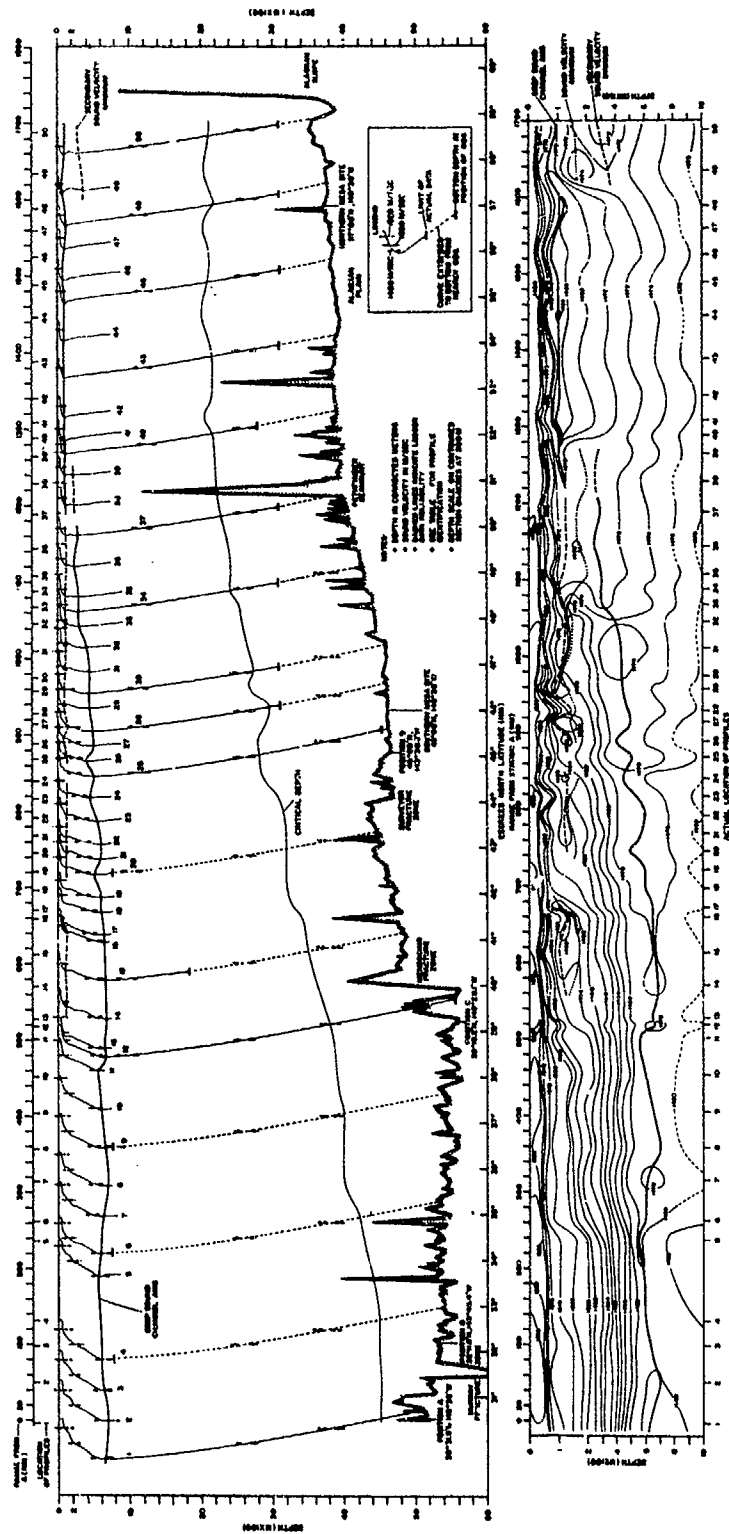
(U) Table E1. Environmental data summary, CHURCH ANCHOR exercise area. * (U)

Time (Z)	Date (September 1973)	Position		Wind		Wave Height, ft	Swell	
		N Lat	W Long.	Dir Deg True	Speed, kt		Dir Deg True	Height ft
1500	2nd	38° 30'	143° 0'	260	7	0.5	270	5
2100	2nd	38° 27'	143° 43'	280	10	1.0	310	5
0300	3rd	38° 30'	143° 32'	280	10	1.5	290	5
0900	3rd	38° 31'	143° 30'	250	5	0.5	290	3
0300	9th	31° 10'	143° 50'	90	10 to 12	2.0	105	4
0900	9th	31° 18'	143° 47'	90	12	2.0	90	4
1500	9th	31° 17'	143° 57'	70	5	1.0	80	3
2100	9th	31° 18'	143° 40'	315	5 to 7	1.0	315	3
0300	20th	31° 08'	143° 37'	000	7 to 10	1.5	330	5
0900	20th	31° 18'	143° 46'	20	7 to 10	1.5	330	5
1500	20th	31° 07'	143° 46'	20	7 to 10	1.0	330	4
2100	20th	31° 13'	143° 48'	50	7 to 10	1.0	330	4

*Measurements from PACIFIC APOLLO

CONFIDENTIAL

UNCLASSIFIED



(U) Figure E-1. Sound-speed structure in the CHURCH ANCHOR exercise area. (U)

UNCLASSIFIED

SECRET

APPENDIX F DATA QUALITY AND ANALYSIS ERRORS

(U) There are at least three major categories into which the errors accrued during the measurement and analysis process may be grouped. The first category, which will not be discussed in this section, includes all hardware-dependent errors, such as variations in hydrophone sensitivity, calibration errors, and perhaps self-noise, or flow-noise in the case of towed arrays. These are discussed in Appendices A and B. The two error categories which will be discussed here include errors which enter when determining horizontal arrival angles and the errors which are introduced when sets of beam response power levels from a line-array are combined by one means or another to obtain an estimate of the horizontal directionality of the noise field.

BEAM RESPONSE DATA

(C) There are four main types of errors encountered when determining horizontal arrival angles for the beam response data. The first is due to the angular nature of both the measurement tool acoustical characteristics (beam patterns) and the noise field vertical arrival structure. Because of the acoustical propagation characteristics of the medium, a nearby noise can arrive at the array via a ray path having a large vertical angle at the array location, and which usually increases as the source-to-array range decreases. As the arrival angle becomes more vertical, the assumed horizontal angle tends more to broadside than it actually is as a result of the conical shape of the beams. The maximum possible error of this type is when the source is very near and along the endfire direction. In this case the bottom-bounce arrival could reach the array at an angle which is nearly perpendicular to the array axis. The azimuth of the source determined from the beam response could be off as much as 90 deg. Fortunately, the very strong nearby sources can usually be identified and the contaminated data excluded from the analysis process. Also, as the ranges to the sources increase, the arrival angles tend to group near the horizontal, where this type of error is minimum.

(U) The second type of error is a result of the beamwidth possessing finite dimensions. The noise received on a beam of an array has arrived from all azimuths covered by the beam and its sidelobes. However, only one power level is obtained, and an assumption must be made during the analysis or display of this datum as to its angular origin. This type of error increases as the width of the beams increase and the sidelobe suppression decreases. This error also increases when the noise field becomes dominated by discrete sources and the noise has been assumed to result from a distribution of sources which is continuous with azimuth. Assuming that the noise field is composed of discrete sources, when in fact it is fairly continuous, also leads to error. The nature of the measured data should determine which of the two assumptions or combinations of the two assumptions should be made. It should not be assumed *a priori*.

SECRET

SECRET

(C) The third form of error is a result of the array tilt when the array is towed at slow speeds. More than 50 percent of the time during the CHURCH ANCHOR noise measurement periods the TASS depth sensors indicated that the aft end of the array was sufficiently lower than the forward end to give an array tilt greater than 10 deg. This in effect, shifted above-horizontal arrivals toward the forward end of the array and shifted below-horizontal arrivals toward the aft end of the array. Hence, a noise source from which the array received both above- and below-horizontal arrivals could be interpreted to have been on two different azimuths. This effect is maximum for a source on broadside and diminished near endfire. The LAMBDA did not have depth sensors during the CHURCH ANCHOR experiments; hence, its tilt can only be estimated. On the basis of the similarity in the physical characteristics of TASS and LAMBDA, with the exception of the length difference, assuming a 10 deg tilt for LAMBDA does not seem unreasonable.

(C) The final form of error in assigning azimuthal arrival angles for the received noise power is perhaps the most easily understood and in many cases the most significant. This is the error which results from not knowing the true array heading. The TASS array contained an array heading sensor which is believed to have been accurate within 2 deg. The LAMBDA array, however, did not have an array heading sensor. The array was assumed to have the same heading as the ship. The validity of this assumption depends on a number of factors, such as the net force exerted on the array by currents and tow-cable being in the same direction as the net force exerted on the ship by the screws, surface currents, winds and towcable, and that adequate time is allowed for array equilibration after a turn. It is likely that for some tow directions the assumption that the two net forces are in the same direction may be invalid. The effect of this type of error would be a positive and negative deviation in array heading around the ship's heading as the ship proceeded around the polygon. When measurements are taken before complete array equilibration, the array heading lags behind the ship's heading, giving a constant clockwise shift in the data for a polygon which is traversed in a clockwise direction.

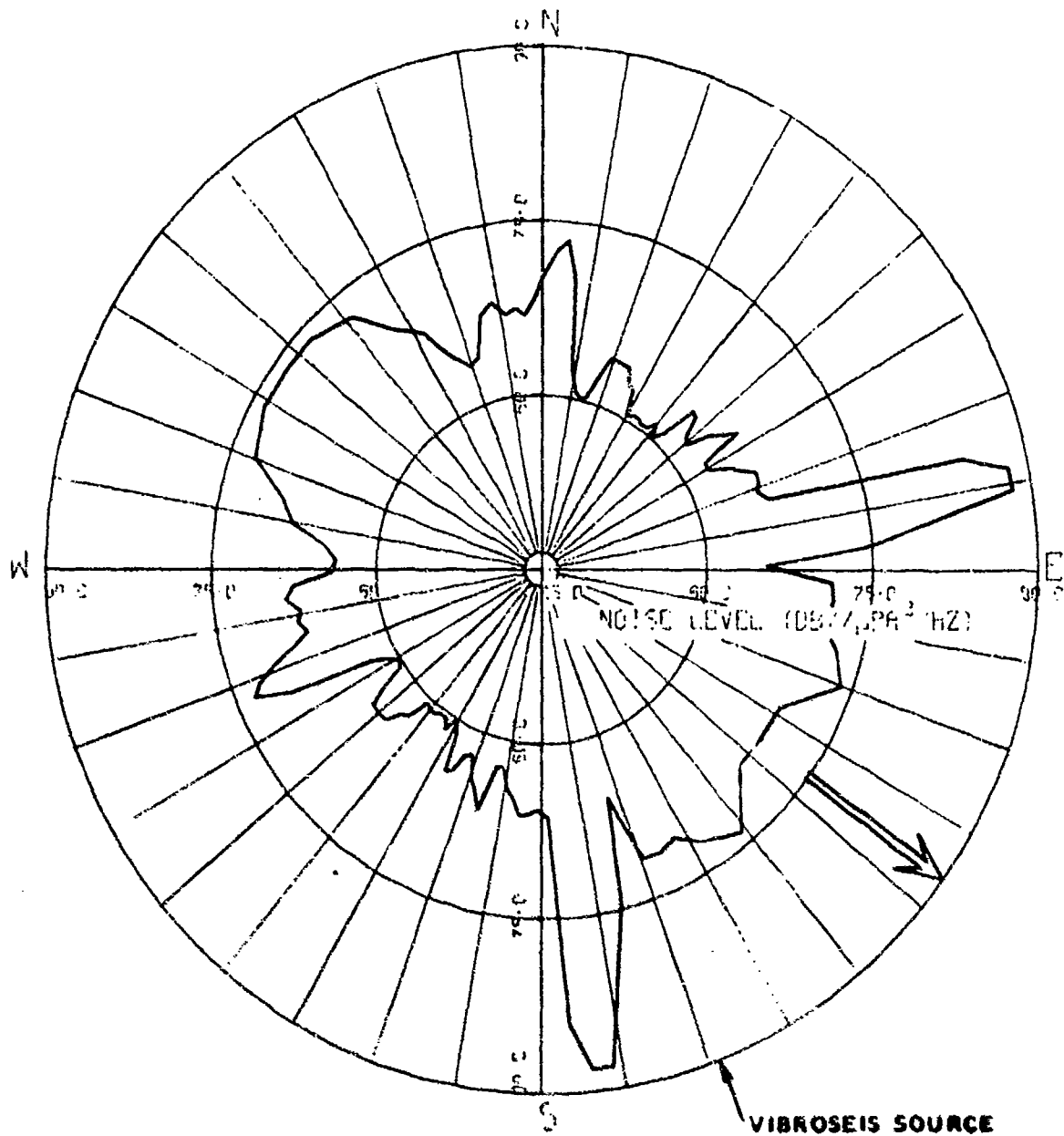
(S) The opportunity to assess the magnitude of the error introduced by assuming the array heading is equal to the ship's heading was afforded by the LAMBDA 38-Hz data of polygon 2. During this polygon the Vibroseis source was operating at a range of approximately 120 nmi along an azimuth of 159 deg. At 38 Hz, the Vibroseis introduced into the water enough sound energy to be easily distinguishable on the LAMBDA beam response data. Figures F-1 through F-5 are beam response curves for the affected data. These data have been plotted with the array heading assumed to be equal to the ship's heading. The arrow at 159 deg indicates the true azimuth to the Vibroseis source. The error in the location of the azimuth of the Vibroseis source is in a constant clockwise direction, ranging from 6 to 30 deg, with a mean of approximately 17 deg.

(U) The fluctuation in the bearing errors indicated in Figs F-1 through F-5 could have been caused by the water mass at the array depth having a velocity relative to the surface water masses in the direction of approximately 310 deg, or by the wind at the surface blowing in the direction of approximately 130 deg. It could also result from some combination of the two.

SECRET

SECRET

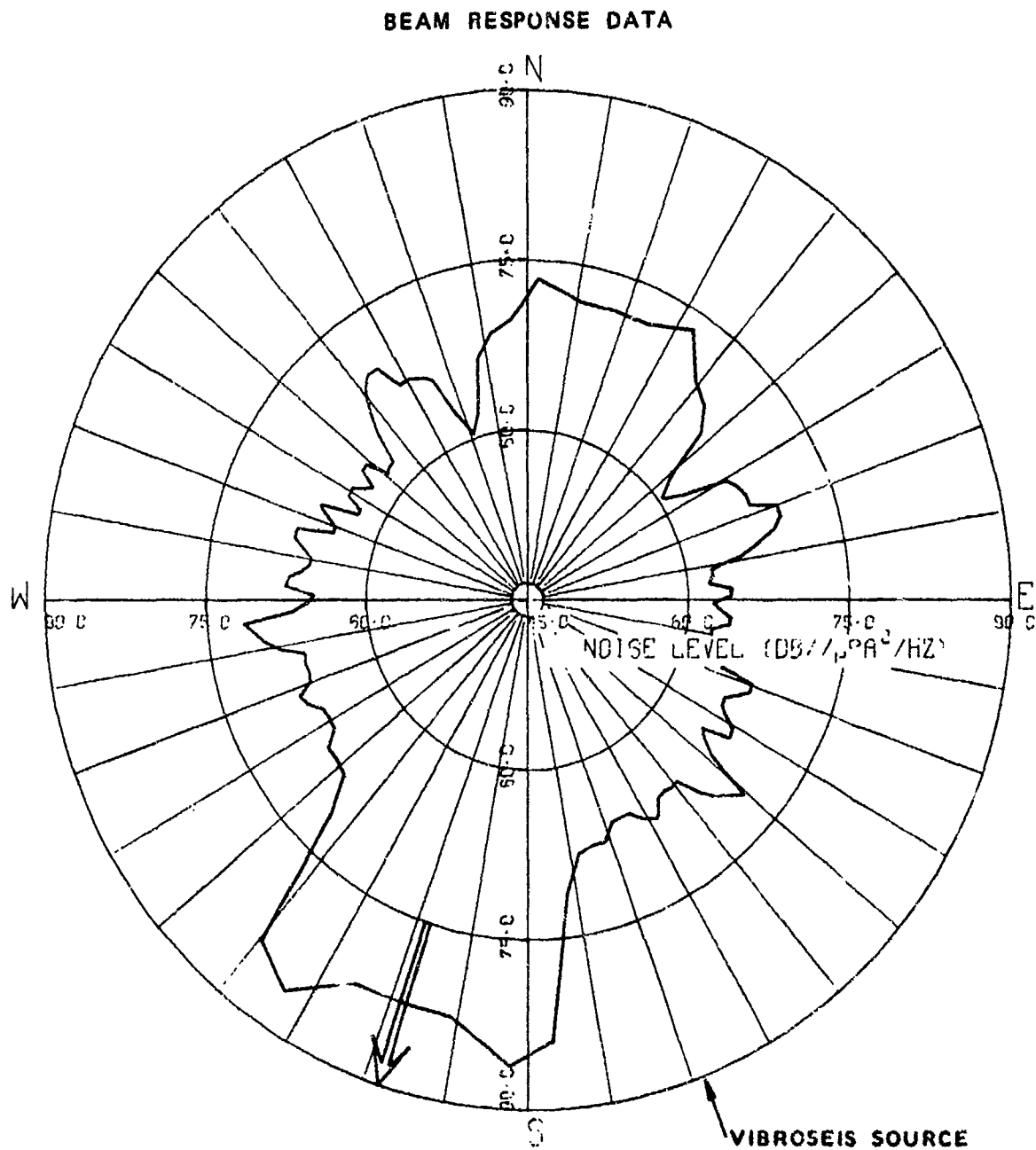
BEAM RESPONSE DATA



(U) Figure F-1. LAMBDA 38-Hz beam response data with Vibroseis source at 159 deg, polygon 2, leg 1 at η -3. (S)

SECRET

SECRET

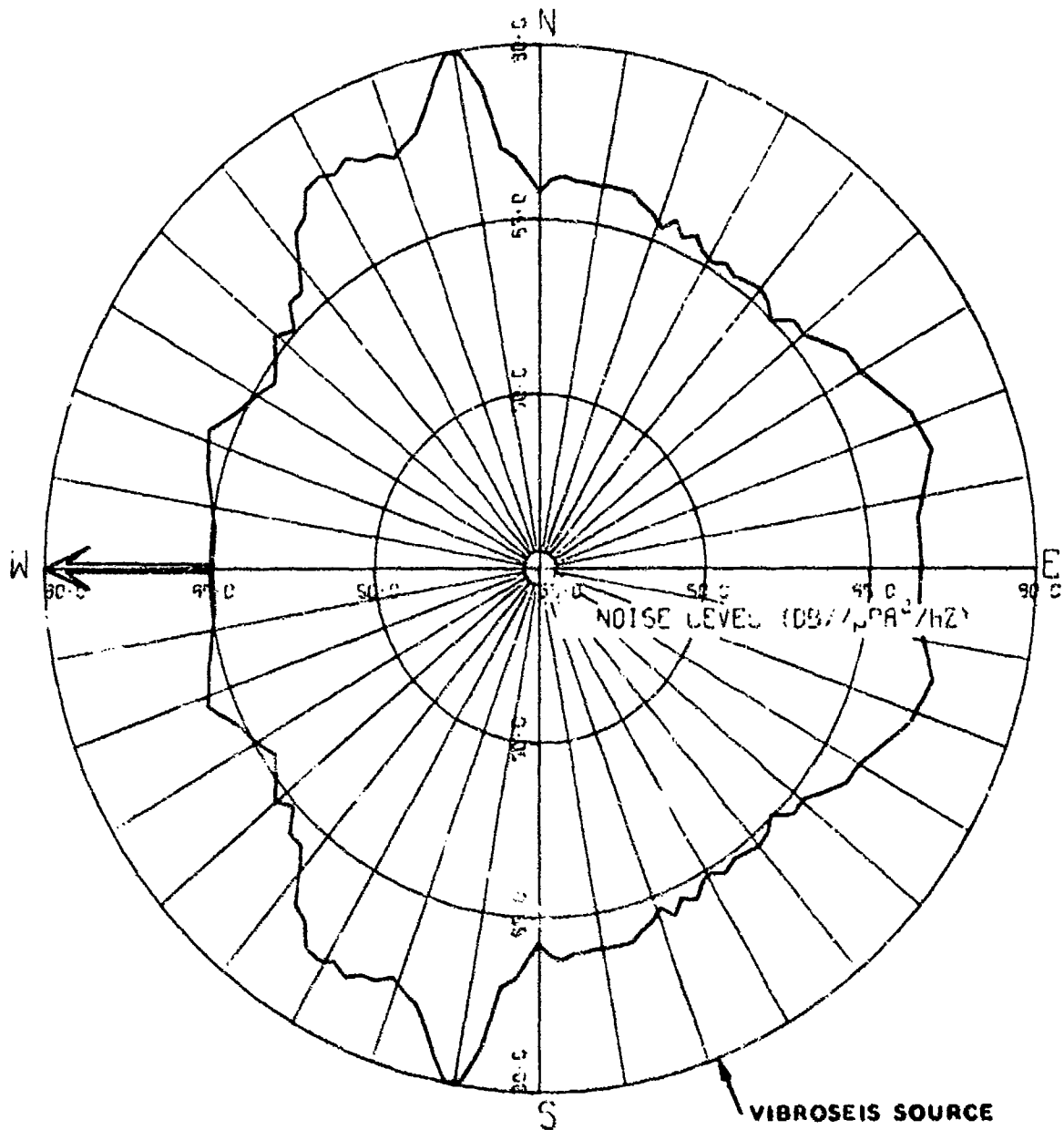


(U) Figure F-2. LAMBDA 38-Hz beam response data with Vibroseis source at 159 deg, polygon 2, leg 2 at η -3. (S)

SECRET

SECRET

BEAM RESPONSE DATA

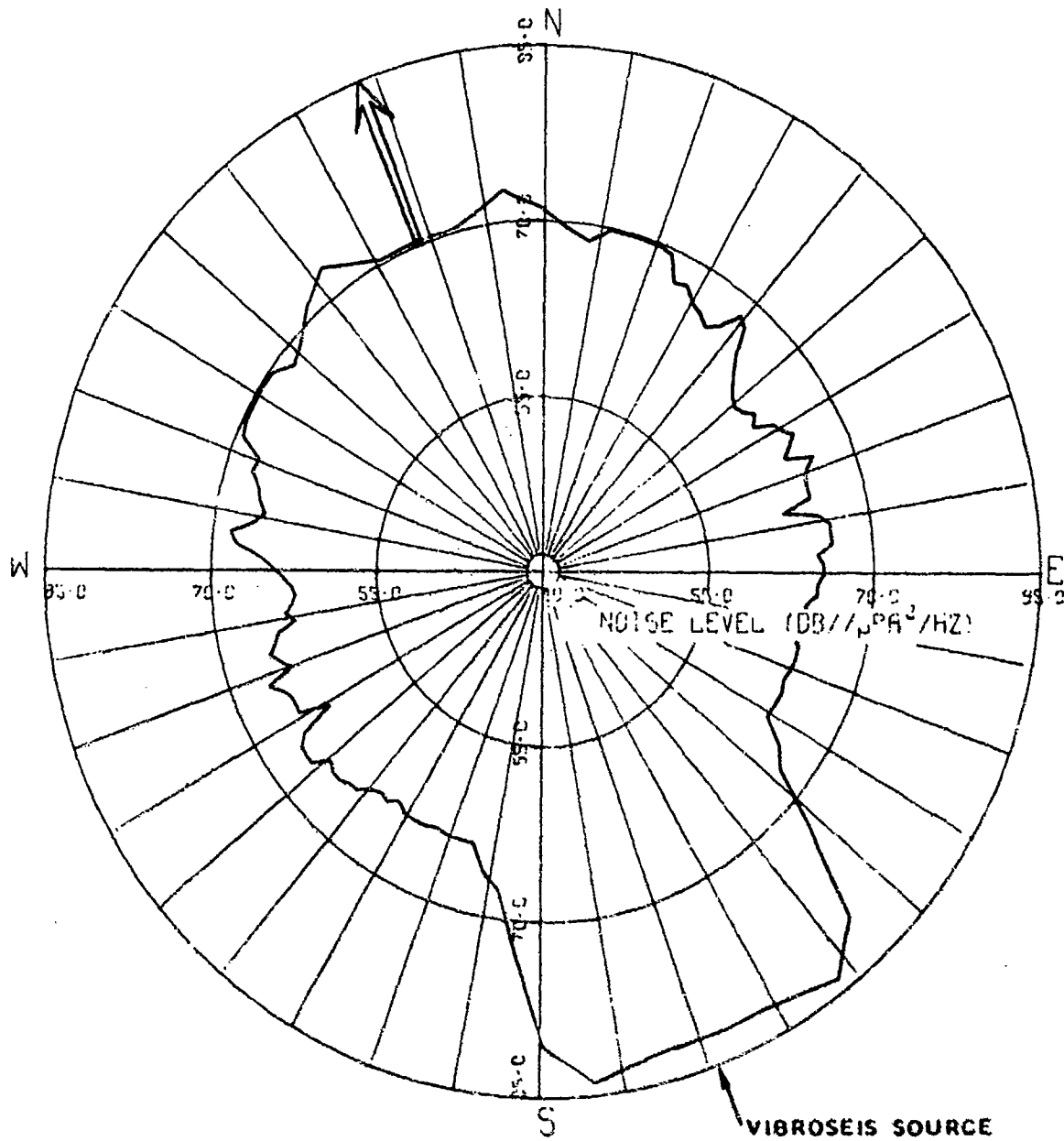


(U) Figure F-3. LAMBDA 38-Hz beam response data with Vibroseis source at 159 deg, polygon 2, leg 3 at η -3. (S)

SECRET

SECRET

BEAM RESPONSE DATA

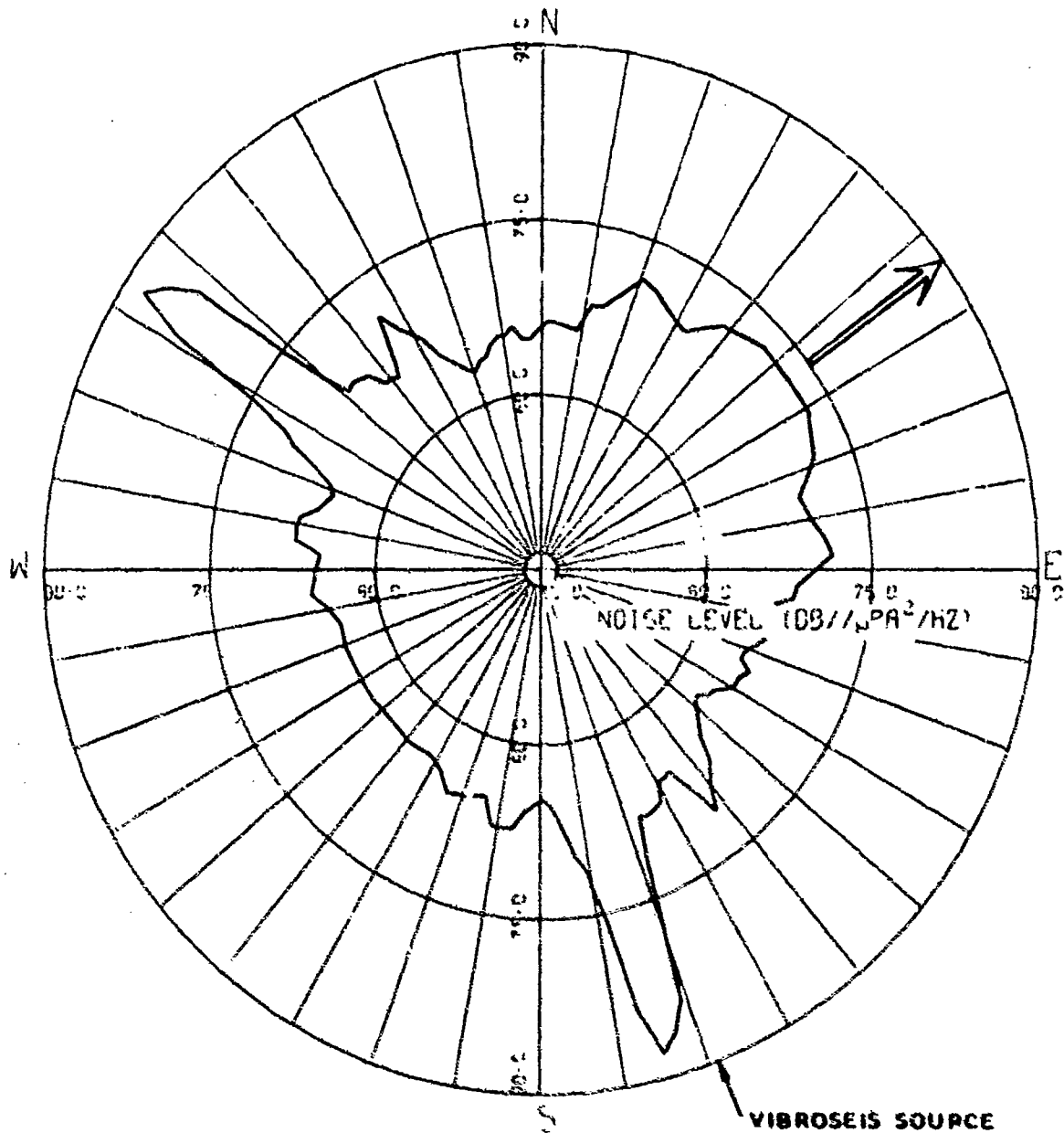


(U) Figure F-4. LAMBDA 38-Hz beam response data with Vibroseis source at 159 deg, polygon 2, leg 4 at η -3. (S)

SECRET

SECRET

BEAM RESPONSE DATA



(U) Figure F-5. LAMBDA 38-Hz beam response data with Vibroseis source at 159 deg, polygon 2, leg 5 at η -3. (S)

SECRET

SECRET

(C) A constant clockwise bearing error could have been caused by a number of factors related to the electronics, the experimental technique, or the physical environment. It is unlikely that the physical environment could have been the cause in this case since the TASS did not experience the same phenomena only 20 nmi away. One of the possible electronic sources was a constant time shift in the multiplexer; however, this would have been discovered by the calibration procedures executed periodically throughout the experiment. The most plausible explanation is related to the experimental technique. The LAMBDA array is approximately 4000 ft long and 3 in. in diameter and experiences considerable drag force due to its extreme length. The tow cable is approximately 1-1/2 in. in diameter and tends to "bore" a hole in the water, with the array trying to travel through the same hole. The extent to which this is accomplished is dependent upon the relative drag of the array compared to the force exerted by the side of the "hole" on the cable in a direction normal to the cable axis to resist the tendency of the cable to slice through the side of the "hole." As the array length increases, the drag increases, which increases the tendency of the cable to slice through the water instead of traveling along the "hole." Thus, the time required for array equilibration increases with array length. If after one leg a bearing error exists due to incomplete equilibration, the error could accrue until, after five legs, the error could be sizable. The buildup of the error, of course, could not continue without limit. At some point an equilibrium condition must be established. At what point, or during which leg this would happen is not clear, if indeed this is the responsible mechanism. In the present study it is assumed that sufficient time was not allowed for array equilibration and that an equilibrium state was established by the first leg of the second polygon at each location, giving a mean heading error of 17 deg, with the fluctuation in heading resulting from relative displacements in water masses at the surface and at array depth. Hence, the uncertainty in the rate of accumulation of the error during the first polygon decreased the confidence in those data sufficiently to warrant emphasizing, in this report, the data from the second LAMBDA polygon of each day, whenever possible, with a constant 17-deg shift in the array heading for each leg. No correction was possible for fluctuations in array heading due to currents. Polygon 3 data were utilized without correction in the absence of polygon 4 data.

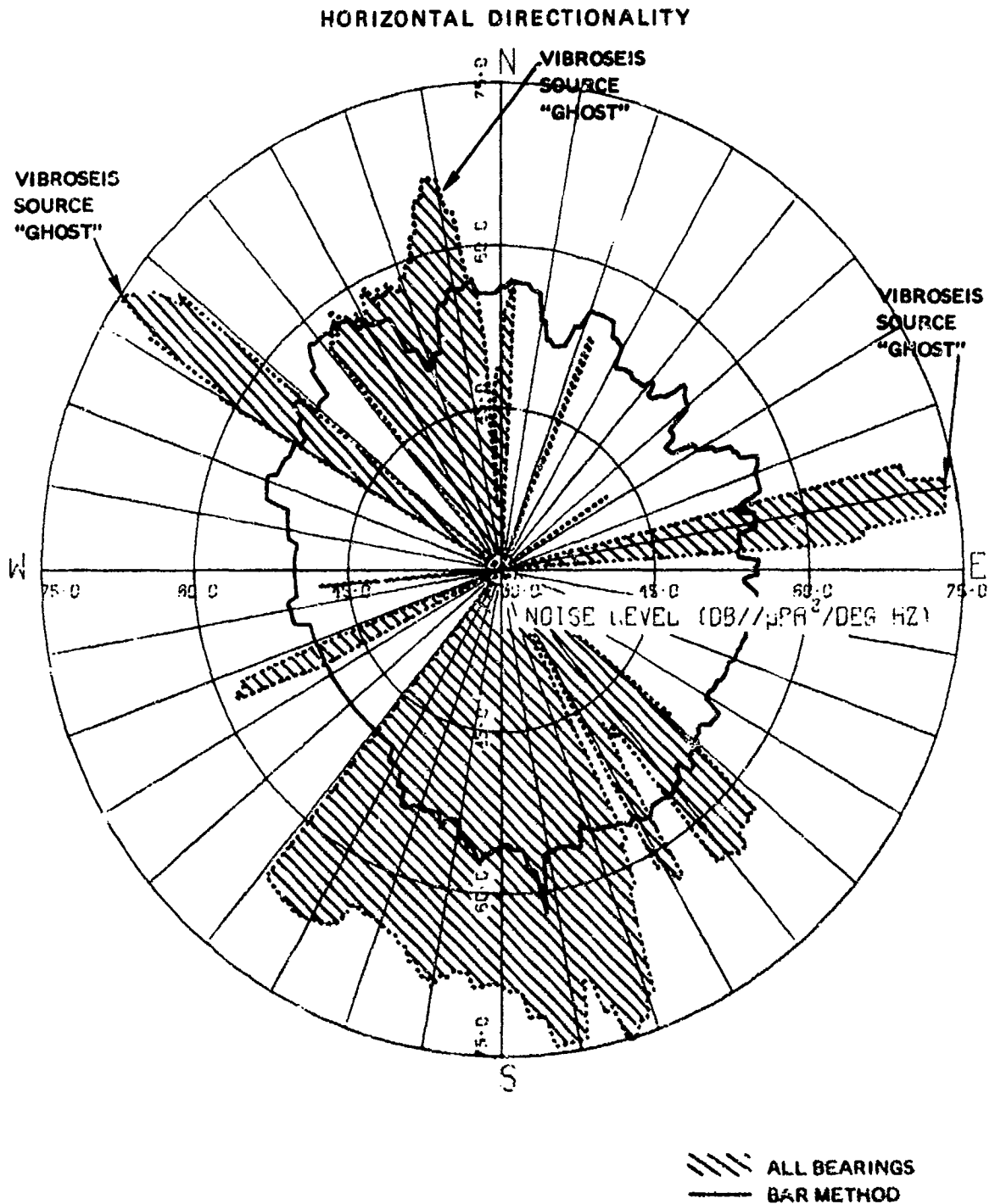
HORIZONTAL DIRECTIONALITY

(U) The faithful reproduction of the noise field horizontal directionality depends on a number of factors. Three of the most significant are the beamwidths of the array, the relative nonstationarity of the noise field, and the nature of the ambiguity resolution algorithms. Only the effect of the algorithms will be considered in this section and only on a limited basis. For a more detailed discussion refer to Appendix D.

(U) Figures F-1 through F-5 are examples of beam response data with known bearing errors. Figure F-6 contains the noise field horizontal directionality which resulted when the beam response data for these five legs were utilized to determine the noise field horizontal directionality without first eliminating the array heading errors. The shaded result is the All-Bearings assessment, and the other is the BAR method

SECRET

SECRET



(U) Figure F-6. Comparison of the 38-Hz All-Bearings and BAR results with array heading errors for LAMBDA polygon 2 at η -3 with the Vibroseis source operating along an azimuth of 159 deg. (S)

SECRET

SECRET

result. The areas within the azimuths which have no shading are azimuths of negative power which were calculated by the All-Bearings method.

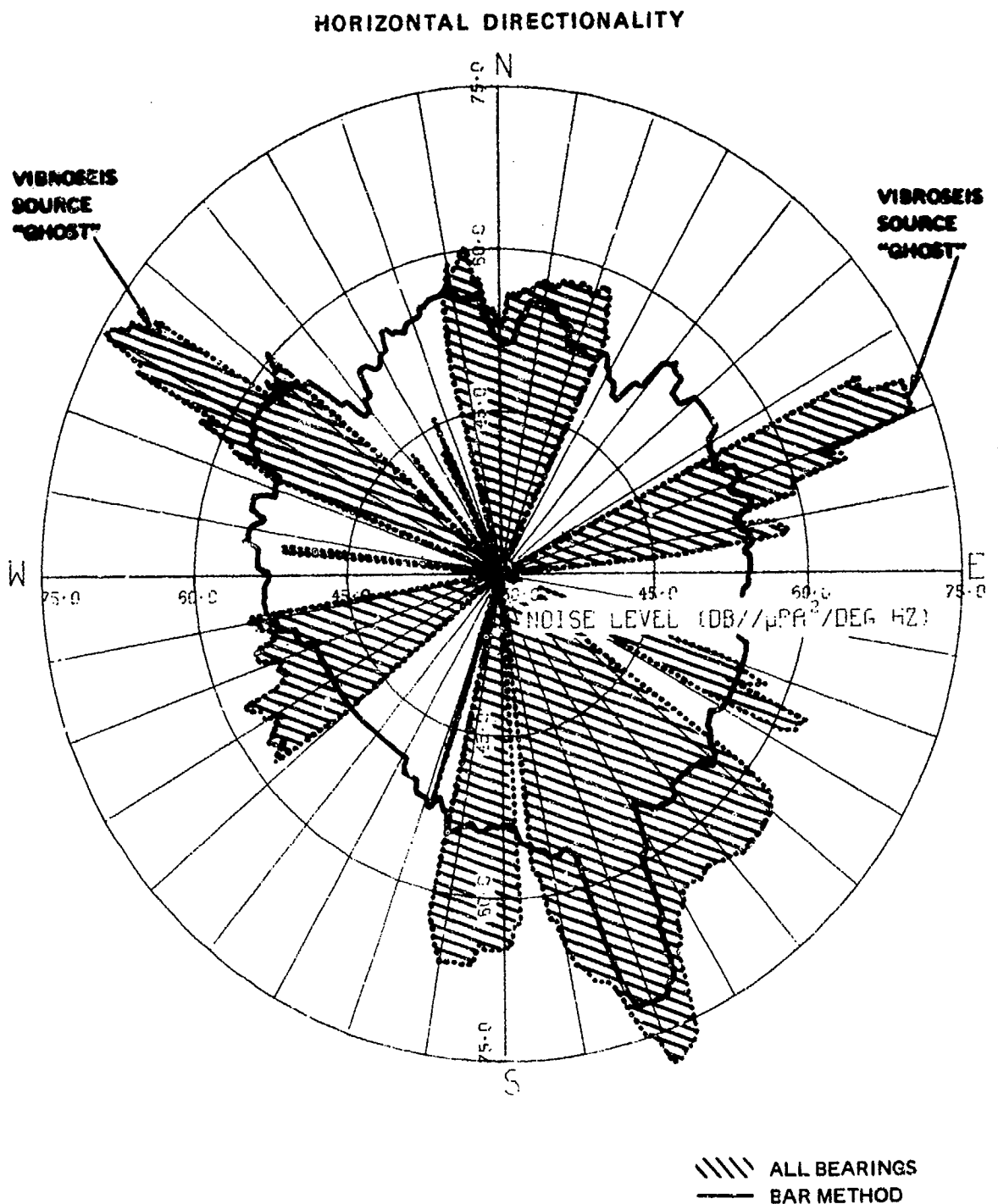
(U) The signal from the Vibroseis source does not appear on the same azimuth of each leg because of the bearing errors. It therefore appears as a transient to the resolution algorithms. The ambiguous beam counterpart is also seen as a transient. Hence, the algorithms cannot distinguish between the true sources and the ambiguous sources. The net result is that all are discriminated against equally. In other words, no ambiguities were resolved. In the All-Bearings assessment, the source is visible on at least five different azimuths. In the BAR assessment, it is nowhere evident since, as a transient, it has been completely eliminated.

(U) Figure F-7 illustrates the results when the corrected array headings were used. The regions of negative power produced by the All-Bearings method are smaller and the true azimuth of the source has a higher level than those along the ambiguous azimuths. However, the ambiguous sources (ghosts) are still of significant level. The BAR assessment now displays a large level along the appropriate azimuth with none of the ambiguous beam effects.

(U) The ambiguity algorithms were not specifically designed to locate large sources. The significance of the above example, however, is that the noise field is composed of many discrete sources and perhaps even distributed sources. To the ambiguity resolution algorithms, the noise from ships is not significantly different from the noise of the Vibroseis source in the above example. The algorithms treat them the same. Hence, the problems the algorithms have with the Vibroseis source (resulting from both the magnitude of the noise level and the apparent transient nature of the source) are the same as those the algorithms would have with noise from ships, whether or not there exists any array heading error. After all, a moving ship can significantly change position in azimuth with respect to the array in the time required to complete a polygon.

SECRET

SECRET



(U) Figure F-7. Comparison of the 38-Hz All-Bearings and BAR results with corrected array headings for LAMBDA polygon 2 at $\eta=3$ with the Vibroseis source operating along an azimuth of 159 deg. (S)

SECRET

UNCLASSIFIED

APPENDIX G STATISTICAL ASSESSMENT OF RANDOMNESS

INTRODUCTION

(U) The deconvolution procedures discussed in the main body of this report require ambiguous beam responses of a line array for two or more array orientations. Implicit in these procedures is the requirement that the noise field remain stationary over the time period required to measure the necessary beam responses.

(U) For one set of array orientations which define a polygon, it is not presently feasible to objectively assess the stationarity of the noise field. This is the case since the noise measurements acquired during each array orientation were separated by sufficient time to allow the array to stabilize after a course change. During such time intervals, changes in the noise field could go undetected. A necessary, but not sufficient, condition for the stationarity requirement is that the beam responses for each array orientation not exhibit nonstationary characteristics.

(U) Onboard the LEE, the beam response measurements were acquired in a manner which allows the assessment of the randomness of the noise levels received on the array's beams during each measurement period. That is, for each array orientation, each beam was sampled with a 1/4-sec sample time every 6 sec for a total of 150 samples.

(U) Nonstationary characteristics such as the tendency for individual noise level assessments of like magnitude to cluster together with respect to time, and time trends in the data will, in general, cause the serial data to appear nonrandom. The serial observations thus acquired were tested for randomness by the three following statistical procedures.

STATISTICAL PROCEDURES

(U) The three statistical procedures applied to the LEE array data which may be used to examine the randomness of the sequential noise measurements for each beam are the Number of Runs Test, Kendall's Test for Correlation, and the Mean-Square Successive Difference Test.

Number of Runs Test

(U) The Number of Runs Test (Ref. 21) is a distribution-free test based on nominal or categorical information; that is, the observations can be unmistakably classified into one of two mutually exclusive categories. For the application at hand,

UNCLASSIFIED

UNCLASSIFIED

the two mutually exclusive categories are above-the-sample-median and below-the-sample-median. The 150 noise-level samples for each beam-frequency combination acquired during a 15-min measurement period onboard the LEE were classified as either above-the-sample-median, A; below-the-sample-median, B; or equal-to-the-sample-median. Neglecting those observations that are equal-to-the-sample-median and those that overloaded the 1/3-octave analyzer, the number of runs in the temporal sequence is determined. Since the samples which overloaded the 1/3-octave analyzer were to be neglected in the other two procedures to be discussed, they were also neglected for the Number of Runs Test; the random allocations hypothesis for the non-overloaded data was not materially affected by this. A run is an unbroken sequence of like events. If the observations in the sample had equally likely *a priori* probability of occupying any position in the temporal sequence, then a frequency distribution for each realizable permutation of the A's and B's may be determined. Usually, realizations with too few or too many runs are suspected as products of nonrandom processes, the former manifesting a tendency for sequential observations to be positively correlated and the latter to be negatively correlated. Also, the deterministic process of a pure unmasked acoustic tone could produce too few or too many runs, depending on its frequency, since the sample interval is a constant 6 sec.

(U) For large samples (the number of samples for one or the other category greater than 20), the realized number of runs and the number of samples in each category can be algebraically combined to produce a realization of a normally distributed random variable with zero mean and unit variance. The standard normal realization thus obtained may be used to assess the randomness of the data sequence for a given beam-frequency combination by comparing the realization to an appropriate standard normal critical value. For example, if one is willing to be wrong 5 percent of the time when the data sequence is in fact random, he will suspect a data sequence as being generated by a nonrandom process when the standard normal run statistic is not contained in the interval $(-1.96, +1.96)$.

Kendall's Test for Correlation

(U) The Kendall's Test for Correlation is a distribution-free test based on ranked observations; that is, no assumptions need be made regarding the probability distribution of the measured data. This test requires more information than the Number of Runs Test. The latter merely requires that the data set be dichotomized, whereas the former takes into account relative magnitudes among the data.

(U) The statistic used in this test is a linear function of the number of rank inversions contained in the observed data set. An inversion exists when an observation in the data sequence is compared to a subsequent observation and it is greater than the subsequent observation. For example, the integer sequence 4, 3, 6, 1, 5, 2, contains nine inversions: 4 is greater than 3, 1, and 2; 3 is greater than 1 and 2; 6 is greater than 1, 5, and 2; and 5 is greater than 2.

UNCLASSIFIED

(U) The rationale for this procedure is that prior to sampling, each of the possible 150-factorial permutations of the observed levels (or their ranks) was equally likely to become the sequence of observations actually obtained when ordered with respect to time. Following this rationale it is not difficult to see that variables which are monotonically related would produce an unusual arrangement with respect to an assumption that the 150-factorial permutations are equally likely.

(U) The sampling distribution for Kendall's correlation statistic is tabulated for moderate sample sizes, up to 40 samples. However, for sample sizes greater than seven (Ref. 22), an algebraic combination of the realization for Kendall's correlation statistic and sample size produces a realization of a normally distributed random variable with zero mean and unit variance, which may be used in the same manner as the unit normal statistic derived for the Number of Runs Test to test for significant departures from the hypothesis that the observed levels are randomly distributed.

Mean-Square Successive Difference Test

(U) The Mean-Square Successive Difference Test (Ref. 23), unlike the previous two tests, is not a distribution-free test. The data in the sequence are assumed to be measurements from a normally distributed population with unknown mean and variance.

(U) If the serial observations are independently distributed, there are two methods available to estimate the population variance, σ^2 . One is the unbiased estimator:

$$S^2 = \frac{1}{n-1} \sum_{i=1}^n (X_i - \bar{X})^2$$

The other is

$$\frac{d^2}{2} = \frac{1}{n-1} \sum_{i=1}^{n-1} (X_{i+1} - X_i)^2,$$

one-half of the mean of the successive differences squared. If the serial observations are not independently distributed, these two statistics estimate different quantities; however, both quantities involve the population variance and the correlation coefficient for adjacent observations. Under the assumption that the serial observations are independently distributed, the quantity

$$Z = \frac{\frac{d^2/2}{S^2} - 1}{\sqrt{(n-2)/(n^2-1)}}$$

is approximately distributed as a unit normal deviate.

UNCLASSIFIED

(U) If the sequential observations are positively correlated, $d^2/2$ underestimates σ^2 more than does S^2 . Hence, positively correlated observations produce a unit normal realization that is negative, and negatively correlated observations produce a unit normal realization that is positive.

(U) The exact distribution for d^2/S^2 for uncorrelated observations has been tabulated for sample sizes that range from 4 to 60 (Ref. 24). The normal approximation appears to be quite good for the 0.05 and the 0.95 significance levels for sample sizes greater than six. It is not nearly as good for the 0.001, 0.01, 0.99, and 0.999 significance levels until the sample size is greater than 60. However, the normal approximation is conservative at these latter values; that is, when the normal approximation is computed for the exact critical values as tabulated in Refs. 23 and 24, they are not as far out in the tails of the standard normal distribution as are the normal critical values. To illustrate the above remarks, the normal approximation computed for the exact critical values of d^2/S^2 are compared with the normal critical values for a sample size of 60 in the following table:

Critical Values Based On	Significance Levels					
	0.001	0.01	0.05	0.95	0.99	0.999
Computation	-3.013	-2.306	-1.649	1.649	2.306	3.014
Normal Tables	-3.090	-2.326	-1.645	1.645	2.326	3.090

(U) Since the normal approximation improves as the sample size increases, it is felt that the approximation is adequate for the 140 to 150 samples acquired during each measurement period for the LEE array.

(U) As with the previous tests, this test produces a realization that is approximately distributed as a unit normal deviate with zero mean; and as with the previous tests, the critical values of the standard normal distribution may be used to test the hypothesis that the serial observations obtained on any one beam-frequency combination for a given measurement period are distributed in a random manner.

ILLUSTRATION OF STATISTICAL PROCEDURES

(U) Tables G-1, G-2, and G-3 have been selected to illustrate the behavior of the Number of Runs Test, Kendall's Test for Correlation, and the Mean-Square Successive Difference Test during periods when the acoustic environment was different.

UNCLASSIFIED

UNCLASSIFIED

SAMPLE SIZE = 159
GAIN CODE = 2
HEADING = 59
LONG. = -143.17
FREQ = 169

DATE - 9/2/73
PASS 11 - LEG 5
ST. TIME = 1830.00
LATITUDE = 38.25
SAMPLE TIME = 1/4

BEAM	N.OV	N.OBS.	N.RUN	N1	N2	Z.RUN	Z.MSSD	Z.TAU	MEDIAN	AUG.	STDEV	BEAM
1	0	135	61	68	67	-1.295	-2.100	-0.555	86.0	86.1	1.99	1
2	0	140	70	66	74	-0.131	-1.037	-1.193	85.5	85.2	1.62	2
3	0	143	61	72	71	-1.929	-2.350	1.283	84.0	83.9	1.70	3
4	0	138	63	68	70	-1.193	-1.931	0.574	83.5	83.3	1.76	4
5	0	139	48	67	72	-3.820	-3.078	6.417	83.0	82.8	1.74	5
6	0	141	74	69	72	0.428	0.414	-0.125	82.5	82.5	1.33	6
7	0	143	72	72	71	-0.083	-0.019	0.868	84.5	84.5	1.62	7
8	0	139	67	70	69	-0.595	0.022	1.681	92.2	82.1	1.82	8
9	0	139	68	67	72	-0.410	-1.202	0.128	81.1	81.0	1.51	9
10	0	138	54	73	65	-2.703	-4.932	5.054	82.7	82.9	2.32	10
11	0	140	69	76	64	-0.253	0.087	-1.334	82.7	82.7	1.96	11
12	0	144	82	74	70	1.515	2.648	1.248	81.1	81.3	1.54	12
13	0	146	44	72	74	-4.981	-8.563	-7.128	88.7	88.5	3.90	13
14	0	145	36	72	73	-6.249	-9.669	8.359	91.6	90.8	4.18	14
15	0	138	70	65	73	0.039	-0.091	3.325	82.0	81.8	1.76	15
16	0	139	71	67	72	0.100	-1.307	0.476	81.5	81.3	1.67	16
17	0	140	68	70	70	-0.508	-2.131	2.913	81.6	81.5	1.80	17
18	0	144	74	76	68	0.295	-0.480	3.605	81.0	80.9	1.63	18
19	0	138	61	72	66	-1.518	-0.978	-2.994	82.2	82.1	1.74	19
20	0	143	67	71	72	-0.922	-1.027	2.976	81.0	80.9	1.61	20
21	0	134	66	66	68	-0.344	-0.849	0.129	80.0	79.9	1.73	21
22	0	143	42	71	72	-5.118	-5.445	7.627	81.0	80.9	1.91	22
23	0	137	74	67	70	0.777	-1.745	3.676	82.0	81.8	1.61	23

(U) Table G-1. Raw data statistical analysis, pass 11, 9/2/73. (U)

UNCLASSIFIED

UNCLASSIFIED

SAMPLE SIZE = 150
GAIN CODE = 2
HEADING = 193
LONG. = -143.17
FREQ = 160

DATE - 9/5/73
PASS 21 - LEG 2
ST. TIME = 2133.10
LATITUDE = 34.50
SAMPLE TIME = 1/4

BEAM	N.OV	N.OBS.	N.RUN	NA	NB	ZRUN	ZMSSD	ZTAU	MEDIAN	AUG.	STDEV	BEAM
1	0	145	68	73	72	-0.916	-0.782	-1.855	81.5	81.5	1.51	1
2	0	138	66	67	71	-0.674	0.118	0.558	78.2	78.1	1.38	2
3	0	141	73	66	75	0.303	0.302	1.601	77.2	77.0	1.37	3
4	0	150	81	74	76	0.821	0.722	3.343	78.0	77.9	1.43	4
5	0	145	73	70	75	-0.069	-2.132	0.469	77.7	77.5	1.58	5
6	0	145	74	69	76	0.111	-0.245	1.758	77.7	77.5	1.48	6
7	0	139	59	69	70	-1.957	-0.725	1.576	78.5	78.5	1.51	7
8	0	145	67	70	75	-1.070	0.401	1.111	78.2	78.1	1.50	8
9	0	142	69	67	75	-0.468	-0.010	1.015	78.7	78.7	1.49	9
10	0	136	69	68	68	0.000	0.172	1.559	78.0	77.8	1.62	10
11	0	137	67	71	66	-0.413	0.893	1.939	78.5	78.3	1.53	11
12	0	139	74	68	71	0.601	0.459	-0.020	78.5	78.3	1.41	12
13	0	140	70	66	74	-0.131	0.058	-0.730	78.2	78.0	1.56	13
14	0	143	77	73	70	0.760	0.394	1.074	78.0	77.9	1.67	14
15	0	150	75	75	75	-0.163	-0.404	0.306	80.5	80.5	1.37	15
16	0	143	63	67	76	-1.553	-1.734	-1.498	80.1	80.0	1.52	16
17	0	143	75	70	73	0.425	1.890	0.283	82.0	81.8	1.65	17
18	0	143	68	75	68	-0.728	-0.445	-0.759	83.0	83.0	1.52	18
19	0	150	70	74	76	-0.981	-2.049	4.488	84.8	84.6	1.83	19
20	0	135	63	66	69	-0.944	-1.761	0.645	82.0	81.9	1.65	20
21	0	137	74	68	69	0.772	0.288	-0.721	83.5	83.4	1.51	21
22	0	135	67	73	62	-0.182	-1.644	3.317	85.0	85.0	1.56	22
23	0	138	62	68	70	-1.364	-0.734	-1.658	87.1	87.0	1.55	23

(U) Table G-2. Raw data statistical analysis, pass 21, 9/5/73. (U)

UNCLASSIFIED

UNCLASSIFIED

SAMPLE SIZE = 150
GAIN CODE = 2
HEADING = 279
LONG. = 143.18
FREQ = 160

DATE - 9/9/73
PASS 61 - LEG 3
ST. TIME = 45.00
LATITUDE = 31.20
SAMPLE TIME = 1/4

BEAM	N.OV	N.OBS.	N.RUN	NA	NB	ZRUN	ZMSSD	ZT.AU	MEDIAN	AUG.	STDEV	BEAM
1	0	140	69	67	76	-0.542	-6.620	2.064	82.2	82.4	2.52	1
2	0	137	68	66	71	-0.241	-7.366	-0.608	81.5	81.7	3.10	2
3	3	135	53	67	68	-2.677	-7.226	-1.362	84.0	84.3	2.87	3
4	4	136	69	65	71	0.022	-6.474	1.273	82.5	82.5	3.01	4
5	0	140	57	66	74	-2.343	-7.209	-1.773	83.7	83.8	2.48	5
6	0	150	61	76	74	-2.456	-5.159	-4.583	83.8	83.9	2.18	6
7	0	150	66	74	76	-1.636	-3.225	3.547	85.8	86.0	2.12	7
8	0	143	72	70	73	-0.078	-3.560	4.855	85.5	85.4	2.40	8
9	0	146	53	72	74	-3.486	-6.600	5.930	83.2	83.5	2.27	9
10	0	146	48	73	73	-4.318	-6.749	3.971	84.2	84.4	2.40	10
11	0	150	57	75	75	-3.113	-7.676	0.059	81.3	81.5	2.71	11
12	0	139	74	71	68	0.601	-5.317	1.283	79.0	80.7	2.32	12
13	0	145	69	75	70	-0.736	-6.286	-2.193	81.1	81.3	2.47	13
14	0	138	66	66	72	-0.662	-7.944	-0.661	80.1	80.5	2.97	14
15	0	146	79	73	73	0.830	-6.731	1.215	80.1	80.5	2.79	15
16	0	143	62	70	73	-1.757	-7.774	2.573	79.6	79.9	2.94	16
17	0	138	56	72	66	-2.374	-8.645	3.000	78.7	79.1	3.11	17
18	0	143	72	71	72	-0.083	-6.959	4.226	80.0	80.3	3.19	18
19	0	147	60	71	76	-2.388	-7.179	3.908	81.6	82.9	2.64	19
20	0	146	62	71	75	-1.985	-7.577	4.474	81.6	82.2	2.70	20
21	0	142	60	72	70	-2.019	-5.846	3.759	82.7	82.7	2.55	21
22	0	150	61	75	75	-2.457	-6.900	0.576	84.0	84.4	2.55	22
23	0	142	67	71	71	-0.842	-6.253	-0.522	81.5	82.0	2.86	23

(U) Table G-3. Raw data statistical analysis, pass 61, 9/9/73. (U)

UNCLASSIFIED

UNCLASSIFIED

(U) Common entries on each figure are:

DATE – Observation date.

PASS – A coded value used to identify a set of measurements.

ST. TIME – Time of day in GMT at beginning of measurement period on observation date.

LATITUDE – Nominal latitude at which measurements were acquired.

SAMPLE TIME – One-third octave analyzer integration time in seconds for each observation.

SAMPLE SIZE – Total observations acquired during the measurement period.

GAIN CODE – The numeral 2 indicates the data were acquired with the beamformer in the high-gain mode.

HEADING – Nominal array heading during the measurement period.

LONG – Nominal longitude at which these measurements were acquired.

FREQ – One-third octave band center frequency.

BEAM – Beam Number	Beam Axis deg
1	17/343
2	30/330
3	38/322
4	46/314
5	53/307
6	59/301
7	64/296
8	70/290
9	75/285
10	80/280
11	85/275
12	90/270
13	95/265
14	100/260
15	105/255
16	110/250
17	116/244

UNCLASSIFIED

UNCLASSIFIED

Beam Number	Beam Axis deg
18	121/239
19	127/233
20	134/226
21	142/218
22	150/210
23	163/197

N.OV – Number of samples which overloaded the 1/3-octave analyzer.

N.OBS – Number of observations used in the Number of Runs Test.

(N.OBS) = (SAMPLE SIZE) – (N.OV) – (number of observations which are equal to the sample median).

N.RUN – Number of runs with respect to the sample median that were observed in the time-ordered sample of size (N.OBS).

NA – Number of runs above the sample median.

NB – Number of runs below the sample median.

ZRUN – A realization of a normally distributed random variable with zero mean and unit variance which is derived from (N.OBS), (N.RUN), (NA), and (NB). See Ref. 21 for a discussion of this statistic.

ZMSSD – A realization of a normally distributed random variable with zero mean and unit variance which is derived from two different assessments of the population variance for a sequence of normally distributed data. See Ref. 25 for a discussion of this statistic.

ZTAU – A realization of a normally distributed random variable with zero mean and unit variance which is a function of the realization of the Kendall Rank Correlation Coefficient and SAMPLE SIZE. See Ref. 22 for a discussion of this statistic.

MEDIAN – Sample median.

AVG. – Sample arithmetic mean.

STDEV. – Sample standard deviation.

The units for MEDIAN, AVG., and STDEV. are decibels referenced to 10 millivolts for a 1/3-octave bandwidth; that is, these statistics are derived from 1/3-octave raw data which have not been adjusted for beam sensitivity, beamwidth, or bandwidth.

UNCLASSIFIED

UNCLASSIFIED

(U) The tabulation shown in Table G-1 is selected to demonstrate the behavior of the statistics derived from the 150 samples acquired beginning at 1830Z on 2 September 1973. During the period when these data were obtained, a merchant vessel which was nominally 10 nmi away was closing on the LEE. This vessel was to rendezvous with the LEE about 1 hr after acquisition of these data. The merchant vessel is evidenced on beams 13 and 14 and again on beam 22. The arrivals on beams 13 and 14 are probably the result of acoustic energy descending on the line array, whereas the arrivals on beam 22 are probably the result of acoustic energy ascending to the line array.

(U) All three statistics discussed in this appendix are extremely significant on beams 13, 14, and 22; that is, the evidence indicates that there are too few runs in the 150 sequential samples to have occurred in a random manner (the Number of Runs Test), that the sequential data are positively correlated (the Mean-Square Successive Difference Test), and that significant trends exist in the samples (the Kendall Correlation Test). It is interesting to note that while all statistics for beams 13 and 14 are significant, the Kendall Correlation Test Statistic, ZTAU, indicates that the 150 samples for beam 13 contain a negative temporal trend, while the 150 samples for beam 14 contain a positive temporal trend. This manifestation is expected if an acoustic source shifts from one beam to another adjacent beam during the data acquisition period.

(U) The variability in the samples as summarized by the respective standard deviations appears to be unusually high for beams 13 and 14 and moderately high for beam 22 when compared with the standard deviation for the remaining beams. The median and the average levels on beams 13 and 14 are quite high when compared to adjacent beams. But, this corroborating evidence would be expected for a nearby acoustic source.

(U) The samples for beams 5 and 10 exhibit nonrandom characteristics in that the three statistics ZRUN, ZMSSD, and ZTAU are significant. The acoustic energy sampled on these beams would not be expected to be related to the merchant vessel unless through sidelobes for those beams. Of course, it is also possible that these beams were experiencing another source or sources.

(U) The tabulation shown in Table G-2 is selected to demonstrate the behavior of the statistics during a time period when there were no known nearby ships to affect the noise measurements. These data were acquired during the 15-min period which began at 2133Z on 5 September 1973. Other than for beams 4, 5, 19, and 22, there appears to be no nonrandomness evident in these samples. One would be alerted to a positive trend in the noise measurements on beam 4; however, the RUNS and Mean-Square Successive Difference statistics are not significantly different from zero for beam 4. The beam 5 statistic for the Mean-Square Successive Difference Test is significantly different from zero at the .05 level of significance, but the other two

UNCLASSIFIED

CONFIDENTIAL

statistics for this beam are not significant. This indication of positive correlation between successive samples could be a random occurrence. The evidence is fairly strong that there may have been a nonrandom sequence of data acquired on beam 19. The Mean-Square Successive Difference and Kendall Correlation statistics indicate the data were probably positively correlated and that they manifest a positive trend. The average level and standard deviation are high for beam 19 when compared with its neighboring beams. Despite the indication of positive trend for beam 22 there is little ancillary evidence to substantiate the hypothesis that the data sequence is nonrandom. Considering the statistical evidence for all 23 beams, one would feel justified to conclude that in total the noise measurements acquired during the specified measurement period behaved in a random manner. That is, events of a systematic and nonstationary nature are scarce in these data.

(C) Finally, the statistics presented in Table G-3 indicate nonrandom events on many beams with respect to the number of Runs Test and the Kendall Correlation Test. However, the Mean-Square Successive Difference Test statistic, ZMSSD, is significantly different from zero for all 23 beams. The acoustic events which caused this indication of positively correlated serial data were distant explosions. The explosions were detonated some 2740 nmi away from the TASS array. By the time the explosive pulses arrived at the array they were spread over about 30 sec. Hence, during the 15-min measurement period there appeared at least one 30-sec sequence of data that was much higher in level than usual. This is the type of phenomenon that the Mean-Square Successive Difference Test would readily detect, and so it has on all beams regardless of explosion location.

CONFIDENTIAL

SECRET

APPENDIX H RESULTS UTILIZING ADAPTIVE PROCESSING

(U) This appendix includes only a few select examples to illustrate the differences between the resolved horizontal directionality results obtained from adaptive processing prior to deconvolution and the results obtained from onboard processing. It is not intended to provide a data base for the adaptive processing results, nor will a lengthy discussion be attempted regarding the attributes, problems, or mathematics of the type of adaptive processing. The resolved horizontal directionalities obtained from the adaptively processed data and how the results differ from the results obtained from the onboard processed data are the primary concern of this appendix. The complete data set is contained in Ref. 5.

(S) The LAMBDA data were analyzed both onboard and ashore. The post-exercise data analysis techniques were much more elaborate, requiring more extensive computing capabilities than existed at sea. The onboard data processing included the forming of conventional beams with Hamming shading. The number of beams utilized in the onboard results varied from 21 at 11 Hz, to 65 at 38 Hz. Ashore, however, beams were formed every 1/2 deg from forward endfire to aft endfire, and results for unshaded conventional beamforming and adaptive beamforming were obtained. The particular type of adaptive processing is discussed in Ref. 26.

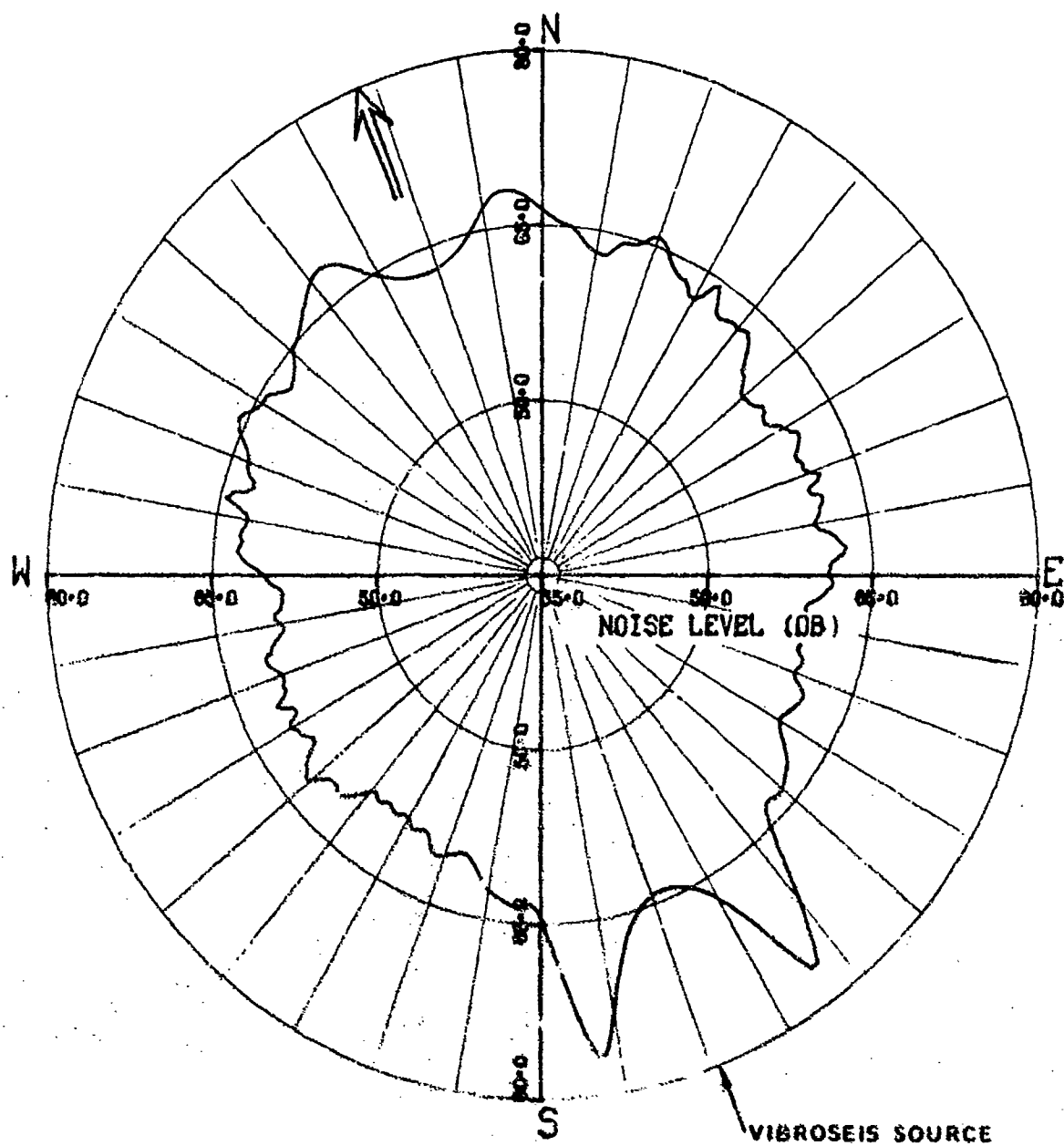
(S) Figures H-1, H-2, and H-3 are 38-Hz beam response plots for the adaptive, conventional, and onboard processing respectively. The levels in the first two figures are only relative levels. The fourth leg of polygon 2 at $\eta=3$ is used in this example because of the Vibroseis source operating about 120 miles away along an azimuth of 159 deg. The bearing errors have not been corrected in these data, thus illustrating the magnitude of the error more adequately than was done with the onboard results and enabling a direct comparison with the onboard results given in Appendix F.

(U) The results of the adaptive processing (Fig. H-1) are quite similar to those for the conventional processing (Fig. H-2) along all azimuths except in the vicinity of the source near endfire. Since a beam is effectively being formed for each 1/2 deg of azimuth, the directionality pattern along the azimuths near the source azimuth will take the form of the beam response at that azimuth. Hence, in these two figures the shapes of the near-endfire beams are evident. The half-power point of the adaptive beam is about 5 deg, whereas it is about 10 deg for the conventional beam. As a result, the adaptive beam has been able to resolve approximately 5 dB lower along the endfire direction than the conventional beam. The near-endfire beams resulting from

SECRET

SECRET

ADAPTIVE AMBIGUOUS PLOT

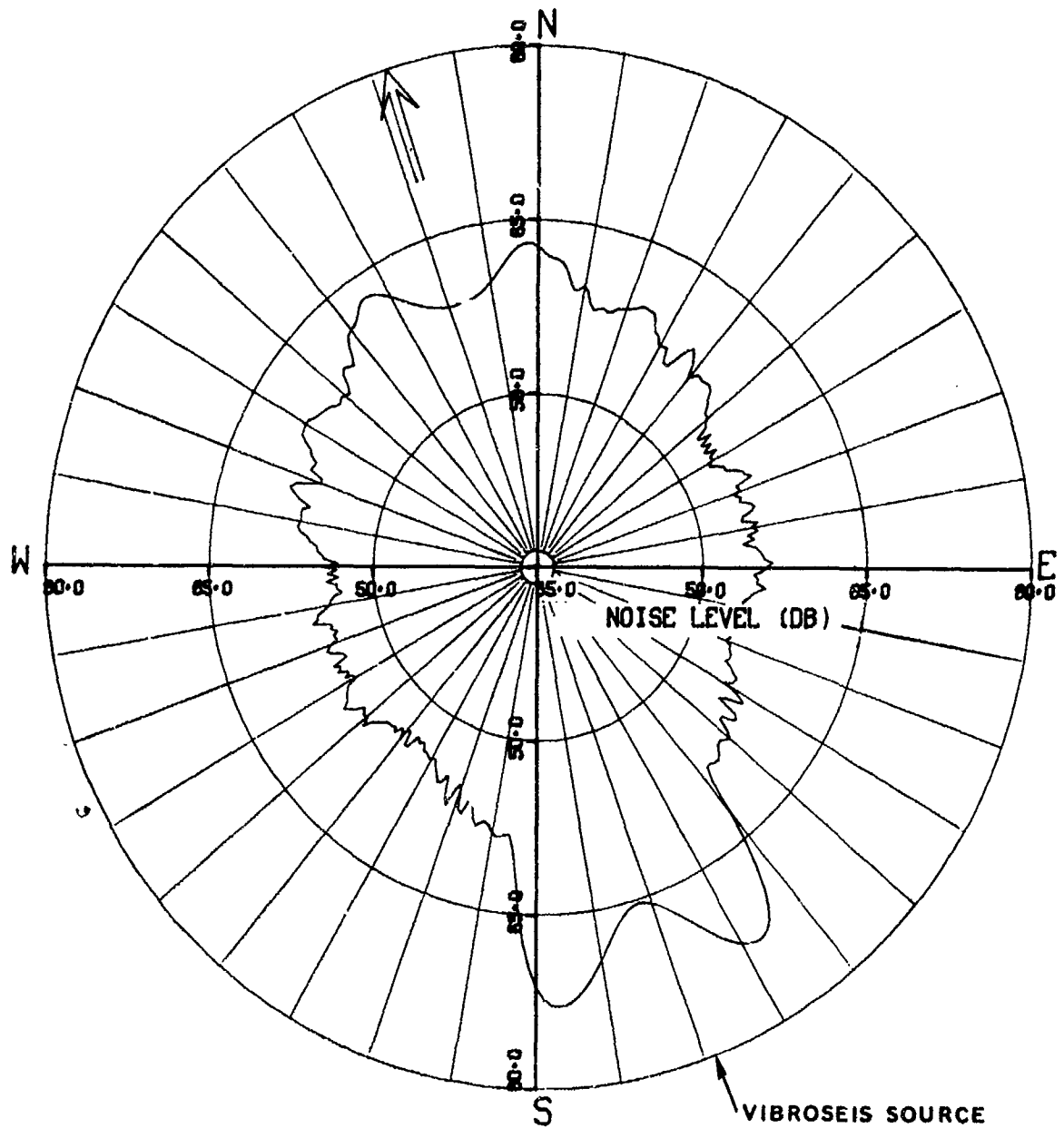


(U) Figure H-1. LAMBDA polygon 2, leg 4, 38-Hz beam response data obtained by adaptive beamforming procedures. (S)

SECRET

SECRET

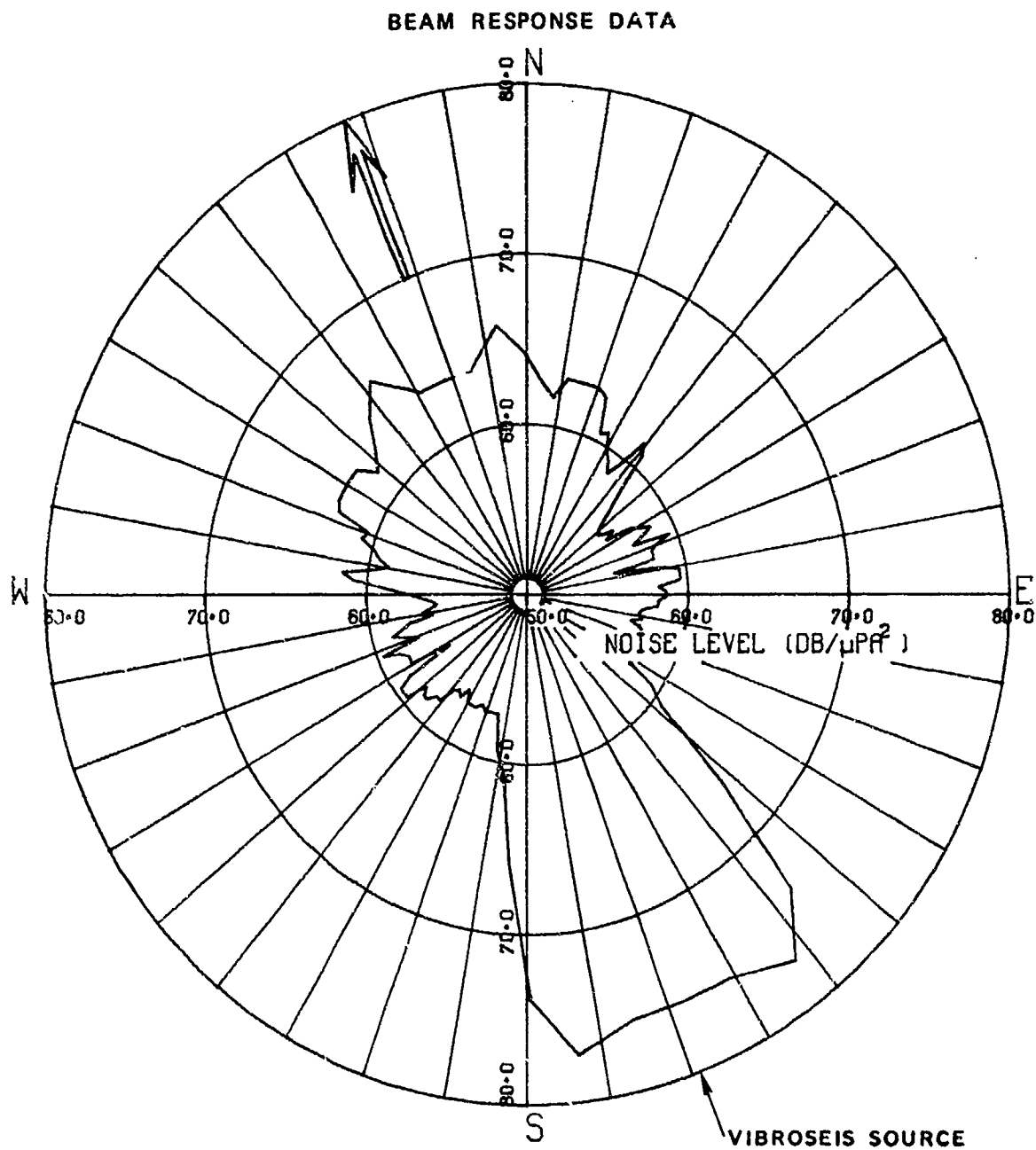
CONVENTIONAL BEAM RESPONSE



(U) Figure H-2. LAMBDA polygon 2, leg 4, 38-Hz beam response data obtained by post-exercise conventional beamforming procedures. (S)

SECRET

SECRET



(U) Figure H-3. LAMBDA polygon 2, leg 4, 38-Hz beam response data obtained during onboard analysis. (S)

SECRET

SECRET

the onboard data processing are about 14 or 15 deg between the half-power points; consequently, the relative azimuth to the signal could not be determined closer than 2 or 3 deg and the endfire beam was severely contaminated, as is clearly evident in Fig. H-3. The adaptive beam responses in Figs. H-4, H-5, H-6, and H-7, for the other four legs of the same polygon, show similar results. These figures can be compared directly with the figures in Appendix F, which are the results for the same legs processed onboard. Figure H-8 gives the horizontal directionalities resolved by the BAR and the All-Bearings methods. These results are for uncorrected array headings and can be compared with the results in Fig. E-6 of Appendix E. When the array heading errors are eliminated, the patterns in Fig. H-9 are obtained and can be compared to those in Fig. E-7 from the onboard processed data.

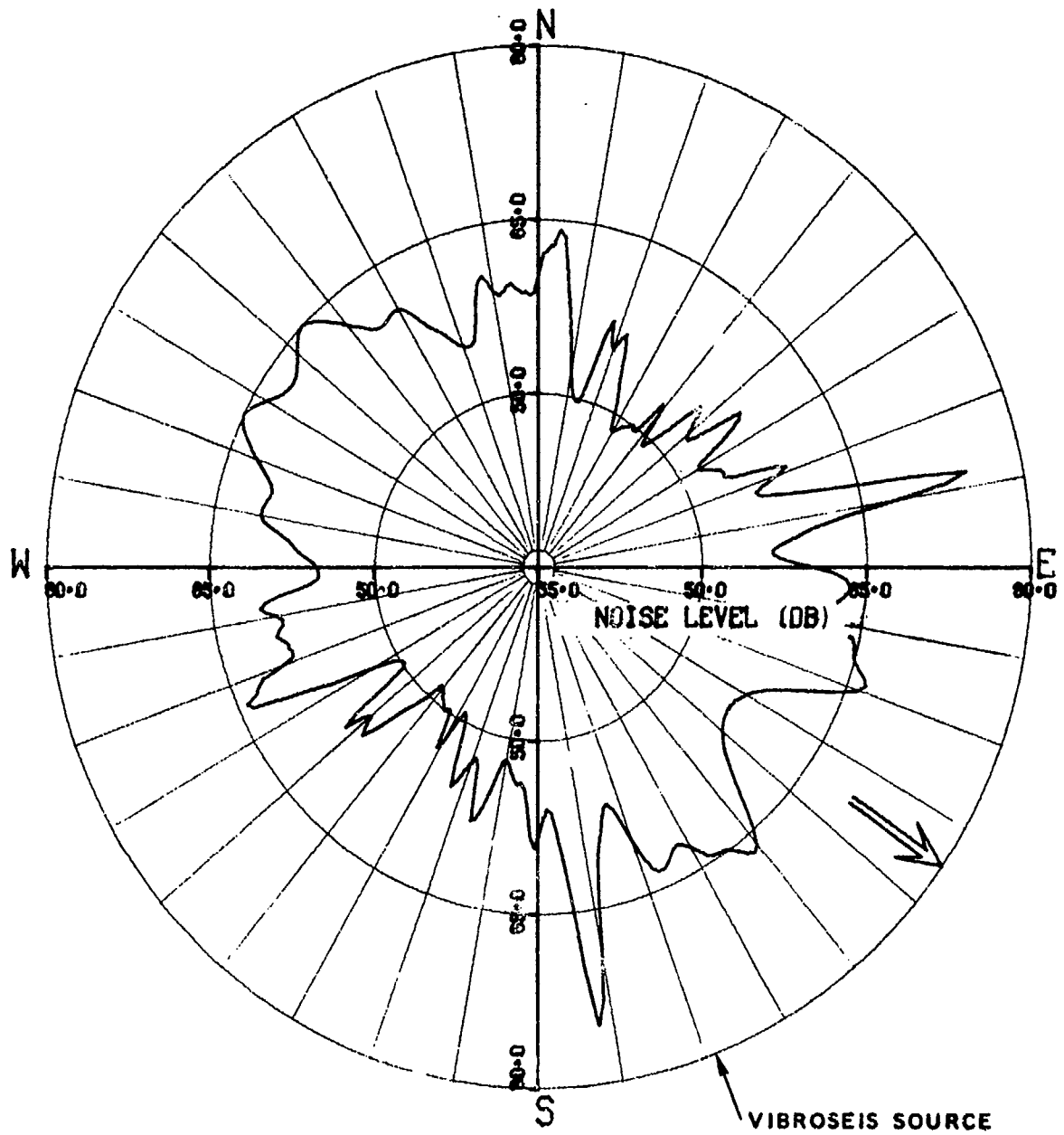
(U) The improvements in the resolution of the beam response plots due to the adaptive processing are remarkable when compared to both the conventional and the onboard processing. If accomplished onboard, adaptive processing could greatly enhance the detection and bearing resolution capabilities of the array. However, when trying to resolve the horizontal directionality of a nonstationary noise field, the effect is more detrimental than it is beneficial, since the apparent nonstationarity of the noise field increases with decreasing beamwidth and the present ambiguity resolution techniques prefer a high degree of stationarity. However, this is not to say that the adaptive processing should not be used or that the data used in the ambiguity resolution algorithms should not come from the adaptively processed data. It simply means, as in the case of onboard data, that if the noise field appears too nonstationary for the adaptive beams, the data should be "smoothed" or sampled to create a new data set which satisfies the necessary stationarity criteria established for noise field resolution. Smoothing or sampling procedures which accomplish this objective have been used successfully in the present study and are discussed in the main body of this document. Appropriate criteria for determining the acceptable beamwidth for a given degree of noise field nonstationarity, however, have not. Establishing such criteria would be a difficult task in itself. It would be neither appropriate nor within the scope of this report.

(U) When the horizontal directionalities obtained from the adaptively processed data were compared with the results obtained from the onboard-processed data for other times and frequencies the results could be generalized as follows. At the higher frequencies (29 and 38 Hz) the increased resolution in the beam response data (caused by the reduction in the beamwidth) and the increased number of adaptive beams combined to make the noise field appear more nonstationary to the ambiguity resolution algorithms than did the beam response data obtained from onboard processing. The net effect was a general degradation in the quality of the resolved results, even though the onboard results at these frequencies were already questionable. As the frequency decreased, the differences in the results from the two types of processing also decreased, and at 11 Hz the differences are relatively minor. In fact, it would be difficult to determine which differences are due to the processing and which are due to how the All-Bearings (and therefore the MAB) method handled the slightly different inputs.

SECRET

SECRET

ADAPTIVE AMBIGUOUS PLOT

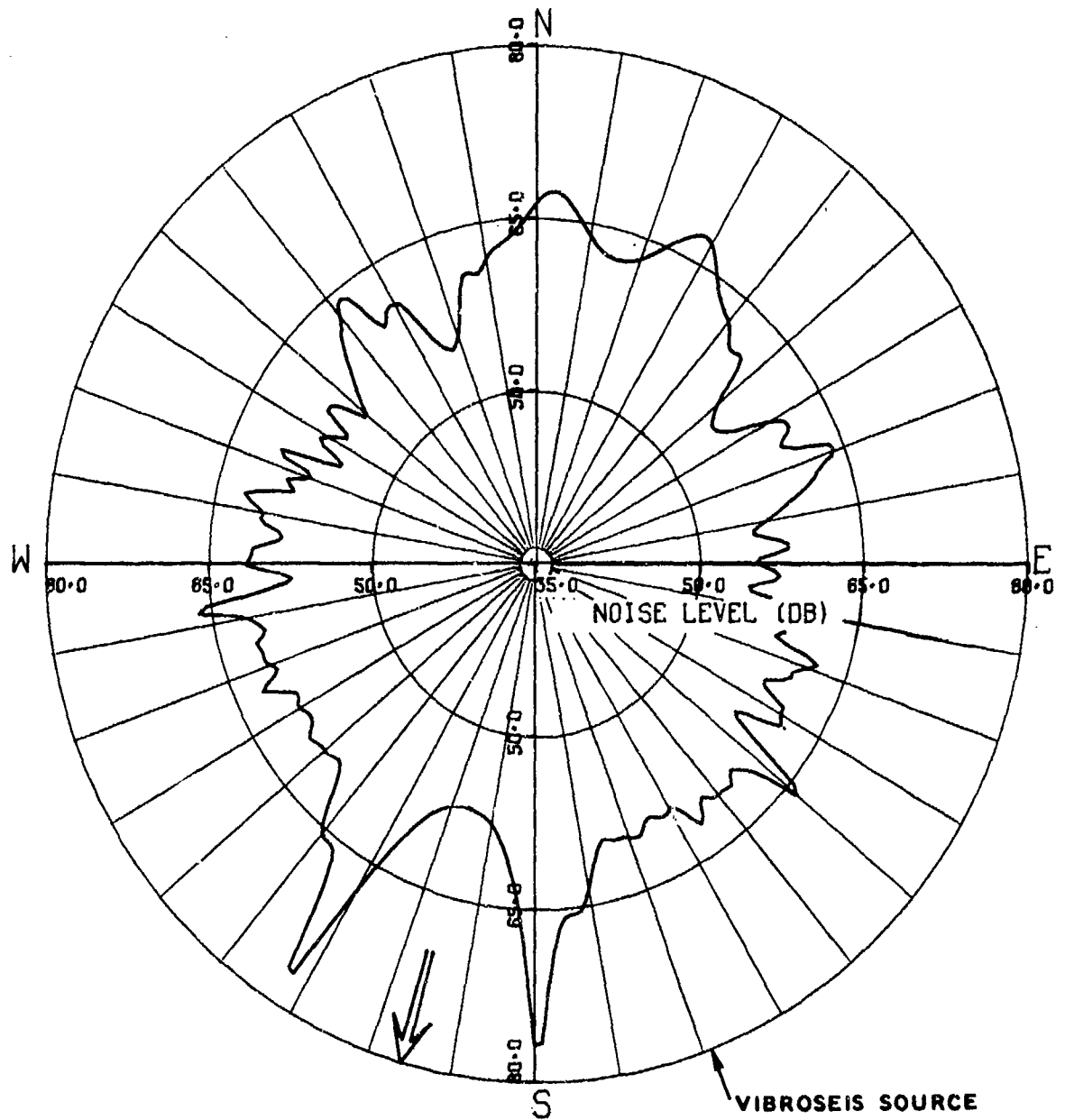


(U) Figure H-4. LAMBDA polygon 2, leg 1, 38-Hz beam response data obtained during onboard analysis (S)

SECRET

SECRET

ADAPTIVE AMBIGUOUS PLOT

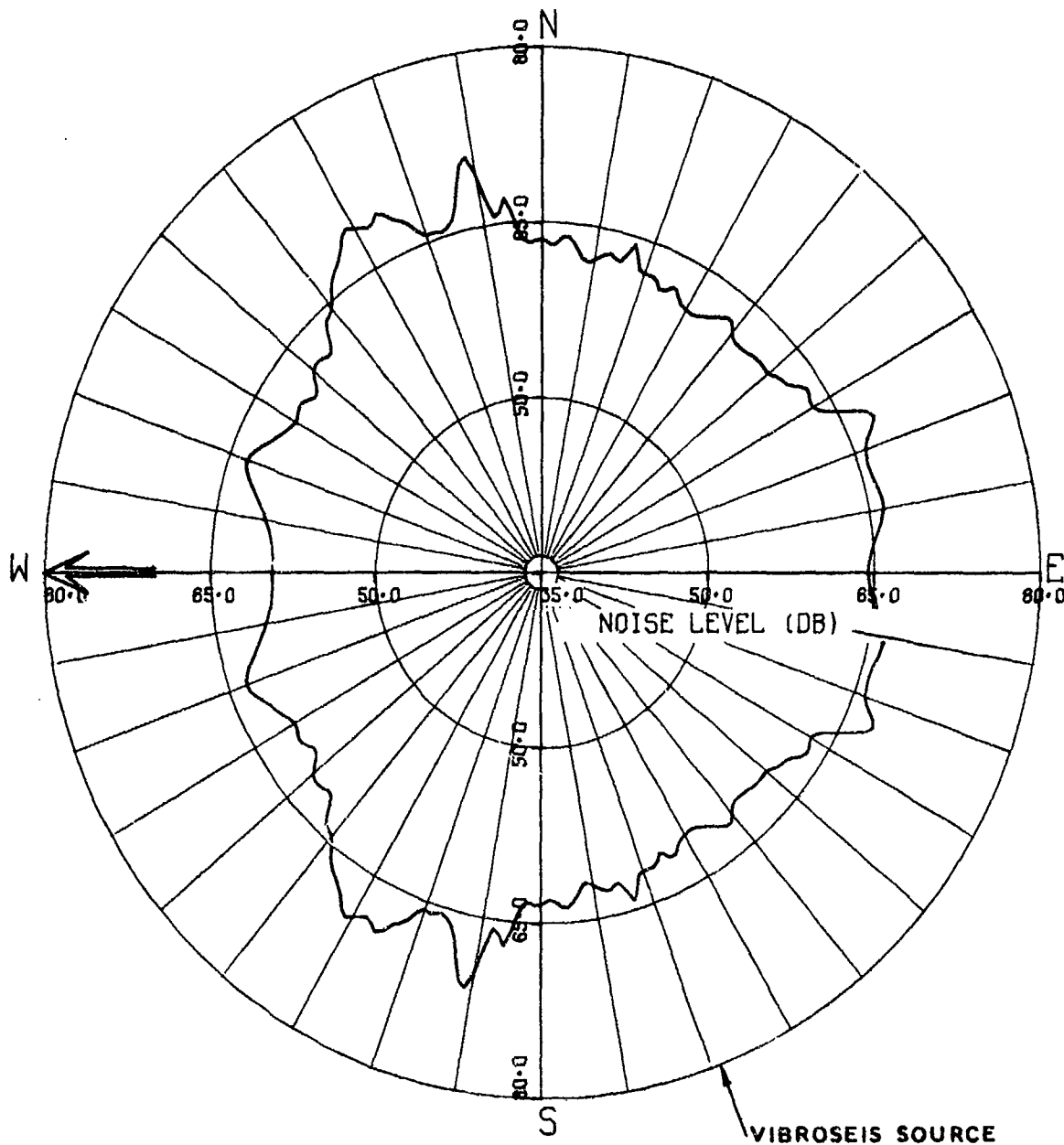


(U) Figure H-5. LAMBDA polygon 2, leg 2, 38-Hz beam response data obtained during onboard analysis. (S)

SECRET

SECRET

ADAPTIVE AMBIGUOUS PLOT

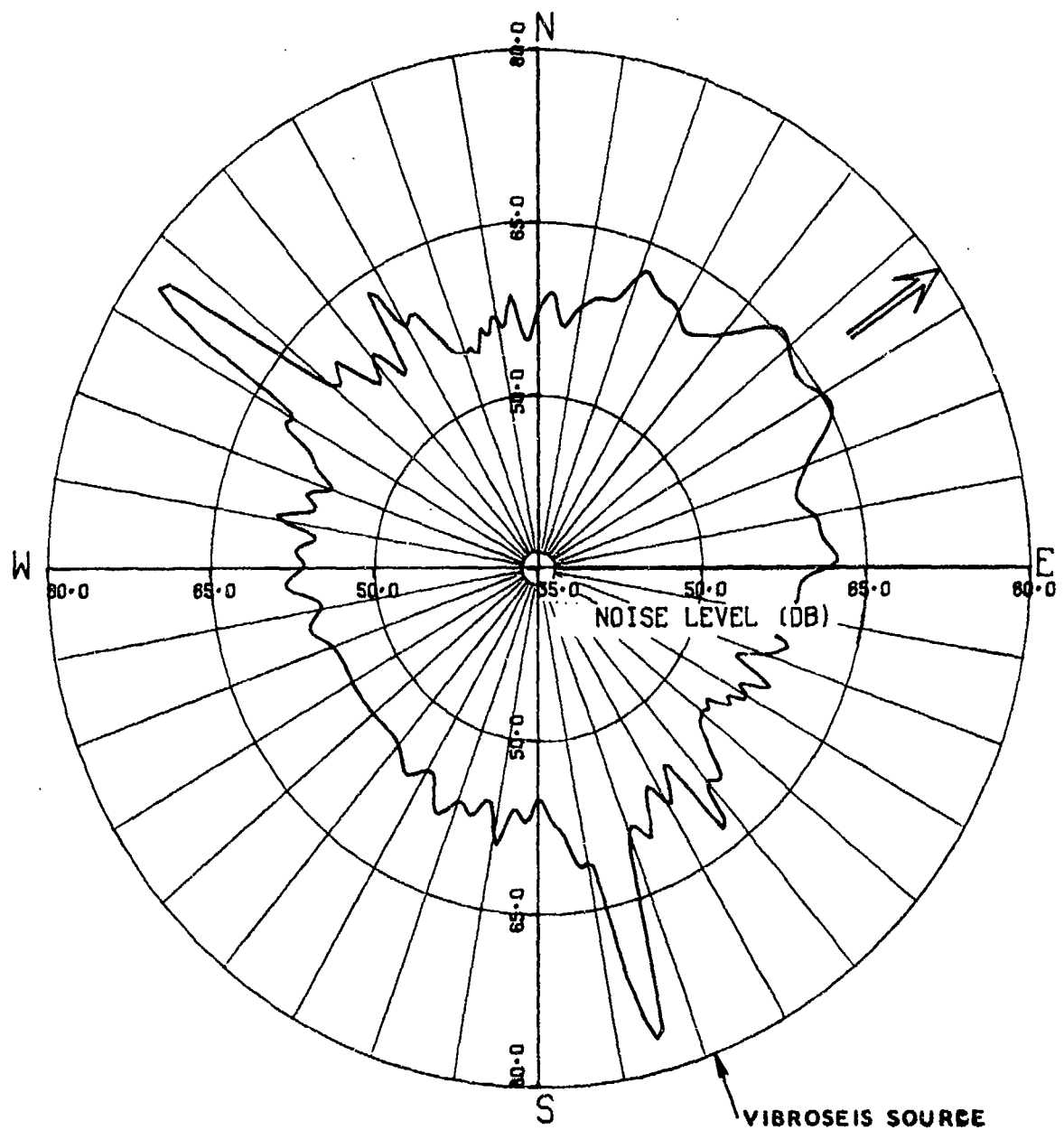


(U) Figure H-6. LAMBDA polygon 2, leg 3, 38-Hz beam response data obtained during onboard analysis. (S)

SECRET

SECRET

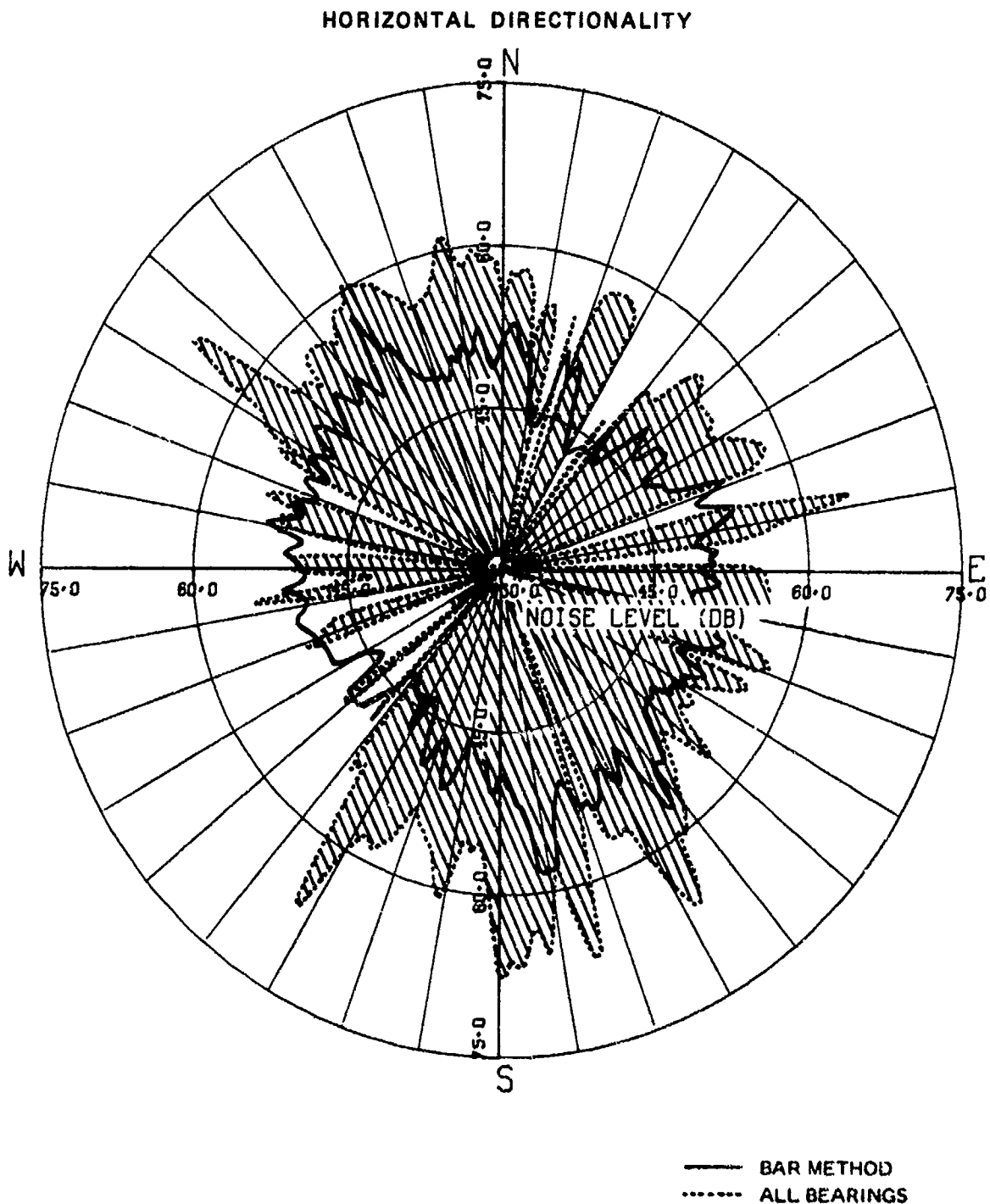
ADAPTIVE AMBIGUOUS PLOT



(U) Figure H-7. LAMBDA polygon 2, leg 5, 38-Hz beam response data obtained during onboard analysis. (S)

SECRET

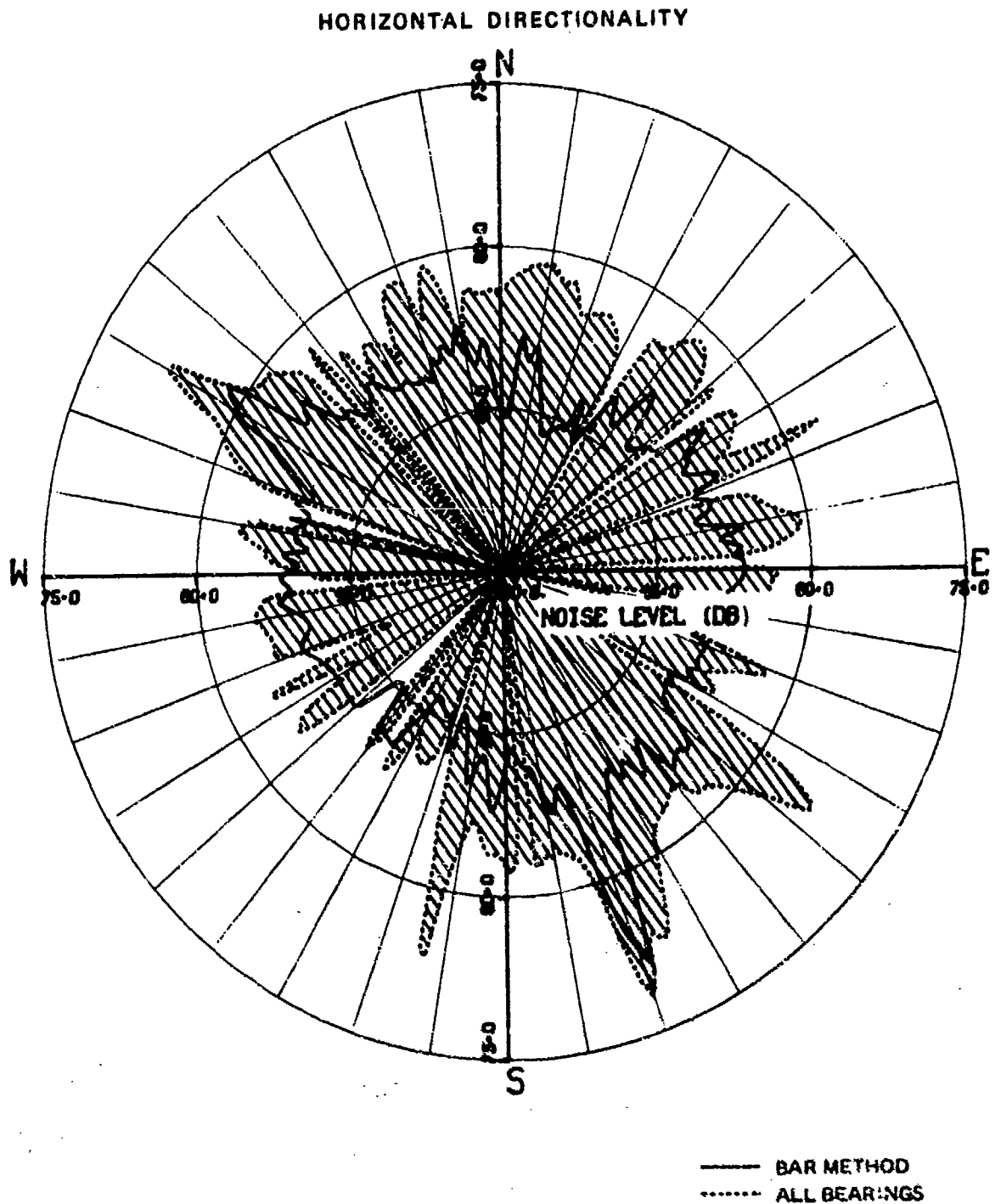
SECRET



(U) Figure H-8. Horizontal directionalities in a 1/8-Hz bandwidth at 38 Hz due to the MAB and BAR methods utilizing the 5 legs of LAMBDA polygon 2 with the original array heading errors. (S)

SECRET

SECRET



(U) Figure H-9. Horizontal directionalities in a 1/8-Hz bandwidth at 38 Hz due to the MAB and BAR methods utilizing the 5 legs of LAMBDA polygon 2 with the original array heading errors corrected. (S)

SECRET



DEPARTMENT OF THE NAVY

OFFICE OF NAVAL RESEARCH
875 NORTH RANDOLPH STREET
SUITE 1425
ARLINGTON VA 22203-1995

IN REPLY REFER TO:

5510/1
Ser 321OA/011/06
31 Jan 06

MEMORANDUM FOR DISTRIBUTION LIST

Subj: DECLASSIFICATION OF LONG RANGE ACOUSTIC PROPAGATION PROJECT
(LRAPP) DOCUMENTS

Ref: (a) SECNAVINST 5510.36

Encl: (1) List of DECLASSIFIED LRAPP Documents

1. In accordance with reference (a), a declassification review has been conducted on a number of classified LRAPP documents.
2. The LRAPP documents listed in enclosure (1) have been downgraded to UNCLASSIFIED and have been approved for public release. These documents should be remarked as follows:

Classification changed to UNCLASSIFIED by authority of the Chief of Naval Operations (N772) letter N772A/6U875630, 20 January 2006.

DISTRIBUTION STATEMENT A: Approved for Public Release; Distribution is unlimited.

3. Questions may be directed to the undersigned on (703) 696-4619, DSN 426-4619.

BRIAN LINK
By direction

Subj: DECLASSIFICATION OF LONG RANGE ACOUSTIC PROPAGATION PROJECT
(LRAPP) DOCUMENTS

DISTRIBUTION LIST:

NAVOCEANO (Code N121LC – Jaime Ratliff)
NRL Washington (Code 5596.3 – Mary Templeman)
PEO LMW Det San Diego (PMS 181)
DTIC-OCQ (Larry Downing)
ARL, U of Texas
Blue Sea Corporation (Dr. Roy Gaul)
ONR 32B (CAPT Paul Stewart)
ONR 321OA (Dr. Ellen Livingston)
APL, U of Washington
APL, Johns Hopkins University
ARL, Penn State University
MPL of Scripps Institution of Oceanography
WHOI
NAVSEA
NAVAIR
NUWC
SAIC

Declassified LRAPP Documents

Report Number	Personal Author	Title	Publication Source (Originator)	Pub. Date	Current Availability	Class.
55	Weinstein, M. S., et al.	SUS QUALITY ASSESSMENT, SQUARE DEAL	Undersea Systems, Inc.	750207	ADA007559; ND	U
BKD2380	Unavailable	WESTLANT 74 PHASE 1 DATA SUMMARY (U)	B-K Dyanmics, Inc.	750301	NS; ND	U
TM-SA23-C44-75	Wilcox, J. D.	MOTION MODEL VALIDATION FROM LRAPP ATLANTIC TEST BED DATA	Naval Underwater Systems Center	750317	ND	U
RAFF7412; 74-482	Scheu, J. E.	SQUARE DEAL SHIPPING DENSITIES (U)	Raff Associates, Inc.	750401	ADC003198; NS; ND	U
PSI TR-004018	Barnes, A. E., et al.	ON THE ESTIMATION OF SHIPPING DENSITIES FROM OBSERVED DATA	Planning Systems Inc.	750401	AD 096582	U
NUSC TD No.4937	LaPlante, R. F., et al.	THE MOORED ACOUSTIC BUOY SYSTEM (MABS)	Naval Underwater Systems Center	750404	ADB003783; ND	U
USI 460-1-75	Weinstein, M. S., et al.	SUS SIGNAL DATA PROCESSING (U) INVESTIGATIONS CONDUCTED UNDER THE DIAGNOSTIC PLAN FOR CHURCH ANCHOR AND SQUARE DEAL SHOT DATA (U)	Underwater Systems, Inc.	750414	ADC002353; ND	U
Unavailable	Ellis, G. E.	SUMMARY OF ENVIRONMENTAL ACOUSTIC DATA PROCESSING	University of Texas, Applied Research Laboratories	750618	ADA011836	U
Unavailable	Edelblute, D. J.	OCEANOGRAPHIC MEASUREMENT SYSTEM TEST AT SANTA CRUZ ACOUSTIC RANGE FACILITY (SCARF)	Lockheed Missiles and Space Co., Inc.	751015	ADB007190	U
Unavailable	Unavailable	SUS SOURCE LEVEL COMMITTEE REPORT	Underwater Systems, Inc.	751105	ADA019469	U
Unavailable	Hampton, L. D.	ACOUSTIC BOTTOM INTERACTION EXPERIMENT DESCRIPTION	University of Texas, Applied Research Laboratories	760102	ADA021330	U
PSI-TR-036030	Turk, L. A., et al.	CHURCH ANCHOR: AREA ASSESSMENT FOR TOWED ARRAYS (U)	Planning Systems Inc.	760301	ND	U
NUC TP 419	Wagstaff, R. A., et al.	HORIZONTAL DIRECTIONALITY OF AMBIENT SEA NOISE IN THE NORTH PACIFIC OCEAN (U)	Naval Undersea Center	760501	ADC007023; NS; ND	U
NRL-MR-3316	Young, A. M., et al.	AN ACOUSTIC MONITORING SYSTEMS FOR THE VIBROSEIS LOW-FREQUENCY UNDERWATER ACOUSTIC SOURCE	Naval Research Laboratory	760601	ADA028239; ND	U
ARL-TR-75-32	Ellis, G. E.	SUMMARY OF ENVIRONMENTAL ACOUSTIC DATA PROCESSING	University of Texas, Applied Research Laboratories	760705	ADA028084; ND	U
Unavailable	Unavailable	SUMMARY OF ENVIRONMENTAL ACOUSTIC DATA PROCESSING	University of Texas, Computer Science Division	761013	ADA032562	U
TTA83676285	Unavailable	ANALYSIS PLAN FOR NARROWBAND/ NARROWBEAM AMBIENT NOISE (U)	Tetra Tech, Inc.	761112	ADC008275; NS; ND	U
USI 564-1-77	Wallace, W. E., et al.	REPORT OF CW WORKSHOP. NORDA, BAY ST. LOUIS, MISS., 28-29 SEPT 1976	Underwater Systems, Inc.	770124	ND	U